Computation of Nonlinear Hydrodynamic Loads on Floating Wind Turbines using Fluid-Impulse Theory

by

Godine Kok Yan Chan

Submitted to the Department of Mechanical Engineering
in partial fulfillment of the requirements for the degree of

Doctor of Philosophy in Mechanical Engineering

at the

MASSACHUSETTS INSTITUTE OF TECHNOLOGY

June 2016

Signature redacted

Author .....
Department of Mechanical Engineering
May 3, 2016

Signature redacted

Certified by .....
Paul D. Sclavounos
Professor
Thesis Supervisor

Signature redacted

Accepted by .....
Rohan Abeyaratne
Chairman, Department Committee on Graduate Students

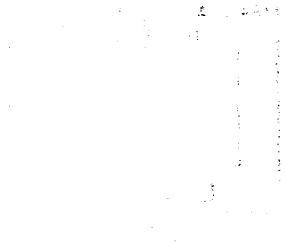

Computation of Nonlinear Hydrodynamic Loads on Floating Wind Turbines using Fluid-Impulse Theory

by

Godine Kok Yan Chan

Submitted to the Department of Mechanical Engineering
on May 3, 2016, in partial fulfillment of the
requirements for the degree of
Doctor of Philosophy in Mechanical Engineering

Abstract

Wind energy is one of the more viable sources of renewable energy and offshore wind turbines represent a promising technology for the cost effective harvesting of this abundant source of energy. To capture wind energy offshore, horizontal-axis wind turbines can be installed on offshore platforms and the study of hydrodynamic loads on these offshore platforms becomes a critical issue for the design of offshore wind turbine systems.

A versatile and efficient hydrodynamics module was developed to evaluate the linear and nonlinear loads on floating wind turbines using a new fluid-impulse formulation — the Fluid Impulse Theory(FIT). The new formulation allows linear and nonlinear loads on floating bodies to be computed in the time domain, and avoids the computationally intensive evaluation of temporal and spatial gradients of the velocity potential in the Bernoulli equation and the discretization of the nonlinear free surface. The module computes linear and nonlinear loads — including hydrostatic, Froude-Krylov, radiation and diffraction, as well as nonlinear effects known to cause ringing, springing and slow-drift loads — directly in the time domain and a stochastic seastate. The accurate evaluation of nonlinear loads by FIT provides an excellent alternative to existing methods for the safe and cost-effective design of offshore floating wind turbines.

The time-domain Green function is used to solve the linear and nonlinear free-surface problems and efficient methods are derived for its computation. The body instantaneous wetted surface is approximated by a panel mesh and the discretization of the free surface is circumvented by using the Green function. The evaluation of the nonlinear loads is based on explicit expressions derived by the fluid-impulse theory, which can be computed efficiently.

Thesis Supervisor: Paul D. Sclavounos
Title: Professor

Acknowledgments

Numerous people contributed to the success of this work. First and foremost, I would like to thank Prof. Paul Sclavounos, my advisor, for his infinite patience and expert guidance throughout the course of my doctoral program here at MIT. No words are enough in expressing my sincere appreciation for his supervision and care throughout my studies. I would also like to thank my committee members, Prof. Lermusiaux, Prof. Techet and Dr. Jonkman for their valuable insight on my project. I would like to especially thank Dr. Jason Jonkman for his kindness and dedication in managing the project as well as providing detailed numerical solutions for this study.

I would like to express my sincerest love and thanks to my family, Mom, Dad and Godfrey; and my extended families, my grandparents, my uncles and aunts and my cousins for their endless love and support. Their encouragement and constant belief in me provided the strength needed in completing this work. Heartfelt thanks especially to my dear Hijung for her never-ending love during the last stretch of my PhD sprint. I also thank God for His everyday blessing and guidance in my journey. Finally, with a heavy heart, I dedicate this work to my Grandmother Chow, who passed away during my final year of doctoral studies at MIT.

Last but not least, a number of present and graduated students at LSPF as well as the Ocean Engineering Department also contributed to the success of this work. I would like to thank my current lab mates, Yu Zhang and Yu Ma, for their generous assistance over lengthy technical discussions amid their demanding academic schedules. I would also like to thank Dr. Sungho Lee for providing valuable advice on my project amid his busy work and family life. In addition, I would like to shout out to my graduated lab mates, Carlos Casanovas and Giorgos Skar. I cannot imagine a life at MIT without all my fantastic office mates in the small and cozy office of 5-329. My sincere thanks also to our Administrative Assistant to the lab, Barbara Smith, for her help in every details pertaining to the lab throughout my studies here at MIT.

This work was sponsored by the U.S. Department of Energy, the National Renewable Energy Center as well as the Massachusetts Clean Energy Center.

Contents

List of Figures

Chapter 1

Introduction

The energy industry continues to make new strides in constructing and deploying offshore wind turbines with the goal to expand modern society's energy portfolio and provide clean energy for today's ever growing economy. Offshore wind shows great potential as one of the future's prominent energy source due to a variety of reasons. For one, wind is inexhaustible and environmental friendly. The horizontal-axis wind turbine is a mature technology, which allows industries to harvest wind energy at utility scale at low cost. The logistics of the offshore environment favor large multi-megawatt turbines in the 6- to 10-MW range for efficient energy production. These turbines can be easily assembled, transported to, and installed at the offshore wind power plant site. The support structure of offshore wind turbines can be either a bottom-mounted structure in shallow waters or a floating platform if the water is deeper than about 50 m. With much of the worldwide energy demand located at coastal regions, it is imperative to utilize the vast wind resources in the offshore environment.

Fortunately, there exists a vast wind resource potential in deeper water in the USA, China, Norway, Japan and many other countries ([8], [10], [21]). In recent years, the offshore wind industry continues to experiment with different designs of floating offshore wind turbines to be deployed in deeper oceans to capture these wind resources [1]. To be able deploy wind turbines on floating support structures for wind

energy production, wave loads exerted on these floaters by ambient sea states over the life of an offshore wind turbine must be properly modeled and predicted to ensure the structure to be safe and cost-effective.

The wave-body problem

The wave-body interaction problem of an offshore floating structure can be summarized as follow. In most seastates, linear wave theory captures most of the leading order aspects of hydrodynamic wave loads on offshore structures. This was theorized by St. Denis and Pierson [6] as an offshore structure's response to a random sea can be estimated by superposing the response to each wave frequency component in the wave spectrum. This allows a reliability-index-based design method for a given sea spectrum to capture most of the leading order effects in a mild sea condition. Therefore, to avoid possible large load responses, offshore floating wind turbines platforms are often designed to have their natural frequencies to be higher or lower than the dominant ocean wave frequencies.

In extreme and severe sea states or large-amplitude body motions, nonlinear effects are of greater importance and interest in addition to the linear effects. Examples of nonlinear effects include nonlinear hydrostatic load by large-amplitude wave elevations, nonlinear Froude-Krylov force and ringing load by steep large-amplitude waves, and nonlinear wave force by large-amplitude body motions. Large amplitude waves causes extreme wave loads which requires more load bearing capability. When encountering steep waves, ringing loads may occur and excite the floating structure which leads to potential system failure due to fatigue of the tower ([7], [29]). Among the nonlinear effects, nonlinear hydrostatic force and nonlinear Froude-Krylov and disturbance forces are of greatest concern because they govern limits of the state of loads on tethers and anchors. For certain offshore wind turbine floater design such as the Tension-Leg Platforms (TLP), the nonlinear extreme wave loads may lead to tether overload and tether slack which are undesirable for the foundation design. Therefore, these nonlinear effects should be taken into consideration when designing

an offshore floating structure for wind turbines, as the energy of these nonlinear effects can reside about the natural frequency of the structure, typically around 1.7-1.8 rad/sec, causing failure of the structure both in the short term and in the long run. This require an efficient and accurate method for analysis of nonlinear wave loads on floating structures for their safe and cost-effective design, making it the primary objective of this work.

Modeling Hydrodynamic Loads

There had been significant advancement in hydrodynamics/wave-body interaction theory in recent years. The scientific community together with the offshore industries had come a long way since Froude [9] and Krylov [16] first established a theoretical approach to the hydrodynamic analysis of a floating body's motion.

Currently, the evaluation of the wave loads on offshore platforms is typically carried out either by Morison's equation or by frequency-domain panel methods with appropriate time-domain transforms for transient analysis. Morison's equation is a strip theory- based time-domain method for slender structures first theorized by Morison, O'Brien, Johnson and Schaaf [20]. The method accounts for fluid inertia, added mass, and viscous effects by selecting appropriate added mass and drag coefficients. Viscous effects can also be accounted for by equipping appropriate drag and inertia coefficients derived from experiments.

For large-volume platforms, frequency domain boundary element method based on the potential flow theory has recently become one of the most popular tools because of its efficiency and reliability. The first application of BEM was pioneered by Hess and Smith [11] and later adapted in wave-body problems by Newman and other scholars ([3], [23], [24]). This method is primarily based on linear theory and model linear and nonlinear potential-flow effects by solving first- and second-order free-surface problems. This leads to the computation of linear and quadratic transfer functions (QTFs). Recent developments in three dimensional time-domain methods

has resulted in several useful computational methods, an example being the commercial code WAMIT, started here at the MIT Ocean Engineering Department [18].

Previous studies have carried out simulations for floating wind turbines using Morison's equation and frequency-domain methods. Investigators carried out computations of the loads and responses of TLP floating wind turbines and documented them in ([2], [32], [34]). Simulations for the Hywind Spar floating wind turbine structure based on Morison's equation were reported by [25]. For the International Energy Agency Offshore Code Comparison Collaboration (IEA OC3) Spar, simulations were reported by [13]. For the semisubmersible WindFloat structure, simulations were presented by [28]. In [26], simulations for the IEA OC3 Continued (OC4) semisubmersible were documented. The conclusions from the simulations reported in these and other studies are summarized here. There is good agreement between methods predicting the linear potential-flow loads from Morison's equation or frequency-domain methods. The accuracy of Morison's method deteriorates as the wavelength of the ambient wave decreases and becomes comparable to the diameter of a cylindrical floater. The agreement between various methods is less satisfactory for predicting the nonlinear low- and high-frequency loads and responses partly because the underlying modeling assumptions differ and partly because the accurate computation of the sum- and difference-frequency QTFs is a complex and time-consuming task. Additional limitation of a frequency domain analysis based on the linear wave and linear dynamics theory is that the amplitudes of ambient wave and body motions have to be small compared to the ambient wavelength. The linearity assumptions on the wave and motion amplitudes hamstrings investigations of crucial hydrodynamic interactions between waves and bodies in severe seas. Excessive computational cost involved with the complexity of fluid and body interaction also limits the development of the three-dimensional fully nonlinear numerical schemes. An alternative to the methods discussed above are time-domain potential flow methods for the computation of second order loads. The nonlinear time-domain solvers have yet to reach the maturity for demanded by the industry.

The Fluid-Impulse Method

The goal of this work is to explore and develop a new versatile, accurate and efficient time-domain potential flow method for the treatment of nonlinear wave-body interaction in irregular waves in the time-domain. The new method, the Fluid-Impulse Theory (FIT), is based on new expressions for nonlinear hydrostatics, Froude-Krylov, and radiation and diffraction loads derived by Sclavounos [30]. Further description of the theory is presented in the theory section of this thesis.

The time-domain fluid-impulse method bridges the gap between long-wavelength approximations in the time-domain Morison's equation and frequency domain methods. It can be used for both slender and large volume offshore structures and allows for the modeling of higher-order transient nonlinear effects in the vicinity of the waterline. In addition, the fluid impulse method allows the evaluation of second-order and higher-order nonlinear effects via compact force expressions that circumvent the discretization of the free surface by taking advantage of the analytical structure of the time-domain Green function.

Overview

The rest of this thesis is organized as follows. Chapter 2 presents theoretical formulations: the boundary value problem for a hydrodynamic wave-body interaction, the force and moment components in FIT formulation, the solution of the disturbance potential by solving a set of integral equation using the transient free-surface Green-function method and the source formulation, and detailed derivation on solving the free-surface impulse component in FIT. Chapter 3 presents numerical algorithms and simulation results: the wave loads obtained by FIT formulation using the Perturbation Theory, the treatment of surfaces and generation of body mesh, the representation of surfaces with constant-strength source elements, verification and comparison studies between FIT and WAMIT, several test cases obtained by FIT for buoy of different sizes, and numerical results obtained by the simplified FIT formulation using the small Ka approximation. Chapter 4 discusses the results and contributions of this

thesis and suggested future work.

Chapter 2

Theory

This chapter discuss the theory behind the computation of hydrodynamic loads using the Fluid-Impulse Theory (FIT). The goal of FIT is to provide a formulation for the computation of nonlinear hydrodynamics loads in the time-domain for body of any size in the ocean. This chapter starts by summarizing the formulation of FIT and discusses the different force and moment components in the formulation. In the formulation, as the ambient wave is assumed to be known, the only unknown is the Radiation and Diffraction (RD) potential, or the disturbance potential. The solution of the disturbance potential is obtained by solving a set of integral equations using the transient Green function and the source formulation. The transient Green function and the source formulation are described theoretically and numerically in their respective subsections. A theoretical framework on expressing the completely nonlinear term, the free-surface impulse force and moment components in surge, heave and pitch, with respect to known body surfaces is then presented for the efficient application of FIT. This allows FIT to be applied efficiently without the need of discretizing the ambient wave free-surface, while accounting for the nonlinear load contributions from the ambient irregular seastate. Finally, a summary on a simplified FIT formulation using the small Ka approximation for surge wave loads on cylinders is presented at the end of this chapter.

2.1 Fluid-Impulse Theory Formulation

Fig. 2-1 illustrates a platform floating on a free surface interacting with a nonlinear ambient wave assumed to be irregular. The reference coordinate system (X, Y, Z) is fixed in space with its origin located on the calm water surface with the positive Z-axis pointing upward. The free-surface elevation resulting from the ambient wave is denoted by the solid line. The dashed line defines a horizontal plane intersecting the Z-axis at the local elevation of the ambient wave profile. The acceleration of gravity is g and the water density is ρ.

The ambient wave velocity potential is denoted by $\phi_I(X, Y, Z, t)$ and assumed to be irregular and traveling in deep water:

$$\text{(polychromatic)} \quad \phi_I(x, y, z, t) = \Re\left\{ \sum_j \frac{igA_j}{\omega_j} e^{\nu_j z - i\nu_j x \cos\beta_j - i\nu_j y \sin\beta_j + i\omega_j t + i\chi_j} \right\} \tag{2.1}$$

$$\text{where} \quad \nu_j = \omega_j^2/g.$$

And the disturbance radiation and diffraction potentials are denoted by $\phi(X, Y, Z, t)$. Both potentials are subject to the Laplace equation in the fluid domain as

$$\frac{\partial^2\phi}{\partial X^2} + \frac{\partial^2\phi}{\partial Y^2} + \frac{\partial^2\phi}{\partial Z^2} = 0. \tag{2.2}$$

On the instantaneous position of the body boundary $S_B(t)$, the normal velocity of the radiation potential is equal to the normal velocity of the body boundary U_n because of its oscillatory motions

$$\frac{\partial\phi}{\partial n} = U_n, \text{ on } S_B. \tag{2.3}$$

In the diffraction problem, the diffraction potential offsets the ambient wave normal velocity on $S_B(t)$

$$\frac{\partial\phi}{\partial n} = -\frac{\partial\phi_I}{\partial n}, \text{ on } S_B. \tag{2.4}$$

For notational simplicity, the radiation and diffraction (RD) potentials are here-

after denoted by the same symbol, with the body boundary conditions from (2.3) and (2.4) applying for each potential, respectively.

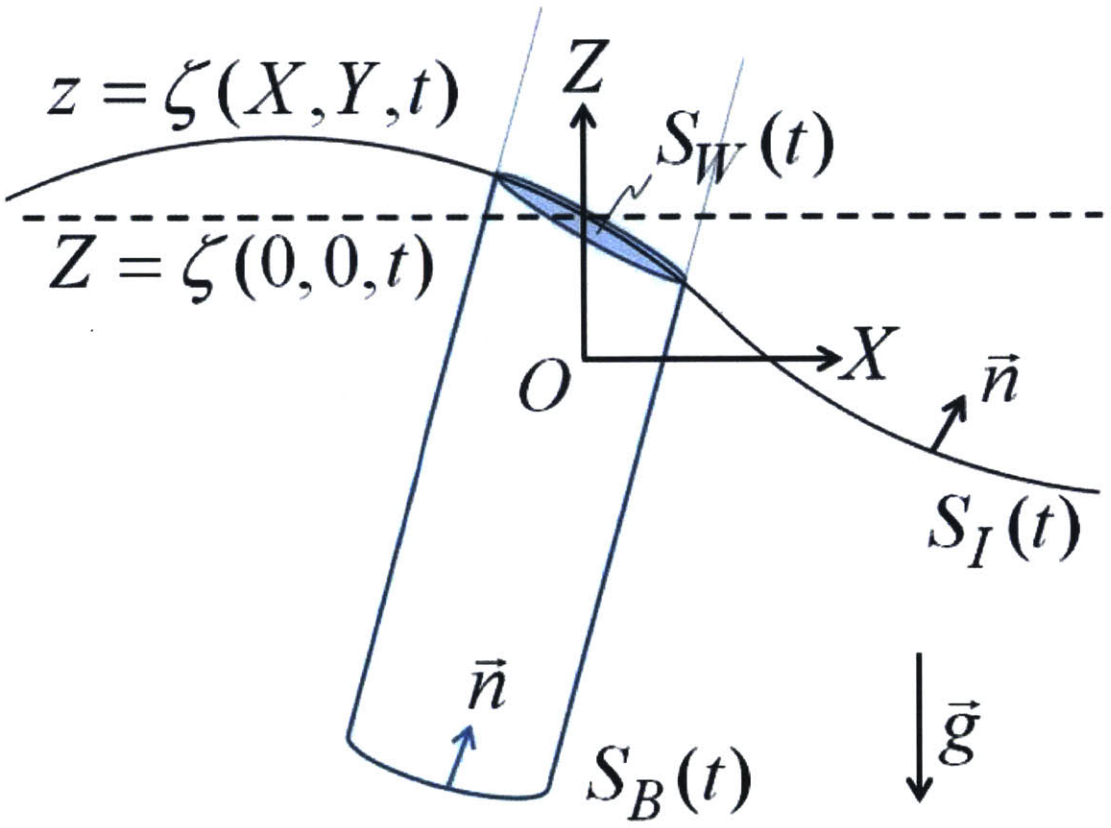

Figure 2-1: Free-surface interaction with floating body

The Fluid Impulse Theory (FIT) derived by [30] is capable of accounting the fully nonlinear free-surface by taking applying a fully nonlinear dynamic and kinematic free-surface condition in the boundary value problem. As this work focuses on studying the leading order nonlinear effects of a wave-body problem, the disturbance RD potential ϕ in FIT was linearized about the ambient wave surface $S_I(t)$ exterior to the body waterline as

$$\frac{\partial^2\phi}{\partial t^2} + g\frac{\partial\phi}{\partial Z} = 0, \text{ on } S_I. \tag{2.5}$$

The conventional definition of the force and moment acting on the body follows from the integration of the hydrodynamic pressure obtained from Bernoulli's equation over the instantaneous body wetted surface

$$\begin{aligned}
\vec{F} &= -\rho \int_{S_B} \Big(\frac{\partial(\phi_I + \phi)}{\partial t} + \frac{1}{2}\nabla(\phi_I + \phi) \cdot \nabla(\phi_I + \phi) + gZ \Big) \vec{n} ds \\
\vec{M} &= -\rho \int_{S_B} \Big(\frac{\partial(\phi_I + \phi)}{\partial t} + \frac{1}{2}\nabla(\phi_I + \phi) \cdot \nabla(\phi_I + \phi) + gZ \Big) \times \Big(\vec{X} \times \vec{n} \Big) ds.
\end{aligned} \tag{2.6}$$

The evaluation of the nonlinear hydrodynamic force and moment given by (2.6) requires the computation of the partial time and space derivatives of the disturbance potential over the instantaneous wetted surface of the body. This computational task requires fine panel meshes that lead to slow convergence in the evaluation of nonlinear forces.

The FIT formulation circumvents the computation of gradients of the disturbance potential by deriving new expressions for the hydrostatic and hydrodynamic forces summarized in the following sections. The total force and moment in (2.6) can be represented as the sum of four components as described in (2.7): 1) nonlinear buoyancy force and moment; 2) Froude-Krylov impulse force and moment; 3) radiation and diffraction body impulse force and moment; and 4) radiation and diffraction free-surface impulse force and moment.

$$\begin{aligned}
\vec{F} &= \vec{F}_H + \vec{F}_{F-K} + \vec{F}_B + \vec{F}_{FS} \\
\vec{M} &= \vec{M}_H + \vec{M}_{F-K} + \vec{M}_B + \vec{M}_{FS}.
\end{aligned} \tag{2.7}$$

These force and moment expresssions are discussed in further details in the following subsections.

2.1.1 Nonlinear Buoyancy Force and Moment

The hydrostatic force and moment acting on the body takes the following form

$$\vec{F}_H = \rho g \forall_W \vec{k} = -\rho g \int\limits_{S_B+S_W} Z\vec{n}ds \tag{2.8}$$

$$\vec{M}_H = -\rho g \int\limits_{S_B+S_W} Z\Big(\vec{X} \times \vec{n}\Big)ds \tag{2.9}$$

In (2.8) and (2.9), $\vec{k}$ is the unit vector pointing in the positive Z-direction and $\forall_W(t)$ is the volume enclosed by the body wetted surface $S_B(t)$ and the nonlinear ambient wave surface interior to the body $S_W(t)$, defined in Fig. 1. The nonlinear hydrostatic force given by (2.8), then, always points upward. In the classical definition of the nonlinear body force obtained by integrating the hydrodynamic pressure from Bernoulli's equation in (2.6), the nonlinear hydrostatic force depends on the shape of the body wetted surface and does not necessarily point upward. (2.8) extends the classical Archimedean buoyancy force in calm water to the unsteady case of nonlinear wave body interactions via the introduction of a time-dependent displacement bounded by the body wetted surface and a dynamic water plane area defined by the ambient wave.

2.1.2 Froude-Krylov Impulse Force and Moment

This force and moment takes the following form

$$\vec{F}_{F-K} = -\rho \frac{d}{dt} \int\limits_{S_B+S_W} \phi_I \vec{n}ds \tag{2.10}$$

$$\vec{M}_{F-K} = -\rho \frac{d}{dt} \int\limits_{S_B+S_W} \phi_I \Big(\vec{X} \times \vec{n}\Big)ds \tag{2.11}$$

The surface integrations in (2.10) and (2.11) are carried out over the instantaneous intersection of the body boundary and the ambient wave profile, which is assumed to be known with the unit normal vector pointing inside the body. An additional integration is carried out over the ambient wave free surface interior to the body. An application of Gauss's theorem provides an alternative definition of the Froude-Krylov impulse as the integral of the ambient wave velocity vector over the volume internal to the body wetted surface and its dynamic water plane area. The evaluation of the new Froude-Krylov force and moment requires knowledge of only the velocity potential of the ambient wave over the body boundary and not its partial time derivative or its spatial gradients.

2.1.3 Radiation and Diffraction Body Impulse Force and Moment

This force and moment takes the following form

$$\vec{F}_B = -\rho \frac{d}{dt} \int_{S_B} \phi \vec{n} ds \tag{2.12}$$

$$\vec{M}_B = -\rho \frac{d}{dt} \int_{S_B} \phi \Big(\vec{X} \times \vec{n} \Big) ds \tag{2.13}$$

The integrations in (2.12) and (2.13) are carried out over the instantaneous body wetted surface defined by its intersection with the ambient wave profile. Again the evaluation of the forces and moments requires only the RD velocity potentials over the body boundary and not their partial time derivative or spatial gradients.

2.1.4 Radiation and Diffraction Free-Surface Impulse Force and Moment

The remaining nonlinear free-surface force and moment invovles integrals of the radiation and diffraction disturbances over the ambient wave free surface $S_I(t)$.

$$\begin{aligned}\vec{F}_{FS} = &- \rho\frac{d}{dt}\int\limits_{S_I}\phi\vec{n}ds - \rho g\vec{k}\int\limits_{S_I}\zeta ds \\ &- \rho\frac{d}{dt}\int\limits_{S_I}\left[\zeta\nabla(\phi_I+\phi) + \frac{1}{2}\zeta^2\frac{\partial}{\partial Z}\nabla(\phi_I+\phi) + ...\right]ds\end{aligned} \tag{2.14}$$

$$\begin{aligned}\vec{M}_{FS} = &- \rho\frac{d}{dt}\int\limits_{S_I}\phi\Big(\vec{X}\times\vec{n}\Big)ds - \rho g\int\limits_{S_I}\zeta(\vec{X}\times\vec{k})ds \\ &- \rho\frac{d}{dt}\int\limits_{S_I}\left\{\zeta\Big[\vec{X}\times\nabla(\phi_I+\phi)\Big] + \frac{1}{2}\zeta^2\frac{\partial}{\partial Z}\Big[\vec{X}\times\nabla(\phi_I+\phi)\Big] + ...\right\}ds\end{aligned} \tag{2.15}$$

Further derivation of this force and moment is discussed in Section 2.4.

2.1.5 Summary

In summary, the nonlinear hydrodynamic force acting on a body floating in an ambient irregular wave of large amplitude has been derived as the sum of a nonlinear buoyancy force pointing upward and the time derivative of a sequence of impulses. The Froude-Krylov nonlinear impulse involves an integral of the ambient wave velocity potential over the instantaneous body wetted surface and the interior water plane area defined by the ambient wave elevation. The body RD nonlinear impulse involves an integral of the RD velocity potentials over the body wetted surface. The free-surface RD nonlinear impulse involves integrals of the RD disturbances over the infinite ambient wave free surface exterior to the body waterline. The forces discussed in this section are based on the assumption that the RD velocity potentials satisfy the linear free-surface condition over the ambient wave free-surface profile. Higher-order nonlinear effects can be accounted for by invoking the fully nonlinear free-surface condition and introducing quadratic and cubic nonlinearities as forcing terms in the right-hand side

of the linear free-surface condition in (2.5) via the perturbation theory.

2.2 Integral Equation for the Disturbance Potential

As discussed in Section 2.1, the ambient wave velocity potential $\phi_I(X, Y, Z, t)$ is assumed to be known *a priori*. To compute the forces and moments presented using FIT, the disturbance potential $\phi(t)$ is the only unknown.

The disturbance potential $\phi(t)$ satisfies the linearized free-surface condition in (2.5) on the ambient wave surface illustrated in Fig. 1. The horizontal dashed planar surface illustrated in the figure intersects the Z-axis at the ordinate $\zeta_I(0, 0, t) \equiv \zeta_I(t)$. To take advantage of the analytical properties of the time-domain Green function, the free-surface condition (2.5) is hereafter assumed to be valid on the planar surface $Z = \zeta_I(t)$. This assumption is justified by the small slope of steep waves in a sea state. Introduce the new coordinate system centered on the dashed planar surface as follows

$$\begin{aligned} x &= X \\ y &= Y \\ z(t) &= Z - \zeta_I(t) \end{aligned} \tag{2.16}$$

The Laplace equation maintains its original form relative to the new coordinate system. The free-surface condition, satisfied by the disturbance potential relative to the new coordinates $\varphi(x = X, y = Y, z = Z - \zeta_I(t), t) = \phi(X, Y, Z, t)$, follows from these identities

$$\begin{aligned} \frac{\partial \phi(t)}{\partial t} &= \frac{\partial \varphi(t)}{\partial t} + \frac{\partial \varphi(t)}{\partial z}\frac{\partial z}{\partial t} = \frac{\partial \varphi(t)}{\partial t} - \dot{\zeta}_I^2(t)\frac{\partial \varphi(t)}{\partial z} \\ \frac{\partial^2 \phi(t)}{\partial t^2} &= \frac{\partial^2 \varphi(t)}{\partial t^2} - 2\dot{\zeta}_I(t)\frac{\partial^2 \varphi(t)}{\partial z \partial t} - \ddot{\zeta}_I(t)\frac{\partial \varphi(t)}{\partial z} + \dot{\zeta}_I^2(t)\frac{\partial^2 \varphi(t)}{\partial z^2} \end{aligned} \tag{2.17}$$

Introducing (2.17) in (2.5), the free-surface condition relative to the new coordinate system becomes

$$\frac{\partial^2 \varphi(t)}{\partial t^2} + [g - \ddot{\zeta}_I(t)]\frac{\partial \varphi(t)}{\partial z} - 2\dot{\zeta}_I(t)\frac{\partial^2 \varphi(t)}{\partial z \partial t} + \dot{\zeta}_I^2(t)\frac{\partial^2 \varphi(t)}{\partial z^2} = 0, z = 0 \tag{2.18}$$

For ambient waves of small steepness, terms involving the time derivatives of the

incident wave elevation are of the order of $\delta = KA$ relative to the leading order terms, where A is the characteristic amplitude of the ambient wave and K is the characteristic wave number. Consequently, the free-surface condition relative to the new coordinate system, with relative errors of $O(\delta)$, becomes the following:

$$\frac{\partial^2 \varphi(t)}{\partial t^2} + g\frac{\partial \varphi(t)}{\partial z} = 0, z = 0 \tag{2.19}$$

The body boundary conditions in (2.3) and (2.4) maintain their form because they involve only spatial derivatives. They are enforced on the instantaneous wetted surface of the body defined relative to the new coordinate system.

From the preceding analysis, it follows that the free-surface condition in (2.19) is enforced on the planar $z = 0$ surface at each time step. Relative to this plane the body wetted surface is more submerged below $z = 0$ when $\zeta_I(t) > 0$ and less submerged when $\zeta_I(t) < 0$. The vertical coordinate of a point of the body wetted surface is given by $z = Z - \zeta_I(t)$, where Z is the vertical coordinate relative to the earth-fixed frame.

The boundary value problem for the disturbance potential becomes a body nonlinear time-domain free-surface problem subject to the linear free-surface condition. Invoking the time-domain Green function, a time-convolution integral equation can be derived for the disturbance potential along the lines of [33], [35]. The disturbance velocity potential is represented by a distribution of sources over the instantaneous wetted surface of the body, as follows

$$\begin{aligned} \varphi(\vec{x}, t) = &- \frac{1}{4\pi} \int\limits_{S_B(t)} ds\ \sigma(\vec{\xi}, t)\Big(\frac{1}{r} - \frac{1}{r'}\Big) \\ &+ \int\limits_0^t d\tau \iint\limits_{S_B(t)} ds\ \sigma(\vec{\xi}, \tau) H_\tau(\vec{x}, \vec{\xi}, t - \tau) \end{aligned} \tag{2.20}$$

The unknown source strength distribution $\sigma(\vec{\xi}, t)$ for $t > 0$ is determined from the solution of the integral equation obtained by enforcing the body boundary condition

as follows

$$\vec{n}\cdot\nabla\varphi(\vec{x},t)=\frac{\partial\varphi(t)}{\partial n}=\vec{n}\cdot\nabla\Bigg[\iint\limits_{S_B(t)}ds\;\sigma(\vec{\xi},t)\Big(-\frac{1}{4\pi}\Big)\Big(\frac{1}{r}-\frac{1}{r'}\Big)+\int\limits_0^t d\tau\iint\limits_{S_B(\tau)}ds\;\sigma(\vec{\xi},\tau)H_\tau(\vec{x},\vec{\xi},t-\tau)\Bigg] \tag{2.21}$$

The left-hand side of (2.21) is a known normal velocity on the body wetted surface for the RD problems via (2.3) and (2.4), respectively.

Invoking the following notation,

$$\begin{aligned}\vec{x}&=(x,y,z)\\ \vec{\xi}&=(\xi,\eta,\zeta)\\ r&=[(x-\xi)^2+(y-\eta)^2+(z-\zeta)^2]^{1/2}\\ r'&=[(x-\xi)^2+(y-\eta)^2+(z+\zeta)^2]^{1/2}\end{aligned} \tag{2.22}$$

the time-domain Green function is defined as follows

$$\begin{aligned}G^{(0)}(\vec{x},\vec{\xi})&=-\frac{1}{4\pi}\Big(\frac{1}{r}-\frac{1}{r'}\Big)\\ H_\tau(\vec{x},\vec{\xi},t)&=-\frac{1}{2\pi}\int\limits_0^\infty dk\;\sqrt{gk}e^{k(z+\zeta)}\sin[\sqrt{gk}t]J_0(kR)\\ R&=[(x-\xi)^2+(y-\eta)^2]^{1/2}\end{aligned} \tag{2.23}$$

The integral equation in (2.20) through (2.23) is solved by discretizing the instantaneous body wetted surface with planar panels and advancing the time-convolution integral ahead in time starting at $t=0$.

The velocity potential of the incident wave $\varphi(\vec{x},t)$ is based on the standard representation of an irregular wave train in a sea state. The solution of the integral equation in (2.21) provides the disturbance velocity potential over the instantaneous position of the wetted surface via (2.20). The substitution of the incident and disturbance potentials in (2.10) to (2.13) allows the evaluation of the fluid-impulse Froude-Krylov

and body forces. This is carried out by first integrating the velocity potentials over the body wetted surface and then taking the time derivative of the resulting time-dependent integral. The evaluation of the partial time derivative and spatial gradients of the ambient and disturbance potentials is circumvented. The free-surface impulse force in Eqs. (2.14) and (2.15) is evaluated in Section 2.4.

2.3 The Transient Wave Part of the Green Function

The transient wave part of the Green function (2.23) described by Wehausen & Laitone [35] can be evaluated in several different ways. Its formulation is listed again below as:

$$
\begin{aligned}
H_\tau(\vec{x},\vec{\xi},t-\tau) &= -\frac{1}{2\pi}\int_0^\infty dk\ \sqrt{gk}e^{kZ}\sin[\sqrt{gk}(t-\tau)]J_0(kR) \\
r &= [(x-\xi)^2+(y-\eta)^2+(z-\zeta)^2]^{1/2} \\
r' &= [(x-\xi)^2+(y-\eta)^2+(z+\zeta)^2]^{1/2} \\
Z &= (z+\zeta) \\
R &= [(x-\xi)^2+(y-\eta)^2]^{1/2}.
\end{aligned}
\tag{2.24}
$$

In this work, the wave part of the Green Function was computed numerically by two methods: 1) by solving the ordinary differential equation as described by Clement [5]; or 2) by the methods described by Newman [22].

2.3.1 Clement

As derived by Clement [5], the wave part of the Green function $H_\tau(\vec{x},\vec{\xi},t-\tau)$ stated above can be evaluated by solving an ordinary differential equation. Rewriting $H_\tau(\vec{x},\vec{\xi},t-\tau)$ as:

$$
H_\tau(\vec{x},\vec{\xi},t-\tau) = F(r,Z,t-\tau) = -\frac{1}{2\pi}\sqrt{g}\int_0^\infty dk\ \sqrt{k}e^{kZ}\sin[\sqrt{gk}(t-\tau)]J_0(kR)
\tag{2.25}
$$

Let $r_1 = \sqrt{r^2+Z^2}$, with a change of variable ($kr_1 \to \lambda$), Jami [12] showed that the memory part of the Green function can be expressed as a function of two variables (μ,T)

$$
F(r,Z,t-\tau) = -\frac{1}{2\pi}\sqrt{g}r_1^{-3/2}\tilde{F}(\mu,T).
\tag{2.26}
$$

with

$$\tilde{F}(\mu,T) = \int_0^\infty d\lambda\ \sqrt{\lambda} e^{-\lambda\mu} \sin[\sqrt{\lambda}T] J_0(\lambda\sqrt{1-\mu^2})$$
$$\text{where} \quad \mu = -Z/r_1 \quad and \quad T = \sqrt{g}(t-\tau)/\sqrt{r_1}. \tag{2.27}$$

$\tilde{F}$ satisfies the following fourth-order differential equation:

$$\tilde{F}^{(4)} + \mu\tau\tilde{F}^{(3)} + \Big(\frac{1}{4}\tau^2 + 4\mu\Big)\tilde{F}^{(2)} + \frac{7}{4}\tau\tilde{F}^{(1)} + \frac{9}{4}\tilde{F} = 0. \tag{2.28}$$

with the initial conditions

$$\tilde{F}^{(2k)}(\mu,0) = 0, \quad \tilde{F}^{(2k+1)}(\mu,0) = (-1)^k(k+1)!P_{k+1}(\mu); \quad k = 0,1,... \tag{2.29}$$

where $\tilde{F}^{(k)}$ denotes the k^{th}-order differentiation of $\tilde{F}$ with respect to τ.
Further study by Chuang et. al [4] stated that a Taylor series expansion method can be applied to solve the differential equation (2.28) with low computational cost. Eq. (2.28) is rewritten as:

$$K_F^{(4)} + \mu\tau K_F^{(3)} + \Big(\frac{1}{4}\tau^2 + A\mu\Big)K_F^{(2)} + B\tau K_F^{(1)} + CK_F = 0$$
$$\text{where} \quad A = 4; \quad B = \frac{7}{4}; \quad C = \frac{9}{4} \quad \text{for} \quad K_F = \tilde{F}. \tag{2.30}$$

Introducing the expression:

$$K_F(\tau) = a_0 + \sum_{n=1}^{\infty} a_n(\tau - \tau_1)^n. \tag{2.31}$$

Based on the work of Chuang et. al [4], the coefficients a_n can be obtained using the closed form solution:

$$a_4 = -\frac{1}{24\kappa_1}(6\kappa_3 a_3 + 2\kappa_2 a_2 + \kappa_8 a_1 + \kappa_9 a_0)$$
$$a_{n+4} = \frac{1}{y_{n+4}}(y_{n+3}a_{n+3} + y_{n+2}a_{n+2} + y_{n+1}a_{n+1} + y_n a_n), \quad \text{for} \quad n = 1, 2, 3, ...$$

where

$$\begin{aligned} y_{n+4} &= \kappa_1(n+4)(n+3)(n+2)(n+1) \\ y_{n+3} &= \kappa_3(n+3)(n+2)(n+1) \\ y_{n+2} &= \kappa_2(n+2)(n+1)n + \kappa_6(n+2)(n+1) \\ y_{n+1} &= \kappa_5(n+1)n + \kappa_8(n+1) \\ y_n &= \kappa_4 n(n-1) + \kappa_7 n + \kappa_9. \end{aligned} \tag{2.32}$$

Once these coefficients are obtained, $\tilde{F}$ can be computed and therefore the wave part of the Green function can be evaluated very efficiently from the computational perspective.

To compute the derivate of $\tilde{F}$ for the evaluation of the derivative of the Green function, by the extension of the Taylor series method presented by Chuang et. al [4], the differential equation can be solved by taking (2.30) with new constants:

$$A = 6; \quad B = \frac{11}{4}; \quad C = \frac{21}{4} \quad \text{for} \quad K_F = \tilde{K}. \tag{2.33}$$

2.3.2 Newman

Another way of evaluating the transient wave part of the Green function is described in Newman [22]. Transforming (2.24) using the spherical coordinates (r_1, θ), with the angle θ measured from the negative vertical axis.
Nondimensionalize the phusical parameters again with repect to g and r_1:

$$\theta = \arccos(\mu) = \arccos(-Z/r_1), \quad T = \sqrt{g}(t-\tau)/\sqrt{r_1}. \tag{2.34}$$

The transient wave part becomes

$$\begin{aligned} &H_\tau(\vec{x}, \vec{\xi}, t-\tau) = \Big(-\frac{1}{4\pi}\Big) g^{\frac{1}{2}} r_1^{-\frac{3}{2}} \Re\{\hat{F}(\theta, T)\} \\ &\text{where} \\ &\hat{F} = -4i \int_0^\infty \omega^2 e^{i\omega T - \omega^2 \cos\theta} J_0(\omega^2 \sin\theta) d\omega; \quad \omega = k^{1/2} \end{aligned} \tag{2.35}$$

The computational domain is now $(0 < T < \infty, 0 \leq \theta \leq \pi/2)$.

For large value of T, asympototic expansion was derived in [22]. The function can now be decomposed into two parts:

$$\hat{F} = f_0 + f_1 + f_2 \tag{2.36}$$

The first part of the integral, integrating $\hat{F}$ in (2.35) up to $iT/2$, can be expanded using Watson's Lemma, and can be expressed as:

$$f_0 \simeq -4 \sum_{n=0} \frac{(2n+2)!}{n!} T^{-2n-3} P_n(\cos\theta) \tag{2.37}$$

The second part of the integral, f_1 was proven to be exponentially small for all values of θ, and through a series of transformation outlined in [22], f_2 can be rewritten into:

$$f_2 \simeq \frac{-4i}{\sqrt{2\sin\theta}} e^{-\frac{1}{4}T^2 e^{-i\theta} - i\frac{\theta}{2} + i\frac{\pi}{4}} \sum_{n=0} \left(\frac{i}{\sin\theta}\right)^n \sum_{m=0} d_{nm} \omega_2^{1-2m-2n} e^{-im\theta} \tag{2.38}$$

where $d_{00} = 1$, $d_{0m} = 0$ for $m > 0$, and for $n \geq 1$

$$d_{nm} = c_n \frac{(2m + 2n - 2)!}{(2n-2)! 2^{2m} m!} \tag{2.39}$$

and

$$c_n = \frac{[\Gamma(n + \frac{1}{2}]^2}{\pi 2^n n!} \tag{2.40}$$

2.4 Free-Surface Impulse Force

Linearing the equations (2.14) and (2.15) above the free-surface using linear FSC (2.5):

$$\zeta = -\frac{1}{g}\frac{\partial \phi}{\partial t}, \text{ on } S_I. \tag{2.41}$$

Keeping terms up to leading order quadratic effects, the free-surface impulse force and moment expressions become:

$$\vec{F}_{FS} = -\rho \frac{d}{dt}\int\limits_{S_I} \phi \vec{n} ds + \rho \vec{k} \int\limits_{S_I} \frac{\partial \phi}{\partial t} ds + \rho \frac{d}{dt}\int\limits_{S_I} \frac{1}{g}\frac{\partial \phi}{\partial t}\nabla(\phi_I + \phi) ds \tag{2.42}$$

$$\begin{aligned} \vec{M}_{FS} = &-\rho \frac{d}{dt}\int\limits_{S_I} \phi\Big(\vec{X} \times \vec{n}\Big) ds + \rho \int\limits_{S_I} \frac{\partial \phi}{\partial t}(\vec{X} \times \vec{k}) ds \\ &- \rho \frac{d}{dt}\int\limits_{S_I} \frac{1}{g}\frac{\partial \phi}{\partial t}\Big[\vec{X} \times \nabla(\phi_I + \phi)\Big] ds \end{aligned} \tag{2.43}$$

The unit normal vector to the ambient wave free surface may be expressed in terms of the gradients of the free-surface elevation. Denoting by δ the order of magnitude of the ambient wave slope obtains the following, with errors quadratic in the wave slope

$$\begin{aligned} \vec{n} &= \frac{\nabla(Z - \zeta_I(X,Y,t))}{|\nabla(Z - \zeta_I(X,Y,t))|} = \frac{-\vec{i}\zeta_{I_X} - \vec{j}\zeta_{I_Y} + \vec{k}}{\sqrt{1 + \zeta_{I_X}^2 + \zeta_{I_Y}^2}} \\ &= (-\vec{i}\zeta_{I_X} - \vec{j}\zeta_{I_Y} + \vec{k})[1 + O(\delta^2)] \end{aligned} \tag{2.44}$$

Invoking again the linear FSC (2.41), and keeping the leading order unit normal vector:

$$\vec{n} = \Big(\frac{1}{g}\frac{\partial^2 \phi_I}{\partial X \partial t}, \frac{1}{g}\frac{\partial^2 \phi_I}{\partial Y \partial t}, 1\Big) \tag{2.45}$$

Substituting (2.45) in (2.42) and (2.43), the force in the surge and heave are respectively:

$$\vec{F}_{FS-1} = -\frac{\rho}{g}\frac{d}{dt}\int_{S_I} \phi\frac{\partial^2\phi_I}{\partial X \partial t}ds + \frac{\rho}{g}\frac{d}{dt}\int_{S_I}\left[\frac{\partial\phi}{\partial t}\frac{\partial}{\partial X}(\phi_I+\phi)\right]ds \tag{2.46}$$

$$\vec{F}_{FS,3} = -\rho\frac{d}{dt}\int_{S_I}\phi ds + \rho\int_{S_I}\frac{\partial\phi}{\partial t}ds + \frac{\rho}{g}\frac{d}{dt}\int_{S_I}\left[\frac{\partial\phi}{\partial t}\frac{\partial}{\partial Z}(\phi_I+\phi)\right]ds \tag{2.47}$$

By moving the derivative of the first term of the force expression inside of the integral and keeping terms to the leading order, the first term of the heave force expression can be shown to cancel with the second term, thus leaving only the last term of the force expression to be computed:

$$\vec{F}_{FS,3} = \frac{\rho}{g}\frac{d}{dt}\int_{S_I}\left(\frac{\partial\phi}{\partial t}\frac{\partial}{\partial Z}(\phi_I+\phi)\right)ds \tag{2.48}$$

In the pitch direction, following (2.44), the cross product between the position vector and the unit normal vector and the gradient of velocity potentials $\vec{X}\times\vec{n}$, $\vec{X}\times\vec{k}$, $\vec{X}\times\nabla\varphi_I$ and $\vec{X}\times\nabla\varphi$ in the pitch direction are respectively:

$$\begin{aligned}
&\left(\vec{X}\times\vec{n}\right)_5 = (z\zeta_{I_X}-x)\vec{j}+O(\delta^2);\\
&\left(\vec{X}\times\vec{k}\right)_5 = -x\vec{j};\\
&\left(\vec{X}\times\nabla\varphi_I\right)_5 = \left(z\frac{\partial\phi_I}{\partial X}-x\frac{\partial\phi_I}{\partial Z}\right)\vec{j};\\
&\left(\vec{X}\times\nabla\varphi\right)_5 = \left(z\frac{\partial\phi}{\partial X}-x\frac{\partial\phi}{\partial Z}\right)\vec{j};
\end{aligned} \tag{2.49}$$

The pitch moment is thus:

$$\begin{aligned}
\vec{M}_{FS,5} &= -\rho\frac{d}{dt}\int_{S_I}\phi\left(z\zeta_{I_X}-x\right)ds + \rho\int_{S_I}\frac{\partial\phi}{\partial t}(-x)ds\\
&+\frac{\rho}{g}\frac{d}{dt}\int_{S_I}\left[\frac{\partial\phi}{\partial t}\left(\left(z\frac{\partial\phi_I}{\partial X}-x\frac{\partial\phi_I}{\partial Z}\right)+\left(z\frac{\partial\phi}{\partial X}-x\frac{\partial\phi}{\partial Z}\right)\right)\right]ds+O(\delta^2)
\end{aligned} \tag{2.50}$$

For small wave steepness, the pitch moment is evaluated on $z = 0$, the remainder of the first and second integral cancels and the moment expression is reduced to:

$$\vec{M}_{FS,5} = -\frac{\rho}{g}\frac{d}{dt}\int_{S_I} x\frac{\partial\phi}{\partial t}\left(\frac{\partial\phi_I}{\partial Z} + \frac{\partial\phi}{\partial Z}\right)ds \tag{2.51}$$

The fluid-impulse force and moment in (2.14) and (2.15) involves quadratic and cubic products of the incident and disturbance potentials. This section described the transformation of the expressions using the lienar FSC as well as assuming small ambient wave steepness. To further simplifed the expressions, the ambient wave free-surface can be linearized locally at the ambient wave waterplane at the body. Thus all integral over the ambient free-surface are evaluated at $z = 0$ with $z = Z - \zeta_I(t)$.

The following subsections discuss the free-surface impulse force futher based on these assumptions.

Before starting the derivations of the free-surface impulse force and moment in the surge, heave and pitch direction, the definitions of the incident wave velocity potential and the disturbance potential are revisited here:

φ_I in irregular waves in deep water, according to (2.1), is:

$$\text{(polychromatic)} \quad \varphi_I(x,y,z,t) = \Re\left\{\sum_j \frac{igA_j}{\omega_j} e^{\nu_j z - i\nu_j x\cos\beta_j - i\nu_j y\sin\beta_j + i\omega_j t + i\chi_j}\right\}$$
$$\nu_j = \omega_j^2/g. \tag{2.52}$$

And the disturbance velocity potential is:

$$
\begin{aligned}
&\varphi(x,y,z,t) = \varphi^{(0)}(x,y,z,t) + \varphi^{(M)}(x,y,z,t) \\
&\varphi^{(0)}(x,y,z,t) = \int_{S_B(\tau)} ds_\xi \sigma(\vec{\xi},t)\Big(\frac{1}{r} - \frac{1}{r'}\Big) \\
&\varphi^{(M)}(x,y,z,t) = \int_0^t d\tau \int_{S_B(\tau)} d\xi \sigma(\vec{\xi},\tau) H_\tau(\vec{x},\vec{\xi},t-\tau) \\
&H_\tau(\vec{x},\vec{\xi},t-\tau) = -\frac{1}{2\pi}\sum_j \int_0^\infty dk_j \ \sqrt{gk_j} e^{k_j(z+\zeta)} \sin[\sqrt{gk_j}(t-\tau)] J_0(k_j R) \\
&\text{where} \quad J_0(k_j R) = \frac{1}{2\pi}\int_{-\pi}^{\pi} e^{ik_j R\cos\theta_j} d\theta_j; \quad R = [(x-\xi)^2 + (y-\eta)^2]^{1/2} \\
&\text{and} \quad x - \xi = R\cos\psi; \quad y - \eta = R\sin\psi
\end{aligned}
\tag{2.53}
$$

Again with small wave steepness approximation, $\varphi^{(0)}(x,y,0,t) = 0,\ t > 0$ by definition. Thus $\frac{\partial}{\partial t}\varphi^{(0)}(x,y,0,t) = 0,\ t > 0$.

$$
\begin{aligned}
&\varphi(x,y,0,t) = \varphi^{(M)}(x,y,0,t) = \int_0^t d\tau \int_{S_B(\tau)} d\xi \sigma(\vec{\xi},\tau) H_\tau(\vec{x},\vec{\xi},t-\tau) \\
&H_\tau(\vec{x},\vec{\xi},t-\tau) = -\frac{1}{2\pi}\sum_j \int_0^\infty dk_j \ \sqrt{gk_j} e^{k_j\zeta} \sin[\sqrt{gk_j}(t-\tau)] J_0(k_j R)
\end{aligned}
\tag{2.54}
$$

The analysis proceeds by evaluating the free-surface impulse force on $z = 0$; The function H_τ can be rewritten as:

$$
\begin{aligned}
&\text{let} \quad u_j = k_j\cos\gamma_j; \quad v_j = k_j\sin\gamma_j; \quad \text{thus} \quad du_j dv_j = k_j dk_j d\gamma_j \\
&H_\tau(\vec{x},\vec{\xi},t-\tau) = -\frac{1}{4\pi^2}\sum_j \int_{-\pi}^{\pi} d\theta_j \int_0^\infty dk_j \ \sqrt{gk_j} e^{k_j\zeta} \sin[\sqrt{gk_j}(t-\tau)] e^{ik_j R\cos\theta_j}
\end{aligned}
\tag{2.55}
$$

Let $\theta_j = \gamma_j - \psi_j, \quad d\theta_j = d\gamma_j, \quad k_j^2 = u_j^2 + v_j^2$:

$$
e^{ik_j R\cos\theta_j} = e^{iu_j(x-\xi)+iv_j(y-\eta)} \tag{2.56}
$$

H_τ is then:

$$H_\tau(\vec{x},\vec{\xi},t-\tau) = -\frac{1}{4\pi^2}\sum_j \iint_{-\infty}^{\infty} du_j dv_j \sqrt{\frac{g}{k_j}} e^{k_j\zeta}\sin[\sqrt{gk_j}(t-\tau)]e^{iu_j(x-\xi)+iv_j(y-\eta)} \tag{2.57}$$

2.4.1 Free-surface impulse force in Surge

The X-direction free-surface impulse force (2.46) can be rewritten into two terms: an ID term which involves cross-products of the incident and disturbance potentials, and a DD term which involves a quadratic product of the disturbance potential:

$$\begin{aligned}
\vec{F}_{FS,1} &= \vec{F}_{FS,1-ID} + \vec{F}_{FS,1-DD} \\
\vec{F}_{FS,1-ID} &= -\frac{\rho}{g}\frac{d}{dt}\int_{z=0}\left(\varphi\frac{\partial^2\varphi_I}{\partial x\partial t} - \frac{\partial\varphi}{\partial t}\frac{\partial\varphi_I}{\partial x}\right)ds \\
\vec{F}_{FS,1-DD} &= \frac{\rho}{g}\frac{d}{dt}\int_{z=0}\left(\frac{\partial\varphi}{\partial t}\frac{\partial\varphi_I}{\partial x}\right)ds
\end{aligned} \tag{2.58}$$

For the first term, the ID component in (2.58), the ambient wave free-surface $S_I(t)$ can be split into the difference between the infinte free-surface $S_\infty(t)$ and the ambient wave surface inside of the body $S_W(t)$:

$$\begin{aligned}
\vec{F}_{FS,1-ID} &= -\frac{\rho}{g}\frac{d}{dt}\left(\int_{S_\infty} - \int_{S_W}\right)\left(\varphi\frac{\partial^2\varphi_I}{\partial x\partial t} - \frac{\partial\varphi}{\partial t}\frac{\partial\varphi_I}{\partial x}\right)ds \\
&= \frac{d}{dt}\left\{\frac{\rho}{g}\int_{S_W}\left(\varphi\frac{\partial^2\varphi_I}{\partial x\partial t} - \frac{\partial\varphi(t)}{\partial t}\frac{\partial\varphi_I}{\partial x}\right)ds - \frac{\rho}{g}\int_{S_\infty}\left(\varphi\frac{\partial^2\varphi_I}{\partial x\partial t} - \frac{\partial\varphi}{\partial t}\frac{\partial\varphi_I}{\partial x}\right)ds\right\}
\end{aligned} \tag{2.59}$$

The impulses for this force expression can then be identified to be an integral over $S_W(t)$ and another over $S_\infty(t)$, which is equivalent to a 2D infinite integral over the x- and y-direction:

$$\begin{aligned}
\vec{F}_{FS,1-ID} &= \frac{d}{dt}\vec{I}_{FS,1-ID} \\
\vec{I}_{FS,1-ID,S_W} &= \frac{\rho}{g}\int\limits_{S_W}\Big(\varphi\frac{\partial^2\varphi_I}{\partial x\partial t} - \frac{\partial\varphi}{\partial t}\frac{\partial\varphi_I}{\partial x}\Big)ds \\
\vec{I}_{FS,1-ID,S_\infty} &= -\frac{\rho}{g}\int\limits_{-\infty}^{\infty}\!\!\iint\Big(\varphi\frac{\partial^2\varphi_I}{\partial x\partial t} - \frac{\partial\varphi}{\partial t}\frac{\partial\varphi_I}{\partial x}\Big)dxdy
\end{aligned} \tag{2.60}$$

This utilizes the property that both the incident wave and both components of the disturbance potential and their time partial derivatives are continuous across the body waterline and over the $z = 0$ plane. The first impulse over the finite surface $S_W(t)$ can be evaluated numerically directly by quadrature with information about all components inside the integral obtained with the expression of $\varphi_I(t)$ and $\varphi(t)$ listed in (2.52) through (2.57) and by taking their spatial and time derivatives. Note that the value and the time derivative of the impulsive part of the disturbance potential $\varphi^{(0)}(t)$ are zero on $z = 0$ as discussed before. Therefore only the memory part of the disturbance potential $\varphi^{(M)}(t)$ contributes to the surface integral over $S_W(t)$.

The second integral in (2.60) is over the entire $z = 0$ plane and its computation by numerical means would be time consuming if computed directly. An efficient way of computing this integral in the time-domain can be derived by taking advantage of the Green function and its analytical representation listed in (2.54) and (2.57). Again, the value and the time derivative of the impulsive part of the disturbance potential $\varphi^{(0)}(t)$ are zero on $z = 0$ and only the memory part of the disturbance potential $\varphi^{(M)}(t)$ contributes to the surface integral.

Substituting (2.52) through (2.57) in the second integral in (2.60) and invoking the definitions of the delta functions:

$$\begin{aligned}\int_{-\infty}^{\infty} dx e^{ix(u_j-\nu_j\cos\beta_j)} &= 2\pi\delta(u_j-\nu_j\cos\beta_j)\\ \int_{-\infty}^{\infty} dy e^{iy(v_j-\nu_j\sin\beta_j)} &= 2\pi\delta(v_j-\nu_j\sin\beta_j)\end{aligned} \tag{2.61}$$

$$\iint_{-\infty}^{\infty} dxdy e^{iu_jx-i\nu_jx\cos\beta_j+iv_jy-i\nu_jy\sin\beta_j} = 4\pi^2\delta(u_j-\nu_j\cos\beta_j)\delta(v_j-\nu_j\sin\beta_j) \tag{2.62}$$

and the relation:

$$\frac{d}{dt}\int_0^t F(\tau)d\tau = F(t) \tag{2.63}$$

The final expression for $\vec{F}_{FS,1-ID}(t)$ can be expressed as:

$$\begin{aligned}&\vec{F}_{FS,1-ID}\\ &= \frac{\rho}{g}\frac{d}{dt}\int_{S_W}\left[\varphi\frac{\partial^2\varphi_I}{\partial x\partial t}-\frac{\partial\varphi}{\partial t}\frac{\partial\varphi_I}{\partial x}\right]ds-\rho\Re\sum_j\left\{A_j\omega_j\cos\beta_j e^{i\omega_jt+i\chi_j}K(\nu_j,\beta_j,t)\right\}\\ &\text{where}\quad K(\nu_j,\beta_j,t)=\int_{S_B}d\xi\sigma(\vec{\xi},t)e^{\nu_j\zeta-i\nu_j\xi\cos\beta_j-i\nu_j\eta\sin\beta_j}\end{aligned} \tag{2.64}$$

For detailed steps on the mathematical derivations please see Appendix A.

For the second term, the DD component in (2.58) contains an integration of a quadratic product of the disturbance potential of the $z = 0$ plane outside the body waterline. The time derivatives maybe transferred under the integral sign by utilizing the Reynolds transport theorem:

$$\begin{aligned}\vec{F}_{FS,1-DD} &= \frac{\rho}{g}\frac{d}{dt}\int\limits_{z=0}\left(\frac{\partial\varphi}{\partial t}\frac{\partial\varphi}{\partial x}\right)ds \\ &= \frac{\rho}{g}\int\limits_{z=0}\frac{d}{dt}\left(\frac{\partial\varphi}{\partial t}\frac{\partial\varphi}{\partial x}\right)ds + \frac{\rho}{g}\oint\limits_{C_W} dl\; U_n\frac{\partial\varphi}{\partial t}\frac{\partial\varphi}{\partial x}\end{aligned} \tag{2.65}$$

The last integral over the body waterline in (2.65) involves the normal oscillatory velocity of the body which is of the same order as the disturbance potential, therefore it is of cubic order and is omitted. Note that for a ship advancing with a significant forward speed, this integral is of the same order as the first term and should be considered when computing free-surface impulse force.

Performing a formal differentiation of the terms under the integral sign in (2.65) gives:

$$\frac{d}{dt}\left(\frac{\partial\varphi}{\partial t}\frac{\partial\varphi}{\partial x}\right) = \frac{\partial^2\varphi}{\partial t^2}\frac{\partial\varphi}{\partial x} + \frac{1}{2}\frac{\partial}{\partial x}\left(\frac{\partial\varphi}{\partial t}\right)^2 \tag{2.66}$$

Upon substitution in (2.65) the DD component of the free-surface impulse force can be expressed as:

$$\vec{F}_{FS,1-DD} = \frac{\rho}{g}\int\limits_{-\infty}^{\infty}dx\int\limits_{-\infty}^{\infty}dy\frac{\partial^2\varphi}{\partial t^2}\frac{\partial\varphi}{\partial x} - \frac{\rho}{g}\int\limits_{S_W}\frac{\partial^2\varphi}{\partial t^2}\frac{\partial\varphi}{\partial x}ds + \frac{\rho}{2g}\oint\limits_{C_W} dl\;\vec{n}_1\left(\frac{\partial\varphi}{\partial t}\right)^2 \tag{2.67}$$

The Stokes' theorem was invoked over the $z = 0$ plane in (2.67) to reduce the integral of the x-derivative in the last term of (2.66) to an integral over the body waterline. The integral of the first term in the right hand side of (2.66) over the body interior waterplane area was also added and subtracted. The second and third term in (2.67) can be evaluated directly using the definition (2.54) of the disturbance potential over the according surface and waterline.

For the evaluation of the infinite integral in (2.67), invoke the free surface condition (2.19) satisfied by the total disturbance potential and introduce the velocity potential decomposition into the instantaneous and memory components:

$$\frac{\partial^2\varphi}{\partial t^2}\frac{\partial\varphi}{\partial x} = -g\frac{\partial\varphi}{\partial z}\frac{\partial\varphi}{\partial x} = -g\frac{\partial\varphi^{(M)}}{\partial z}\frac{\partial\varphi^{(M)}}{\partial x} - g\frac{\partial\varphi^{(0)}}{\partial z}\frac{\partial\varphi^{(M)}}{\partial x},\ z=0 \tag{2.68}$$

(2.68) was obtained by utilizing the property that the value and the x-derivative of the velocity potential component $\varphi^{(0)}$ is zero on the z=0 plane at all times. The infinite integral in (2.67) is therefore:

$$\frac{\rho}{g}\int_{-\infty}^{\infty}dx\int_{-\infty}^{\infty}dy\frac{\partial^2\varphi}{\partial t^2}\frac{\partial\varphi}{\partial x} = \frac{\rho}{g}(-g)\int_{-\infty}^{\infty}dx\int_{-\infty}^{\infty}dy\left(\frac{\partial\varphi^{(M)}}{\partial z}\frac{\partial\varphi^{(M)}}{\partial x} + \frac{\partial\varphi^{(0)}}{\partial z}\frac{\partial\varphi^{(M)}}{\partial x}\right) \tag{2.69}$$

The memory component of the disturbance velocity potential is harmonic in the lower half space for z<0 and it vanishes at infinity. Therefore, by utilizing the familiar vector identity over a closed surface bounded by the $z = 0$ plane and a semi-spherical surface at infinity over which the integrand vanishes:

$$\int_{-\infty}^{\infty}dx\int_{-\infty}^{\infty}dy\Big(\frac{\partial\varphi^{(M)}}{\partial n}\nabla\varphi^{(M)} - \frac{1}{2}\vec{n}\varphi^{(M)}\cdot\varphi^{(M)}\Big) = 0 \tag{2.70}$$

The unit vector $\vec{n}$ points in the vertical direction. The x-component of (2.70) is:

$$\int_{-\infty}^{\infty}dx\int_{-\infty}^{\infty}dy\Big(\frac{\partial\varphi^{(M)}}{\partial n}\frac{\partial\varphi^{(M)}}{\partial x}\Big) = 0 \tag{2.71}$$

Combining (2.69) and (2.71) gives:

$$\frac{\rho}{g}\int_{-\infty}^{\infty}dx\int_{-\infty}^{\infty}dy\frac{\partial^2\varphi}{\partial t^2}\frac{\partial\varphi}{\partial x} = -\rho\int_{-\infty}^{\infty}dx\int_{-\infty}^{\infty}dy\frac{\partial\varphi^{(0)}}{\partial z}\frac{\partial\varphi^{(M)}}{\partial x} \tag{2.72}$$

The Rankine source $1/r$ its image $1/r$ and their Z-derivatives follows the following Fourier representations on the $z = 0$ plane

$$\frac{1}{r} = \frac{1}{2\pi}\iint_{-\infty}^{\infty} du_1 dv_1 e^{-(u_1^2+v_1^2)^{1/2}|z-\zeta_1|+iu_1(x-\xi_1)+iv_1(y-\eta_1)}$$

$$\frac{\partial}{\partial z}\left(\frac{1}{r}\right)_{r=0} = -\frac{\partial}{\partial z}\left(\frac{1}{r'}\right)_{r=0} = -\frac{1}{2\pi}\iint_{-\infty}^{\infty} du_1 dv_1 (u_1^2+v_1^2)^{1/2} e^{(u_1^2+v_1^2)^{1/2}\zeta_1+iu_1(x-\xi_1)+iv_1(y-\eta_1)} \tag{2.73}$$

Note that the infinite integrals over u and v are subjected to a summation series for polychromatic waves. Since the final expression for the DD component does not involve the incident wave velocity potential, the effects of irregular waves are implied to be included when computing source strength σ at any time and thus the summation is skipped for simplicity in this derivation.

Combining (2.73) with the definition of the impulsive velocity potential $\varphi^{(0)}$ in (2.53), the z-derivative of the impulsive potential is:

$$\frac{\partial \varphi^{(0)}}{\partial z}(x,y,0,t) = -\frac{1}{4\pi^2}\iint_{-\infty}^{\infty} du_1 dv_1 (u_1^2+v_1^2)^{1/2} \int_{S_B(t)} d\xi_1 \sigma(\vec{\xi_1},t) e^{(u_1^2+v_1^2)^{1/2}\zeta_1+iu_1(x-\xi_1)+iv_1(y-\eta_1)} \tag{2.74}$$

The first partial x-derivative of the disturbance potential at $z = 0$ is:

$$\frac{\partial \varphi^{(M)}}{\partial x}(x,y,0,t) = -\frac{1}{4\pi^2}\int_0^t d\tau \int_{S_B(\tau)} d\xi_2 \sigma(\vec{\xi_2},\tau) \iint_{-\infty}^{\infty} du_2 dv_2 \; iu_2 e^{k_2\zeta_2}\sqrt{\frac{g}{k_2}}\sin[\sqrt{gk_2}(t-\tau)] e^{iu_2(x-\xi_2)+iv_2(y-\eta_2)} \tag{2.75}$$

Substituting (2.74) and (2.75) into (2.72) and invoking the identity for delta functions again:

$$\iint_{-\infty}^{\infty} dxdy e^{i(u_1+u_2)x+i(v_1+v_2)y} = 4\pi^2\delta(u_1+u_2)\delta(v_1+v_2) \tag{2.76}$$

Using also the properties of the delta function:

$$\iint_{-\infty}^{\infty} du_2 dv_2 F(u_2,v_2)\delta(u_1+u_2)\delta(v_1+v_2) = F(-u_1,-v_1) \tag{2.77}$$

where

$$F(u_2,v_2) = -iu_1\sqrt{\frac{g}{k_1}}\sin[\sqrt{gk_1}(t-\tau)]e^{k_1\zeta_2+iu_1\xi_2+iv_1\eta_2} \tag{2.78}$$

The final expression for the DD component of the free-surface impulse force in surge is:

$$\begin{aligned}\vec{F}_{FS,1-DD} = \rho \int_{S_B(t)} ds_{\xi_1}\sigma(\vec{\xi_1},t)\frac{\partial^2\varphi^{(M)}(\vec{\xi_1},t)}{\partial\xi_1\partial\zeta_1} \\ - \frac{\rho}{g}\int_{S_W}\frac{\partial^2\varphi^{(M)}}{\partial t^2}\frac{\partial\varphi^{(M)}}{\partial x}ds + \frac{\rho}{2g}\oint_{C_W}\left(\frac{\partial\varphi^{(M)}}{\partial t}\right)^2 n_1 dl \\ \text{where}\quad \varphi^{(M)}(\vec{\xi_1},t) = \int_0^t d\tau \int_{S_B(\tau)} ds_{\xi_2}\sigma(\vec{\xi_2},\tau)H_\tau(\vec{\xi_1},\vec{\xi_2},t-\tau)\end{aligned} \tag{2.79}$$

For detailed steps on the mathematical derivations please see Appendix A.

The free-surface RD impulse force and moment is then evaluated using the expression (2.64) and (2.79) and the results are shown in the next chapter.

2.4.2 Free-surface impulse force in Heave

The Z-direction free-surface impulse force in (2.48), like the surge force, can be rewritten into two terms: an ID term which involves cross-products of the incident and disturbance potentials, and a DD term which involves a quadratic product of the disturbance potential:

$$\begin{aligned} \vec{F}_{FS,3} &= \vec{F}_{FS,3-ID} + \vec{F}_{FS,3-DD} \\ \vec{F}_{FS,3-ID} &= \frac{\rho}{g}\frac{d}{dt}\int\limits_{S_I}\left(\frac{\partial\varphi}{\partial t}\frac{\partial\varphi_I}{\partial z}\right)ds \\ \vec{F}_{FS,3-DD} &= \frac{\rho}{g}\frac{d}{dt}\int\limits_{S_I}\left(\frac{\partial\varphi}{\partial t}\frac{\partial\varphi}{\partial z}\right)ds \end{aligned} \tag{2.80}$$

First consider the ID term, applying the linear free-surface condition for both the incident and the disturbance velocity potential:

$$\frac{\partial\varphi_I}{\partial z} = -\frac{1}{g}\frac{\partial^2\varphi_I}{\partial t^2} \tag{2.81}$$

$\vec{F}_{FS,3-ID}(t)$ becomes:

$$\vec{F}_{FS,3-ID} = -\frac{\rho}{g^2}\frac{d}{dt}\int\limits_{S_I}\left(\frac{\partial\varphi}{\partial t}\frac{\partial^2\varphi_I}{\partial t^2}\right)ds \tag{2.82}$$

Similiar to the surge force, the ambient wave free-surface $S_I(t)$ can be rewritten into the difference between the infinte free-surface $S_\infty(t)$ and the ambient wave surface inside of the body $S_W(t)$.

Thus this force expression can then be identified to be an integral over $S_W(t)$ and another over $S_\infty(t)$:

$$\begin{aligned}
\vec{F}_{FS,3-ID} &= \frac{d}{dt}\vec{I}_{FS,3-ID} \\
\vec{I}_{FS,3-ID,S_W} &= \frac{\rho}{g^2}\int\limits_{S_W}\Big(\frac{\partial\varphi}{\partial t}\frac{\partial^2\varphi_I}{\partial t^2}\Big)ds \\
\vec{I}_{FS,3-ID,S_\infty} &= -\frac{\rho}{g^2}\int\limits_{-\infty}^{\infty}\!\!\iint\Big(\frac{\partial\varphi}{\partial t}\frac{\partial^2\varphi_I}{\partial t^2}\Big)dxdy
\end{aligned} \tag{2.83}$$

The first impulse over the finite surface $S_W(t)$ can again be evaluated numerically directly by quadrature and the second integral is evaluated using the Green function and its analytical representation similar to the surge force. Invoking the definitions of delta functions (2.61), the impulse over the infinite surface can be simplified as:

$$\begin{aligned}
&\vec{I}_{FS,3-ID,S_\infty} \\
&\quad = -\rho\Re\Big\{\int\limits_0^t d\tau\sum_j\Big[iA_j\omega_j e^{i\omega_j t+i\chi_j}\cos[\sqrt{g\nu_j}(t-\tau)]K_j(\nu_j,\beta_j,\tau)\Big]\Big\} \\
&\text{where}\quad K_j(\nu_j,\beta_j,\tau) = \int\limits_{S_B(\tau)} d\xi\sigma(\xi,\tau)e^{\nu_j\zeta-i\nu_j\xi\cos\beta_j-i\nu_j\eta\sin\beta_j}
\end{aligned} \tag{2.84}$$

Therefore the ID component of the heave direction free-surface impulse force is:

$$\begin{aligned}
&\vec{F}_{FS,3-ID} \\
&\quad = \frac{\rho}{g^2}\frac{d}{dt}\int\limits_{S_W}\frac{\partial\varphi}{\partial t}\frac{\partial^2\varphi_I}{\partial t^2}ds \\
&\quad\quad - \rho\frac{d}{dt}\int\limits_0^t d\tau\Re\Big\{\sum_j\Big[iA_j\omega_j e^{i\omega_j t+i\chi_j}\cos[\sqrt{g\nu_j}(t-\tau)]K_j(\nu_j,\beta_j,\tau)\Big]\Big\}
\end{aligned} \tag{2.85}$$

For detailed mathematical derivations please see Appendix B.

The second part DD, transforming the equation with the linear FSC (2.81) and rewriting the integral over the ambient wave free-surface $S_I(t)$ into the difference between the infinte free-surface $S_\infty(t)$ and the ambient wave surface inside of the body $S_W(t)$:

$$\begin{aligned}\vec{F}_{FS,3-DD} &= \frac{\rho}{g}\frac{d}{dt}\int\limits_{S_I}\left(\frac{\partial\varphi}{\partial t}\frac{\partial\varphi}{\partial z}\right)ds \\ &= \frac{d}{dt}\left\{\frac{\rho}{g^2}\int\limits_{S_W}\frac{\partial\varphi}{\partial t}\frac{\partial^2\varphi}{\partial t^2}ds + \frac{\rho}{g}\int\limits_{S_\infty}\frac{\partial\varphi}{\partial t}\frac{\partial\varphi}{\partial z}ds\right\}\end{aligned} \tag{2.86}$$

The first integral over the finite surface $S_W(t)$ can be evaluated by quadrature using the expression of the disturbance potential obtained by solving the integral equations on the surface as described in Section 2.2. For the second integral over the infinite free-surface $S_\infty(t)$, seperate the derivative inside the integral over S_∞ into two parts by eliminating $\varphi^{(0)}(t)$ and its derivative on $z = 0$ as their values are zero as discussed in (2.53) and (2.54):

$$\frac{\partial\varphi}{\partial t}\frac{\partial\varphi}{\partial z} = \frac{\partial\varphi^{(M)}}{\partial t}\frac{\partial\varphi^{(0)}}{\partial z} + \frac{\partial\varphi^{(M)}}{\partial t}\frac{\partial\varphi^{(M)}}{\partial z} \tag{2.87}$$

Assuming small wave steepness, the integral over S_∞ can be evaluated on $z = 0$. Transforming the z derivative of the impulsive potential to a time derivative using the linear FSC:

$$\frac{\partial\varphi^{(M)}}{\partial t}\frac{\partial\varphi^{(0)}}{\partial z} = -\frac{1}{g}\frac{\partial\varphi^{(M)}}{\partial t}\frac{\partial^2\varphi^{(0)}}{\partial t^2} \tag{2.88}$$

Recalling that the time partial derivative of impulsive part of the wave potential $\frac{\partial}{\partial t}\varphi^{(0)}(t)$ is zero, the second integral of 2.86 is now reduced to:

$$\vec{I}_{FS,3-DD,S_\infty} = \frac{\rho}{g}\int_{S_\infty}\frac{\partial\varphi^{(M)}}{\partial t}\frac{\partial\varphi^{(M)}}{\partial z}ds = \frac{\rho}{g}\iint\limits_{-\infty}^{\infty}\left(\frac{\partial\varphi^{(M)}}{\partial t}\frac{\partial\varphi^{(M)}}{\partial z}\right)dxdy \tag{2.89}$$

The spatial and temporal derivative of the memory potentials can be found by taking the partial derivative of the disturbance potential in (2.54).

By substituting the expressions for the spatial and temporal derivative of the memory potentials into (2.89) and applying definitions of the delta function again, the impulse over the surface integral on $z = 0$ becomes:

$$\begin{aligned}
&\vec{I}_{FS,3-DD,S_\infty} \\
&= \frac{\rho}{4\pi^2} \int_0^t d\tau_1 \int_{S_B(\tau_1)} ds_{\xi_1} \sigma(\vec{\xi_1}, \tau_1) \int_0^t d\tau_2 \int_{S_B(\tau_2)} ds_{\xi_2} \sigma(\vec{\xi_2}, \tau_2) \\
&\quad \times \int_{-\pi}^{\pi} d\theta \int_0^\infty k dk \ \sqrt{gk} e^{k(\zeta_1+\zeta_2)} \cos[\sqrt{gk}(t-\tau_1)] \sin(\sqrt{gk}(t-\tau_2)) e^{ikR\cos\theta}
\end{aligned} \tag{2.90}$$

Using trigonometric identities:

$$\cos[\sqrt{gk}(t-\tau_1)] \sin(\sqrt{gk}(t-\tau_2)) = \frac{1}{2}\Big\{ \sin(\sqrt{gk}(\tau_1-\tau_2)) + \sin[\sqrt{gk}(2t-(\tau_1+\tau_2))] \Big\} \tag{2.91}$$

(2.90) can then be rewritten as:

$$\begin{aligned}
&\vec{I}_{FS,3-DD,S_\infty} \\
&= -\frac{\rho}{2} \int_0^t d\tau_1 \int_{S_B(\tau_1)} ds_{\xi_1} \sigma(\vec{\xi_1}, \tau_1) \int_0^t d\tau_2 \int_{S_B(\tau_2)} ds_{\xi_2} \sigma(\vec{\xi_2}, \tau_2) \\
&\quad \times \frac{\partial}{\partial \zeta_1} \Big[H_\tau(\vec{\xi_1}, \vec{\xi_2}, \tau_1 - \tau_2) + H_\tau(\vec{\xi_1}, \vec{\xi_2}, 2t - (\tau_1+\tau_2)) \Big] \\
&\quad \text{where} \quad H_\tau(\vec{\xi_1}, \vec{\xi_2}, T) \\
&\qquad = -\frac{1}{4\pi^2} \int_{-\pi}^{\pi} d\theta \int_0^\infty dk \ \sqrt{gk} e^{k(\zeta_1+\zeta_2)} sin[\sqrt{gk}T] e^{ikR\cos\theta}
\end{aligned} \tag{2.92}$$

The final expression of the DD component of the heave free-surface impulse force is then:

$$\begin{aligned}
&\vec{F}_{FS,3-DD} \\
&\quad = \frac{d}{dt}\Bigg\{ \frac{\rho}{g^2} \int\limits_{S_W} \frac{\partial \varphi}{\partial t} \frac{\partial^2 \varphi}{\partial t^2} ds \\
&\qquad - \frac{\rho}{2} \int\limits_0^t d\tau_1 \int_{S_B(\tau_1)} ds_{\xi_1} \sigma(\vec{\xi}_1, \tau_1) \int\limits_0^t d\tau_2 \int_{S_B(\tau_2)} ds_{\xi_2} \sigma(\vec{\xi}_2, \tau_2) \\
&\qquad\quad \times \frac{\partial}{\partial \zeta_1} \Big[H_\tau(\vec{\xi}_1, \vec{\xi}_2, \tau_1 - \tau_2) + H_\tau(\vec{\xi}_1, \vec{\xi}_2, 2t - (\tau_1 + \tau_2)) \Big] \Bigg\}
\end{aligned} \tag{2.93}$$

For detailed mathematical derivations please see Appendix B.

2.4.3 Free-surface impulse force in Pitch

Following the derivation in (2.51), the pitch moment can be split into:

$$\begin{aligned}
\vec{M}_{FS,5} &= \vec{M}_{FS,5-ID} + \vec{M}_{FS,5-DD} \\
\vec{M}_{FS,5-ID} &= \frac{\rho}{g^2}\frac{d}{dt}\int\limits_{S_I}\left(x\frac{\partial\varphi}{\partial t}\frac{\partial^2\varphi_I}{\partial t^2}\right)ds \\
\vec{M}_{FS,5-DD} &= \frac{\rho}{g^2}\frac{d}{dt}\int\limits_{S_I}\left(x\frac{\partial\varphi}{\partial t}\frac{\partial^2\varphi}{\partial t^2}\right)ds
\end{aligned} \tag{2.94}$$

Similiar to surge and heave free-surface impulse force, rewriting again the free-surface integral as the difference between the impulse over the infinite free-surface and the ambient free-surface inside of the body, the ID component is:

$$\vec{M}_{FS,5-ID} = \frac{\rho}{g^2}\frac{d}{dt}\left(\int\limits_{S_\infty} - \int\limits_{S_W}\right)\left(x\frac{\partial\varphi}{\partial t}\frac{\partial^2\varphi_I}{\partial t^2}\right)ds \tag{2.95}$$

The ID impulse in (2.95) can be then be expressed as the sum of two impulses:

$$\begin{aligned}
\vec{M}_{FS,5-ID} &= \frac{d}{dt}\left(\vec{I}_{FS,5-ID,S_W} + \vec{I}_{FS,5-ID,S_\infty}\right); \\
\vec{I}_{FS,5-ID,S_W} &= -\frac{\rho}{g^2}\int\limits_{S_W}\left(x\frac{\partial\varphi}{\partial t}\frac{\partial^2\varphi_I}{\partial t^2}\right)ds \\
\vec{I}_{FS,5-ID,S_\infty} &= \frac{\rho}{g^2}\int\limits_{-\infty}^{\infty}\int\left(x\frac{\partial\varphi}{\partial t}\frac{\partial^2\varphi_I}{\partial t^2}\right)dxdy
\end{aligned} \tag{2.96}$$

Consider the second part of ID impulse over the infinte free-surface in (2.96). Substituting the partial derivatives of the definition of the impulsive and memory potential in (2.52) and (2.53):

$$\vec{I}_{FS,5-ID,S_\infty} = \frac{\rho}{g}\Big(-\frac{1}{4\pi^2}\Big)\Re\Bigg\{\int_0^t d\tau \int_{S_B(\tau)} ds_\xi \sigma(\vec{\xi},\tau)(-igA\omega)e^{i\omega t} \times \int_{-\infty}^{\infty}\int dudv\Big[e^{(u^2+v^2)^{(1/2)}\zeta}\cos[g^{(1/2)}(u^2+v^2)^{(1/4)}(t-\tau)]e^{-iu\xi-iv\eta}\Big] \times \int_{-\infty}^{\infty}\int dxdy\Big[xe^{ix(u-\nu\cos\beta)+iv(y-\nu\sin\beta)}\Big]\Bigg\} \tag{2.97}$$

Let

$$f(u,v) = e^{(u^2+v^2)^{(1/2)}\zeta}\cos[g^{(1/2)}(u^2+v^2)^{(1/4)}(t-\tau)]e^{-iu\xi-iv\eta} \tag{2.98}$$

Applying the definition of the delta functions:

$$\begin{aligned}\int_{-\infty}^{\infty} dx\; xe^{ix(u-\nu\cos\beta)} &= -2\pi i\delta'(u-\nu\cos\beta)\\ \int_{-\infty}^{\infty} dy\; e^{iy(v-\nu\sin\beta)} &= 2\pi\delta(v-\nu\sin\beta)\end{aligned} \tag{2.99}$$

(2.97) becomes:

$$\vec{I}_{FS,5-ID,S_\infty} = \frac{\rho}{g}\Big(\frac{1}{4\pi^2}\Big)\Re\Bigg\{\int_0^t d\tau \int_{S_B(\tau)} ds_\xi \sigma(\vec{\xi},\tau)(igA\omega)e^{i\omega t} \times (-4\pi^2 i)\int_{-\infty}^{\infty}\int dudv f(u,v)\delta'(u-\nu\cos\beta)\delta(v-\nu\sin\beta)\Bigg\} \tag{2.100}$$

Utilizing again property of delta functions:

$$\int_{-\infty}^{\infty}\int dudvf(u,v)\delta'(u-\nu\cos\beta)\delta(v-\nu\sin\beta) = -f'(\nu\cos\beta,\nu\sin\beta) \tag{2.101}$$

Thus the impulse over $S_\infty(t)$ is:

$$\vec{I}_{FS,5-ID,S_\infty} = \rho A\omega\Re\left\{e^{i\omega t}\int_0^t d\tau\int_{S_B(\tau)} ds_\xi\sigma(\vec{\xi},\tau)\Big[-f'(\nu\cos\beta,\nu\sin\beta)\Big]\right\} \tag{2.102}$$

The free-surface pitch ID moment is then:

$$\begin{aligned}\vec{M}_{FS,5-ID} &= -\frac{\rho}{g^2}\frac{d}{dt}\int_{S_W}\left(x\frac{\partial\varphi}{\partial t}\frac{\partial^2\varphi_I}{\partial t^2}\right)ds \\ &+ \rho A\omega\Re\left\{e^{i\omega t}\int_0^t d\tau\int_{S_B(\tau)} ds_\xi\sigma(\vec{\xi},\tau)\Big[Q_1+Q_2+Q_3\Big]e^{\nu\zeta-i\nu\xi\cos\beta-i\nu\eta\sin\beta}\right\}\end{aligned} \tag{2.103}$$

where

$$Q_1 = -\zeta\cos\beta\cos[\sqrt{g\nu}(t-\tau)];$$

$$Q_2 = \frac{1}{2}\sqrt{\frac{g}{\nu}}\cos\beta(t-\tau)\sin[\sqrt{g\nu}(t-\tau)];$$

$$Q_3 = i\xi\cos[\sqrt{g\nu}(t-\tau)].$$

For detailed steps on the mathematical derivations please see Appendix C.

The second part of the free-surface pitch moment is the DD component in (2.94). Similiar to the heave forec, rewriting the integral over the ambient wave free-surface $S_I(t)$ into the difference between the infinte free-surface $S_\infty(t)$ and the ambient wave surface inside of the body $S_W(t)$:

$$\begin{aligned}\vec{M}_{FS,5-DD} &= -\frac{\rho}{g}\frac{d}{dt}\int_{S_I}\left(x\frac{\partial\varphi}{\partial t}\frac{\partial\varphi}{\partial z}\right)ds \\ &= \frac{d}{dt}\left\{-\frac{\rho}{g^2}\int_{S_W} x\frac{\partial\varphi}{\partial t}\frac{\partial^2\varphi}{\partial t^2}ds - \frac{\rho}{g}\int_{S_\infty} x\frac{\partial\varphi}{\partial t}\frac{\partial\varphi}{\partial z}ds\right\}\end{aligned} \tag{2.104}$$

Recalling again $\partial\varphi^{(0)}/\partial t = 0$, the impulse of the DD component is then:

$$\vec{I}_{FS,5-DD} = -\frac{\rho}{g}\int_{S_\infty} x\frac{\partial\varphi^{(M)}}{\partial t}\frac{\partial\varphi^{(M)}}{\partial z}ds = -\frac{\rho}{g}\iint_{-\infty}^{\infty}\Big(x\frac{\partial\varphi^{(M)}}{\partial t}\frac{\partial\varphi^{(M)}}{\partial z}\Big)dxdy \tag{2.105}$$

Substituting the partial derivatives of 2.54 into the impulse:

$$\begin{aligned}
&-\frac{\rho}{g}\int_{S_\infty} x\frac{\partial\varphi^{(M)}}{\partial t}\frac{\partial\varphi^{(M)}}{\partial z}ds \\
&= -\rho\Big(-\frac{1}{4\pi^2}\Big)^2\int_0^t d\tau_1\int_{S_B(\tau_1)} ds_{\xi_1}\sigma(\vec{\xi}_1,\tau_1)\int_0^t d\tau_2\int_{S_B(\tau_2)} ds_{\xi_2}\sigma(\vec{\xi}_2,\tau_2) \\
&\quad\times\iint_{-\infty}^{\infty} du_1dv_1\ F_1(u_1,v_1)\iint_{-\infty}^{\infty} du_2dv_2\ F_2(u_2,v_2) \\
&\quad\times\iint_{-\infty}^{\infty} dxdy\ xe^{i(u_1+u_2)x+i(v_1+v_2)y}
\end{aligned} \tag{2.106}$$

where:

$$\begin{aligned}
F_1(u_1,v_1) &= e^{(u_1^2+v_1^2)^{(1/2)}\zeta_1}\cos[g^{(1/2)}(u_1^2+v_1^2)^{(1/4)}(t-\tau_1)]e^{-iu_1\xi_1-iv_1\eta_1} \\
F_2(u_2,v_2) &= e^{(u_2^2+v_2^2)^{(1/2)}\zeta_2}g^{(1/2)}(u_2^2+v_2^2)^{(1/4)}\sin[(g^{(1/2)}(u_2^2+v_2^2)^{(1/4)}(t-\tau_2))]e^{-iu_2\xi_2-iv_2\eta_2}
\end{aligned} \tag{2.107}$$

Invoking the identity:

$$\int_{-\infty}^{\infty} dx\int_{-\infty}^{\infty} dy\ xe^{i(u_1+u_2)x+i(v_1+v_2)y} = -4\pi^2 i\delta'(u_1+u_2)\delta(v_1+v_2) \tag{2.108}$$

Using also the properties of the delta function:

$$\iint_{-\infty}^{\infty} du_1dv_1F_1(u_1,v_1)\delta'(u_1+u_2)\delta(v_1+v_2) = -F_1'(-u_2,-v_2) \tag{2.109}$$

The impulse can then be expressed as:

$$
\begin{aligned}
&-\frac{\rho}{g}\int_{S_\infty} x\frac{\partial\varphi^{(M)}}{\partial t}\frac{\partial\varphi^{(M)}}{\partial z}ds \\
&=-\rho\Big(\frac{1}{4\pi^2}\Big)^2(-4\pi^2 i)\int_0^t d\tau_1 \int\limits_{S_B(\tau_1)} ds_{\xi_1}\sigma(\vec{\xi}_1,\tau_1)\int_0^t d\tau_2 \int\limits_{S_B(\tau_2)} ds_{\xi_2}\sigma(\vec{\xi}_2,\tau_2) \\
&\quad\times\iint_{-\infty}^{\infty} du_2dv_2\ F_2(u_2,v_2)\Big(-F_1'(-u_2,-v_2)\Big)
\end{aligned}
\tag{2.110}
$$

The impulse is then:

$$
\begin{aligned}
&-\frac{\rho}{g}\int_{S_\infty} x\frac{\partial\varphi^{(M)}}{\partial t}\frac{\partial\varphi^{(M)}}{\partial z}ds \\
&=\rho\int_0^t d\tau_1 \int\limits_{S_B(\tau_1)} ds_{\xi_1}\sigma(\vec{\xi}_1,\tau_1)\int_0^t d\tau_2 \int\limits_{S_B(\tau_2)} ds_{\xi_2}\sigma(\vec{\xi}_2,\tau_2) \\
&\quad\times\Bigg\{-\frac{\zeta_1}{2}\frac{\partial}{\partial\xi_1}\Big[H_\tau(\vec{\xi}_1,\vec{\xi}_2,\tau_1-\tau_2)+H_\tau(\vec{\xi}_1,\vec{\xi}_2,2t-(\tau_1+\tau_2))\Big] \\
&\qquad+\frac{(t-\tau_1)}{2k}\int d\zeta_1\frac{\partial}{\partial\xi_1}\frac{\partial}{\partial\tau_2}\Big[H_\tau(\vec{\xi}_1,\vec{\xi}_2,\tau_1-\tau_2)+H_\tau(\vec{\xi}_1,\vec{\xi}_2,2t-(\tau_1+\tau_2))\Big] \\
&\qquad+\frac{\xi_1}{2}\frac{\partial}{\partial\zeta_1}\Big[H_\tau(\vec{\xi}_1,\vec{\xi}_2,\tau_1-\tau_2)+H_\tau(\vec{\xi}_1,\vec{\xi}_2,2t-(\tau_1+\tau_2))\Big]\Bigg\}
\end{aligned}
\tag{2.111}
$$

where $H_\tau(\vec{\xi}_1,\vec{\xi}_2,T)$

$$
=-\frac{1}{4\pi^2}\int_{-\pi}^{\pi}d\theta\int_0^\infty dk\ \sqrt{gk}e^{k(\zeta_1+\zeta_2)}sin[\sqrt{gk}T]e^{ikR\cos\theta}
$$

The DD free-surface pitch moment is then:

$$
\begin{aligned}
\vec{M}_{FS,5-DD} = \frac{d}{dt}\Bigg\{ & -\frac{\rho}{g^2}\int\limits_{S_W} x\frac{\partial\varphi}{\partial t}\frac{\partial^2\varphi}{\partial t^2}ds \\
& + \rho\int\limits_0^t d\tau_1 \int\limits_{S_B(\tau_1)} ds_{\xi_1}\sigma(\vec{\xi_1},\tau_1)\int\limits_0^t d\tau_2 \int\limits_{S_B(\tau_2)} ds_{\xi_2}\sigma(\vec{\xi_2},\tau_2) \\
& \times\Bigg\{ -\frac{\zeta_1}{2}\frac{\partial}{\partial\xi_1}\Big[H_\tau(\vec{\xi_1},\vec{\xi_2},\tau_1-\tau_2)+H_\tau(\vec{\xi_1},\vec{\xi_2},2t-(\tau_1+\tau_2))\Big] \\
& + \frac{(t-\tau_1)}{2k}\int d\zeta_1\frac{\partial}{\partial\xi_1}\frac{\partial}{\partial\tau_2}\Big[H_\tau(\vec{\xi_1},\vec{\xi_2},\tau_1-\tau_2)+H_\tau(\vec{\xi_1},\vec{\xi_2},2t-(\tau_1+\tau_2))\Big] \\
& + \frac{\xi_1}{2}\frac{\partial}{\partial\zeta_1}\Big[H_\tau(\vec{\xi_1},\vec{\xi_2},\tau_1-\tau_2)+H_\tau(\vec{\xi_1},\vec{\xi_2},2t-(\tau_1+\tau_2))\Big]\Bigg\}\Bigg\}
\end{aligned}
\tag{2.112}
$$

For detailed steps on the mathematical derivations please see Appendix C.

2.5 Nonlinear loads on a vertical cylinder in irregular waves of small Ka

This section discuss the method presented by Sclavounos [31] on computing nonlinear surge force acting on a vertical circular cylinder in irregular waves.

For a vertical cylinder fixed in space (a diffraction problem), the Fluid-Impulse Theory can be used to approximate nonlinear loads to leading order by the 2D croos-flow potential.

The ambient waves are assumed to be irregular. The expressions presented in this section are valid for small values of Ka, where K is a characteristic wavenumber and a is the cylinder radius.

The characteristic wavelegnth in a seastate is often large relative to the cylinder diameters of offshore structures and wind turbines. In such cases Ka is a small parameter and the diffraction potential near the cylinder may be approximated to leading order by the 2D cross-flow potential:

$$\varphi(r,\theta) = -u_1 \frac{a}{r}\cos\theta, \quad u_1 = \frac{\partial \varphi_I}{\partial x}(r=0) \tag{2.113}$$

Recalling the incident wave velocity potential in irregular waves in deep water as:

$$\text{(polychromatic)} \quad \varphi_I(x,y,z,t) = \Re\left\{ \sum_j \frac{igA_j}{\omega_j} e^{\nu_j z - i\nu_j x\cos\beta_j - i\nu_j y\sin\beta_j + i\omega_j t + i\chi_j} \right\} \tag{2.114}$$

In uni-directional waves:

$$u_1 = \frac{\partial \varphi_I}{\partial x}(r=0) = \Re\left\{ \sum_j A_j\omega_j e^{\nu_j z + i\omega_j t + i\chi_j} \right\} \tag{2.115}$$

And $\dot{u}_1(z)|_{x=0}$ as:

$$\dot{u}_1(z)|_{x=0} = \Re\left\{ \sum_j iA_j\omega_j^2 e^{\nu_j z + i\omega_j t + i\chi_j} \right\} \tag{2.116}$$

Substituting (2.113) into F-K and RD disturbance body force, the expressions become equal in the limit of small Ka and their sum is:

$$F_{X,F-K} + F_{X,D} = 2\rho\pi a^2 \int_{-T}^{\zeta_I} dz \dot{u}_1(z)|_{x=0} + 2\rho\pi a^2 \frac{\partial \zeta_I}{\partial t}\Big|_{x=0} u_1|_{x=0,z=\zeta_I} \tag{2.117}$$

For the free-surface impulse force, introduce (2.113) into (2.58), the DD term vanishs identically. The ID component is then the leading order force. The force expression therefore becomes:

$$F_{X,FS} = 2\rho\pi a^2 \int_{-T}^{\zeta_I} dz(u_1 u_{1x} + u_3 u_{1z}) - \rho\pi a^2 u_1 u_3|_{x=0,z=\zeta_I}; \quad u_3 = \frac{\partial \zeta_I}{\partial t} + u_1 \frac{\partial \zeta_I}{\partial x}; \tag{2.118}$$

where at $x = 0$ and in unidirectional waves:

$$\begin{aligned} u_{1x} &= \Re\left\{ \sum_j \frac{-iA_j\nu_j^3}{g} e^{\nu_j z + i\omega_j t + i\chi_j} \right\} \\ u_{1z} &= \Re\left\{ \sum_j \frac{A_j\nu_j^3}{g} e^{\nu_j z + i\omega_j t + i\chi_j} \right\} \end{aligned} \tag{2.119}$$

and

$$\begin{aligned} \frac{\partial \zeta_I}{\partial t} &= \Re\left\{ \sum_j iA_j\omega_j e^{i\omega_j t + i\chi_j} \right\} \\ \frac{\partial \zeta_I}{\partial x} &= \Re\left\{ \sum_j -iA_j\nu_j e^{i\omega_j t + i\chi_j} \right\} \end{aligned} \tag{2.120}$$

By applying the small Ka approximation, the full FIT expression which can compute nonlinear loads for finite Ka was reduced from 2D surface integrals to a 1D integral for numerical evaluation of nonlinear wave loads. This drastically reduces computational resources and provide an efficient method for the computation of nonlinear wave loads for slender vertical cylinders in the ocean.

Chapter 3

Numerical Analysis and Results

This chapter discusses the methods used in numerical analysis and results obtained using FIT with its theory described in Chapter 2. The results in this chapter aims to verify the accuracy of FIT and study its efficiency and effectiveness in computing nonlinear wave effects.

Numerically, the Fluid-Impulse Theory offers the advantage of only requiring the discretization of the instantaneous body surface $S_B(t)$ and the ambient wave surface inside of the body $S_W(t)$ for the computation of linear and nonlinear force and moment in all directions. The forces and moments in the formulation of FIT were described by a summation of several time derivatives of impulses over these surfaces. Therefore when computing force and moment using FIT, only these two surfaces needed to be discretized. This allows FIT to compute nonlinear wave loads efficiently. It is also a versatile method, as the FIT is not limited by the small wave amplitude, small wave steepness, or long wavelength assumption.

This chapter is structured as follow: First, Section 3.1 describe the application of the perturbation theory to simplify the fully nonlinear FIT formulation into linear and leading order nonlinear effects for numerical computation; Section 3.2 then describes the treatment of body meshes in discrete formulations; Section 3.3 further explains the application of quadrilateral constant-strength source elements on body

surfaces for numerical computation; After reviewing discrete formulations and application of appropriate numerical methods, Section 3.4 presents a verification study between linear FIT and frequency-domain method WAMIT, and a comparison between the computation of surge 2nd order quadratic hydrodynamic force between FIT and WAMIT; Convergence studies on different perimeters when computing 2nd order quadratic solutions from FIT is presented in Section 3.5, and a mesh convergence study is also presented between FIT and WAMIT in Section 3.6; To further study FIT numerically, computation results for buoys of different sizes are then presented in Section 3.7; Finally, a numerical study on the simplified FIT formulation using the small Ka approximation is presented in Section 3.8.

3.1 Perturbation Theory

Recalling the force formulation of FIT in Chapter 2:

$$\vec{F} = \vec{F}_H + \vec{F}_{F-K} + \vec{F}_D + \vec{F}_{FS} \tag{3.1}$$

By assuming a small steepness for the ambient surface wave, which is a reasonable assumption due to the high gravitational force, the following perturbation expansion for the velocity potential and free-surface elevation can be assumed as

$$\begin{aligned} \varphi_I &= \varphi_I^{(1)} + \varphi_I^{(2)} + \varphi_I^{(3)} + ... \\ \varphi &= \varphi^{(1)} + \varphi^{(2)} + \varphi^{(3)} + ... \\ \zeta_I &= \zeta_I^{(1)} + \zeta_I^{(2)} + \zeta_I^{(3)} + ... \end{aligned} \tag{3.2}$$

For the inclusion of only first order potentials, the formulation of FIT can be seperated into 1st order and 2nd order force and moments. In the surge direction, by applying the perturbation theory in (3.1), 1st order body forces includes only Froude-Krylov impulse force and RD body impulse force over the mean body surface $\bar{S}_B$:

$$\vec{F}_1^{(1)} = \vec{F}_{F-K,1}^{(1)} + \vec{F}_{D,1}^{(1)} = -\rho \frac{d}{dt} \int_{\bar{S}_B} \varphi_I^{(1)} \vec{n}_1 ds - \rho \frac{d}{dt} \int_{\bar{S}_B} \varphi^{(1)} \vec{n}_1 ds \tag{3.3}$$

Using the Taylor-series expansion, 2nd order forces includes components from Froude-Krylov, RD body over the differential surface $\triangle S$ and linearized ambient wave free-surface inside of the body $S_W(t)$, as depicted in Figure 3-1, as well as free-surface forces described in section 2.4:

$$\vec{F}_1^{(2)} = \vec{F}_{F-K,1}^{(2)} + \vec{F}_{B,1}^{(2)} + \vec{F}_{FS,1}^{(2)};$$

$$\vec{F}_{F-K,1}^{(2)} + \vec{F}_{B,1}^{(2)}$$

$$= -\rho\frac{d}{dt}\oint_{C_W} \zeta_I^{(1)}\varphi_I^{(1)}\vec{n}_1 dl - \rho\frac{d}{dt}\int_{\bar{S}_W} \varphi_I^{(1)}|_{z=0}\frac{\partial\zeta_I^{(1)}}{\partial x}ds - \rho\frac{d}{dt}\oint_{C_W} \zeta_I^{(1)}\varphi^{(1)}\vec{n}_1 dl \quad (3.4)$$

$$\vec{F}_{FS,1}^{(2)} = \vec{F}_{FS,1-ID}^{(2)} + \vec{F}_{FS,1-DD}^{(2)}$$

with both ID and DD component evaluated with $\varphi_I^{(1)}$ and $\varphi^{(1)}$.

The heave force and pitch moment follow the same derivation.

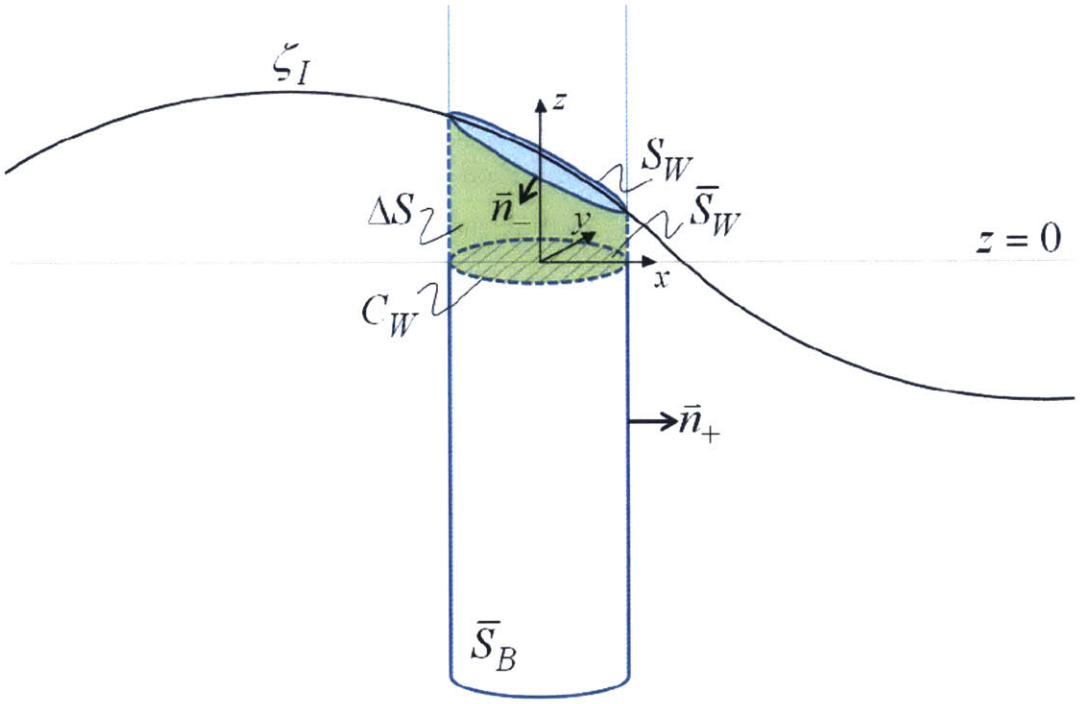

Figure 3-1: Surfaces and vectors included in numerical analysis using FIT

3.2 Treatment of surfaces and Generation of body Mesh

In FIT, the body boundary condition is imposed on field points on the exact body surface, which is often referred to as collocation points. For a vertical cylinder, these points locate on the vertical wall as well as the bottom surface. An accurate evaluation of influence coefficients between source points and field points is required to determine strengths of source panel-elements upon the body boundary condition. The evaluation of influence coefficient becomes tricky when the field point is in the proximity of or identical with the source point. To prevent a singularity in the numerical computation, a source point is designed to be located a little off a field point as illustrated in the figure below for the vertical wall of the cylinder. The source point on the bottom surface is simply located at a vertical depth with a slight smaller draft than the full draft. This method enhances the computational stability and provides an accurate solution.

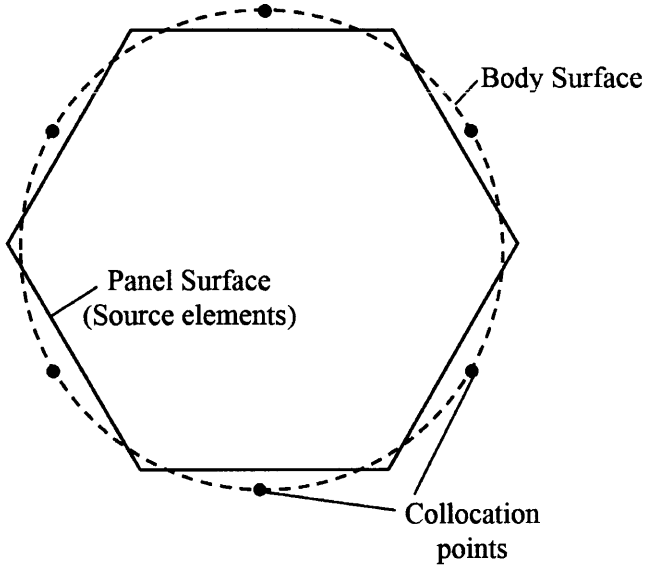

Figure 3-2: Top view of a cylindrical body and numerical panel elements surrounding the body surface (Simplified in terms of the number of panel elements)

Several body sizes were studied in this work, the MIT/NREL TLP body was studied with three mesh density for initial convergence studies, presented in Subsection

3.5.3, while two slenderer bodies were computed with converged meshes generated with the knowledge of mesh convergence on the MIT/NREL TLP. The cylindrical MIT/NREL TLP buoy with a radius of 9 m and a draft of 47.89 m was represented by a body mesh of 720 panels, with 24 azimuthal, 41 vertical, and 9 bottom panels (Fig. 3-3); 1440 panels, with 36 azimuthal, 31 vertical, and 9 bottom panels (Fig. 3-4); and 2,400 panels, with 48 azimuthal, 41 vertical, and 9 bottom panels (Fig. 3-5). The ambient wave free-surface inside of the body $\bar{S}_W$ use the same mesh as the bottom surface but located at $z = 0$. The two slenderer cylinders are of radius 3m and 1.75m, with a 43.2m draft and a 30m draft respectively. The buoy with 3m radius was represented by a body mesh of 936 panels, with 18 azimuthal, 42 vertical, and 9 bottom panels (Fig. 3-6), while the buoy with 1.75m radius was represented by a body mesh of 684 panels, with 18 azimuthal, 30 vertical, and 9 bottom panels (Fig. 3-7).

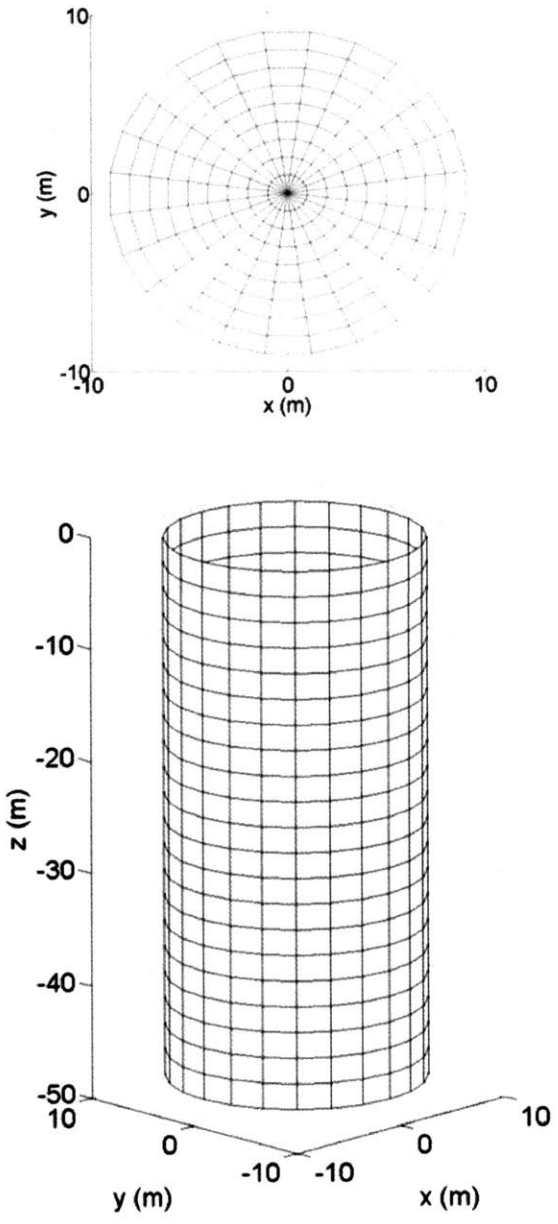

Figure 3-3: Body mesh with 720 panels for MIT/NREL TLP, r=9m, T=47.89m

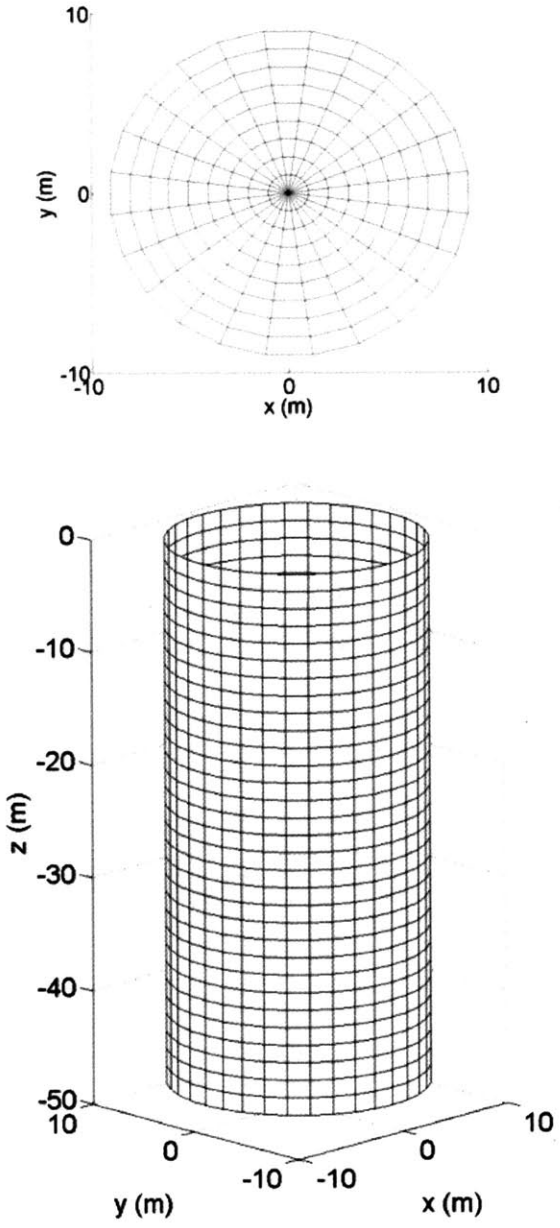

Figure 3-4: Body mesh with 1440 panels for MIT/NREL TLP, r=9m, T=47.89m

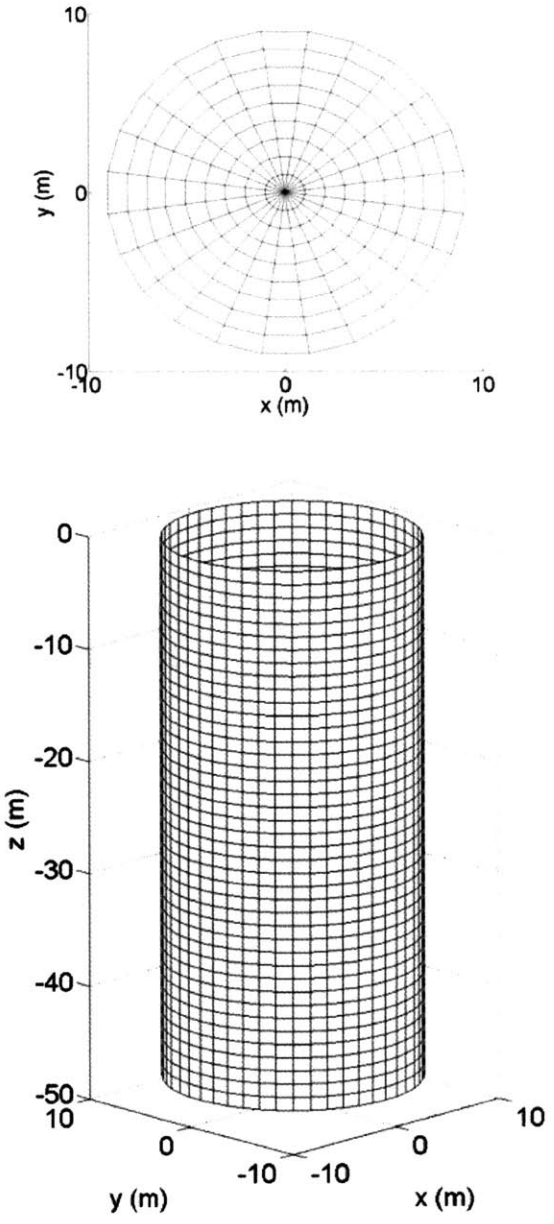

Figure 3-5: Body mesh with 2400 panels for MIT/NREL TLP, r=9m, T=47.89m

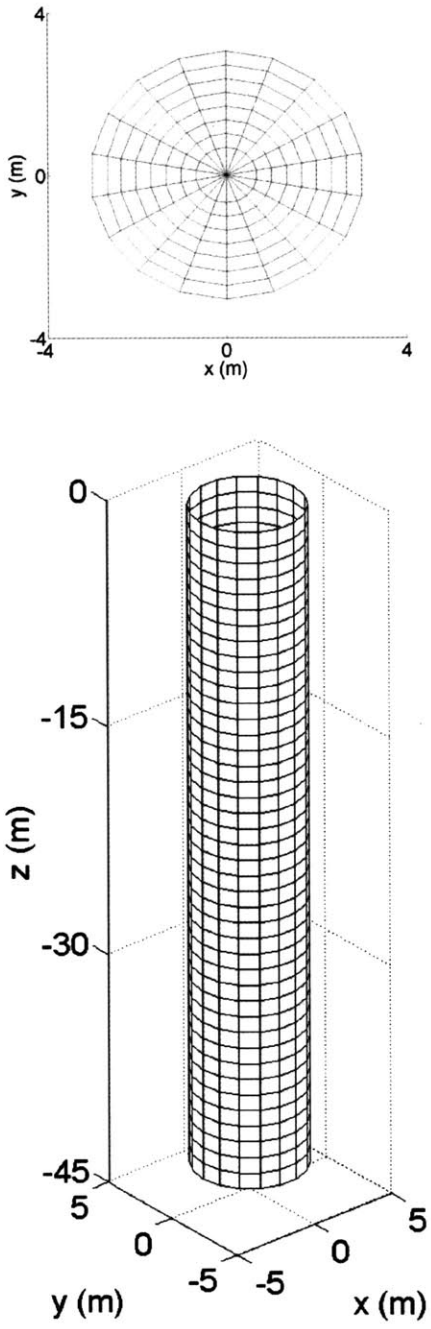

Figure 3-6: Body mesh with 936 panels, r=3m, T=43.2m

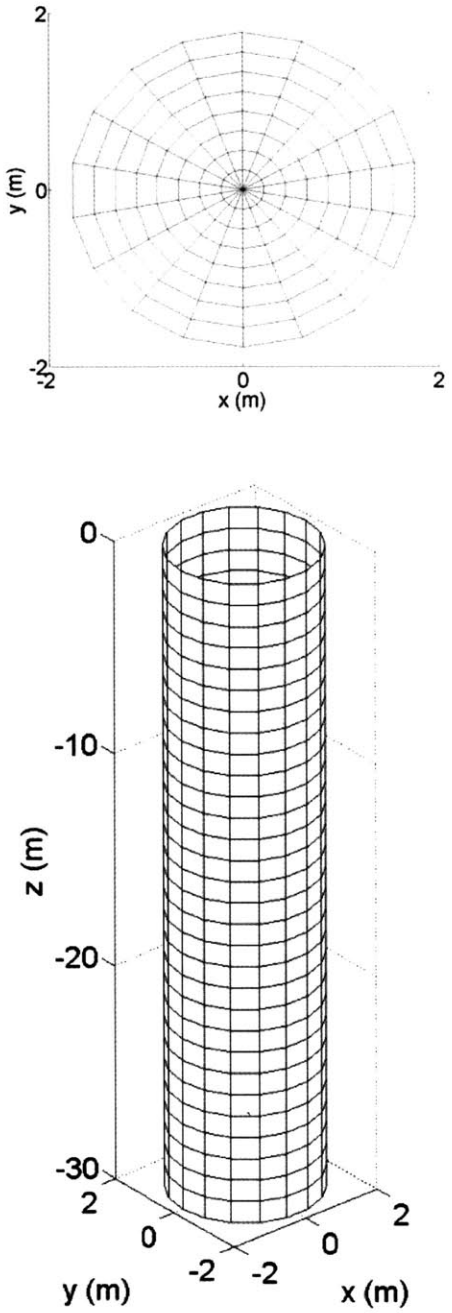

Figure 3-7: Body mesh with 684 panels, r=1.75m, T=30m

3.3 A Quadrilateral Constant-Strength Source Panel Element

A quadrilateral constant-strength source element is presently taken as the 3D Panel element to represent the floating body boundary in order to model its hydrodynamic interaction with surface waves. At each quadrilateral element the singularity strength is uniformly distributed over each element. The strength of this element is the primary unknown and a panel code using N elements can be constructed to solve for those N constants based on the body boundary condition presented in the previous and subsequent chapters.

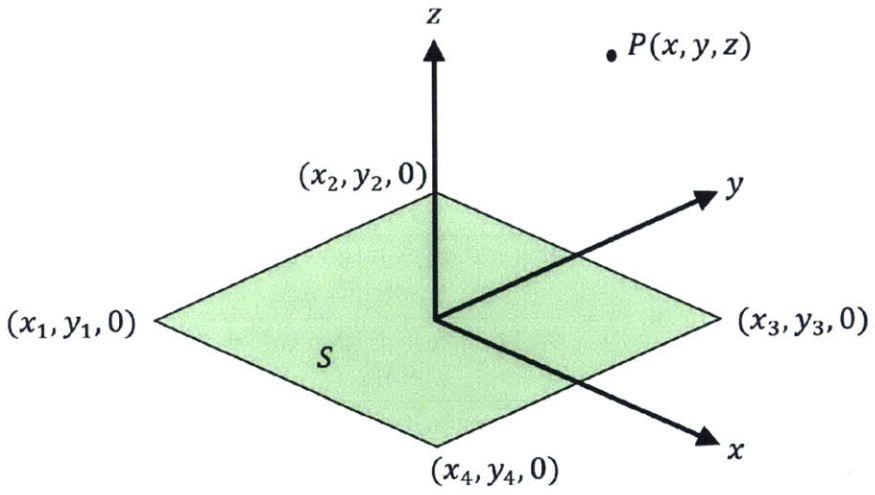

Figure 3-8: A Quadrilateral uniform-strength source element

Consider a surface element with a uniform-strength source distribution σ per area bounded by four straight lines as shown in Fig. 3-8. The four corner points of the element are denoted as $(x_1, y_1, 0)$, $(x_2, y_2, 0)$, $(x_3, y_3, 0)$, $(x_4, y_4, 0)$. The velocity potential at a point $P(x, y, z)$ in the 3D domain due to this element is

$$\varphi(x, y, z) = \frac{-\sigma}{4\pi} \int_S \left(\frac{1}{\sqrt{(x - x_0)^2 + (y - y_0)^2 + z^2}} \right) ds \tag{3.5}$$

And the velocity components can be obtained by differentiating the velocity po-

tential:

$$(u, v, w) = \left(\frac{\partial \varphi}{\partial x}, \frac{\partial \varphi}{\partial y}, \frac{\partial \varphi}{\partial z}\right) \tag{3.6}$$

The closed form solution of the velocity potential and velocity components in x,y and z due to the quadrilateral constant-strength source element is taken from Section 10.4.1 in Katz [15].

When the point P is sufficiently far from the center of the element $(x_0, y_0, 0)$, the quadrilateral source element of an area A can be approximated by an equivalent point source and this will help to increase the computational efficiency and lower the computational cost. When the point is far from the element, the velocity potential can be approximated as follows.

$$\varphi(x, y, z) = \frac{-\sigma}{4\pi}\left(\frac{A}{\sqrt{(x - x_0)^2 + (y - y_0)^2 + z^2}}\right) \tag{3.7}$$

Thus the velocity components are the differential of the potential:

$$\begin{aligned} u(x, y, z) &= \frac{\sigma A(x - x_0)}{4\pi[(x - x_0)^2 + (y - y_0)^2 + z^2]^{3/2}} \\ v(x, y, z) &= \frac{\sigma A(y - y_0)}{4\pi[(x - x_0)^2 + (y - y_0)^2 + z^2]^{3/2}} \\ w(x, y, z) &= \frac{\sigma A(z - z_0)}{4\pi[(x - x_0)^2 + (y - y_0)^2 + z^2]^{3/2}} \end{aligned} \tag{3.8}$$

A far field analysis was performed by Lee [19] and it was found that the approximations above are valid if the distance is more than approximately 1 panel diameter either in horizontal or vertical direction.

3.4 Comparsion of wave-loads between FIT and WAMIT

The solutions for the diffraction problem (also known as the wave-excitation problem) was first obtained by FIT and the results were analyzed and compared with the potential-flow method of FAST's HydroDyn module [14], based on frequency-domain solutions from WAMIT and converted to the time domain through frequency-to-time domain transforms [17]. The cylindrical MIT/NREL TLP buoy with a radius of 9 m and a draft of 47.89 m was treated in a random severe sea state with a 6-m significant wave height and a 12-sec peak-spectral wave period as shown in Figure 3-9 and 3-10, the time-series of wave elevation is plotted in Figure 3-11. A body mesh of 2,400 panels, with 48 azimuthal, 41 vertical, and 9 bottom panels was selected for FIT and a body mesh of 32,400 panels was selected for WAMIT and a comparison was made between the solutions of FIT and WAMIT. The panels were taken to be flat and the source strengths were assumed to be constant on each panel as discussed in Section 3.3 (also the low-order method in WAMIT). The time step of the time-domain simulations in FIT was 0.1 sec with a memory interval in the solution of the linear time convolution equation of 18 sec. For the convergence studies on different perimeters used in FIT, please refer to Section 3.5. The WAMIT solution uses a time step of 0.1 s for the frequency-to-time-domain transforms of the WAMIT solution. The WAMIT solution, in turn, is based on the pressure-integration method considering the first-order and full quadratic interaction of first-order terms, including the full difference- and sum-frequency QTFs but not including the second-order potential, based on a frequency discretization of 0.05 rad/s. The WAMIT solutions were computed at NREL courtesy of Dr. Jonkman.

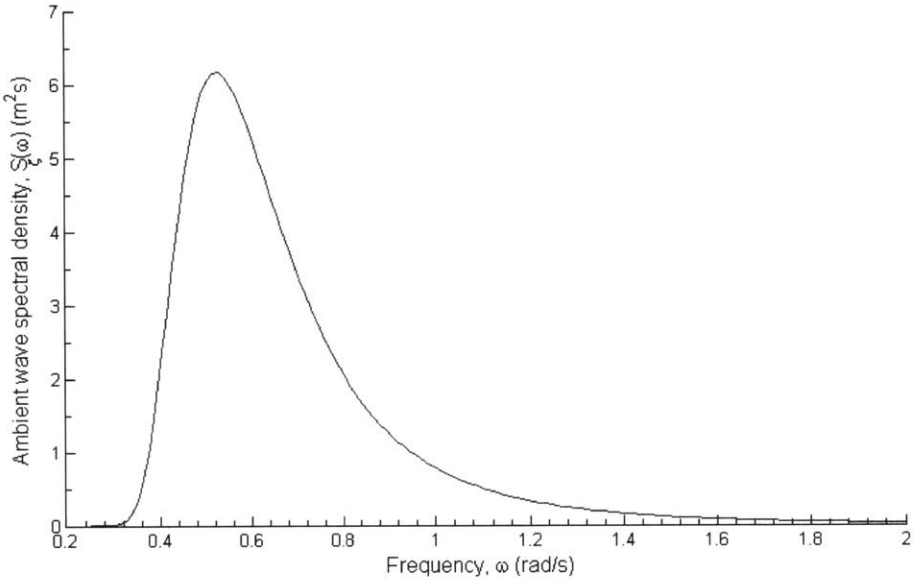

Figure 3-9: Wave spectral density of the JONSWAP seastate

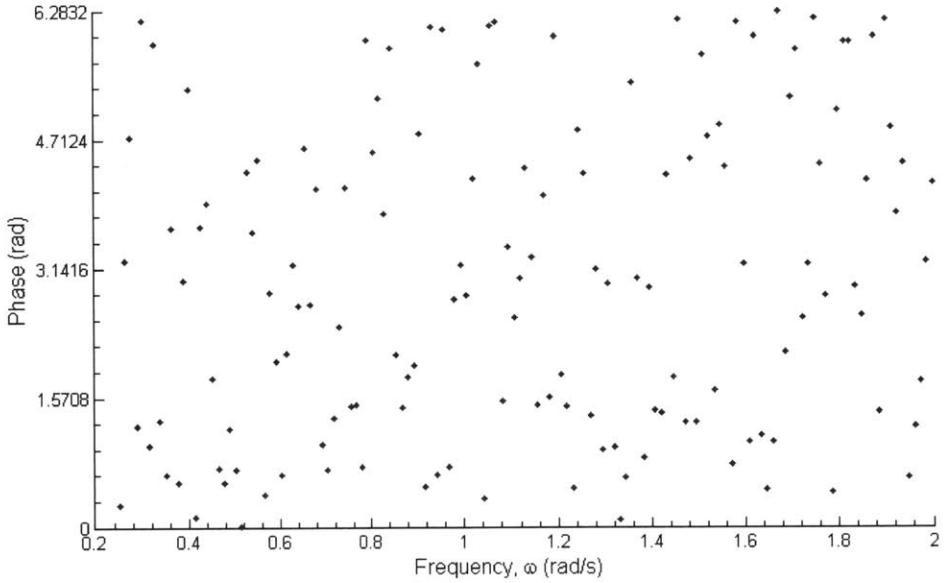

Figure 3-10: Phase of the JONSWAP irregular wave

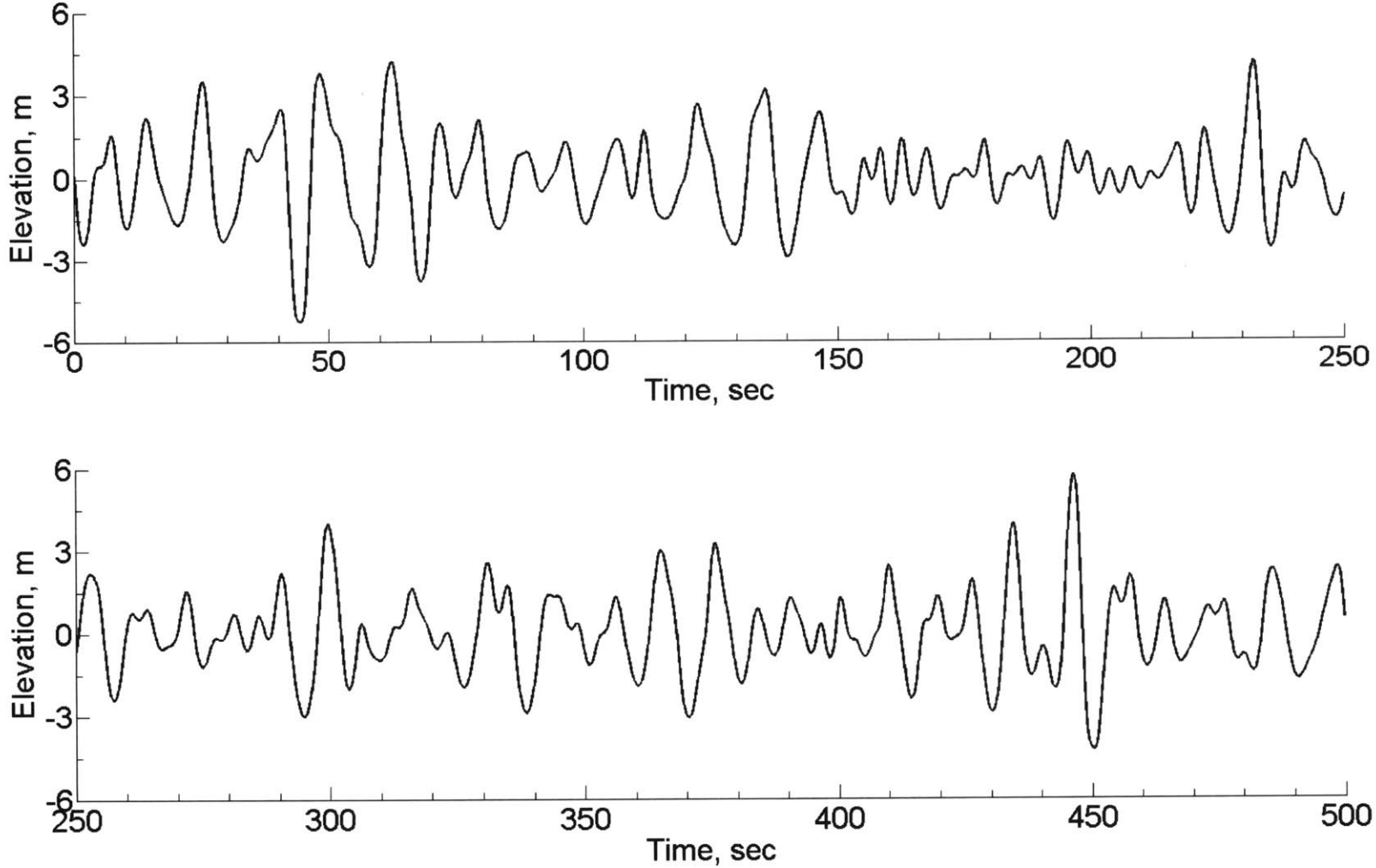

Figure 3-11: Wave elevation of the JONSWAP seastate

3.4.1 1st Order Solutions

The linear solutions between FIT and WAMIT were first compared for a verification study.

The linear formulation of FIT was described in Section 3.1. First order solution of WAMIT can be found in Chapter 2 of WAMIT Theory Manual by Lee [18]:

$$\vec{F}^{(1)} = -\rho g \int_{\bar{S}_B} Z\vec{n}ds - \rho \int_{\bar{S}_B} \frac{\partial \Phi^{(1)}}{\partial t}\vec{n}ds; \quad \text{where} \quad \Phi^{(1)} = \varphi_I^{(1)} + \varphi^{(1)} \tag{3.9}$$

The time-marching solutions and fitted PSDs of the surge, heave and pitch linear solutions are plotted in the following pages. The solutions obtained by FIT and WAMIT were found to be in very good agreement. This verifies the accuracy of the linear solution of the FIT module, and suggested that the computation of source strength and velocity potentials to be correct in the FIT theory. This provides confidence in the computation of velocity potentials using FIT in the numerical code and allow the code to be used to computed linear and second order solutions, as discussed in the following sections.

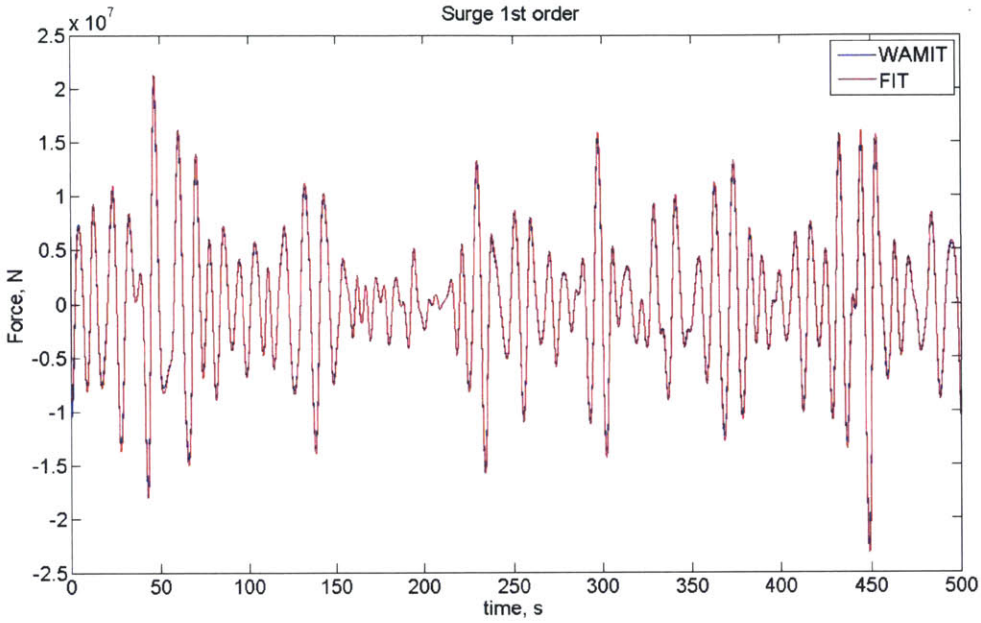

Figure 3-12: Surge 1st order

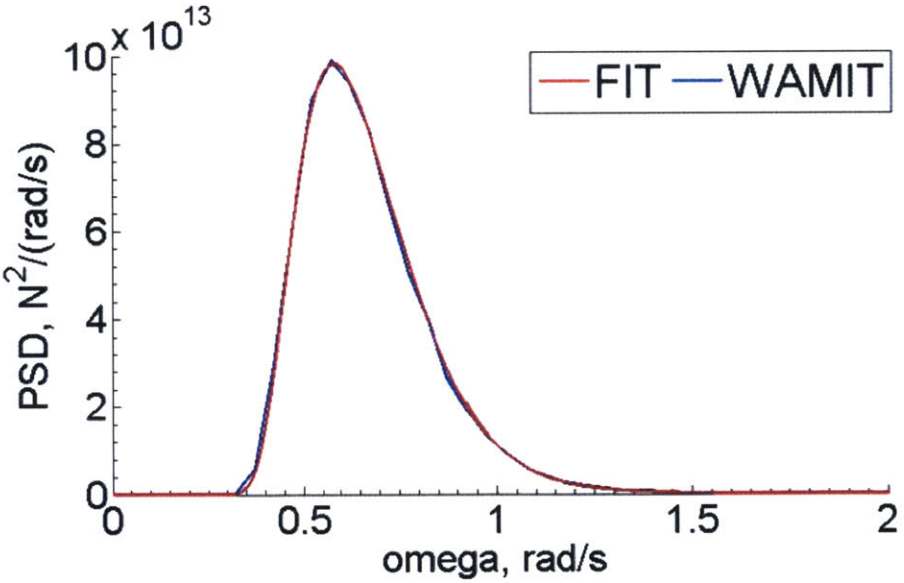

Figure 3-13: Surge 1st order PSD

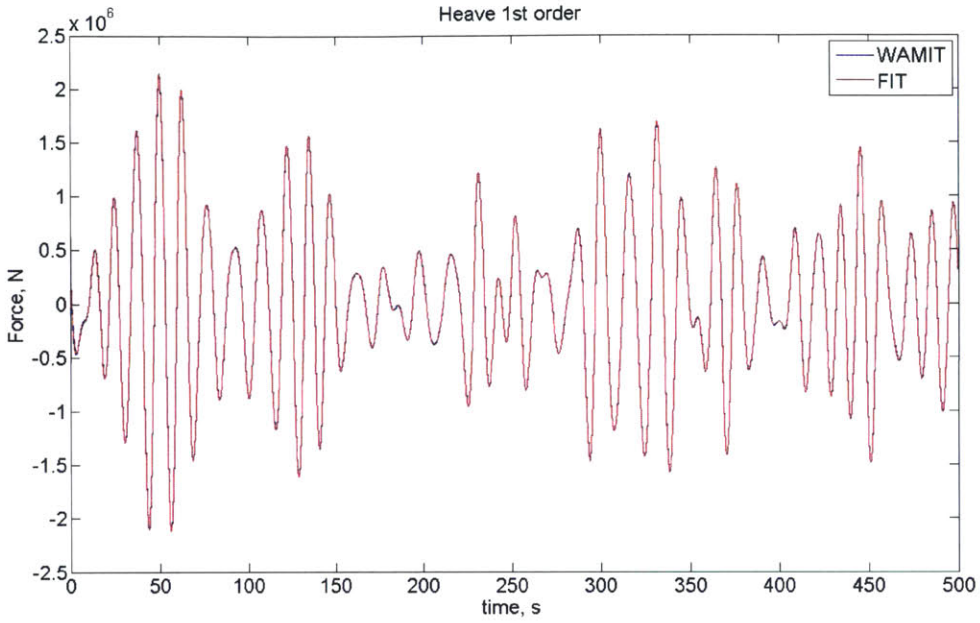

Figure 3-14: Heave 1st order

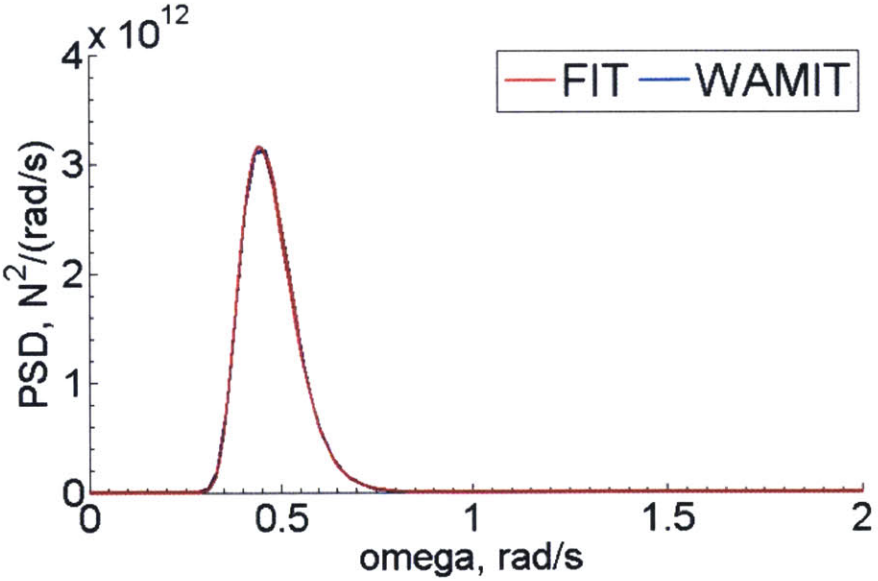

Figure 3-15: Heave 1st order PSD

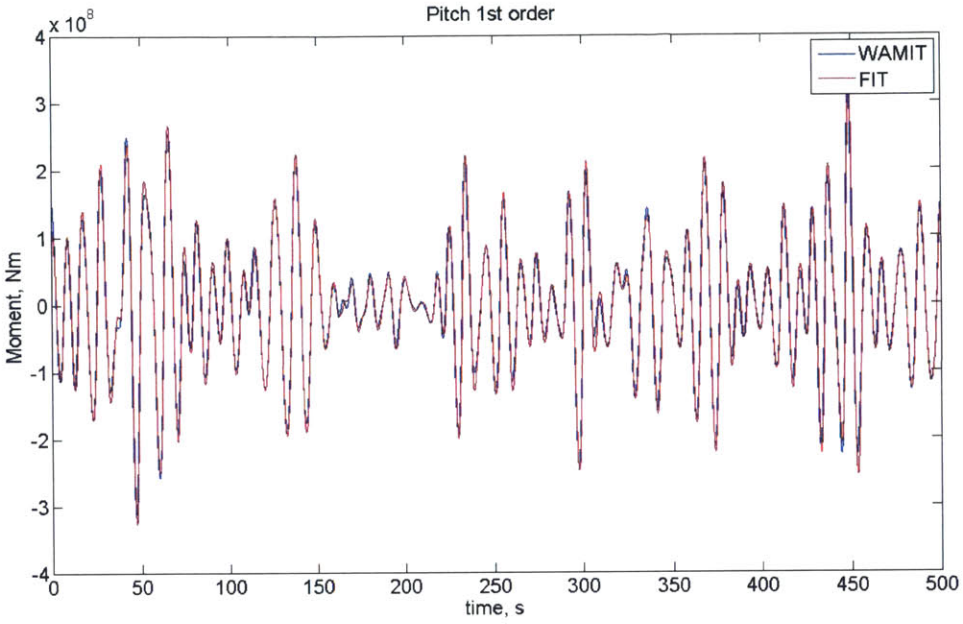

Figure 3-16: Pitch 1st order

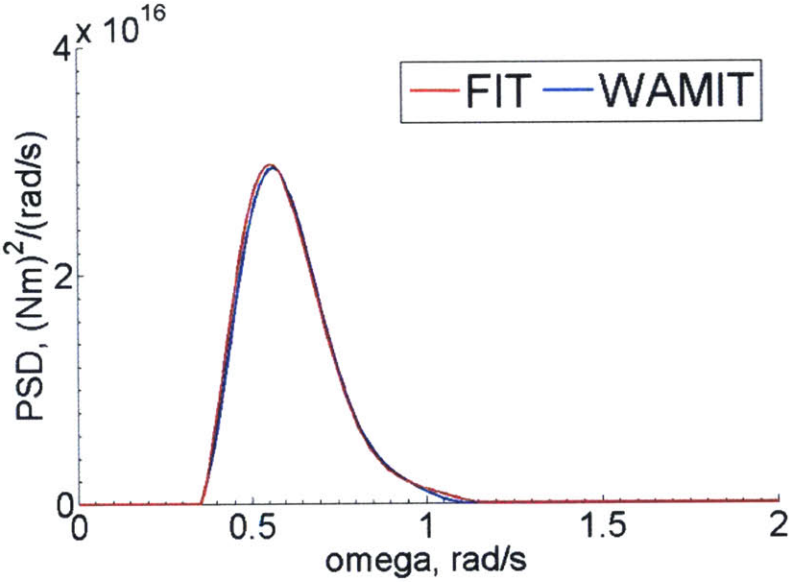

Figure 3-17: Pitch 1st order PSD

3.4.2 Hydrodynamic Force in Surge Comparison Between FIT and WAMIT

One of the primary mode of motion for an offshore platform is in the surge direction, assuming uni-directional wave coming in from the surge direction. This subsection presents the surge solutions comparison between FIT and WAMIT.

The cylindrical MIT/NREL TLP buoy was treated again in the random severe sea state shown in Figure 3-9 and 3-10. The same body meshes and frequency-to-time domain transform were used in this section as Subsection 3.4.1. The body is fixed in space and the problem was treated as a diffraction problem of a fixed cylinder in irregular waves.

The first order solution was discussed Subsection 3.4.1. The second order solution excluding the second-order incident-wave potentials (1st order potentials only) for a diffraction problem in FIT was obtained and analyzed according to the perturbation theory in Section 3.1.

According to Lee [18], second order surge quadratic force for a stationary truncated cylinder in WAMIT is:

$$\vec{F}_1^{(2)} = -\rho \int_{\bar{S}_B} \frac{1}{2} \nabla\Phi^{(1)} \cdot \nabla\Phi^{(1)} n_1 ds \tag{3.10}$$

A series of time-marching graphs and their respective PSDs are plotted in this subsection, including a comparison of total (Fig. 3-18 to 3-20), 1st order (Fig. 3-21 to 3-22), and 2nd quadratic surge hydrodynamic forces (Fig. 3-23 to 3-25) between FIT and WAMIT.

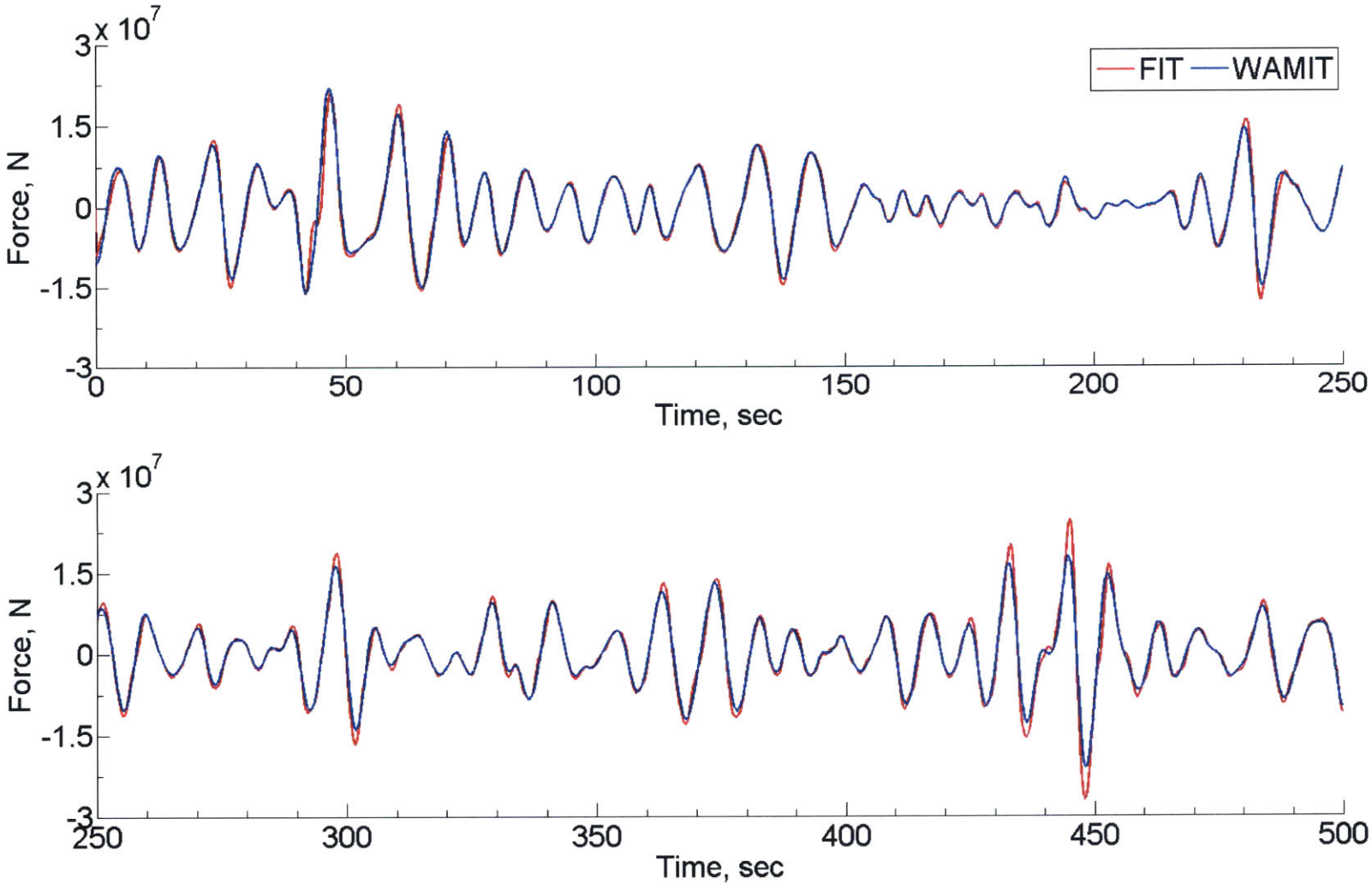

Figure 3-18: Total surge hydrodynamic force from FIT and WAMIT, r=9m, T=47.89m

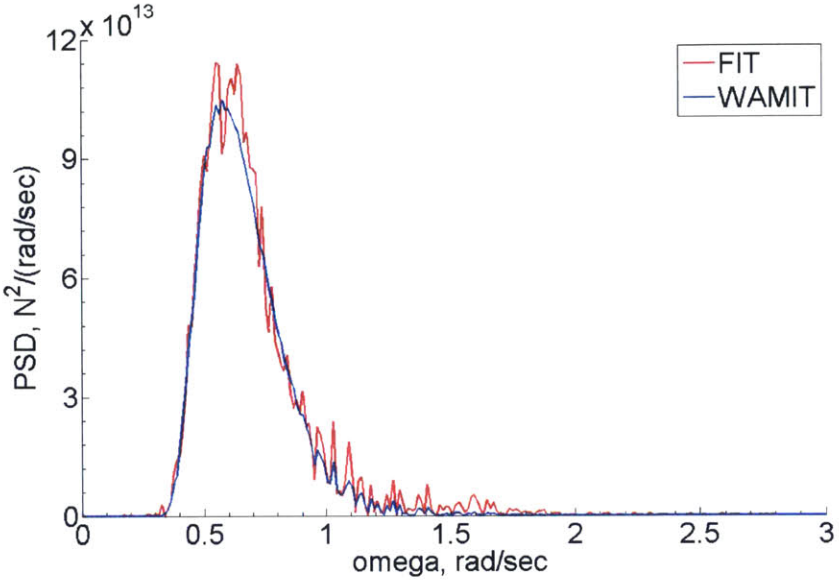

Figure 3-19: PSD comparison of total surge force between FIT and WAMIT, r=9m, T=47.89m

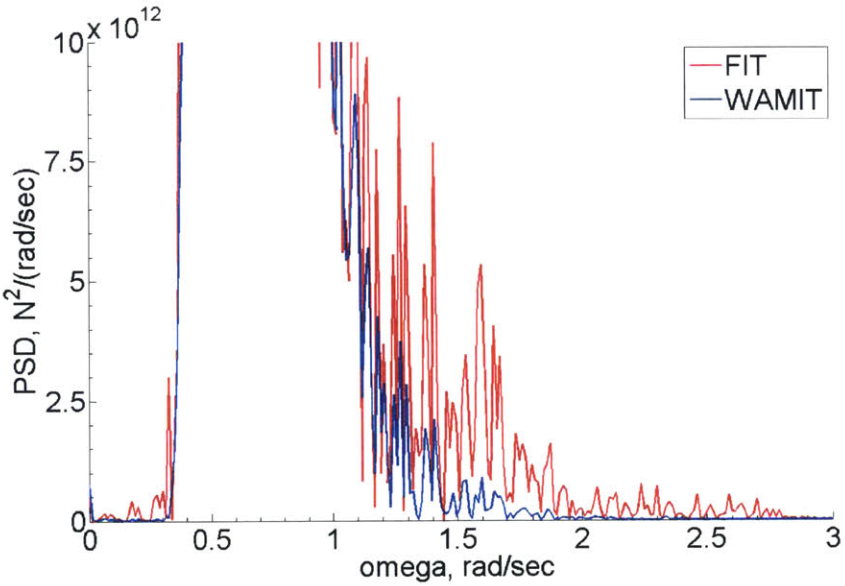

Figure 3-20: Close up PSD comparison of total surge force between FIT and WAMIT, r=9m, T=47.89m

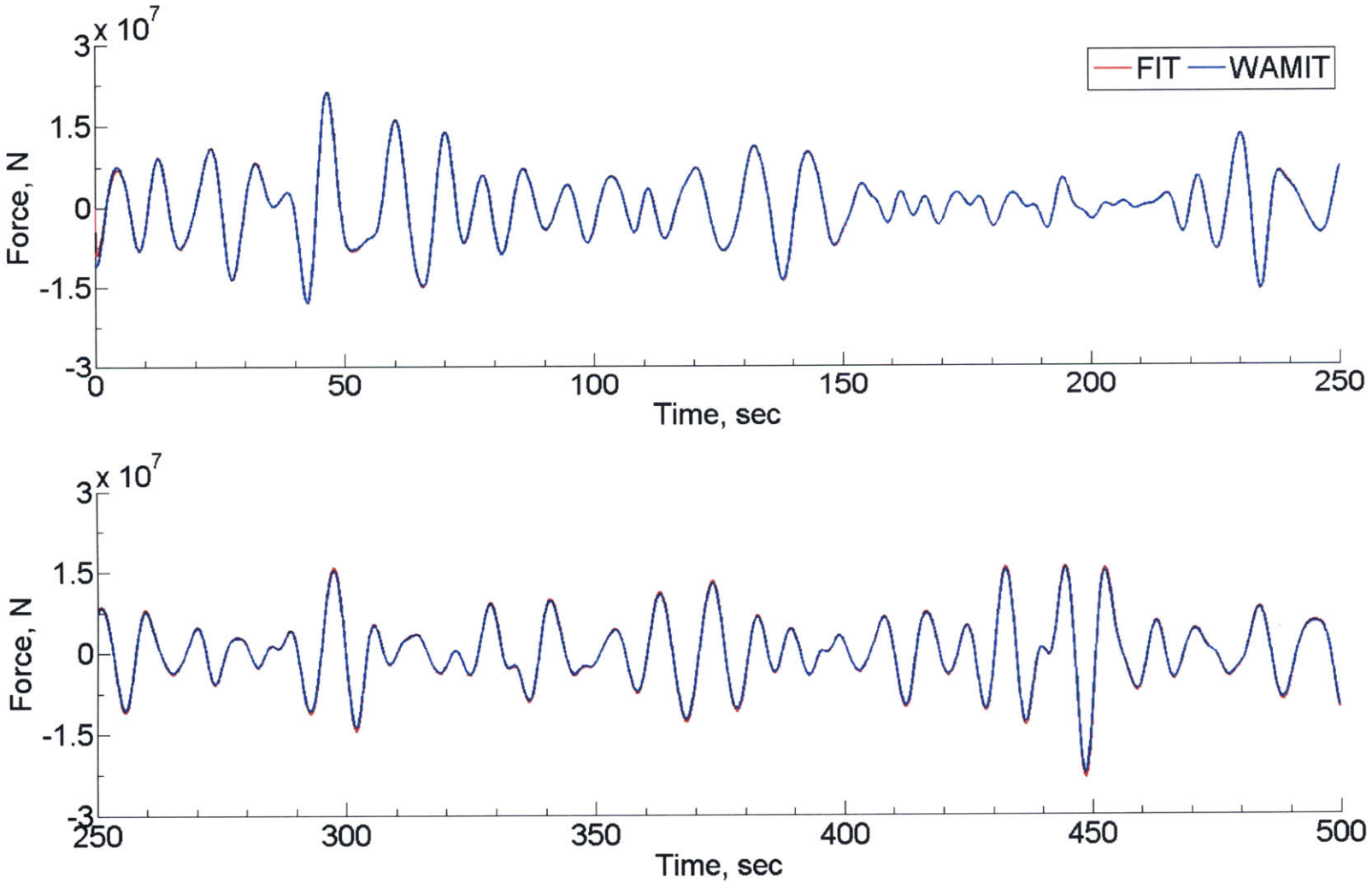

Figure 3-21: 1st order surge hydrodynamic force from FIT and WAMIT, r=9m, T=47.89m

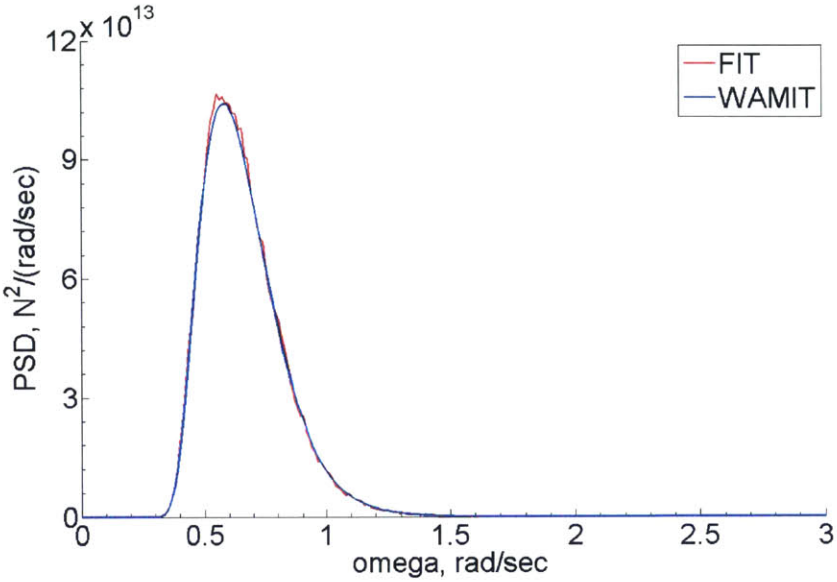

Figure 3-22: PSD comparison of 1st order surge force between FIT and WAMIT, r=9m, T=47.89m

The numerical solutions for the total hydrodynamic force obtained by FIT and WAMIT were in good agreement as shown in Figure 3-18, with the solution from FIT capturing larger responses at the peaks over the time-marching solution, as well as displaying some higher order nonlinearities. The PSD analysis of the total hydrodynamic forces between FIT and WAMIT in Figure 3-19 and 3-20 confirms the observation from the time-marching solution, as FIT produced responses with larger amplitude at the leading order wave frequency at about 0.53 rad/sec, and also captured more nonlinear effects at sum- (1.4 to 1.8 rad/sec) and difference- (0.3 to 0.4 rad/sec) frequency range. Same with results presented in Subsection 3.4.1, the linear solutions match perfectly as demonstrated in the linear time-marching and PSD comparison in Figure 3-21 and 3-22. Plotting the 2nd order time-marching solutions (Fig. 3-23) and PSDs (Fig. 3-24 and 3-25) further revealed that aside from capturing more nonlinearities at sum- and difference frequency ranges, significant nonlinear effects were present at other frequency ranges. The nonlinear effects computed by FIT scatter across the entire frequency spectrum between 0 to 3 rad/sec, and was capable of capturing contributions between 2 to 3 rad/sec in which WAMIT did not produce any wave loads.

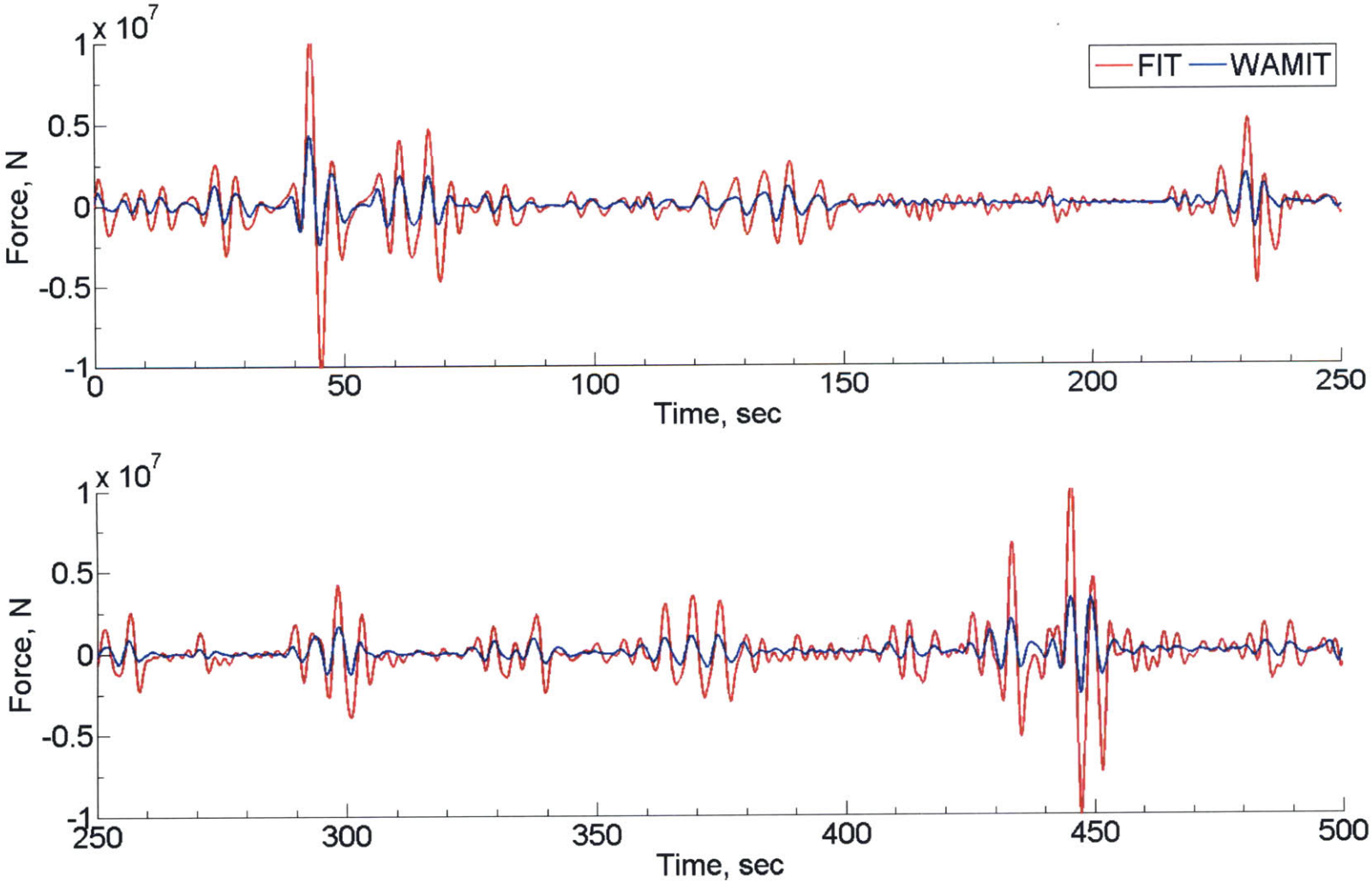

Figure 3-23: 2nd order surge quadratic hydrodynamic force from FIT and WAMIT, r=9m, T=47.89m

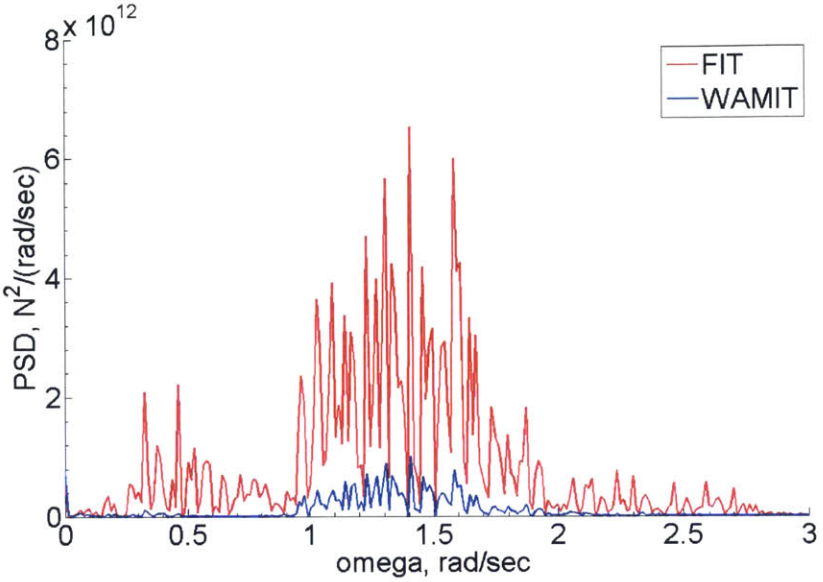

Figure 3-24: PSD comparison of 2nd order surge force between FIT and WAMIT, r=9m, T=47.89m

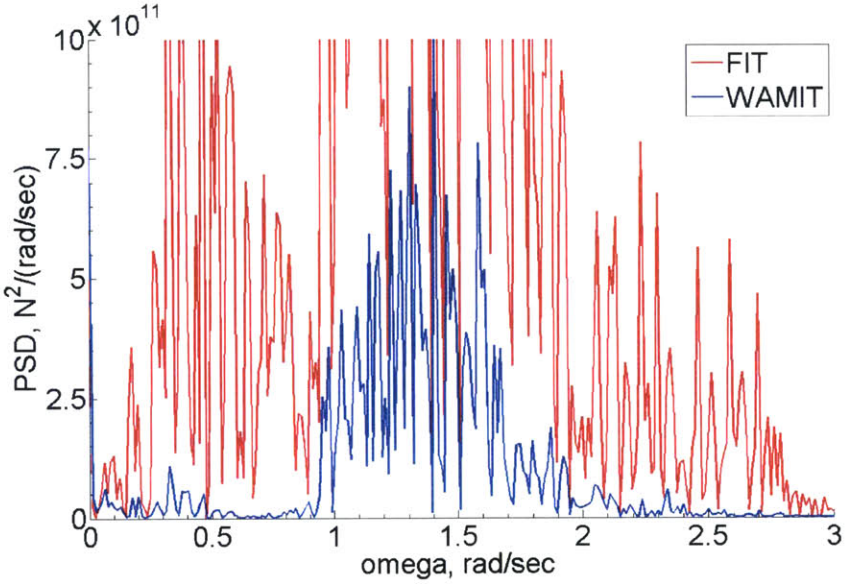

Figure 3-25: Close up PSD comparison of 2nd order surge force between FIT and WAMIT, r=9m, T=47.89m

3.5 Convergence Tests on FIT 2nd Order Surge Quadratic Solution

This section summarizes the convergence tests performed on the computation of 2nd order quadratic surge hydrodynamic force. In summary, convergence were achieved with different perimeters for the efficient computation of nonlinear loads using FIT. The different perimeters are listed as follow:

Subsection 3.5.1 describes the memory time convergence for the FIT solutions. It was found in the convergence study that the memory function and its derivative decays towards zero as time increases. It was found that pass 18 seconds of memory time interval, the magnitude of the memory function and its derivative is sufficiently close to zero, leading to the conclusion that 18 seconds of memory time is sufficient for numerical solutions obtained using FIT.

Subsection 3.5.2 describes the size of time step ($\triangle t$) convergence for the FIT solutions. It was found that 0.1 seconds is sufficient for converged solutions.

Subsection 3.5.3 describes the mesh convergence for the FIT solutions. It was found that 2400 panels are sufficient for converged solutions.

3.5.1 Memory Time Convergence

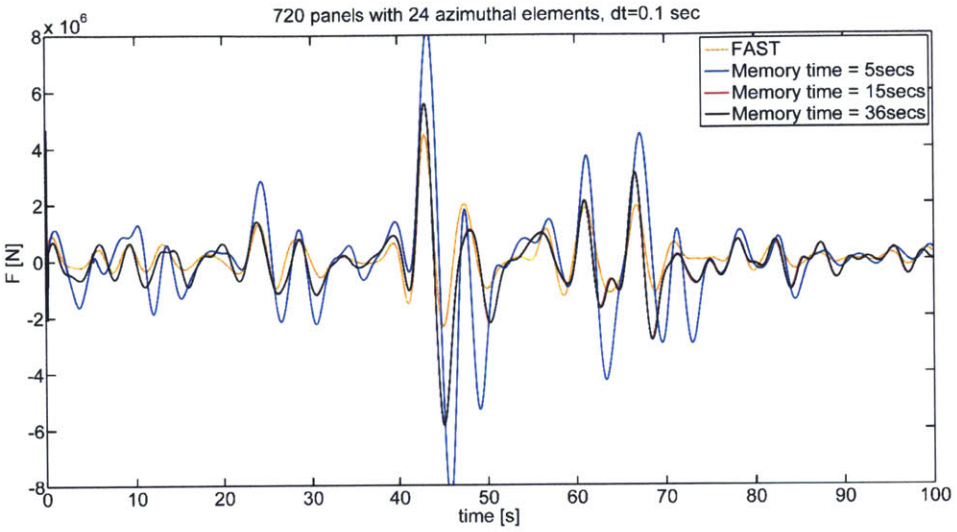

Figure 3-26: Convergence study for memory time length t = 0 to 100s

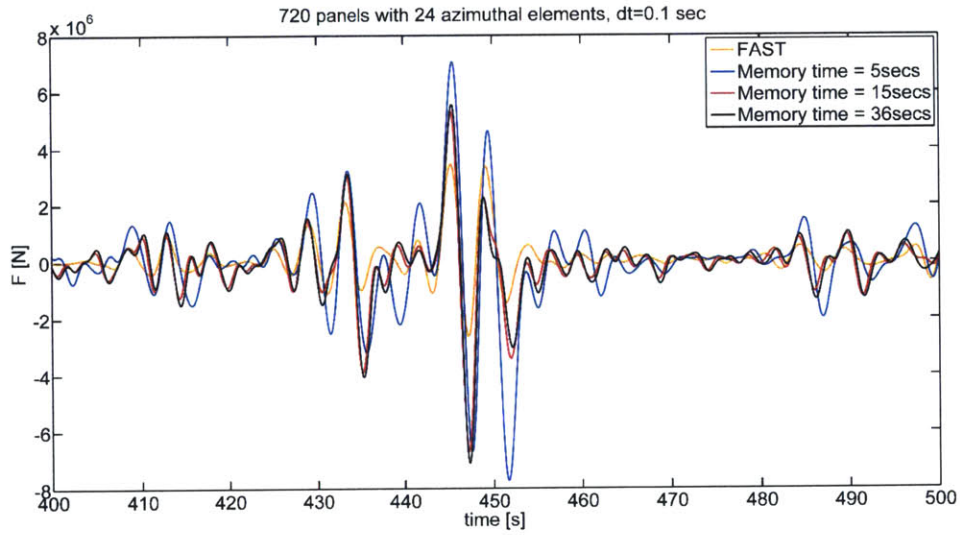

Figure 3-27: Convergence study for memory time length t = 400 to 500s

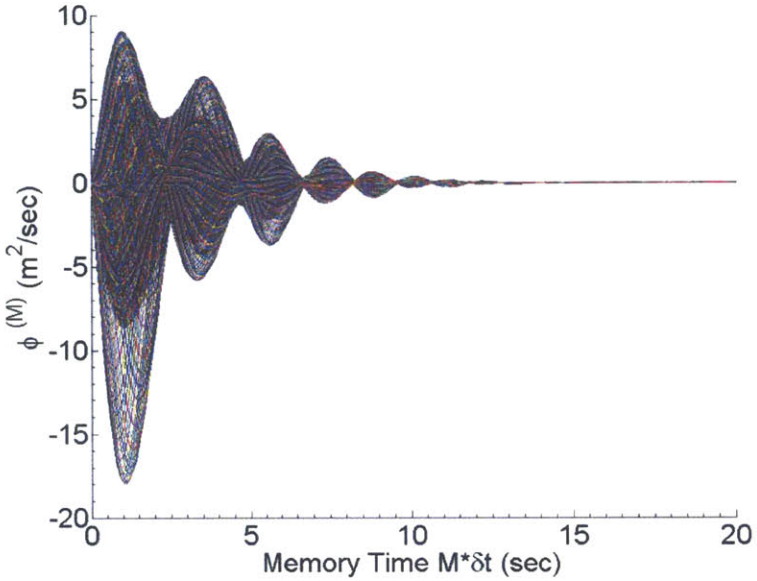

Figure 3-28: Contribution of memory effects from each time step on Memory function, (z=0)

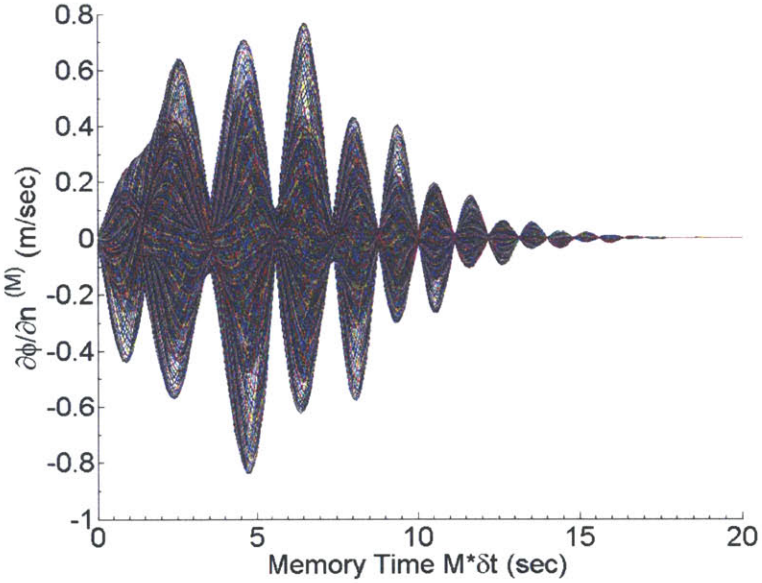

Figure 3-29: Contribution of memory effects from each time step on derivative of Memory function, (z=0)

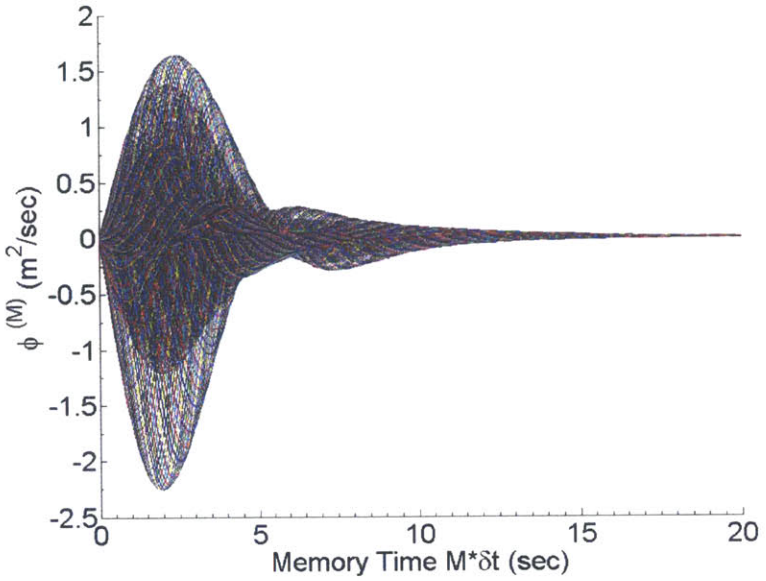

Figure 3-30: Contribution of memory effects from each time step on Memory function, (z=1/2draft)

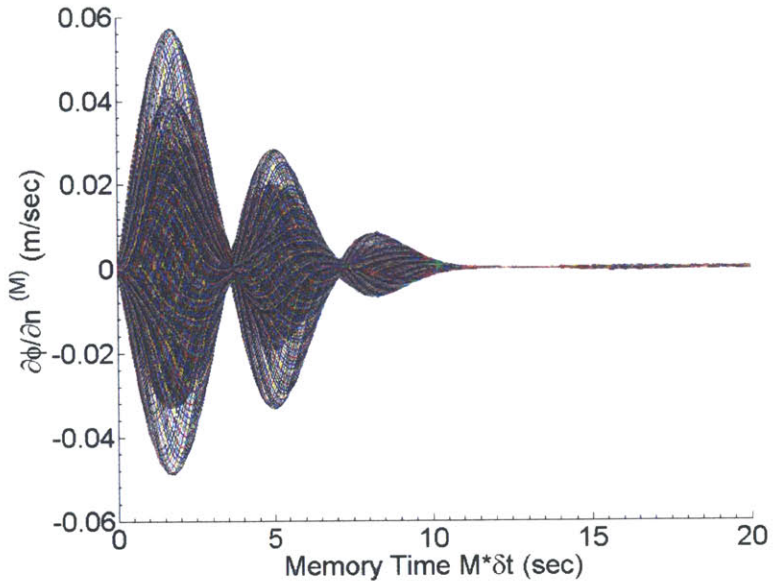

Figure 3-31: Contribution of memory effects from each time step on derivative of Memory function, (z=1/2draft)

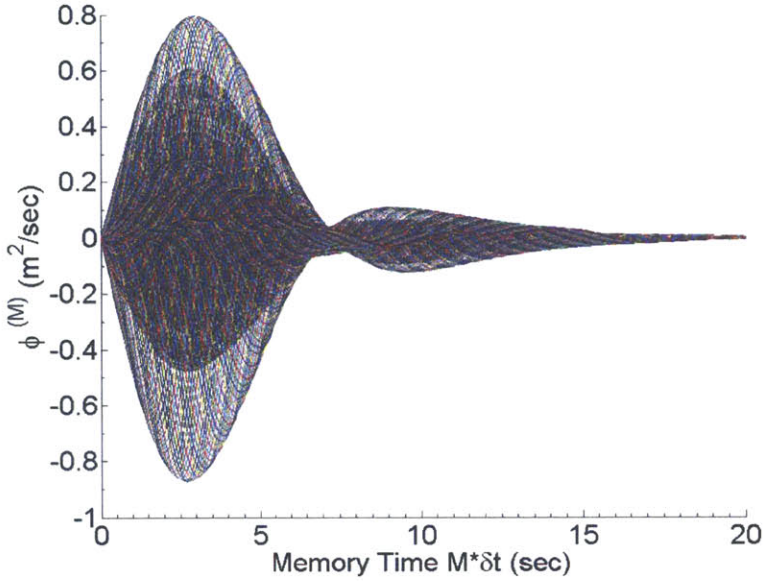

Figure 3-32: Contribution of memory effects from each time step on Memory function, (z=draft)

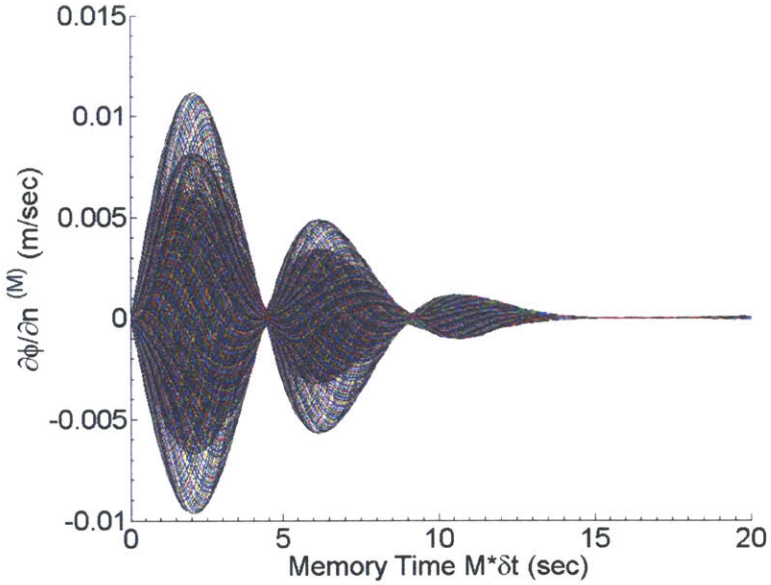

Figure 3-33: Contribution of memory effects from each time step on derivative of Memory function, (z=draft)

3.5.2 Size of Time Step Convergence

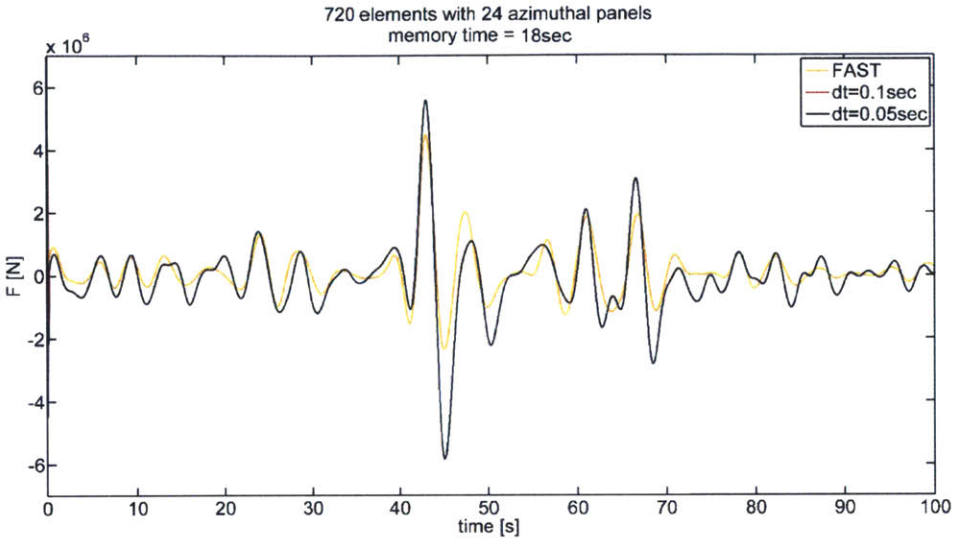

Figure 3-34: Convergence study for $\triangle t$ t = 0 to 100s

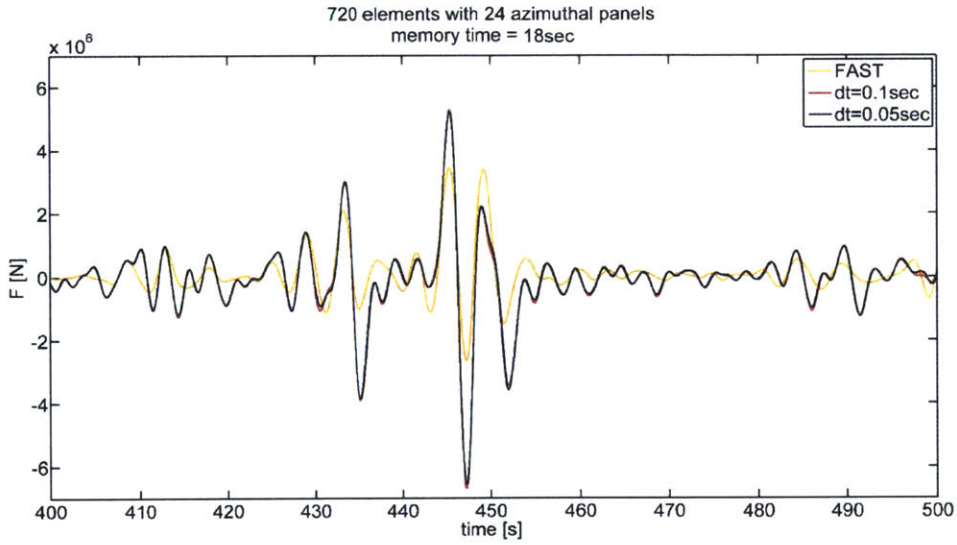

Figure 3-35: Convergence study for $\triangle t$ t = 400 to 500s

Note that dt=0.2s or larger time steps does not lead to a converged solution.

3.5.3 Mesh Convergence for FIT

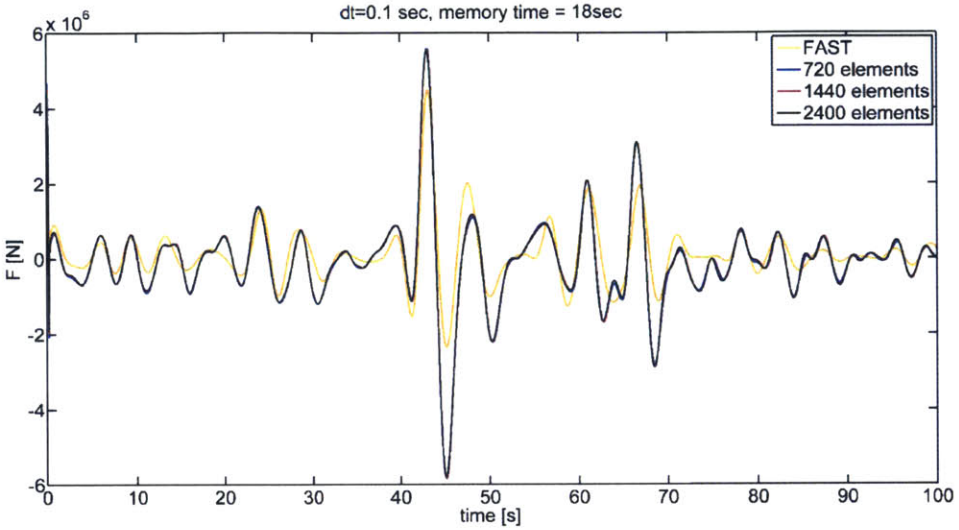

Figure 3-36: Convergence study for mesh density t = 0 to 100s

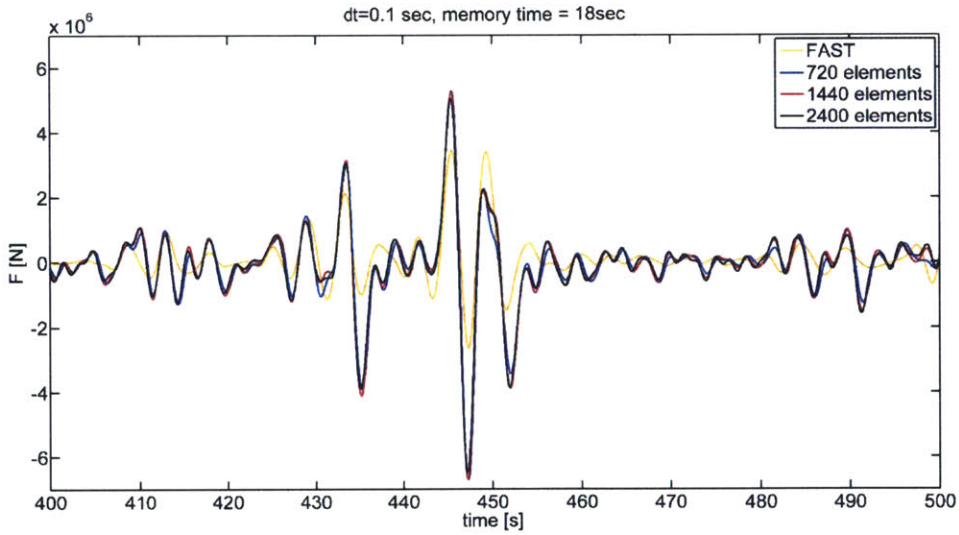

Figure 3-37: Convergence study for mesh density t = 400 to 500s

3.6 Mesh Convergence between FIT and WAMIT on 2nd order solutions

The rate of mesh convergence was compared between the 2nd order quadratic surge solutions obtained using FIT and WAMIT.

In this study, only the mesh convergence between FIT and WAMIT was compared, as the two sets of simulations were ran on different platforms with different computer system specifications and hardware. By studying the rate of mesh convergence between the two methods, the comparison provides a preliminary understanding of the efficiency on computing nonlinear effects between the time-domain method FIT and the frequency-domain method WAMIT. It was found that FIT requires less panels on meshes than WAMIT to achieve convergence of nonlinear solutions. This suggests that for computation of nonlinear effects, FIT is efficient in discretization of surfaces and can conserve computational resources when applied appropriately.

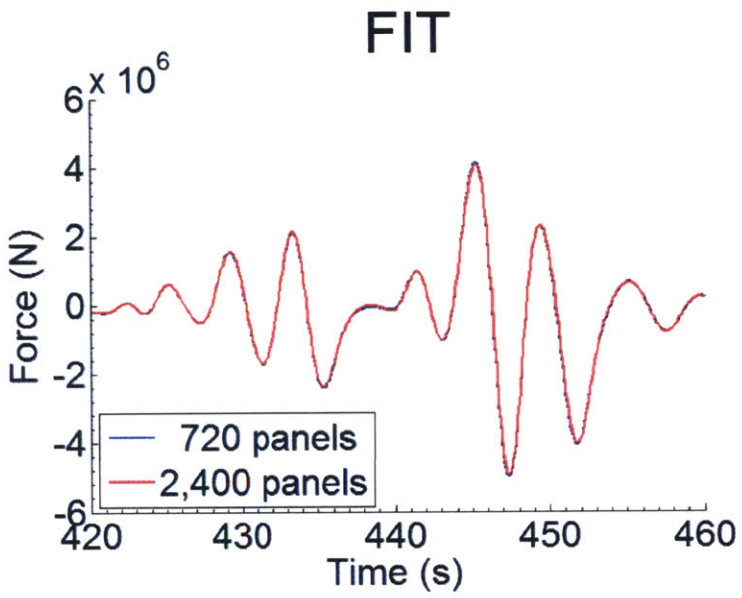

Figure 3-38: Mesh convergence for FIT

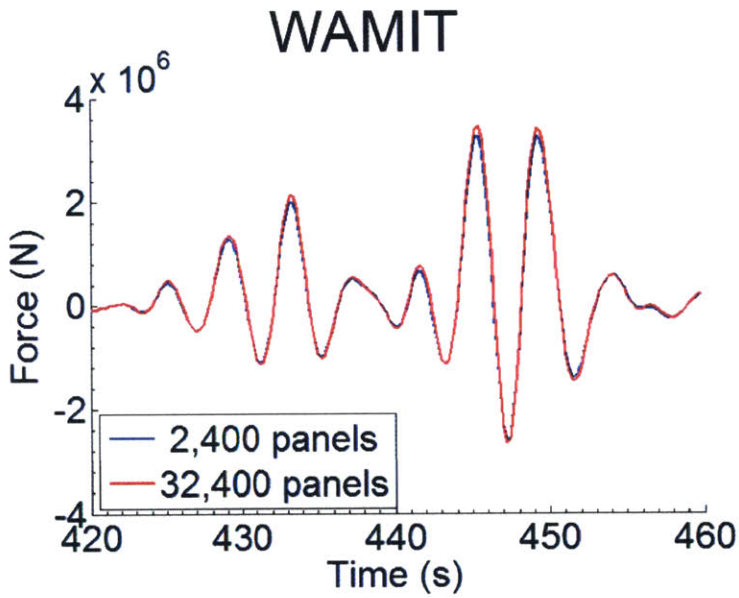

Figure 3-39: Mesh convergence for WAMIT

3.7 Numerical Solutions from FIT

Following the linear verification between FIT and WAMIT, a series of simulations computing surge hydrodynamic forces was carried out to further understand the performances and capabilities of FIT. The wave-body problem was treated to be a cylinder fixed in space and the diffraction problem was solved. Two test cases were carried out with the MIT/NREL TLP (9m radius and 47.89m draft) and a slenderer buoy (1.75m radius and 30m draft) treated in a random severe sea state produced according to the JONSWAP spectrum with a 6-m significant wave height and a 12-sec peak-spectral wave period as shown in Figure 3-9 and 3-10. Another test case was carried out with a cylinder (3m radius and 43.2m draft) treated in an irregular sea state obtained in OC5 [27] shown in Figure 3-40 and 3-41.

For each case, the results are presented in the following order:

- Time-marching comparison between the total, 1st and 2nd order surge hydrodynamic force
- PSD comparison between the total, 1st and 2nd order surge hydrodynamic force
- Time-marching comparison between 1st order surge hydrodynamic force components
- PSD comparison between 1st order surge hydrodynamic force components
- Time-marching comparison between 2nd order surge hydrodynamic force components
- PSD comparison between 2nd order surge hydrodynamic force components
- Time-marching comparison between 2nd order surge free-surface impulse force components
- PSD comparison between 2nd order surge free-surface impulse force components

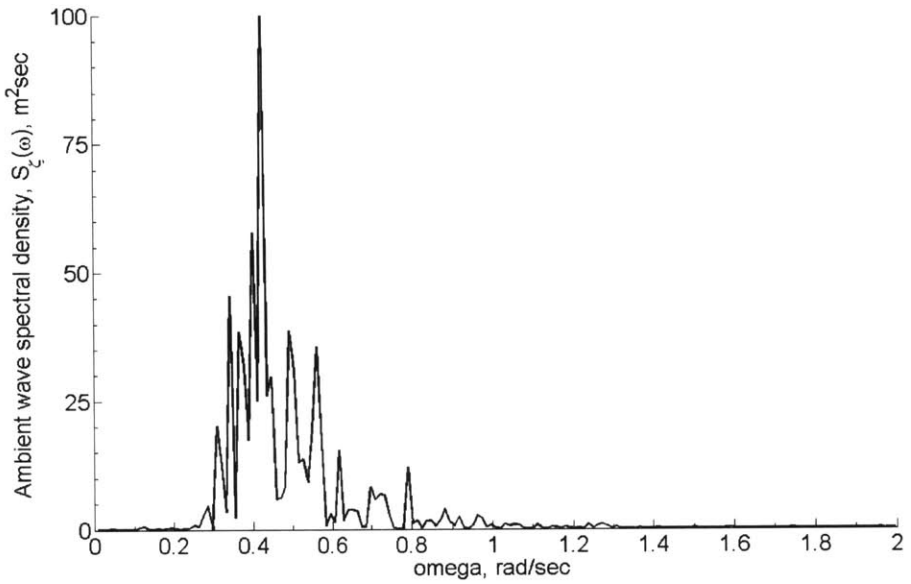

Figure 3-40: Wave spectral density of the OC5 seastate

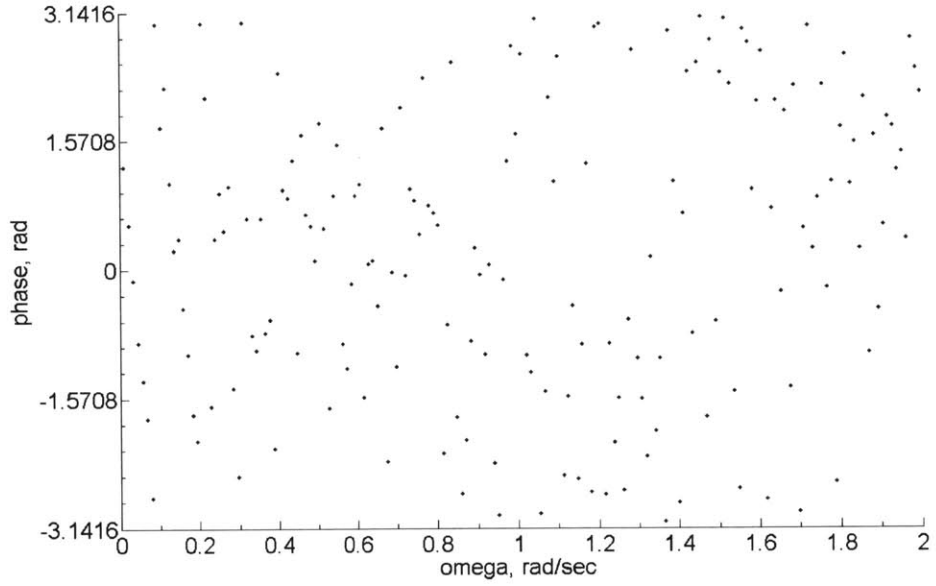

Figure 3-41: Phase of the irregular wave in OC5

3.7.1 MIT/NREL TLP r=9m, T=47.89m

This subsection provides detail results obtained from numerical analysis as described in the introduction of this Section. First, the cylindrical MIT/NREL TLP buoy with a radius of 9 m and a draft of 47.89 m, which was used in numerical simulation in the previous sections, was treated in the random severe sea state generated according to JONSWAP with a 6-m significant wave height and a 12-sec peak-spectral wave period as shown in Figure 3-9 and 3-10. The characteristic wave frequency for this spectrum is $\omega_c = 0.525$rad/sec and the non-dimensionalized perimeter Ka, where $K = \omega_c^2/g$ is the characteristic wave number and a is the radius of the buoy, is $Ka = 0.253$ which is in a finite value range. The 720 panels mesh (Fig. 3-3) was selected to be used in this study. The time step of the time-domain simulations in FIT was 0.1 sec with a memory interval in the solution of the time convolution equation of 18 sec.

In summary, results in this study shows that both linear and nonlinear wave loads are important for a buoy with intermediate size in severe sea state. The time-marching solutions of the comparison of total, 1st and 2nd order surge force and its PSD analyses, as shown in Figure 3-42 to 3-44, shows that linear analysis was able to capture wave loads at the dominant wave frequency range (0.5 to 0.8 rad/sec), while nonlinear analysis provides the 2nd order solution which helps understand wave loads at other frequencies, especially at sum- (1.4 to 1.8 rad/sec) and difference- (0.3 to 0.4 rad/sec) frequency range and when frequency is larger than 2rad/sec. The comparison between 1st order surge hydrodynamic force components in Figure 3-45 and 3-46 shows that both F-K and body disturbance forces are important for linear analysis, with body disturbance force having slightly higher amplitude than its F-K counterpart. The next set of plots shows the comparison between 2nd order surge hydrodynamic force components in Figure 3-47 and 3-48, and the results suggested that 2nd order quadratic effects are significant for all 2nd order components in FIT. It was found that the F-K and body impulse force provide contributions at sum- and difference frequencies, while the free-surface impulse force captures nonlinear

responses at other frequencies, notably with a significant group of energy at frequency larger than 2 rad/sec. The final set of results for the comparison of 2nd order surge free-surface impulse force components as shown in Figure 3-49 and 3-50 illustrates the contributions from the two components, ID and DD, in the free-surface impulse force in FIT. It was found that for this test case, wave loads from the DD component of the free-surface impulse force counteracts the ID component, which is expected as described in the theory section. It was also found that the ID component has a larger magnitude compared to the DD component, and together the two components provide nonlinear wave loads at two frequency ranges, a first group of energy at 0.6 to 1.4 rad/sec, and a second group at 2 to 2.6 rad/sec. These free-surface impulse forces were found to reside at a different frequency ranges from the sum- and difference frequency range.

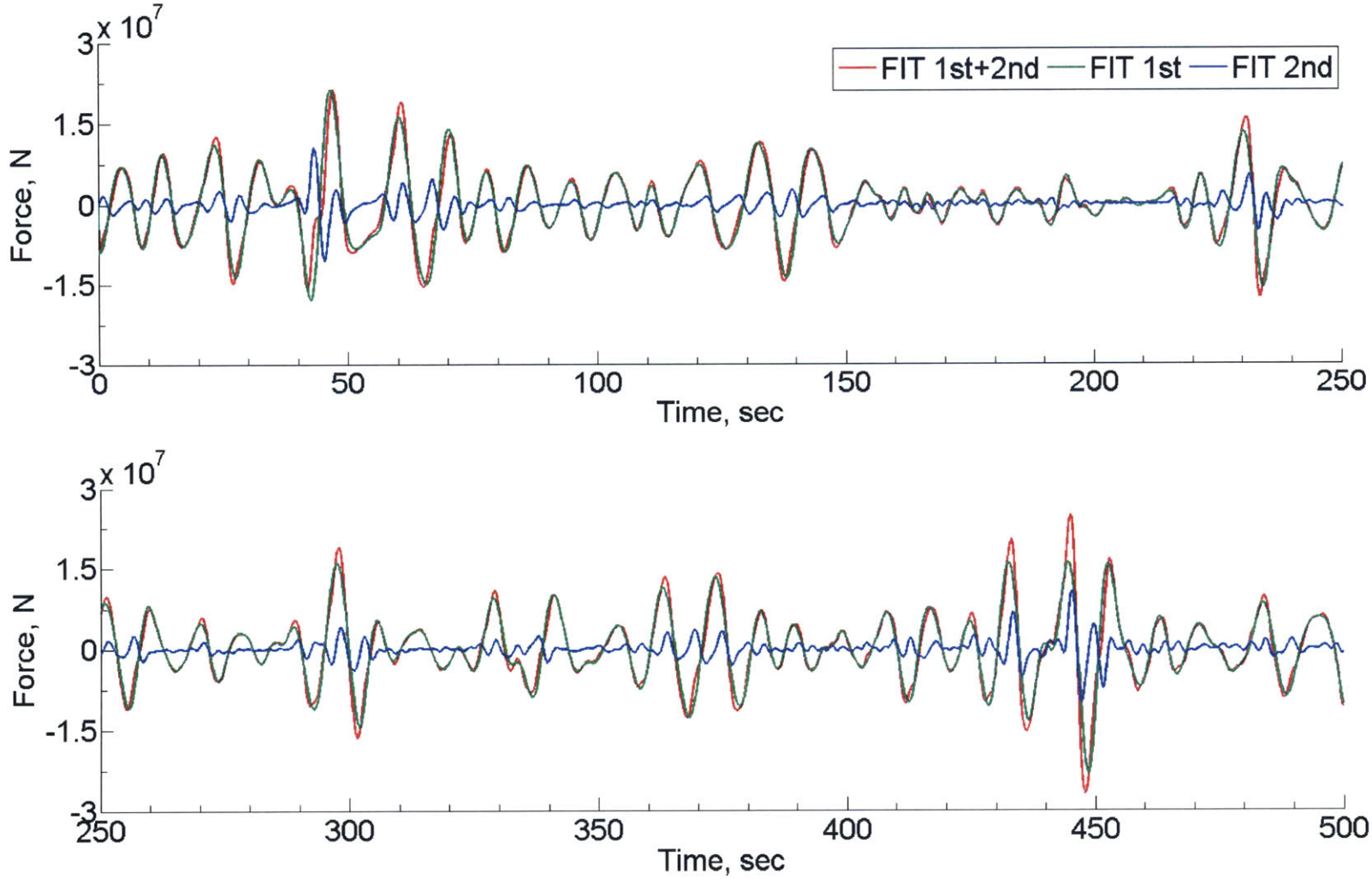

Figure 3-42: Surge hydrodynamic force from FIT, r=9m, T=47.89m

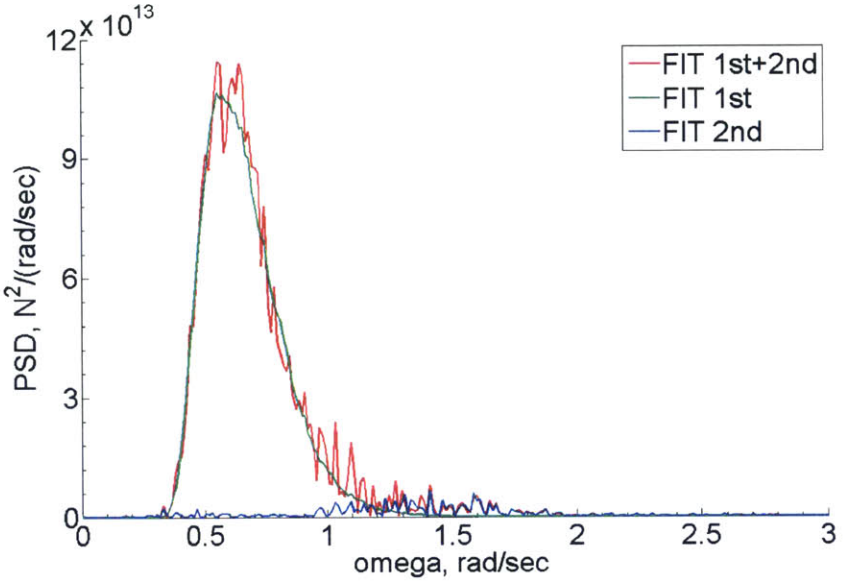

Figure 3-43: PSD comparison between total, 1st and 2nd order surge force from FIT, r=9m, T=47.89m

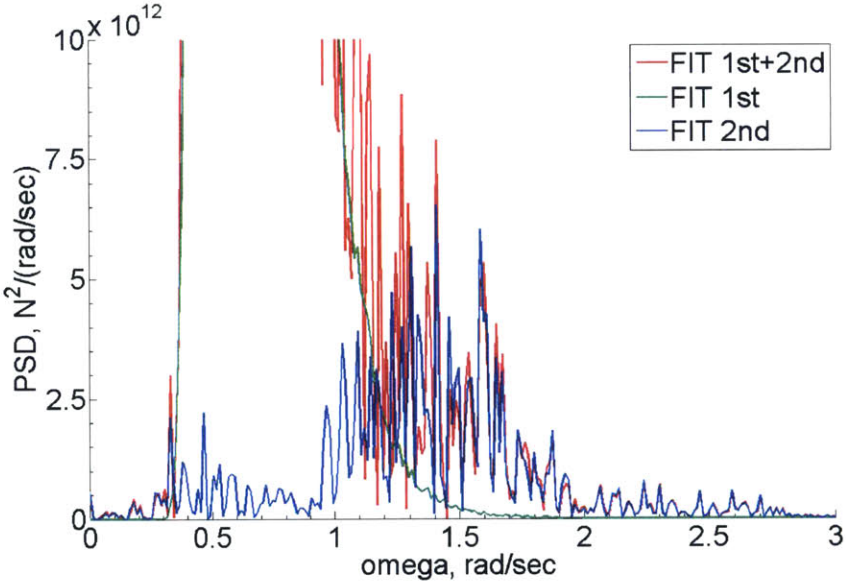

Figure 3-44: Close up of PSD comparison between total, 1st and 2nd order surge force from FIT, r=9m, T=47.89m

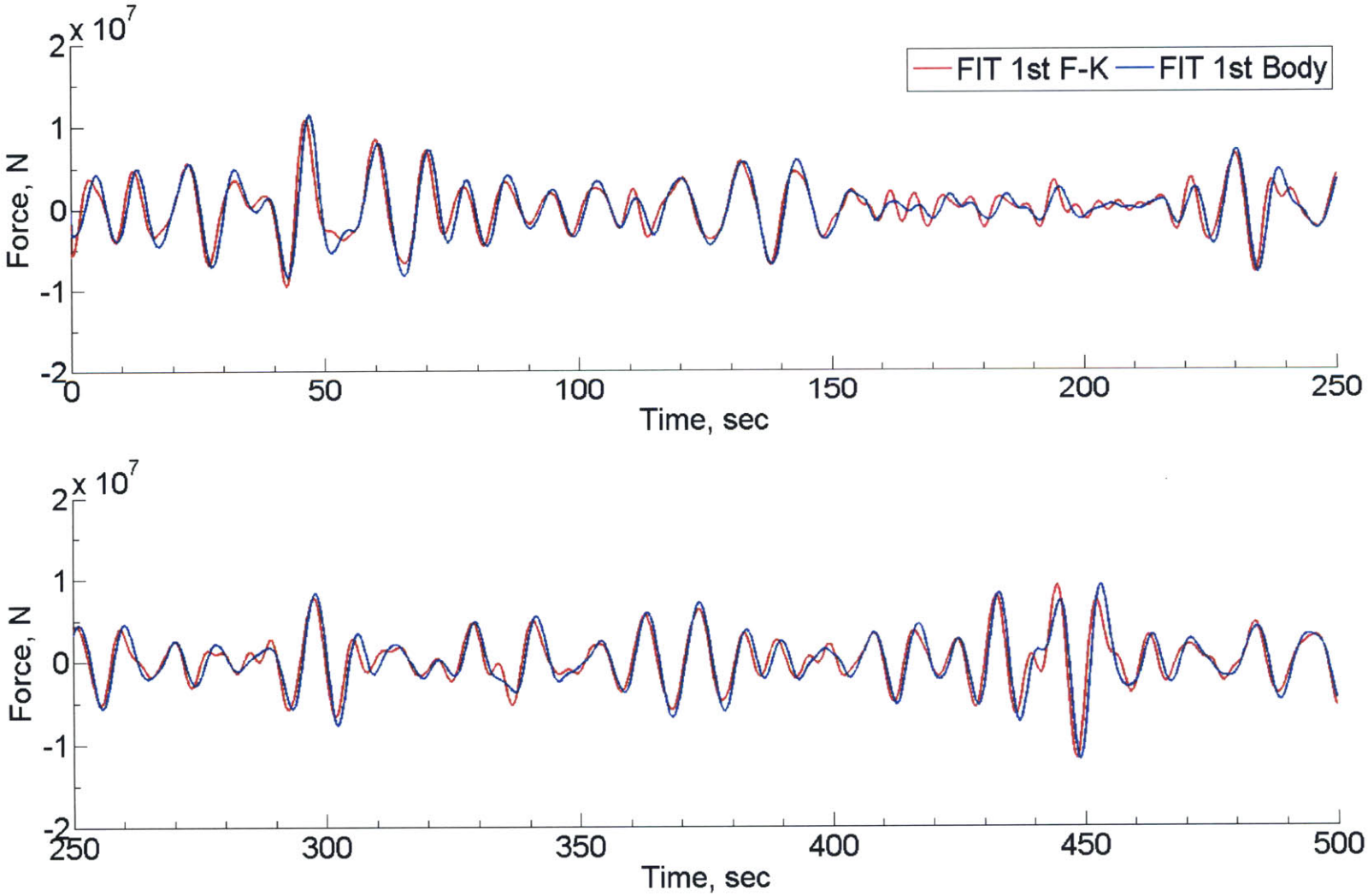

Figure 3-45: 1st order surge hydrodynamic force components from FIT, r=9m, T=47.89m

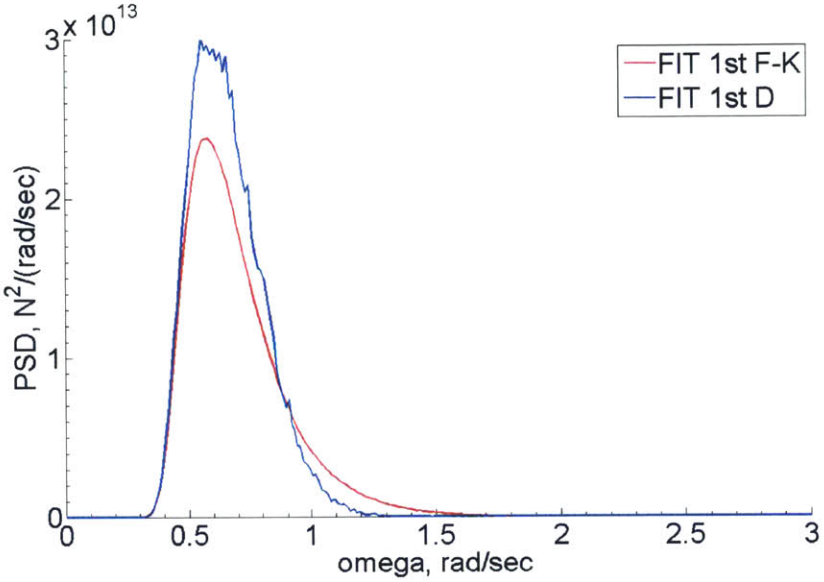

Figure 3-46: PSD comparison of 1st order surge hydrodynamic force components from FIT, r=9m, T=47.89m

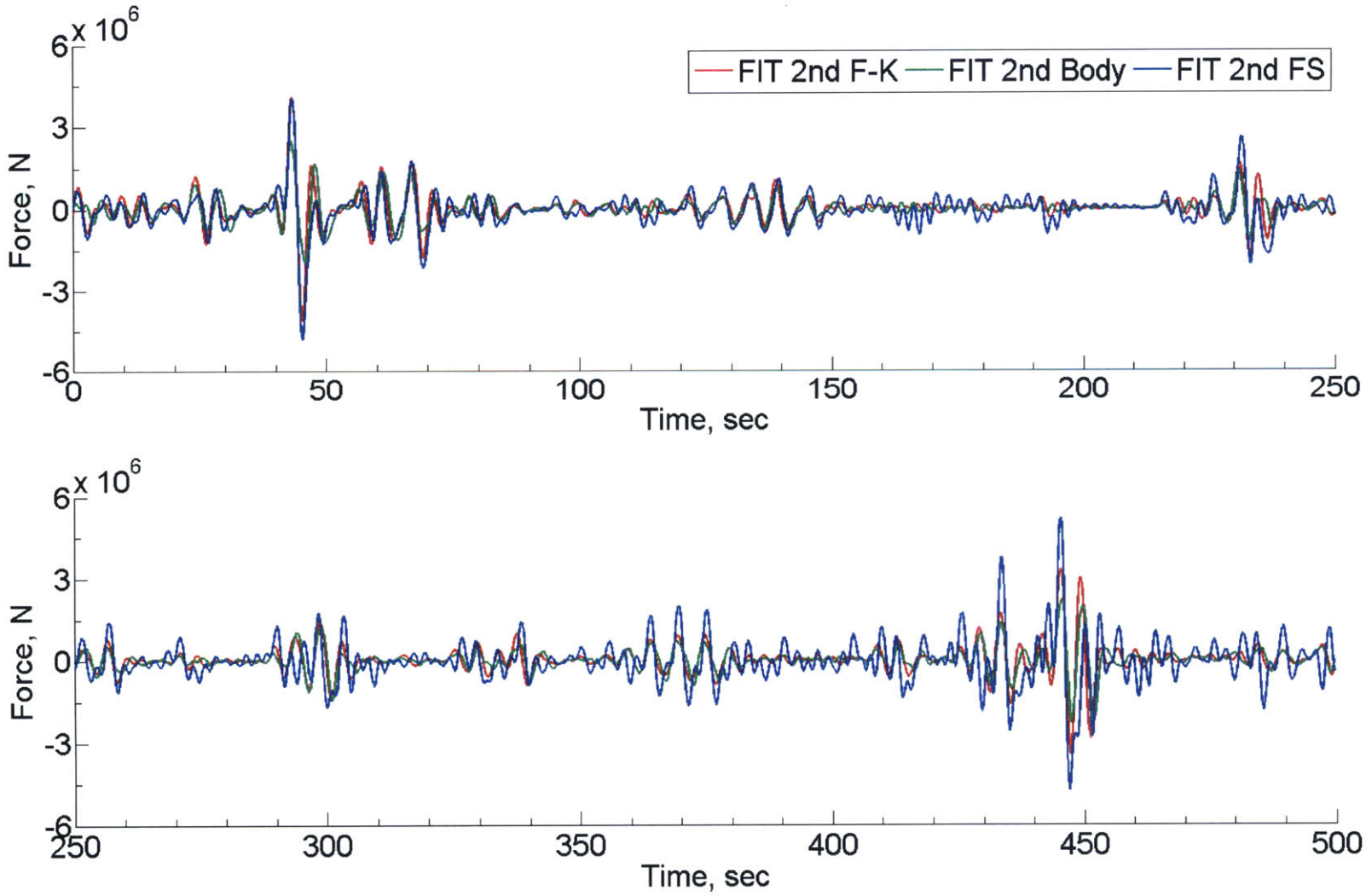

Figure 3-47: 2nd order surge hydrodynamic force components from FIT, r=9m, T=47.89m

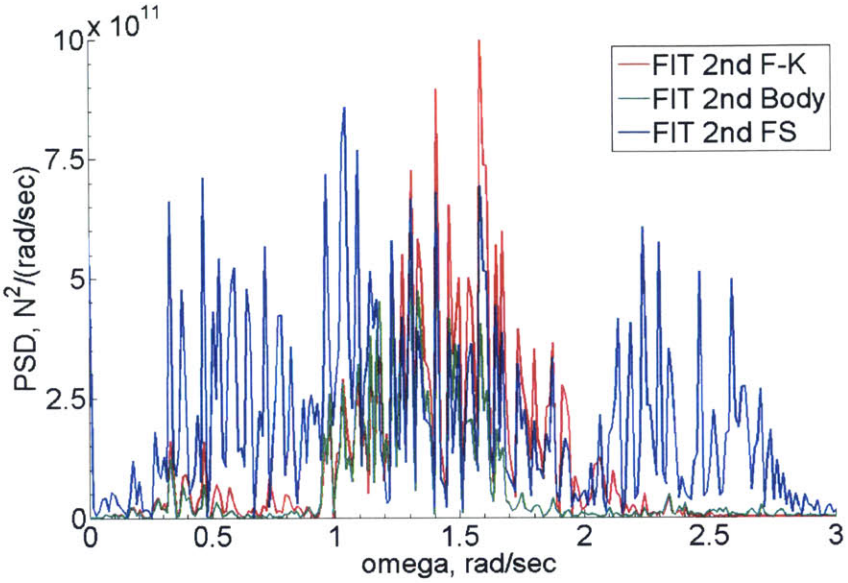

Figure 3-48: PSD comparison of 2nd order surge hydrodynamic force components from FIT, r=9m, T=47.89m

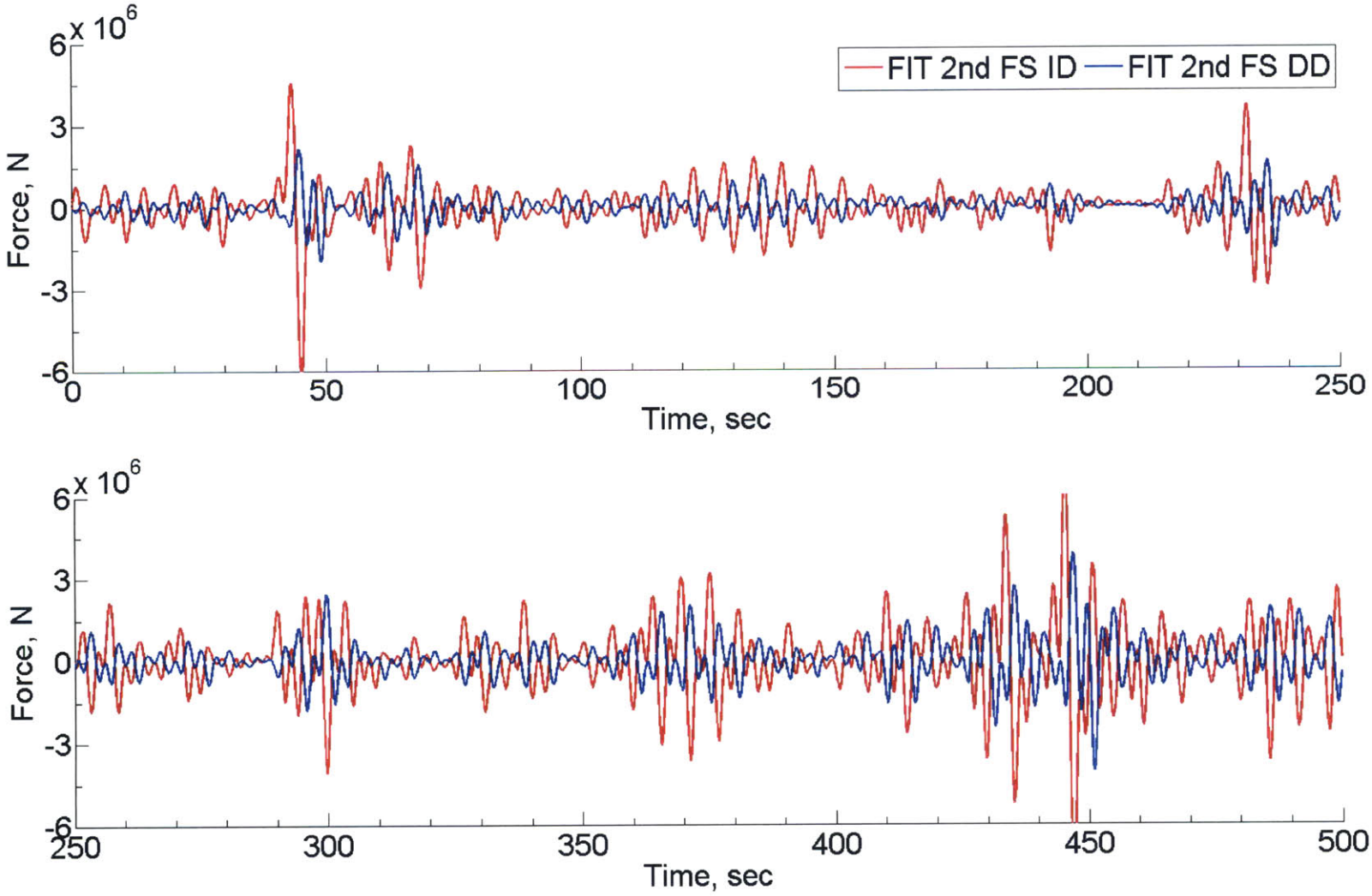

Figure 3-49: 2nd order surge free-surface impulse force components from FIT, r=9m, T=47.89m

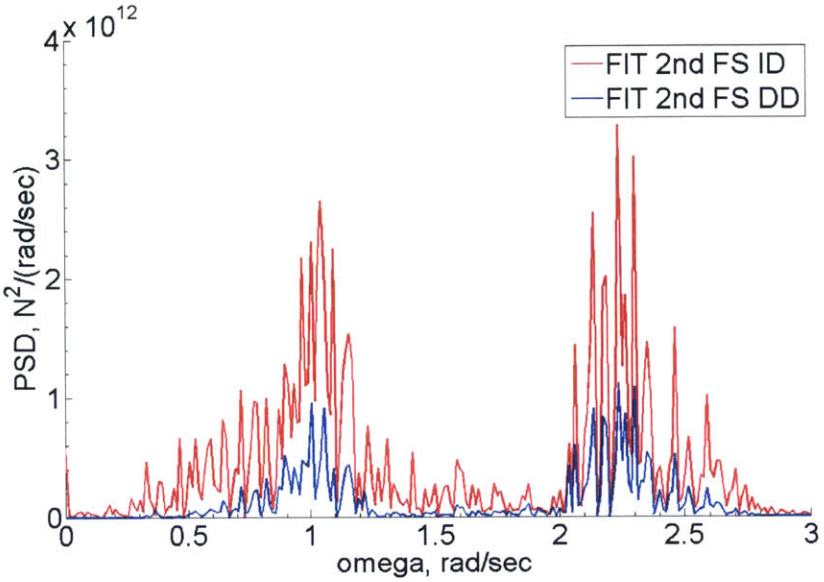

Figure 3-50: PSD comparison of 2nd order surge free-surface impulse force components from r=9m, T=47.89m

3.7.2 r=3m, T=43.2m

After numerical simulations on the cylindrical MIT/NREL TLP buoy, a slender buoy with a radius of 3 m and a draft of 43.2 m was studied. The buoy was treated in a different wave spectrum, an irregular sea state according to OC5 as shown in Figure 3-40 and 3-41. The characteristic wave frequency for this spectrum is $\omega_c = 0.4$rad/sec and the $Ka = 0.0459$ is small. The 936 panels mesh (Fig. 3-6) was selected to be used in this study. The time step of the time-domain simulations in FIT was 0.1 sec with a memory interval in the solution of the time convolution equation maintained at 18 sec.

In summary, results in this simulation suggested that both linear and nonlinear wave loads are important for a slender buoy in severe sea state. The time-marching solutions of the comparison of total, 1st and 2nd order surge force and its PSD analyses, as shown in Figure 3-51 to 3-53, shows that linear analysis is able to capture wave loads at the dominant wave frequency range (0.4 to 0.6 rad/sec), while nonlinear analysis provides the 2nd order solution which helps understand wave loads at sum- (1 to 1.6 rad/sec) and difference- (0.3 to 0.4 rad/sec) frequency range. The comparison between 1st order surge hydrodynamic force components in Figure 3-54 and 3-55 shows that both F-K and body disturbance forces are important for linear analysis, with body disturbance force almost resembles the amplitude and phase of its F-K counterpart. This corresponds to the theory suggested by G.I. Taylor in which the F-K and disturbance forces are close to equal to each other in the case of a slender body (long-wavelength approximation). The next set of plots which shows the comparison between 2nd order surge hydrodynamic force components in Figure 3-56 and 3-57 suggests that 2nd order quadratic effects are significant for all 2nd order components in FIT at sum- and difference frequencies, with the F-K, body and free-surface impulse forces providing comparable contributions to nonlinear wave loads. The final set of results for the comparison of 2nd order surge free-surface impulse force components as shown in Figure 3-58 and 3-59 demonstrates that for a buoy with small Ka values, the contributions from the ID components dominates the DD component as suggested

in [31].

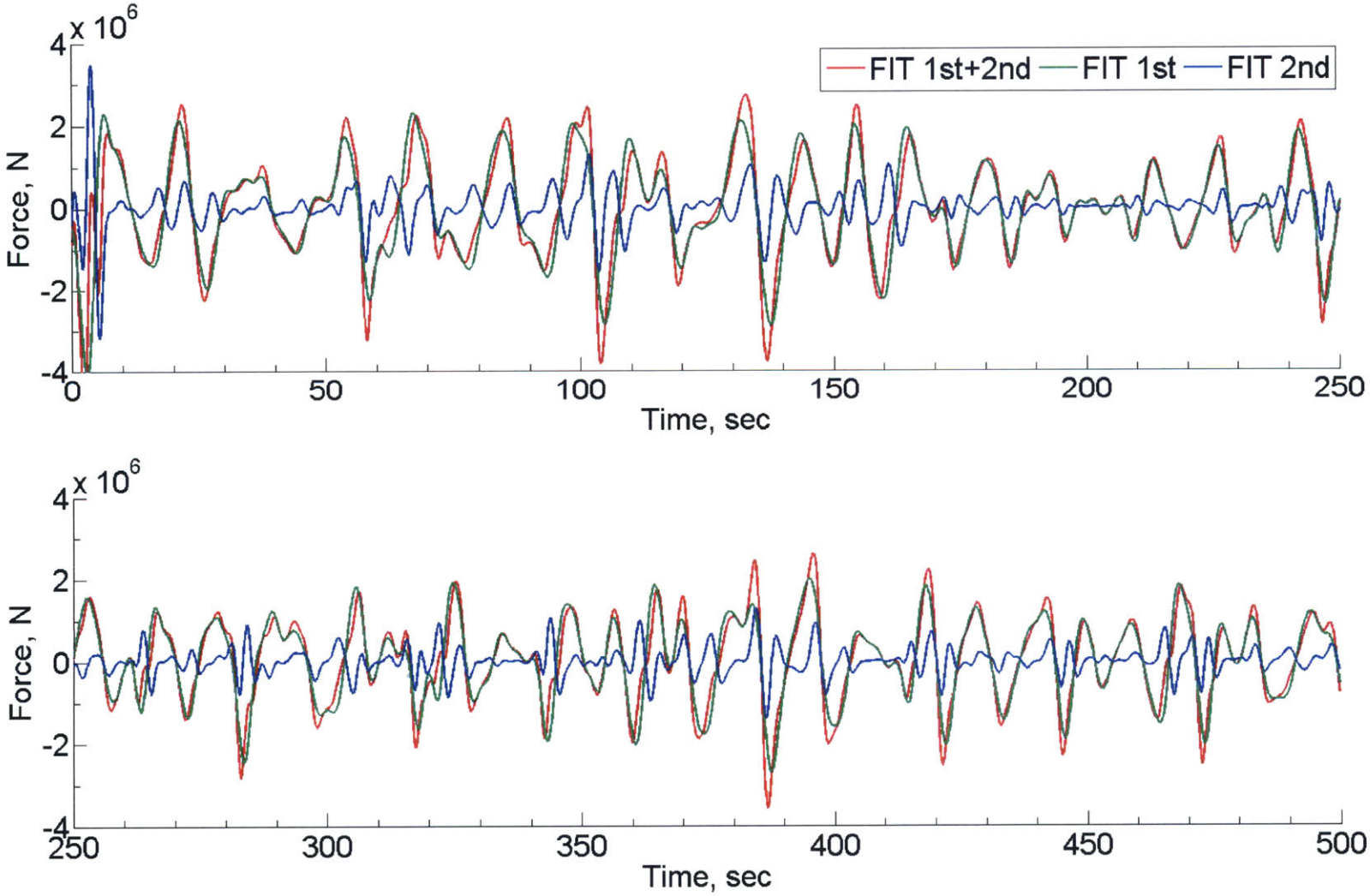

Figure 3-51: Surge hydrodynamic force from FIT, r=3m, T=43.2m

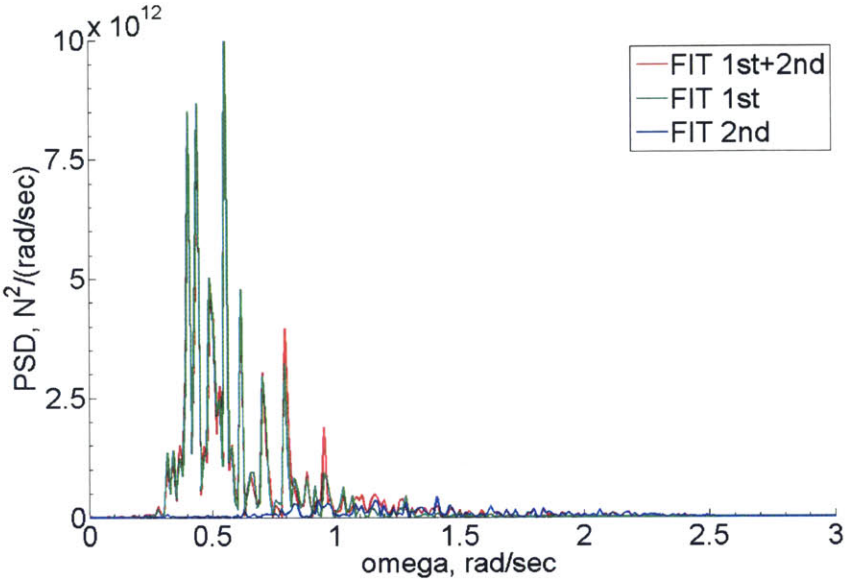

Figure 3-52: PSD comparison between total, 1st and 2nd order surge force from FIT, r=3m, T=43.2m

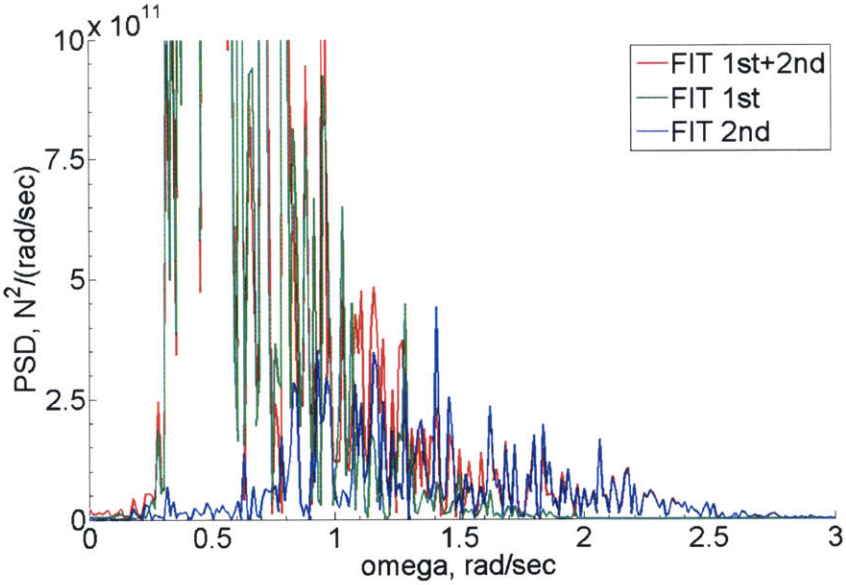

Figure 3-53: Close up of PSD comparison between total, 1st and 2nd order surge force from FIT, r=3m, T=43.2m

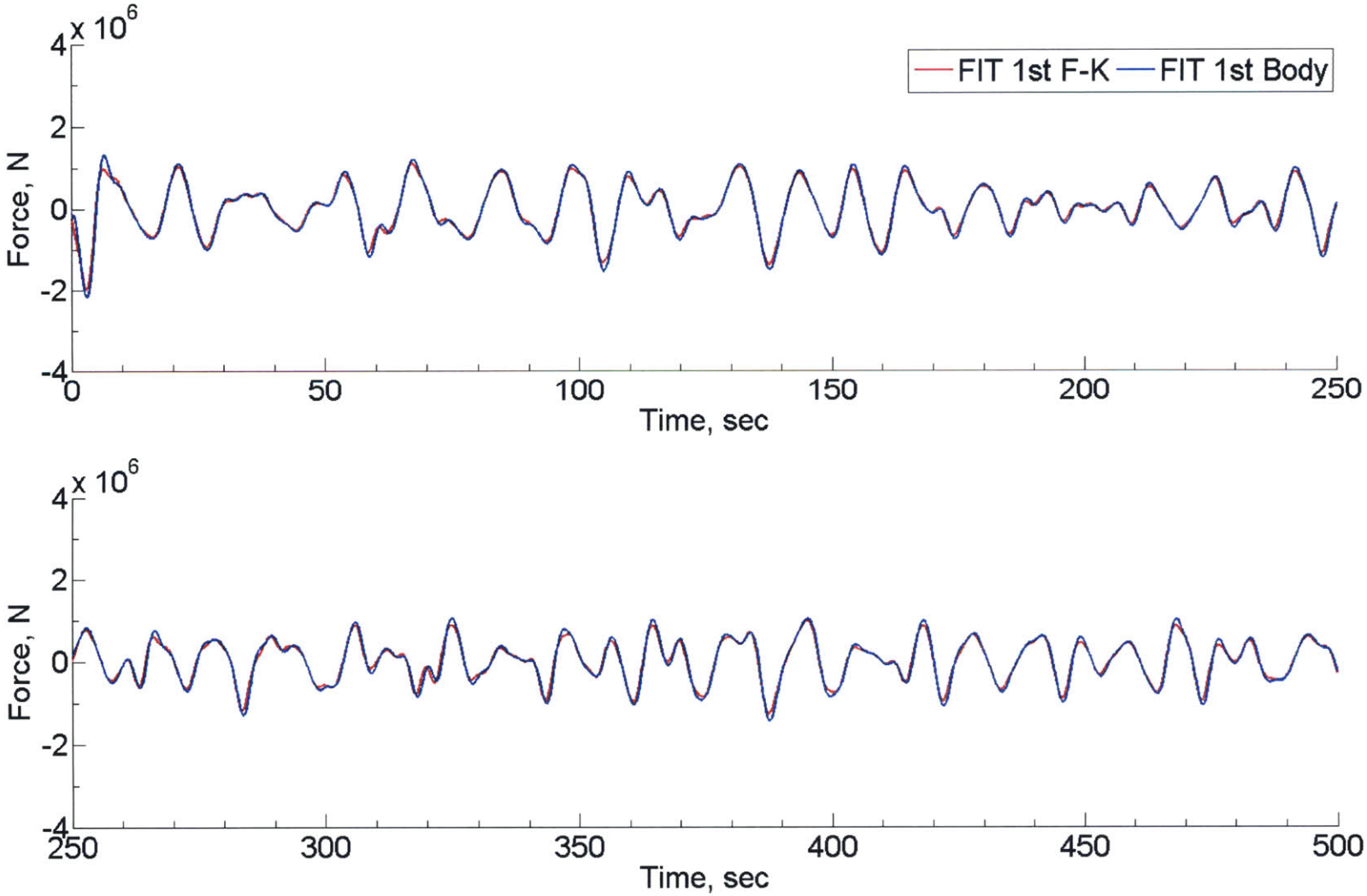

Figure 3-54: 1st order surge hydrodynamic force components from FIT, r=3m, T=43.2m

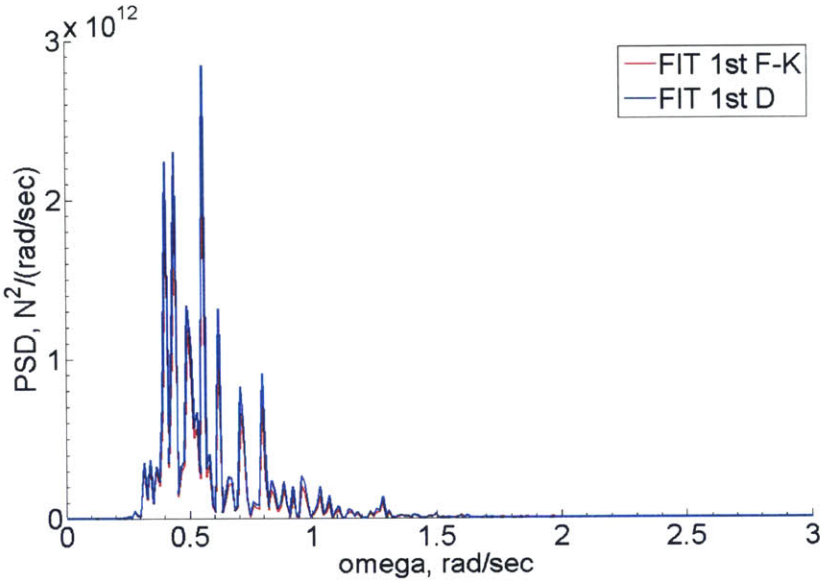

Figure 3-55: PSD comparison of 1st order surge hydrodynamic force components from FIT, r=3m, T=43.2m

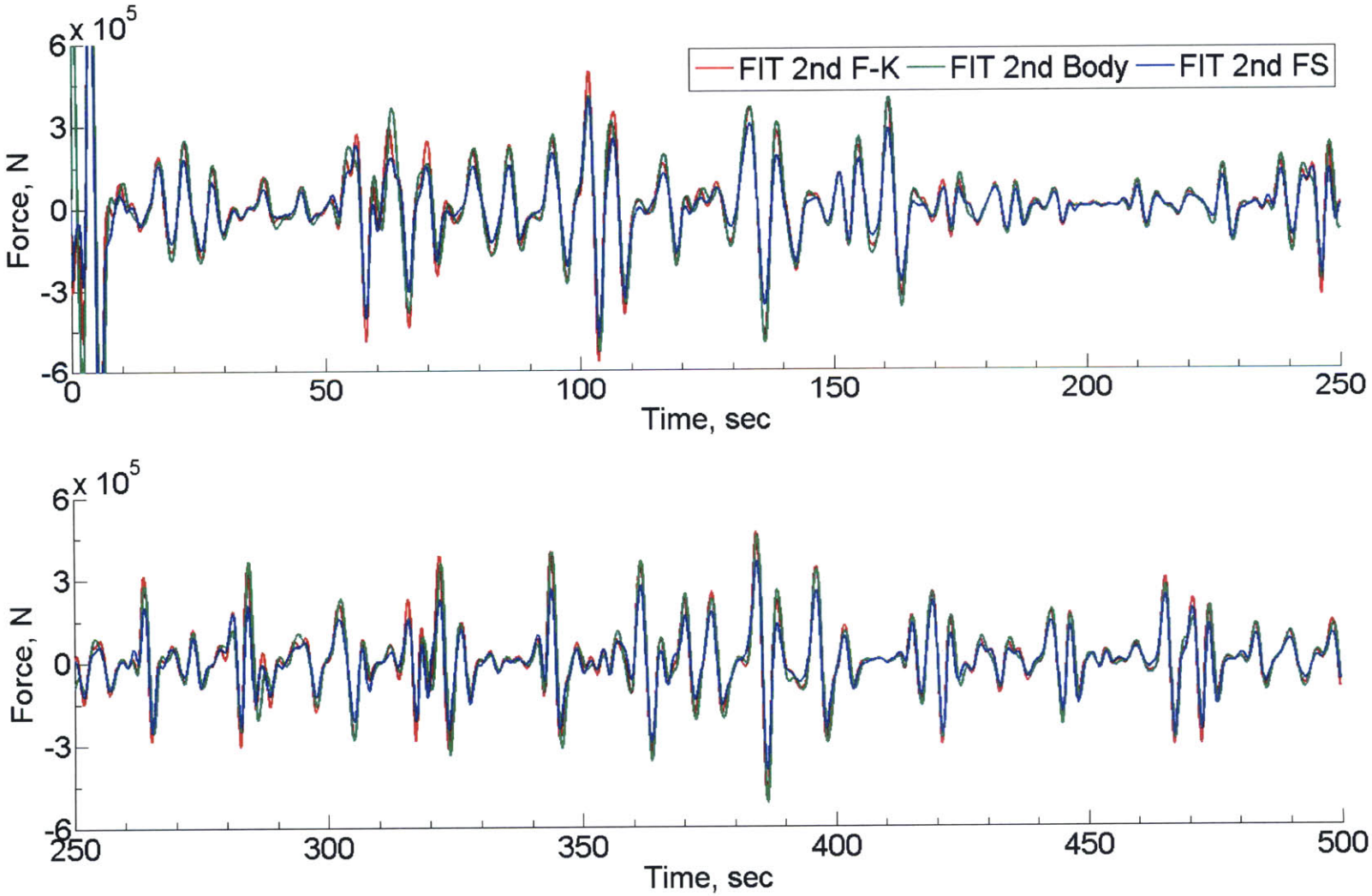

Figure 3-56: 2nd order surge hydrodynamic force components from FIT, r=3m, T=43.2m

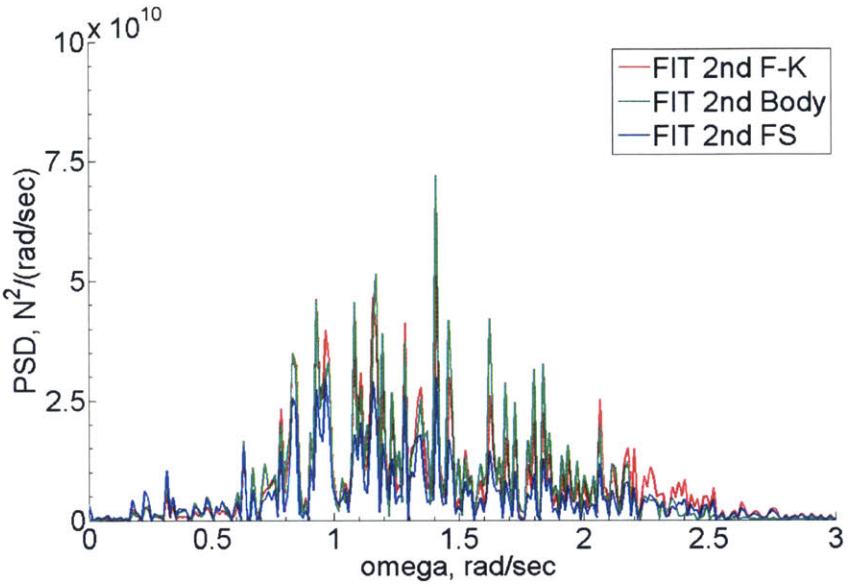

Figure 3-57: PSD comparison of 2nd order surge hydrodynamic force components from FIT, r=3m, T=43.2m

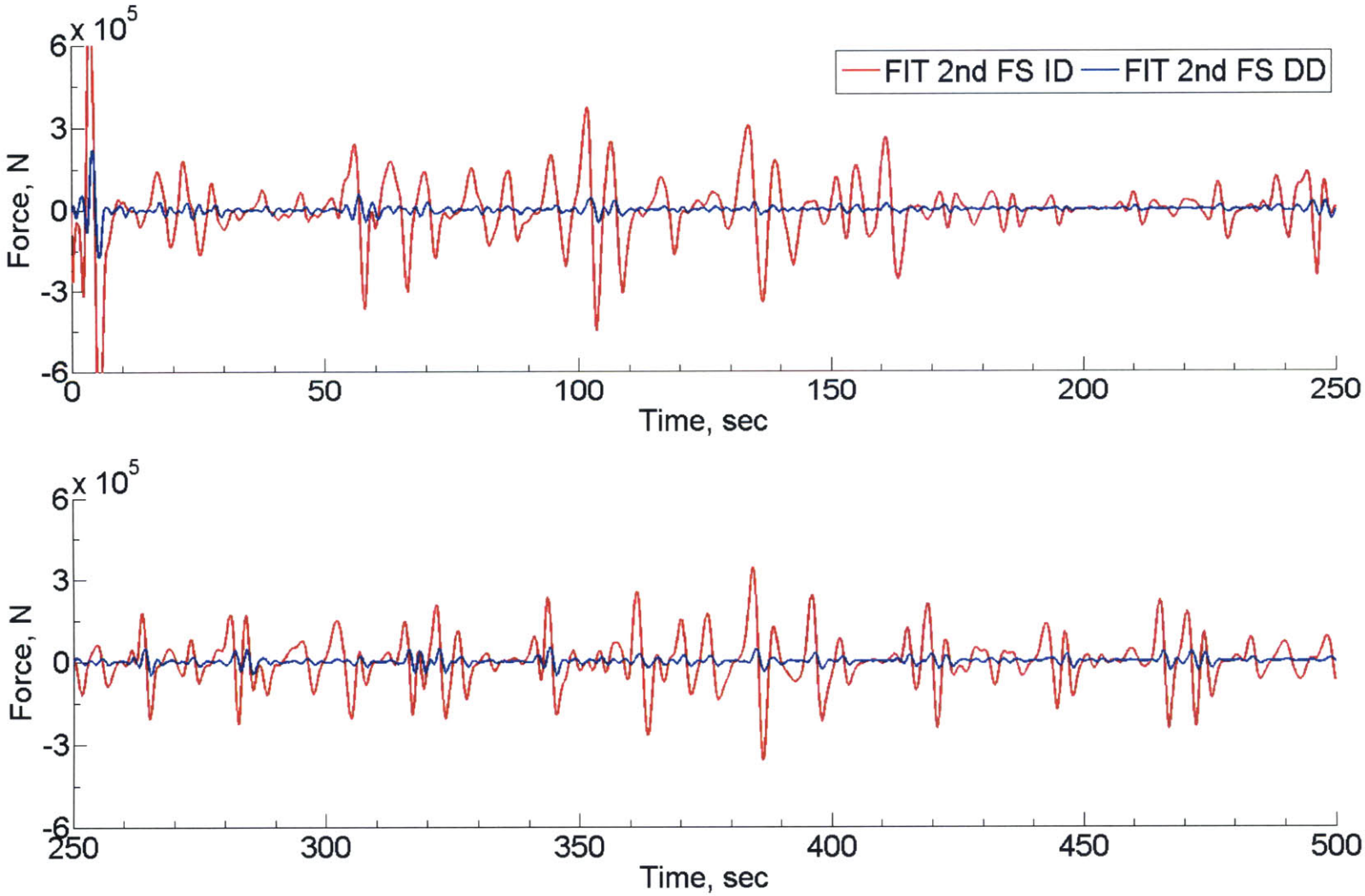

Figure 3-58: 2nd order surge free-surface impulse force components from FIT, r=3m, T=43.2m

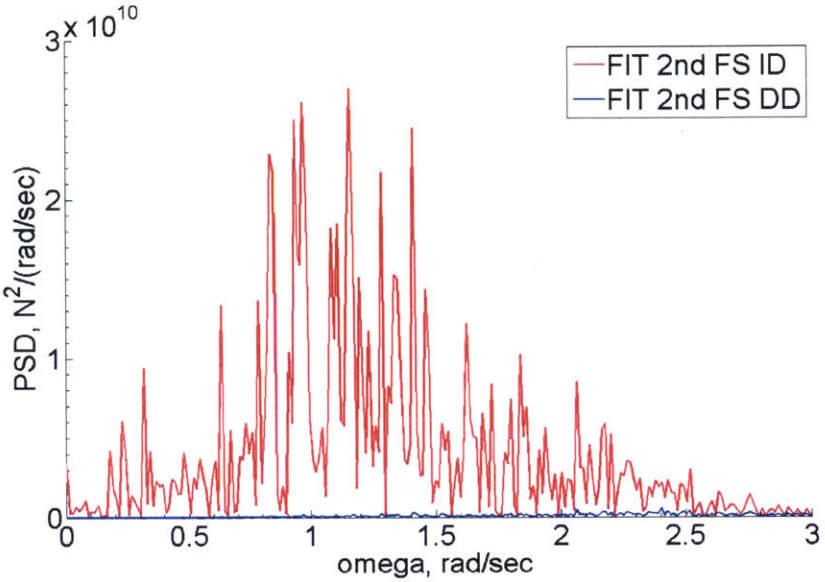

Figure 3-59: PSD comparison of 2nd order surge free-surface impulse force components from r=3m, T=43.2m

3.7.3 r=1.75m, T=30m

Another slender buoy with a radius of 1.75m and a draft of 30m was studied. This study was carried out to verify the slender buoy results obtained with the previous buoy of 3m radius and to provide a comparison to the MIT/NREL TLP as this set of results were obtained using the same JONSWAP spectrum with a 6-m significant wave height and a 12-sec peak-spectral wave period as shown in Figure 3-9 and 3-10. The characteristic wave frequency for this spectrum is again $\omega_c = 0.525$rad/sec, and in this study $Ka = 0.0492$, a small value. The 684 panels mesh (Fig. 3-7) was selected to be used in this study. The time step of the time-domain simulations in FIT was 0.1 sec with a memory interval in the solution of the time convolution equation of 18 sec.

In summary, results in this simulation again suggested that both linear and non-linear wave loads are important. The time-marching solutions of the comparison of total, 1st and 2nd order surge force and its PSD analyses, as shown in Figure 3-60 to 3-62, shows that linear analysis is able to capture wave loads at the dominant wave frequency range (0.5 to 0.8 rad/sec), while nonlinear analysis provides the 2nd order solution which helps understand wave loads at sum- (1.2 to 2 rad/sec) and difference- (0.3 to 0.4 rad/sec) frequency range. The comparison between 1st order surge hydrodynamic force components in Figure 3-63 and 3-64 shows that both F-K and body disturbance forces are important for linear analysis, with body disturbance force almost resembles the amplitude and phase of its F-K counterpart, again agreeing with the theory suggested by G.I. Taylor. The next set of plots which shows the comparison between 2nd order surge hydrodynamic force components in Figure 3-65 and 3-66 suggests that 2nd order quadratic effects are significant for all 2nd order components in FIT at sum- and difference frequencies, with the F-K, body and free-surface impulse forces provide comparable contributions to nonlinear wave loads. The final set of results for the comparison of 2nd order surge free-surface impulse force components as shown in Figure 3-67 and 3-68 demonstrates that for a buoy

with small Ka values, the contributions from the ID components dominates the DD component as suggested in [31].

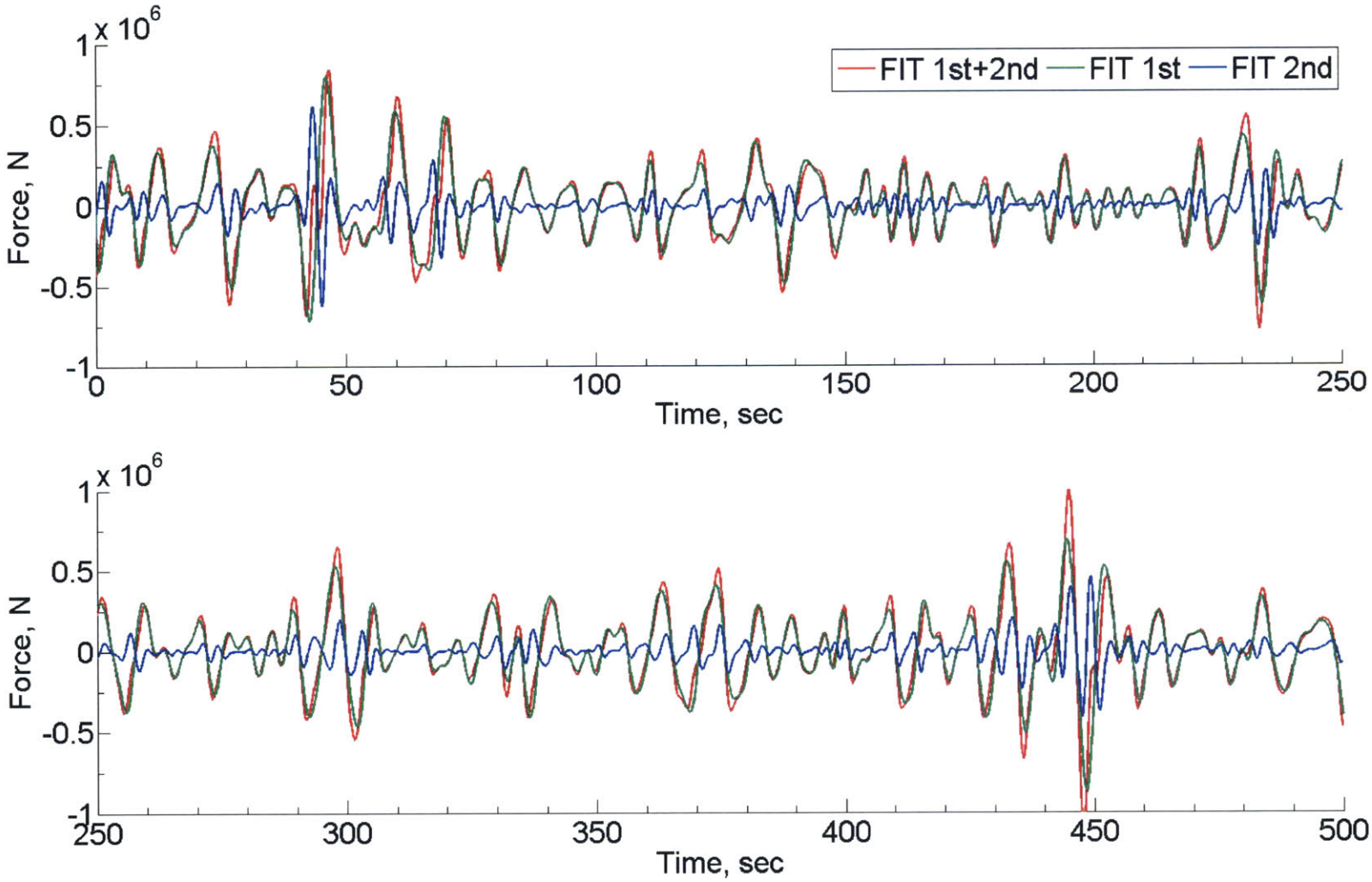

Figure 3-60: Surge hydrodynamic force from FIT, r=1.75m, T=30m

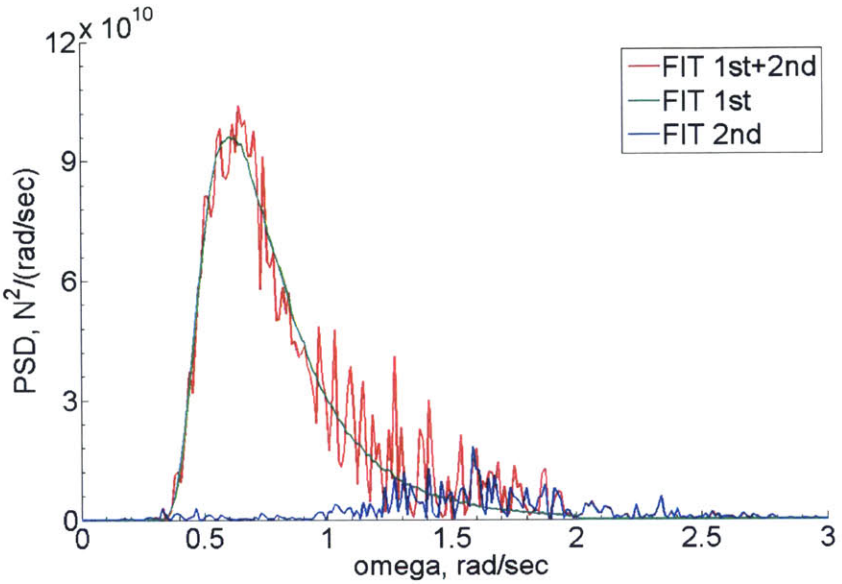

Figure 3-61: PSD comparison between total, 1st and 2nd order surge force from FIT, r=1.75m, T=30m

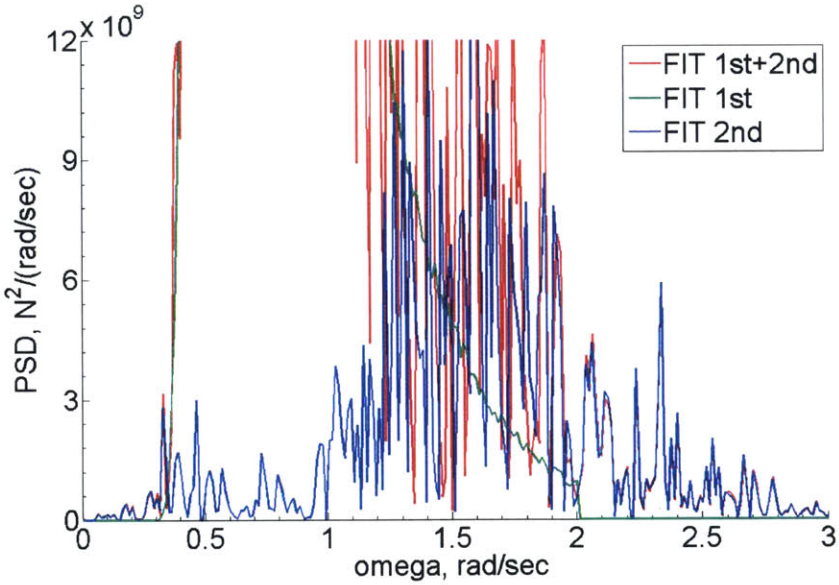

Figure 3-62: Close up of PSD comparison between total, 1st and 2nd order surge force from FIT, r=1.75m, T=30m

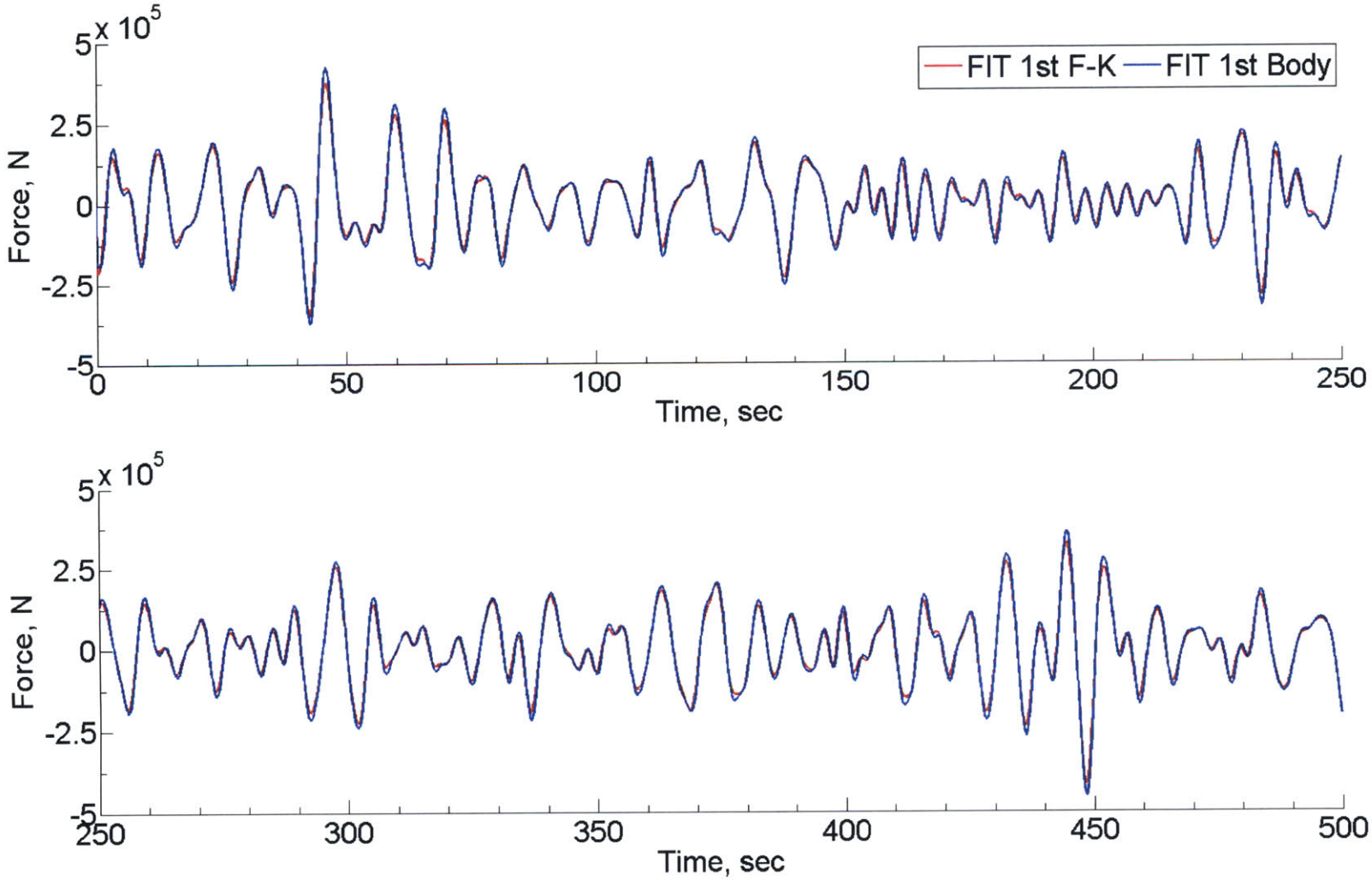

Figure 3-63: 1st order surge hydrodynamic force components from FIT, r=1.75m, T=30m

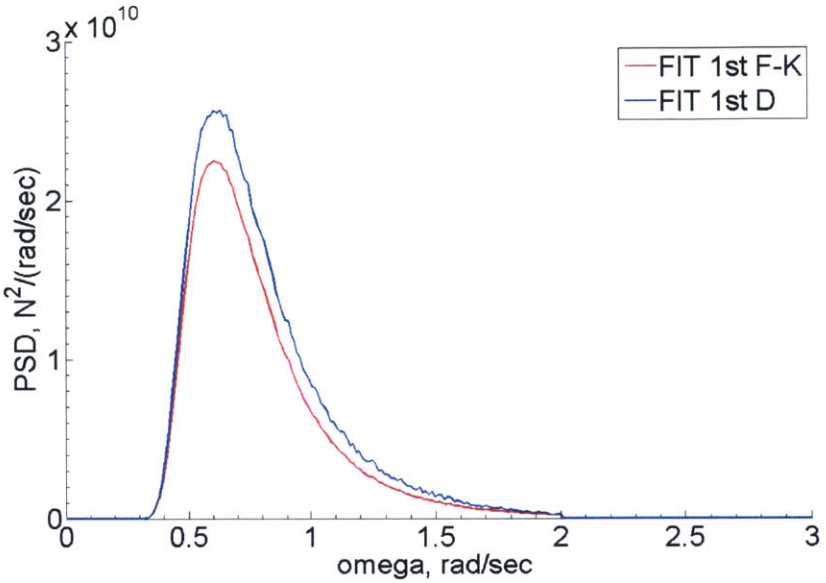

Figure 3-64: PSD comparison of 1st order surge hydrodynamic force components from FIT, r=1.75m, T=30m

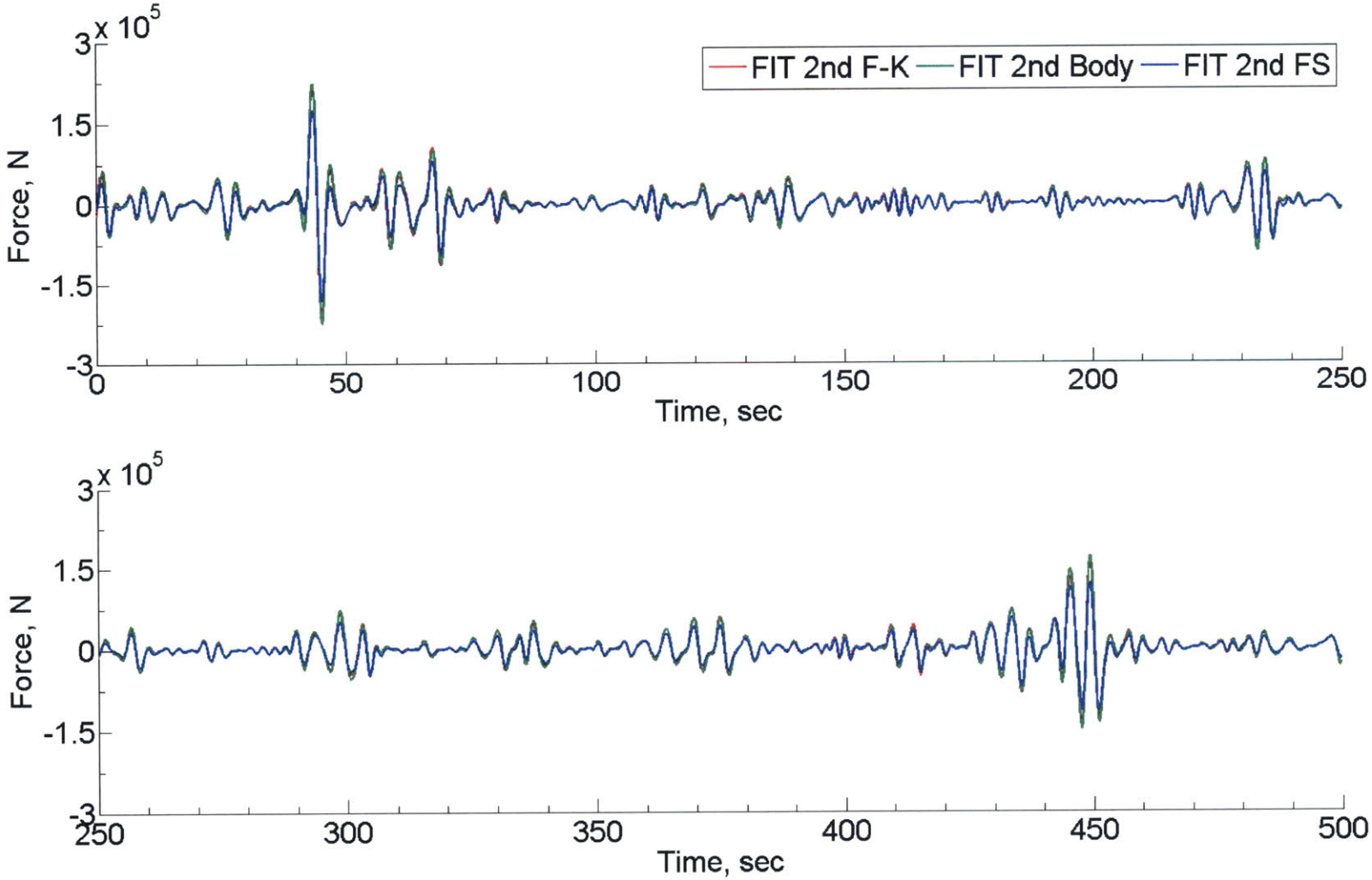

Figure 3-65: 2nd order surge hydrodynamic force components from FIT, r=1.75m, T=30m

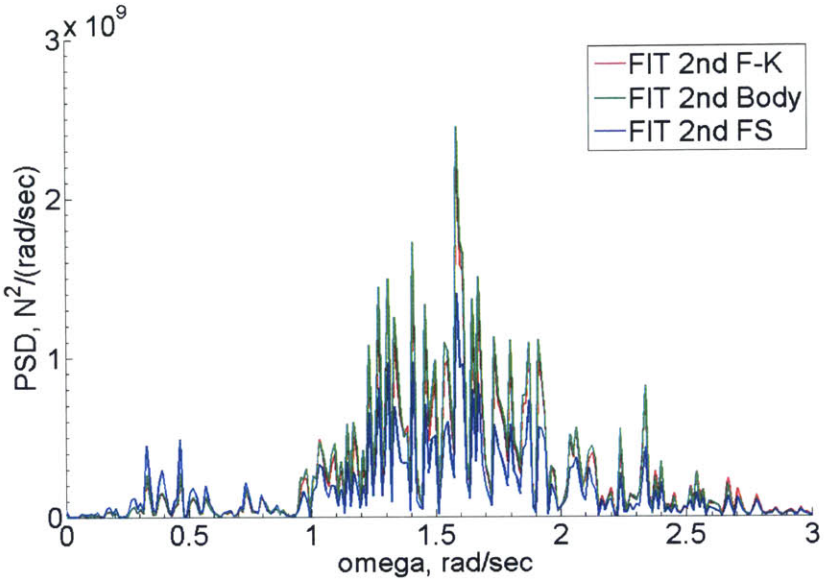

Figure 3-66: PSD comparison of 2nd order surge hydrodynamic force components from r=1.75m, T=30m

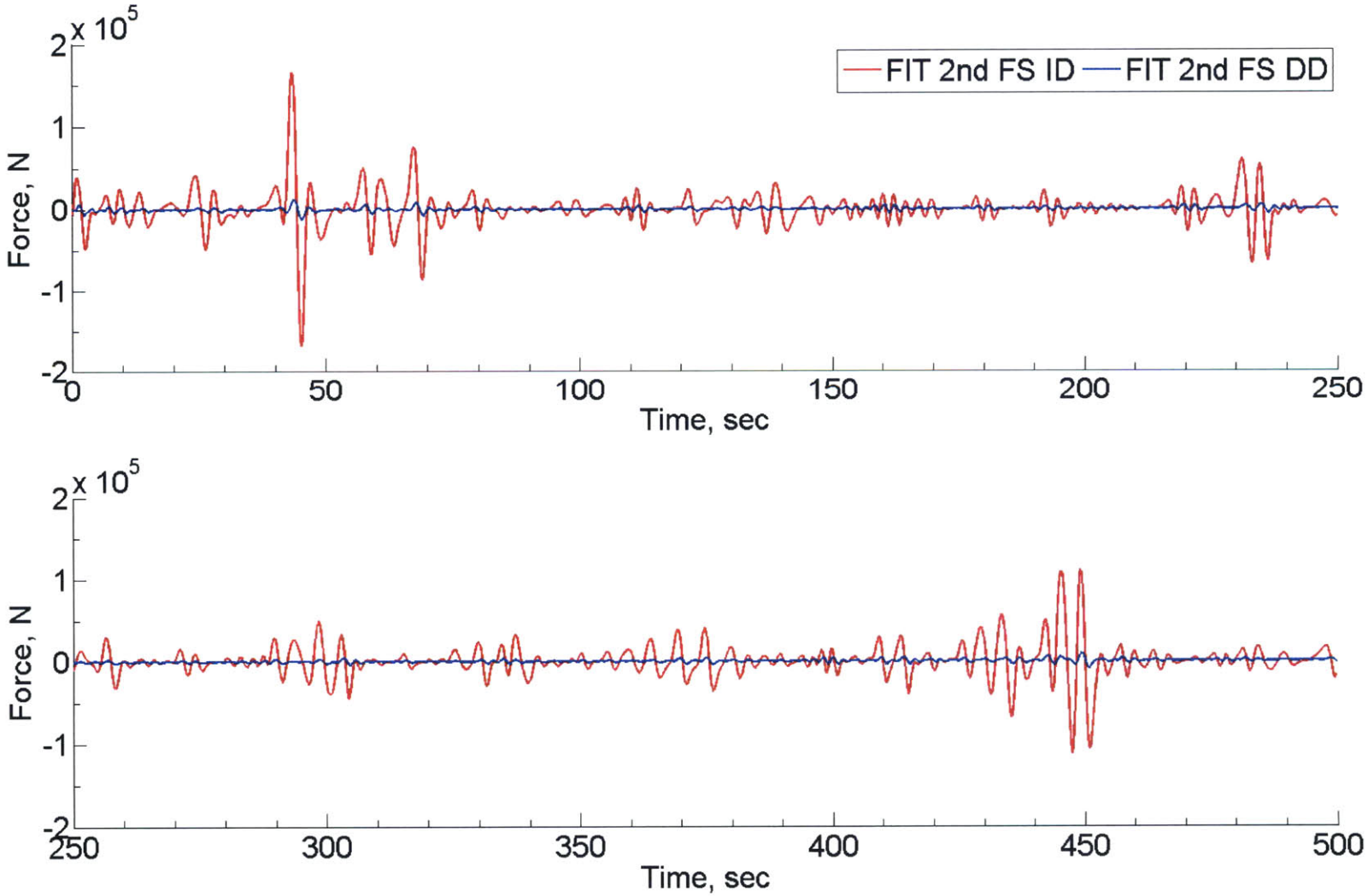

Figure 3-67: 2nd order surge free-surface impulse force components from FIT, r=1.75m, T=30m

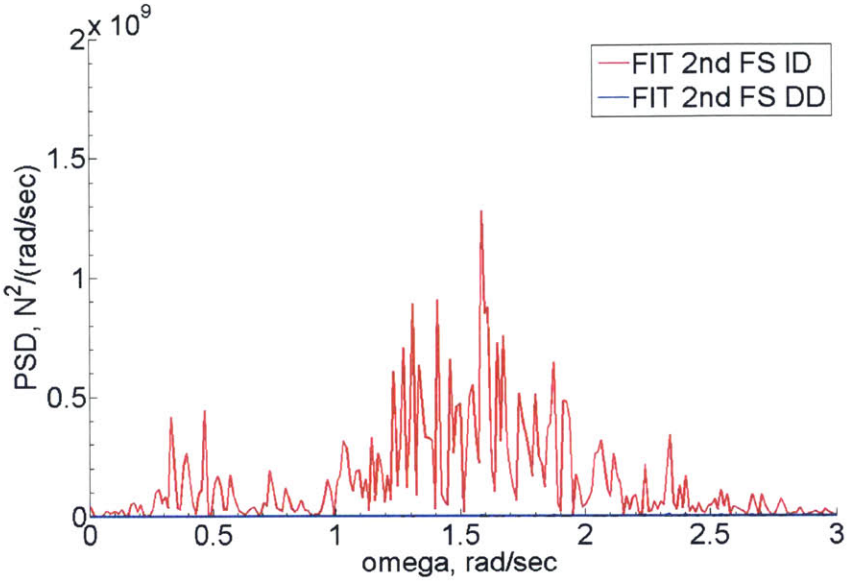

Figure 3-68: PSD comparison of 2nd order surge free-surface impulse force components from r=1.75m, T=30m

3.8 Comparison between Small Ka with FIT full expression

In addition to the numerical study of the FIT full expression in the previous sections, a study on the performance of the FIT small Ka approximation as described in Section 2.5 and [31]. This study was inspired by the results obtained in the previous sections in which the ID component of the free-surface impulse force was found to be much larger than its DD counterpart for slender cylinder. It was therefore hypothesized that the DD component can be omitted when computing nonlinear wave loads for slender cylinder with small Ka. The goal of this study is then to understand if the small Ka approximation improves the computational efficiency of the linear and nonlinear wave loads for slender cylinders while retaining the capability of capture nonlinear contributions from the free-surface impulse force. The advantage of the small Ka approximation is that the method does not require the discretization of surfaces, as it is a slender body method and only require integrations over the vertical direction, which greatly reduces computational cost.

The results are presented as follow. The total surge hydrodynamic force, including the 1st and 2nd order F-K, body impulse and free-surface impulse force, was compared between FIT full expression and its small Ka approximation. The time-marching results and PSDs for the MIT/NREL TLP and for the slender buoys of radius 3m and 1.75m were plotted in the Subsection 3.8.1. The results obtained for the FIT full expression are obtained through the simulations described in Section 3.7, while the results for the small Ka approximation were computed according to the theory presented in Section 2.5. The free-surface impulse force between the two methods on all three buoys were then compared between FIT full expression and its small Ka approximation in Subsection 3.8.2.

3.8.1 1st + 2nd Order Surge Force Comparison

In summary, the small Ka approximation was found to be able to capture the majority of wave loads computed by FIT full expression. The comparison between FIT full expression and small Ka approximation for the two simulations suggests that FIT full expression still captures more nonlinearities at the peaks of the responses in the time-marching solutions in Figure 3-72 and 3-75. The PSDs in Figure 3-74 and ?? agrees with the time-marching solutions and showed that overall the magnitude of the wave loads captured by the full expression is slightly higher than the small Ka approximation over all wave frequencies. Both FIT full expression and small Ka approximation was able to capture nonlinear wave loads at high frequencies. For the comparison between FIT full expression and small Ka approximation for wave loads on the MIT/NREL TLP, which has a an intermediate diameter and a finite Ka value, the approximation becomes less accurate as it over estimate responses at higher frequencies as shown in Figure 3-69 and 3-70. The important conclusion drawn from this study was that for slender cylinders with small Ka, a simplified expression which was reduced to a 1D integral was able to capture the majority of linear and nonlinear wave loads in irregular seastates, allowing efficient evaluation of nonlinear wave loads on slender cylinders using FIT.

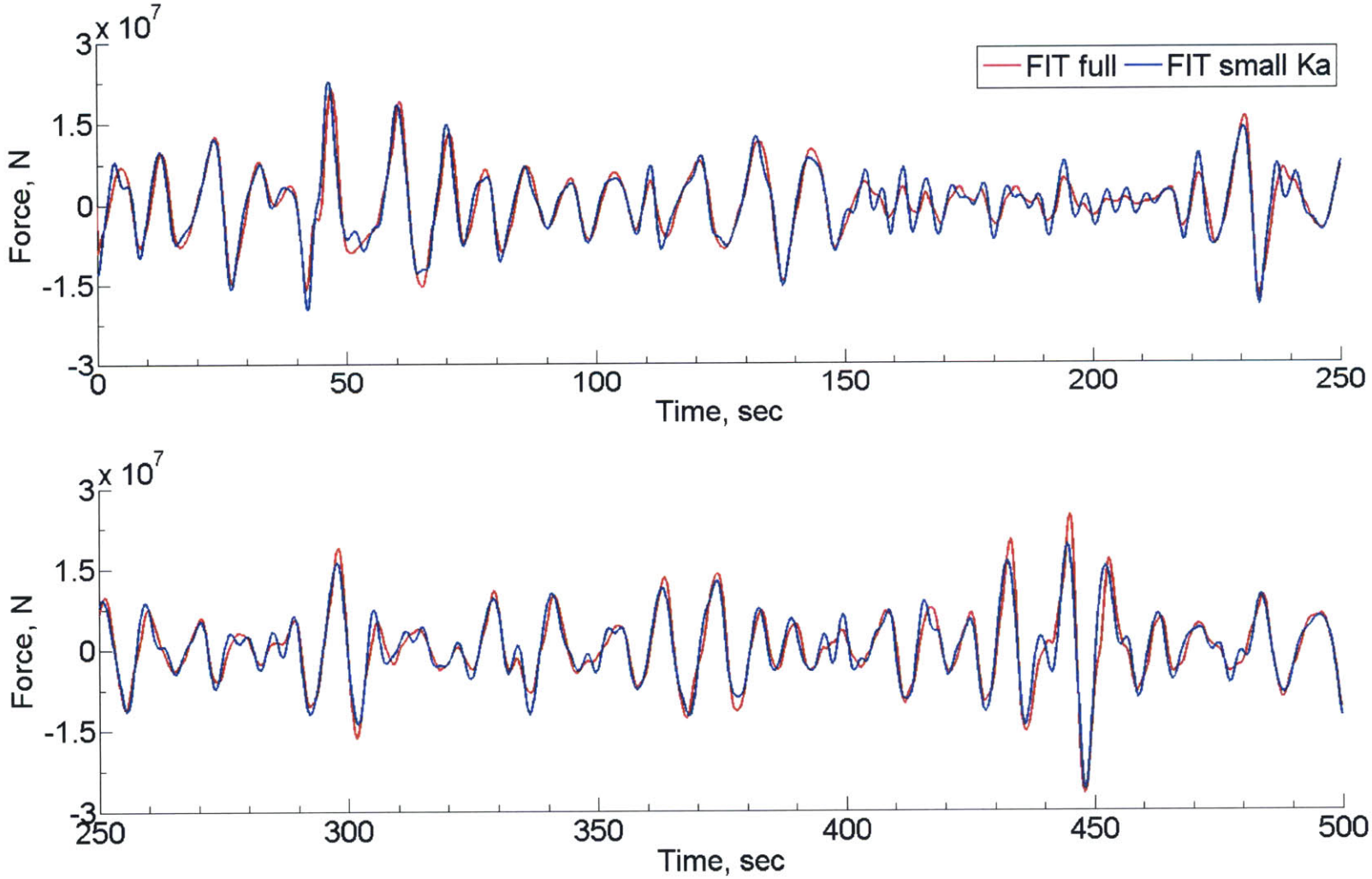

Figure 3-69: Total surge hydrodynamic force between FIT full expression and small Ka approx., r=9m, T=47.89m

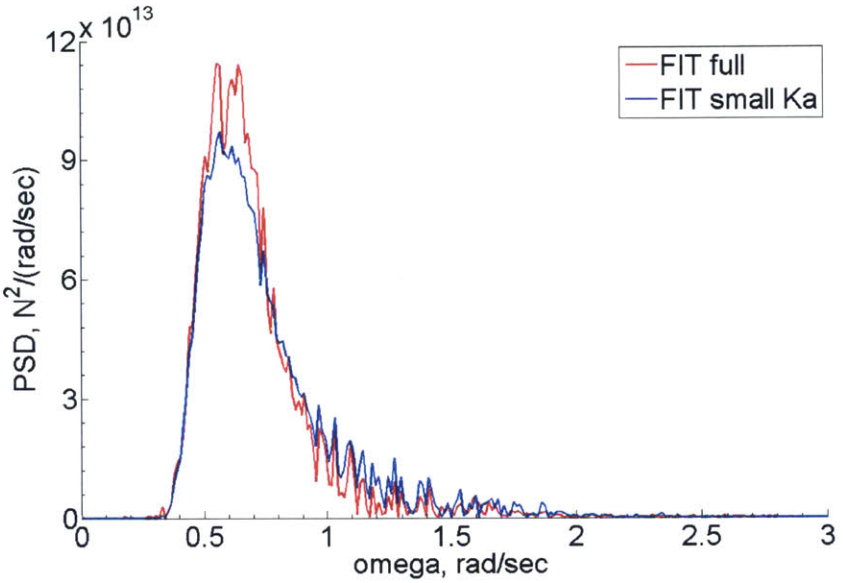

Figure 3-70: PSD comparison between FIT full expression and small Ka approx. for total surge hydrodynamic force, r=9m, T=47.89m

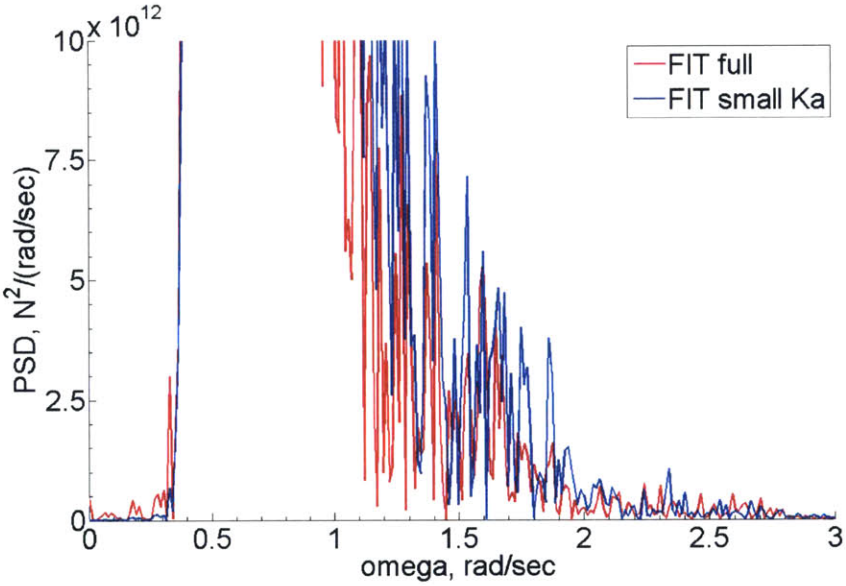

Figure 3-71: Close up of PSD comparison between FIT full expression and small Ka approx. for total surge hydrodynamic force, r=9m, T=47.89m

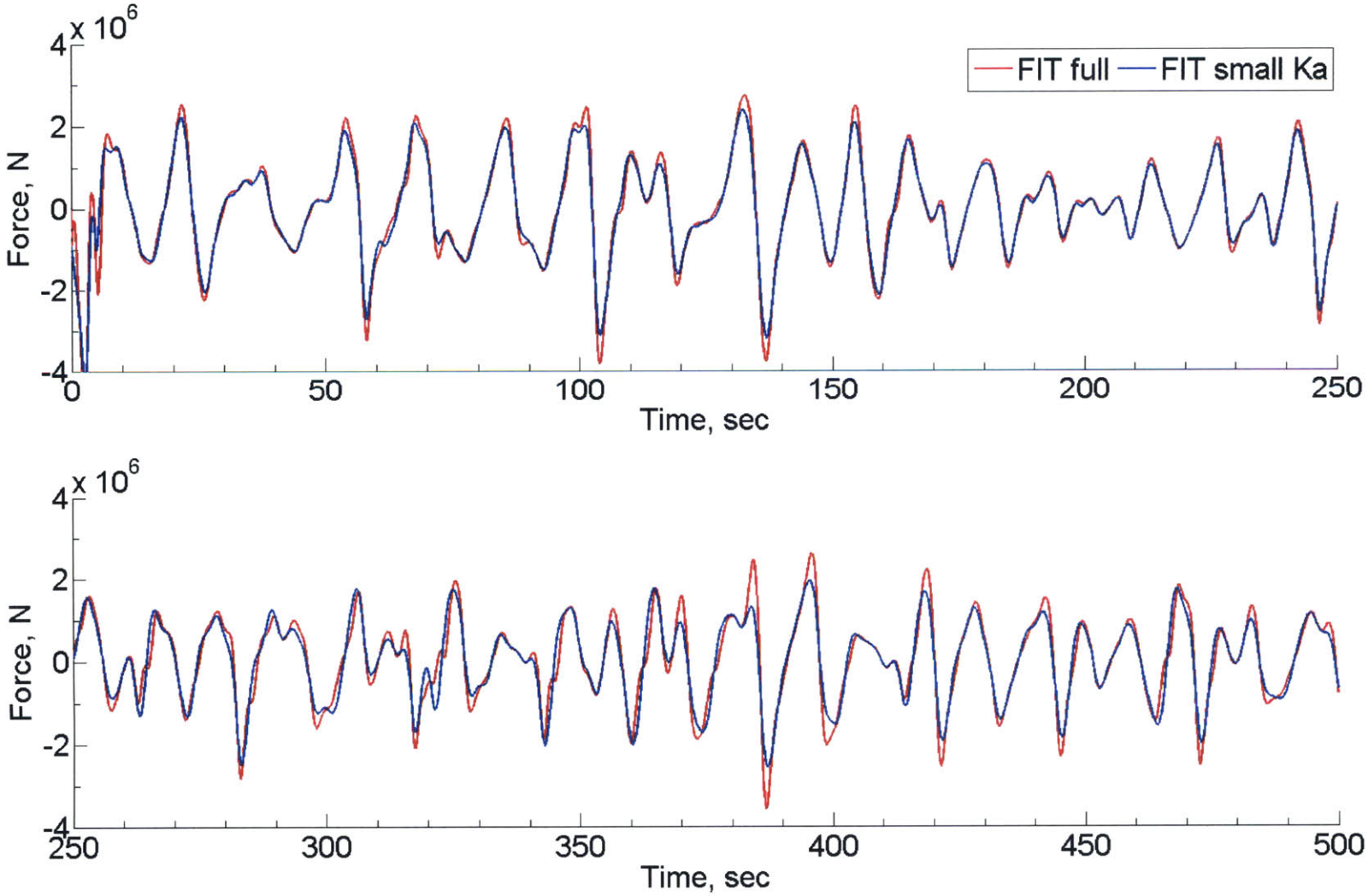

Figure 3-72: Total surge hydrodynamic force between FIT full expression and small Ka approx., r=3m, T=43.2m

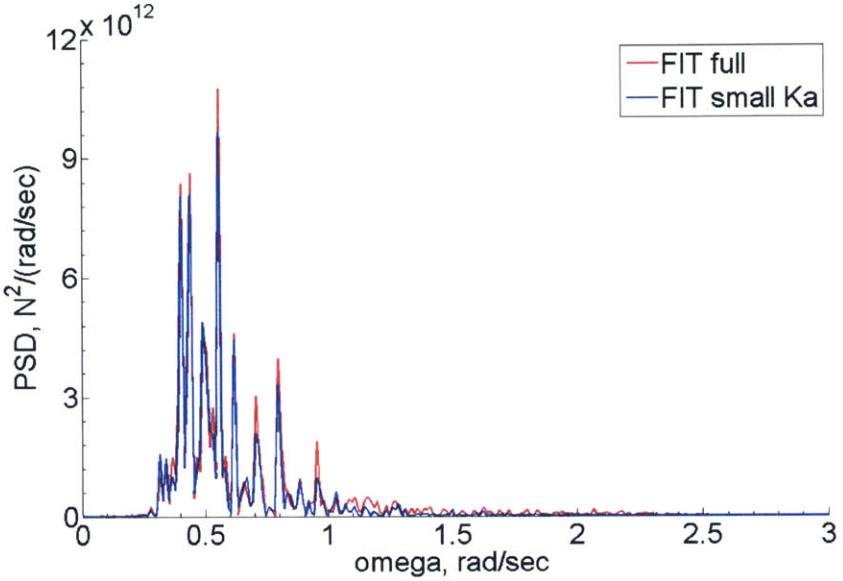

Figure 3-73: PSD comparison between FIT full expression and small Ka approx. for total surge hydrodynamic force, r=3m, T=43.2m

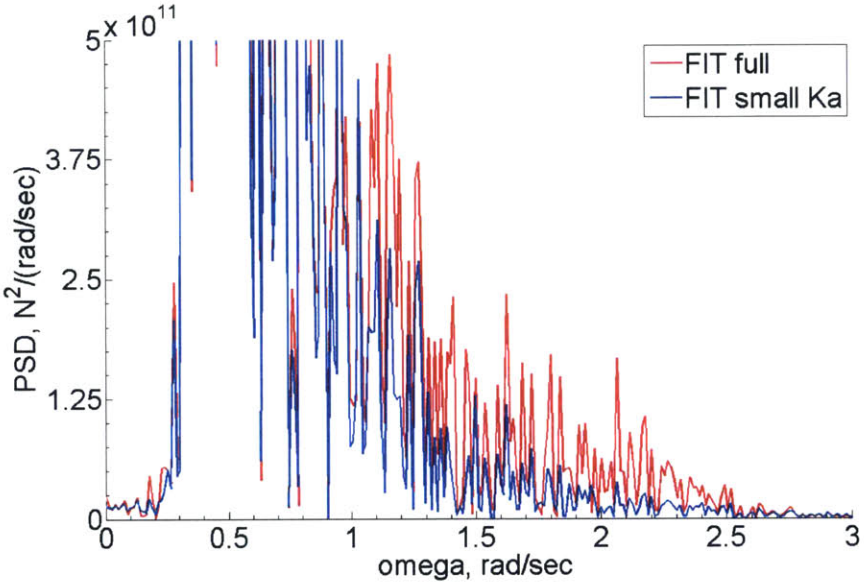

Figure 3-74: Close up of PSD comparison between FIT full expression and small Ka approx. for total surge hydrodynamic force, r=3m, T=43.2m

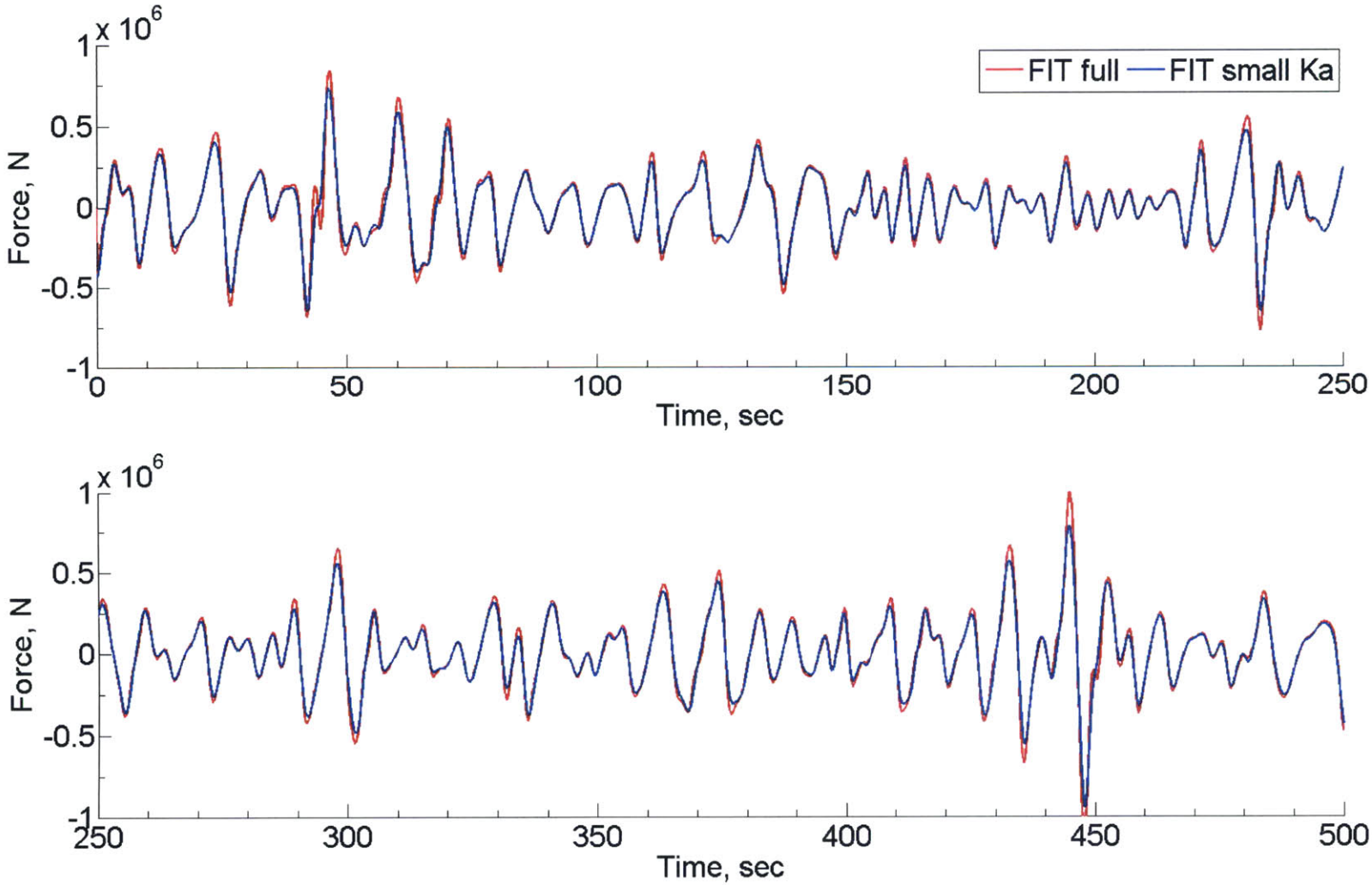

Figure 3-75: Total surge hydrodynamic force between FIT full expression and small Ka approx., r=1.75m, T=30m

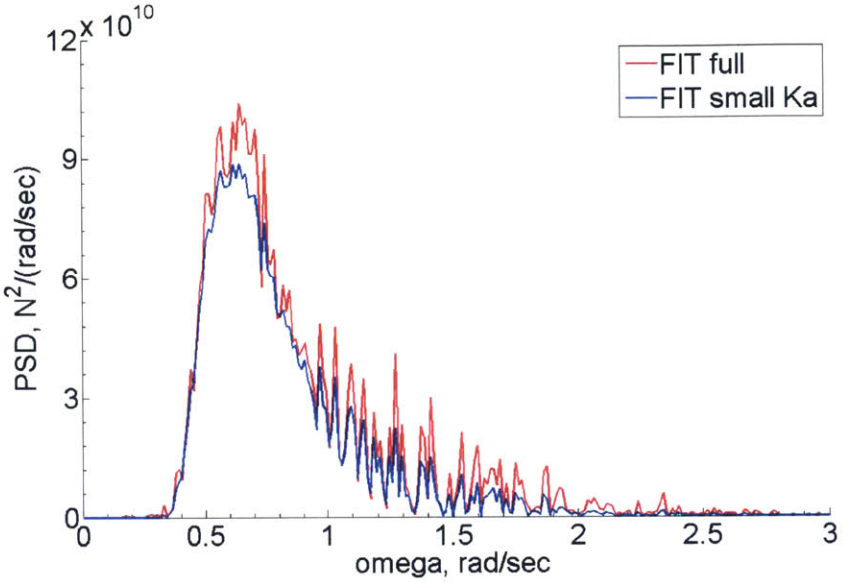

Figure 3-76: PSD comparison between FIT full expression and small Ka approx. for total surge hydrodynamic force, r=1.75m, T=30m

3.8.2 Free-Surface Surge Force Comparison

For the free-surface impulse force, the small Ka approximation falls short on accurately capturing nonlinear wave responses when compared to the FIT full expression for finite Ka, as expected from the theory. It can be seen in Figure 3-77 that the correspondence between time-marching solutions obtained by the two methods are in little agreement. In the PSD graph, Figure 3-78, the FIT full expression was able to capture nonlinear effects over all frequency range while the small Ka approximation provided only wave loads at sum- and difference- frequency. The two numerical comparison between FIT full expressions and small Ka approximation with cylinders with small Ka (slenderer buoy of radius 3m and 1.75m) in Figure 3-79 to 3-82 performs better than finite Ka. The comparisons for the two slender cylinders suggest that although FIT full expression captures more nonlinearities at the peaks of the wave loads in the time-marching solution when compared to the small Ka approximation, both methods were able to capture wave loads at the same sum- and difference- frequency range for nonlinear load analysis.

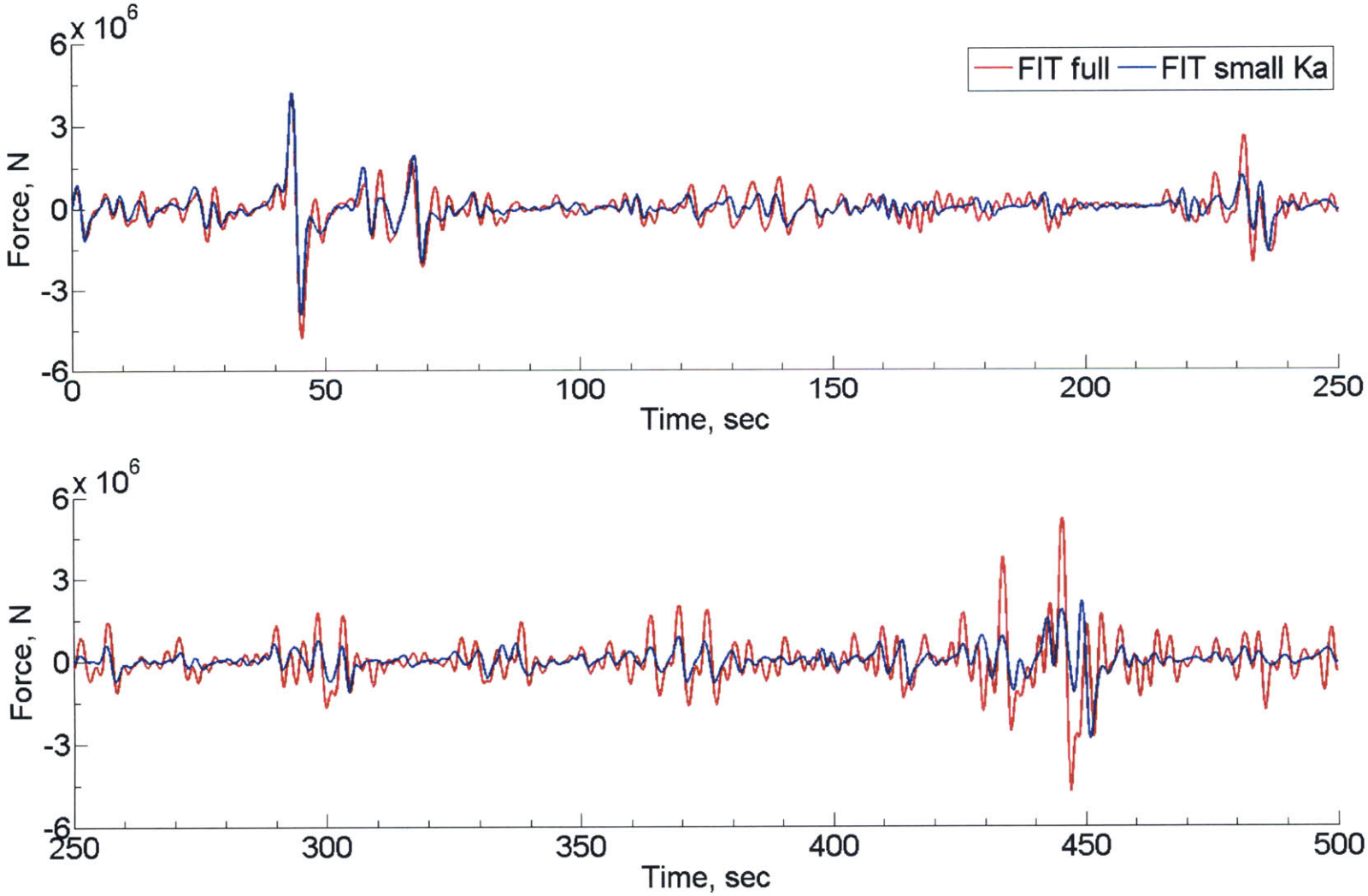

Figure 3-77: Free-surface surge hydrodynamic force between FIT full expression and small Ka approx., r=9m, T=47.89m

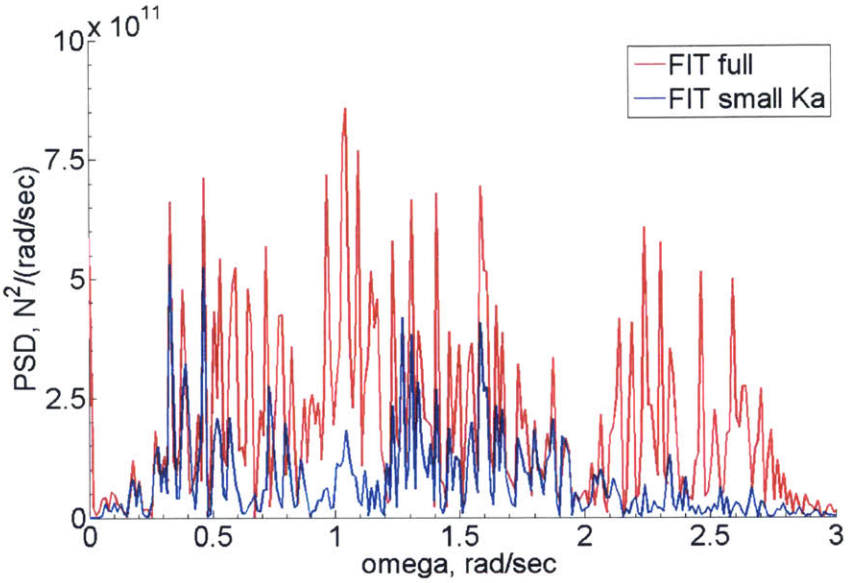

Figure 3-78: PSD comparison between FIT full expression and small Ka approx. for free-surface surge hydrodynamic force, r=9m, T=47.89m

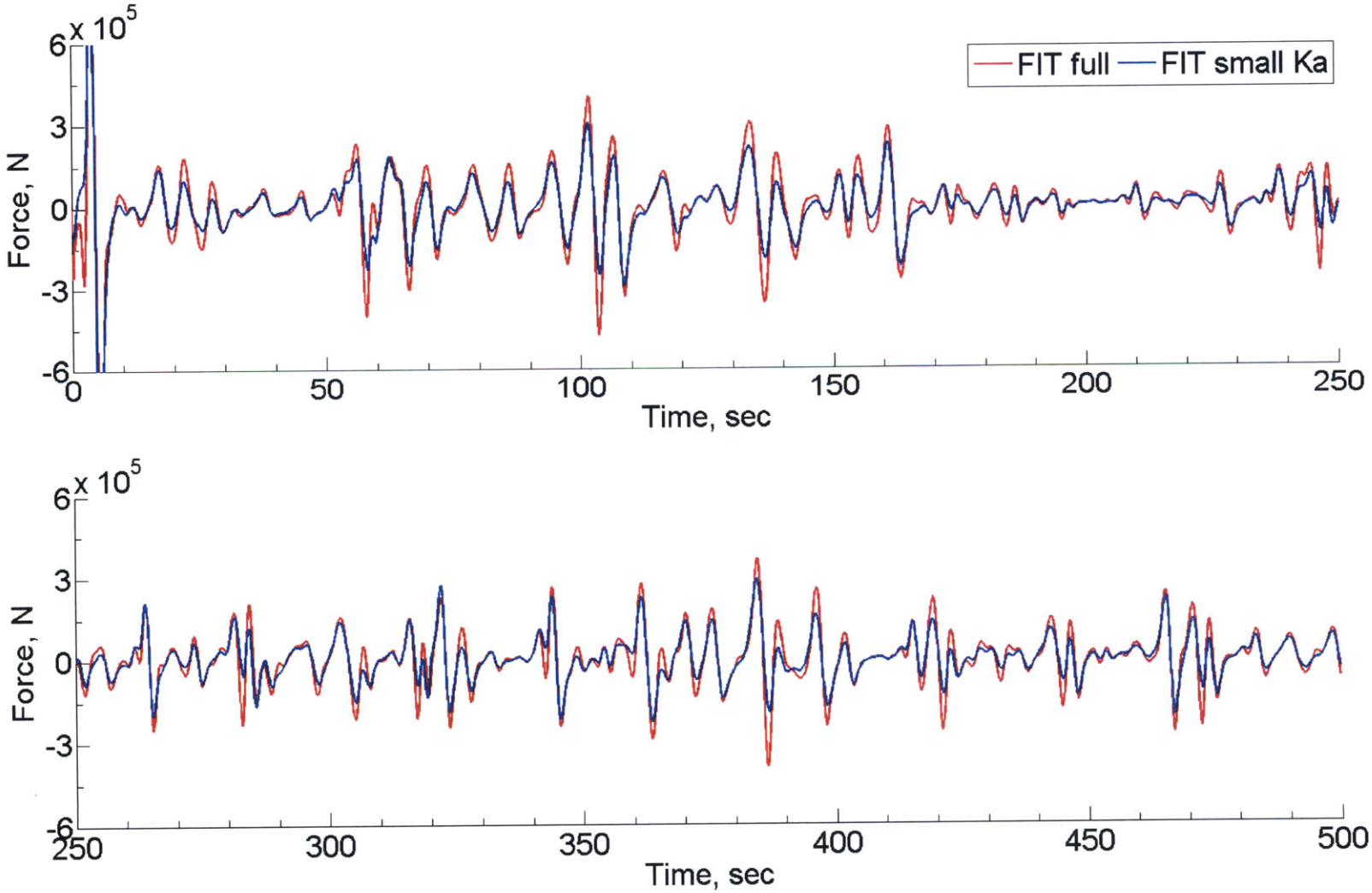

Figure 3-79: Free-surface surge hydrodynamic force between FIT full expression and small Ka approx., r=3m, T=43.2m

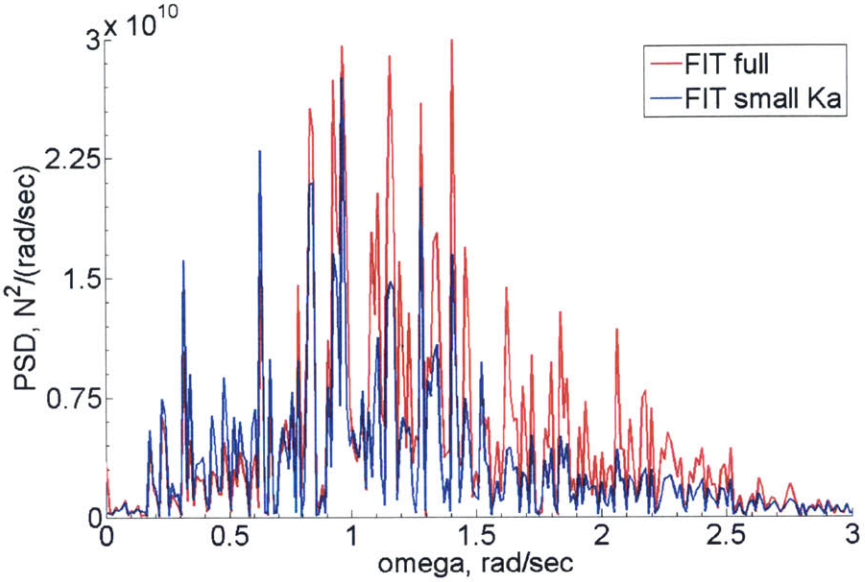

Figure 3-80: PSD comparison between FIT full expression and small Ka approx. for free-surface surge hydrodynamic force, r=3m, T=43.2m

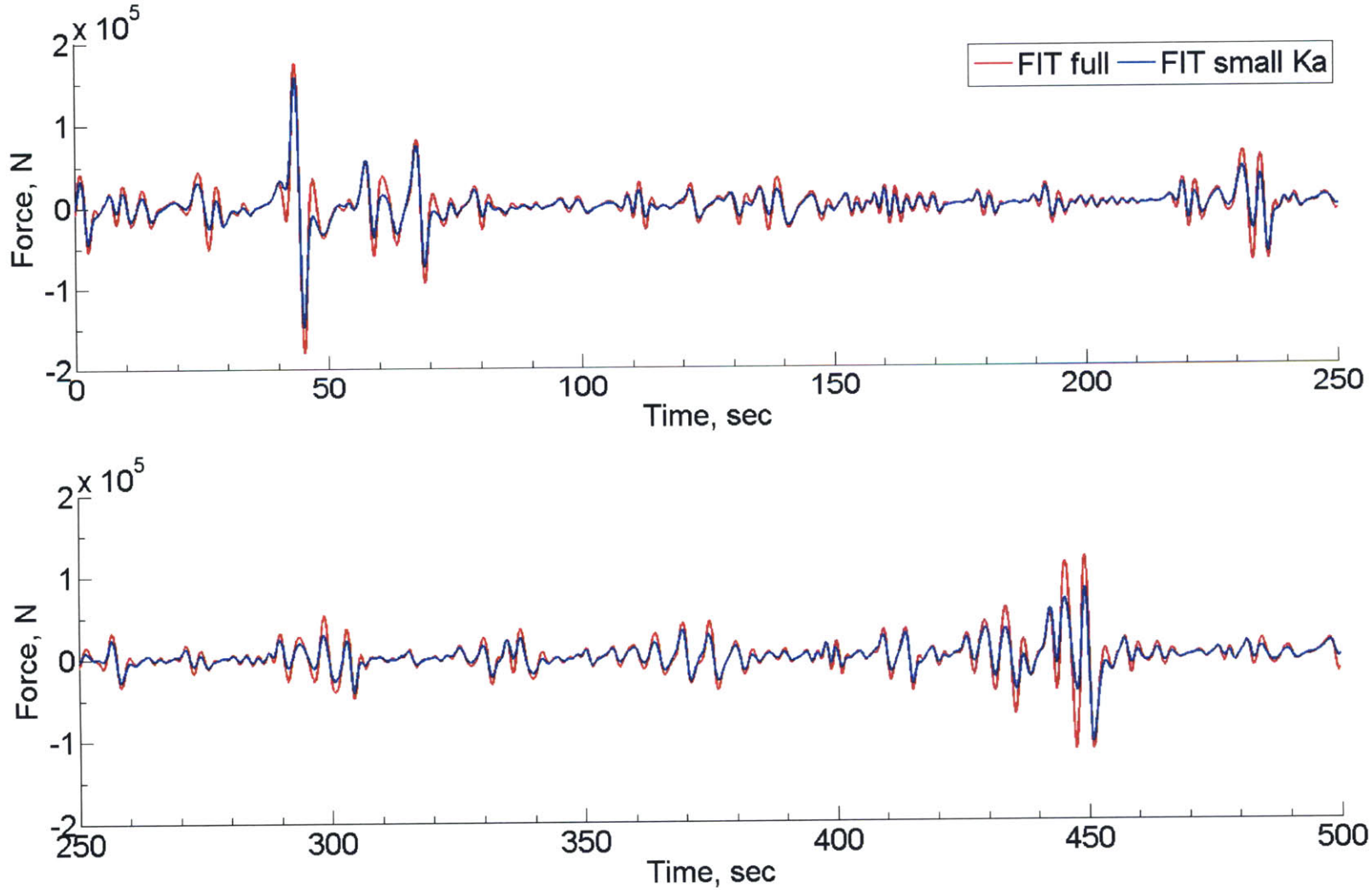

Figure 3-81: Free-surface surge hydrodynamic force between FIT full expression and small Ka approx., r=1.75m, T=30m

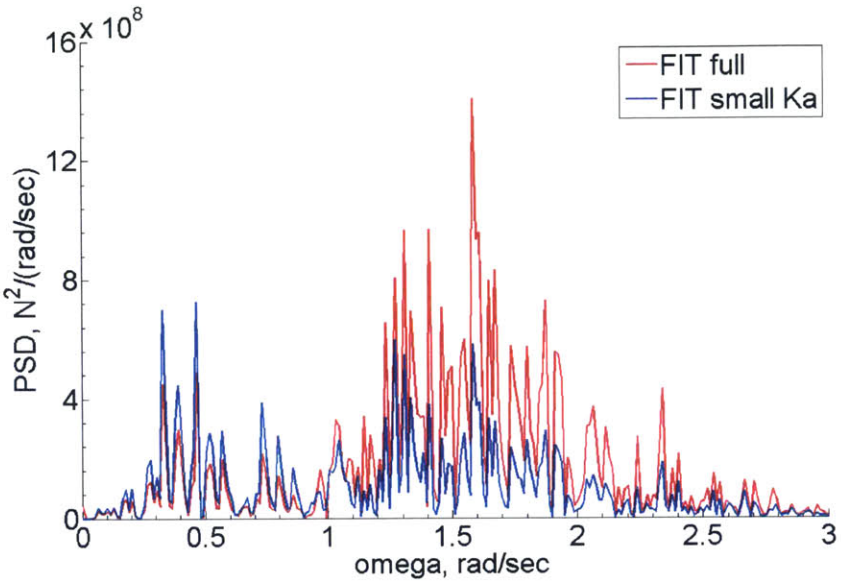

Figure 3-82: PSD comparison between FIT full expression and small Ka approx. for free-surface surge hydrodynamic force, r=1.75m, T=30m

Chapter 4

Discussion and Future Work

This chapter discusses the numerical methods obtained in Chapter 3 and suggests possible future research directions.

The Fluid-Impulse Theory (FIT) was explored theoretically and numerically for the computation of linear and nonlinear hydrodynamic loads on offshore bodies. The objective was to provide a new computation method for the solution of hydrodynamic loads on offshore bodies in the time-domain.

Theoretically, the original fully nonlinear formulation for the computation of hydrodynamic loads from FIT was linearized with the linear free-surface condition for the computation of leading order nonlinear effects. The derivation was performed only under the assumption of a small wave steepness of the ambient wave, which is valid in an offshore environment for wave-body interaction. This allowed the identification of the linear and 2nd order body and free-surface wave-load components in FIT. The equations were then further derived to express hydrodynamic load as a function of the time-domain Green function with integrals over known body surfaces for efficient numerical computation. The discretization of the free surface was circumvented by taking advantage of the analytical structure of the time-domain Green function. The derivations were discussed in detail in the Theory chapter with mathematical formulation attached in the appendices.

Following the theoretical analysis, a three-dimensional time-domain potential-based hydrodynamics solver was developed for simulations of linear and leading order nonlinear wave-body interactions based on the time-domain Green-function method in irregular sea states.

Time domain simulations were carried out on studying hydrodynamic loads on cylindrical offshore floating wind turbine platforms. Several bodies were studied, including the MIT/NREL TLP buoy with 9m radius and 47.89m draft, and two slenderer cylinder with 3m and 1.75m radius with 43.2m and 30m draft respectively. The offshore bodies were treated in a JONSWAP spectrum, which is a random severe sea state with a 6-m significant wave height and a 12-sec peak-spectral wave period, as well as in an irregular sea state obtained from the OC5 experiments. Linear and 2nd order results were separated according to perturbation theory for numerical analysis.

Numerical verification was first performed between 1st order solutions of FIT and the frequency-domain method WAMIT. The results showed that linear comparison between FIT and WAMIT on the MIT/NREL TLP demonstrates very good agreement, which verified the application of the source formulation and the solution of integral equations for the disturbance potential using the impulsive and transient Green functions for numerical computation using FIT.

Following the verification of linear solutions between FIT and WAMIT, the second order surge quadratic solution computed by FIT was studied. Convergence tests were performed to determine the convergence of different perimeters to ensure solution convergence for all simulations in this work. Perimeters studied in the convergence studies included density of meshes, size of time steps and amount of memory time kept in time-marching simulations. In addition to the FIT convergence studies, a comparison of mesh convergence between FIT and WAMIT was performed and FIT was found to be able to achieve convergence with less panels than WAMIT. This

suggested that FIT has the potential to conserve computational cost as discretizing body surfaces with less panels drastically reduces the requirement of computational resources.

After the convergence tests, FIT was applied to compute linear and nonlinear surge responses for cylinders with various sizes. The performances of FIT on computing wave loads can be summarized as follow. Both linear and 2nd order surge wave loads were important when analyzing surge responses on a cylinder in sever sea states, and the loads were adequately captured by FIT. At the 1st order wave frequencies, FIT captured the leading order wave loads which are dominant at that frequency range, while nonlinear wave loads were captured by the module at other frequencies for second order analysis. For 1st order wave loads, FIT correctly depicted the F-K and disturbance solutions in the cases of slender buoys as the two forces coincided with each other at the same frequency ranges with slightly different magnitudes. This corresponded to G.I. Taylor's theory on the F-K and disturbance effects being close to equal to each other under the long-wavelength approximation for slender cylinders. FIT showed that in the case where long-wavelength approximation is no longer valid, i.e. when Ka is finite, disturbance effects has a higher magnitude than F-K effects but occurs at a narrower band of frequencies.

For second order effects, FIT was found to be able to capture leading order second order wave loads at high frequencies. In addition, FIT was found to be able to capture more nonlinear wave loads when compared to frequency-domain method WAMIT. In general, FIT captures more nonlinearities as it computed larger F-K and disturbance body forces at the sum- and difference- frequencies when compared with WAMIT. In addition, FIT suggested that for a buoy with intermediate diameter, the completely nonlinear term, the free-surface impulse force, is crucial when analyzing nonlinear wave loads. It was found that aside from 2nd order F-K and disturbance body forces which occurs at sum- and difference frequency, there exist an additional free-surface impulse force which scatters across the frequencies from 0 to 3 rad/sec,

with peaks at the sum-, diff- and a higher frequency peaking around 2.3rad/sec. For slender buoys, the 2nd order free-surface impulse forces were found to reside at the sum- and difference- frequency range, coinciding with the F-K and disturbance body forces. This difference in behavior could be attributed to the size of the waterplane area inside of the body S_W, which is related to the buoy's radius, as the free-surface impulse force depends directly on the size of S_W. As the size of the water plane area S_W increases, the free-surface impulse force breaks away from the sum- and difference-frequency range and move to other frequencies. This can be an important consideration when designing offshore floating wind turbines as it presents energy at the body's natural frequency ranges, with offshore floating wind turbines typically having 1st flexural modes at around 1.7 rad/sec, causing fatigue of the system or interfering with the tower bending mode frequencies .

By further studying the free-surface impulse force, which has original theoretical formulation consisting of integrals over the ambient wave free-surface, it was found that both ID and DD component on S_W grows larger as the radius of the body becomes larger, and the behavior of the ID component on S_∞ also changes as radius increases. The free-surface impulse force breaks away from the sum- and difference-frequency range and moves to other frequencies as the size of S_W increases. The total ID term was found to be larger than their DD counterpart, suggesting the cross product between incident wave and disturbance potential to be more important on the free-surface. Within the DD term, the components on S_∞ was found to be small compared to contributions from the waterplane are S_W, indicating that this term is more important for buoys with intermediate to large waterplane areas rather than slender buoys.

Overall, the free-surface impulse force obtained by FIT was found to be comparable in magnitude to their F-K and disturbance body counterparts, and the total nonlinear wave loads were found to be significant at higher frequencies for floating cylinder of difference sizes. This suggests that applying the FIT when performing

wave-loads analysis on offshore floating wind turbines can be beneficial to the design of the system as it provides an efficient way to compute nonlinear effects for the study of nonlinear system responses such as ringing, springing and slow-drift loads to ensure the system's safety and cost-effectiveness over the life span of deployment.

To potentially improve the performance of the FIT module, by concluding from the previous studies that the ID component of the free-surface impulse force is much larger than the DD component for slender buoys, a simplified FIT formulation for cylinder with small Ka was studied. The results obtained from this approximation was compared with the results obtained from the FIT full expression. The approximation was found to be in good agreement with full numerical solutions from FIT for computing total surge hydrodynamic forces as well as free-surface impulse forces for slender buoys. It was found that the PSDs of the solutions matched well, with the small Ka approximation slightly underestimating the magnitude of nonlinear loads. There are room for improvement in the simplified formulation to allow the model to capture the full magnitude of the nonlinearities. Further study in this area can prove beneficial to further increase the efficiency of the current FIT module.

In summary, the FIT formulation was explored theoretically for efficient computation of nonlinear wave loads on offshore floating wind turbines. A new hydrodynamics module for the computation linear and nonlinear wave responses using FIT was successfully developed and the module demonstrated that FIT allows computation of important nonlinear wave loads for design of offshore wind turbines. Agreement was found between FIT and frequency-domain method WAMIT for the evaluation of second-order wave loads while FIT computed larger nonlinear wave loads over a wider span of frequencies, especially at frequency ranges close to the typical offshore floating wind turbine's natural frequency of 1.7rad/sec. The module also achieved mesh convergence with less panels when compared to frequency-domain method, as it is a momentum-based method rather than a pressure integration based method, allowing potential savings in computation resources. The new module provides a new time-

domain method for the analysis of nonlinear wave load in severe irregular seastates for the safe and cost-effective design of offshore floating structure, especially for offshore floating wind turbines. Finally, an early exploration of a small Ka approximation method provides potential to further improve efficiency in computing nonlinear wave effects using FIT in the future.

Suggestions for future research topics are as follows. Continued development of the module on computing nonlinear wave loads in other degree of freedoms, including heave and pitch, on the free surface impulse force and moment components to further understand the capability of the FIT formulation is recommended. Further comparisons of the FIT method and numerical modules using other numerical programs, including both time-domain and frequency-domain methods, for future verification studies. The validation of nonlinear wave loads of the floating wind turbine through full-scaled or modeled design experiments would be useful. Viscous forces on the floater can also be added as Morrison like terms functions of the relative wave and body kinematics in future studies. As another application of the present wave-load model based on the Fluid Impulse Theory, sea-keeping problems of ships in extreme wave conditions can be studied further to confirm the applicability of the Fluid Impulse Theory in a wide range of problems in ocean engineering.

Appendices

Appendix A

Free-surface impulse force in Surge

The X-direction free-surface impulse force (2.46) can be rewritten into two terms: an ID term which involves cross-products of the incident and disturbance potentials, and a DD term which involves a quadratic product of the disturbance potential:

$$\begin{aligned}
\vec{F}_{FS,1} &= \vec{F}_{FS,1-ID} + \vec{F}_{FS,1-DD} \\
\vec{F}_{FS,1-ID} &= -\frac{\rho}{g}\frac{d}{dt}\int\limits_{z=0}\left(\varphi\frac{\partial^2\varphi_I}{\partial x\partial t} - \frac{\partial\varphi}{\partial t}\frac{\partial\varphi_I}{\partial x}\right)ds \\
\vec{F}_{FS,1-DD} &= \frac{\rho}{g}\frac{d}{dt}\int\limits_{z=0}\left(\frac{\partial\varphi}{\partial t}\frac{\partial\varphi_I}{\partial x}\right)ds
\end{aligned} \tag{A.1}$$

The ambient wave free-surface $S_I(t)$ can be split into the difference between the infinte free-surface $S_\infty(t)$ and the ambient wave surface inside of the body $S_W(t)$:

$$\begin{aligned}
\vec{F}_{FS,1-ID} &= -\frac{\rho}{g}\frac{d}{dt}\left(\int\limits_{S_\infty} - \int\limits_{S_W}\right)\left(\varphi\frac{\partial^2\varphi_I}{\partial x\partial t} - \frac{\partial\varphi}{\partial t}\frac{\partial\varphi_I}{\partial x}\right)ds \\
&= \frac{d}{dt}\left\{\frac{\rho}{g}\int\limits_{S_W}\left(\varphi\frac{\partial^2\varphi_I}{\partial x\partial t} - \frac{\partial\varphi(t)}{\partial t}\frac{\partial\varphi_I}{\partial x}\right)ds - \frac{\rho}{g}\int\limits_{S_\infty}\left(\varphi\frac{\partial^2\varphi_I}{\partial x\partial t} - \frac{\partial\varphi}{\partial t}\frac{\partial\varphi_I}{\partial x}\right)ds\right\}
\end{aligned} \tag{A.2}$$

The impulses for this force expression can then be identified to be an integral over $S_W(t)$ and another over $S_\infty(t)$:

$$\begin{aligned}
\vec{F}_{FS,1-ID} &= \frac{d}{dt}\vec{I}_{FS,1-ID} \\
\vec{I}_{FS,1-ID,S_W} &= \frac{\rho}{g}\int_{S_W}\Big(\varphi\frac{\partial^2\varphi_I}{\partial x\partial t} - \frac{\partial\varphi}{\partial t}\frac{\partial\varphi_I}{\partial x}\Big)ds \\
\vec{I}_{FS,1-ID,S_\infty} &= -\frac{\rho}{g}\int_{S_\infty}\Big(\varphi\frac{\partial^2\varphi_I}{\partial x\partial t} - \frac{\partial\varphi}{\partial t}\frac{\partial\varphi_I}{\partial x}\Big)ds
\end{aligned} \tag{A.3}$$

Assuming small wave steepness, φ_I and its derivative can be assumed to be evaluated at $z = 0$.

$$\begin{aligned}
\varphi_I(x,y,0,t) &= \Re\Big\{\sum_j \frac{igA_j}{\omega_j}e^{-i\nu_j x\cos\beta_j - i\nu_j y\sin\beta_j + i\omega_j t + i\chi_j}\Big\} \\
\frac{\partial\varphi_I}{\partial x}(x,y,0,t) &= \Re\Big\{\sum_j \frac{igA_j}{\omega_j}(-i\nu_j\cos\beta_j)e^{-i\nu_j x\cos\beta_j - i\nu_j y\sin\beta_j + i\omega_j t + i\chi_j}\Big\} \\
\frac{\partial^2\varphi_I}{\partial x\partial t}(x,y,0,t) &= \Re\Big\{\sum_j \frac{igA_j}{\omega_j}(i\omega_j)(-i\nu_j\cos\beta_j)e^{-i\nu_j x\cos\beta_j - i\nu_j y\sin\beta_j + i\omega_j t + i\chi_j}\Big\}
\end{aligned} \tag{A.4}$$

And the disturbance velocity potential is:

$$\begin{aligned}
&\varphi(x,y,z,t) = \varphi^{(0)}(x,y,z,t) + \varphi^{(M)}(x,y,z,t) \\
&\varphi^{(0)}(x,y,z,t) = \int_{S_B(\tau)} ds_\xi \sigma(\vec{\xi},t)\Big(\frac{1}{r} - \frac{1}{r'}\Big) \\
&\varphi^{(M)}(x,y,z,t) = \int_0^t d\tau \int_{S_B(\tau)} d\xi\sigma(\vec{\xi},\tau)H_\tau(\vec{x},\vec{\xi},t-\tau) \\
&\quad H_\tau(\vec{x},\vec{\xi},t-\tau) = -\frac{1}{2\pi}\sum_j \int_0^\infty dk_j\ \sqrt{gk_j}e^{k_j(z+\zeta)}\sin[\sqrt{gk_j}(t-\tau)]J_0(k_jR) \\
&\quad \text{where}\quad J_0(k_jR) = \frac{1}{2\pi}\int_{-\pi}^{\pi} e^{ik_jR\cos\theta_j}d\theta_j; \quad R = [(x-\xi)^2 + (y-\eta)^2]^{1/2} \\
&\quad \text{and}\quad x - \xi = R\cos\psi; \quad y - \eta = R\sin\psi
\end{aligned} \tag{A.5}$$

Again with small wave steepness approximation, $\varphi^{(0)}(x,y,0,t) = 0,\ t > 0$ by definition. Thus $\frac{\partial}{\partial t}\varphi^{(0)}(x,y,0,t) = 0,\ t > 0$.

$$\begin{aligned}
\varphi(x,y,0,t) = \varphi^{(M)}(x,y,0,t) &= \int_0^t d\tau \int_{S_B(\tau)} d\xi \sigma(\vec{\xi},\tau) H_\tau(\vec{x},\vec{\xi},t-\tau) \\
H_\tau(\vec{x},\vec{\xi},t-\tau) &= -\frac{1}{2\pi}\sum_j \int_0^\infty dk_j\ \sqrt{gk_j} e^{k_j\zeta} \sin[\sqrt{gk_j}(t-\tau)] J_0(k_j R)
\end{aligned} \tag{A.6}$$

The analysis proceeds by evaluating the free-surface impulse force on $z = 0$; The function H_τ can be rewritten as:

$$\begin{aligned}
&\text{let} \quad u_j = k_j \cos\gamma_j; \quad v_j = k_j \sin\gamma_j; \quad \text{thus} \quad du_j dv_j = k_j dk_j d\gamma_j \\
&H_\tau(\vec{x},\vec{\xi},t-\tau) = -\frac{1}{4\pi^2}\sum_j \int_{-\pi}^{\pi} d\theta_j \int_0^\infty dk_j\ \sqrt{gk_j} e^{k_j\zeta} \sin[\sqrt{gk_j}(t-\tau)] e^{ik_j R\cos\theta_j}
\end{aligned} \tag{A.7}$$

Let $\theta_j = \gamma_j - \psi_j, \quad d\theta_j = d\gamma_j, \quad k_j^2 = u_j^2 + v_j^2$:

$$e^{ik_j R\cos\theta_j} = e^{iu_j(x-\xi)+iv_j(y-\eta)} \tag{A.8}$$

H_τ is then:

$$H_\tau(\vec{x},\vec{\xi},t-\tau) = -\frac{1}{4\pi^2}\sum_j \iint_{-\infty}^{\infty} du_j dv_j\ \sqrt{\frac{g}{k_j}} e^{k_j\zeta} \sin[\sqrt{gk_j}(t-\tau)] e^{iu_j(x-\xi)+iv_j(y-\eta)} \tag{A.9}$$

The first partial time derivative of the disturbance potential at $z = 0$ is then:

$$\begin{aligned}
&\frac{\partial\varphi^{(M)}}{\partial t}(x,y,0,t) = \\
&\quad -\frac{1}{4\pi^2}\int_0^t d\tau \int_{S_B(\tau)} d\xi \sigma(\xi,\tau) \\
&\qquad \times \sum_j \iint_{-\infty}^{\infty} du_j dv_j\ e^{k_j\zeta} \sqrt{\frac{g}{k_j}} \sqrt{gk_j} \cos[\sqrt{gk_j}(t-\tau)] e^{iu_j(x-\xi)+iv_j(y-\eta)}
\end{aligned} \tag{A.10}$$

Substituting A.4 and A.10 into A.3, the integral over S_∞ becomes:

$$\vec{I}_{FS,1-ID,S_\infty} = -\frac{\rho}{g}\iint_{-\infty}^{\infty} dxdy\Big(\varphi\frac{\partial^2\varphi_I}{\partial x\partial t} - \frac{\partial\varphi}{\partial t}\frac{\partial\varphi_I}{\partial x}\Big)$$

$$= -\frac{\rho}{g}\iint_{-\infty}^{\infty} dxdy\Bigg\{\Big\{-\frac{1}{4\pi^2}\int_0^t d\tau\int_{S_B(\tau)} d\xi\sigma(\xi,\tau)$$

$$\times\sum_j\iint_{-\infty}^{\infty} du_j dv_j\ \sqrt{\frac{g}{k_j}}e^{k_j\zeta}\sin[\sqrt{gk_j}(t-\tau)]e^{iu_j(x-\xi)+iv_j(y-\eta)}$$

$$\times\Re\Big[\sum_j\frac{igA_j}{\omega_j}(i\omega_j)(-i\nu_j\cos\beta_j)e^{-i\nu_j x\cos\beta_j - i\nu_j y\sin\beta_j + i\omega_j t + i\chi_j}\Big]\Big\}$$

$$-\Big\{-\frac{1}{4\pi^2}\int_0^t d\tau\int_{S_B(\tau)} d\xi\sigma(\xi,\tau)$$

$$\times\sum_j\iint_{-\infty}^{\infty} du_j dv_j\ e^{k_j\zeta}\sqrt{\frac{g}{k_j}}\sqrt{gk_j}\cos[\sqrt{gk_j}(t-\tau)]e^{iu_j(x-\xi)+iv_j(y-\eta)}$$

$$\times\Re\Big[\sum_j\frac{igA_j}{\omega_j}(-i\nu_j\cos\beta_j)e^{-i\nu_j x\cos\beta_j - i\nu_j y\sin\beta_j + i\omega_j t + i\chi_j}\Big]\Big\}\Bigg\} \tag{A.11}$$

Reorganizing (A.11):

$$\vec{I}_{FS,1-ID,S_\infty}$$

$$= \frac{\rho}{g}\frac{1}{4\pi^2}\Re\Bigg\{\int_0^t d\tau\int_{S_B(\tau)} d\xi\sigma(\xi,\tau)$$

$$\times\sum_j\iint_{-\infty}^{\infty} dudv\ \frac{igA_j}{\omega_j}(-i\nu_j\cos\beta_j)e^{k_j\zeta+i\omega_j t+i\chi_j} \tag{A.12}$$

$$\times\Big(ig\sin[\sqrt{gk_j}(t-\tau)] - g\cos[\sqrt{gk_j}(t-\tau)]\Big)$$

$$\times\iint_{-\infty}^{\infty} dxdy\Big[e^{iu_j(x-\xi)-i\nu_j x\cos\beta_j + iv_j(y-\eta)-i\nu_j y\sin\beta_j}\Big]\Bigg\}$$

Applying the definitions of the delta dunctions:

$$\begin{aligned}\int_{-\infty}^{\infty} dx e^{ix(u_j-\nu_j\cos\beta_j)} &= 2\pi\delta(u_j-\nu_j\cos\beta_j)\\ \int_{-\infty}^{\infty} dy e^{iy(v_j-\nu_j\sin\beta_j)} &= 2\pi\delta(v_j-\nu_j\sin\beta_j)\end{aligned} \tag{A.13}$$

$$\iint_{-\infty}^{\infty} dxdy e^{iu_jx-i\nu_jx\cos\beta_j+iv_jy-i\nu_jy\sin\beta_j} = 4\pi^2\delta(u_j-\nu_j\cos\beta_j)\delta(v_j-\nu_j\sin\beta_j) \tag{A.14}$$

Substituting (A.13) into (A.12) and performing the infinite integrals over the delta functions:

$$\begin{aligned}&\vec{I}_{FS,1-ID,S_\infty}\\ &= \frac{\rho}{g}\frac{1}{4\pi^2}\Re\Bigg\{\int_0^t d\tau\int_{S_B(\tau)} d\xi\sigma(\xi,\tau)\\ &\quad\times\sum_j 4\pi^2 e^{-i\nu_j\xi\cos\beta_j-i\nu_j\eta\sin\beta_j}(-i\nu_j\cos\beta_j)\frac{igA_j}{\omega_j}e^{\nu_j\zeta+i\omega_jt+i\chi_j}\\ &\quad\times g\Big(i\sin[\sqrt{g\nu_j}(t-\tau)]-\cos[\sqrt{g\nu_j}(t-\tau)]\Big)\Bigg\}\\ &= \frac{\rho}{g}\Re\Bigg\{\int_0^t d\tau\int_{S_B(\tau)} d\xi\sigma(\xi,\tau)\\ &\quad\times\sum_j(-i\nu_j\cos\beta_j)\frac{igA_j}{\omega_j}e^{\nu_j\zeta+i\omega_jt+i\chi_j}e^{-i\nu_j\xi\cos\beta_j-i\nu_j\eta\sin\beta_j}(-g)e^{-i\sqrt{g\nu_j}(t-\tau)}\Bigg\}\\ &= \rho\Re\Bigg\{\sum_j\frac{-gA_j\nu_j}{\omega_j}\cos\beta_j e^{i\chi_j}e^{i\omega_jt}\int_0^t d\tau e^{-i\omega_j(t-\tau)}\int_{S_B(\tau)} d\xi\sigma(\xi,\tau)e^{\nu_j\zeta-i\nu_j\xi\cos\beta_j-i\nu_j\eta\sin\beta_j}\Bigg\}\\ &= -\rho\Re\Bigg\{\sum_j A_j\omega_j\cos\beta_j e^{i\chi_j}\int_0^t d\tau e^{i\omega_j\tau}\int_{S_B(\tau)} d\xi\sigma(\xi,\tau)e^{\nu_j\zeta-i\nu_j\xi\cos\beta_j-i\nu_j\eta\sin\beta_j}\Bigg\}\end{aligned} \tag{A.15}$$

Applying the relation:

$$\frac{d}{dt}\int_0^t F(\tau)d\tau = F(t) \tag{A.16}$$

The final expression for FS-1 ID is derived as:

$$\begin{aligned}
&\vec{F}_{FS,1-ID}(t) \\
&= \frac{\rho}{g}\frac{d}{dt}\int_{S_W(t)}\left[\varphi(t)\frac{\partial^2\varphi_I(t)}{\partial x\partial t} - \frac{\partial\varphi(t)}{\partial t}\frac{\partial\varphi_I(t)}{\partial x}\right]ds - \rho\Re\sum_j\left\{A_j\omega_j\cos\beta_j e^{i\omega_j t+i\chi_j}K(\nu_j,\beta_j,t)\right\} \\
&\text{where}\quad K(\nu_j,\beta_j,t) = \int_{S_B(t)} d\xi\sigma(\vec{\xi},t)e^{\nu_j\zeta - i\nu_j\xi\cos\beta_j - i\nu_j\eta\sin\beta_j}
\end{aligned} \tag{A.17}$$

The second integral invovles an integration of a quadratic product of the disturbance potential of the $z = 0$ plane outside the body waterline. Invoking the Reynolds transport theorem the time derivatives maybe transferred under the integral sign

$$\begin{aligned}
\vec{F}_{FS,1-DD} &= \frac{\rho}{g}\frac{d}{dt}\int_{z=0}\left(\frac{\partial\varphi}{\partial t}\frac{\partial\varphi}{\partial x}\right)ds \\
&= \frac{\rho}{g}\int_{z=0}\frac{d}{dt}\left(\frac{\partial\varphi}{\partial t}\frac{\partial\varphi}{\partial x}\right)ds + \frac{\rho}{g}\oint_{C_W} dl\ U_n\frac{\partial\varphi}{\partial t}\frac{\partial\varphi}{\partial x}
\end{aligned} \tag{A.18}$$

The last integral over the body waterline involves the normal oscillatory velocity of the body which is of the same order as the disturbance potential, therefore it is of cubic order and is omitted. This would not be the case for a ship advancing with a significant forward speed in which case this integral is of the same order as the first term.

A formal differentiation of the terms under the integral sign leads to

$$\frac{d}{dt}\left(\frac{\partial\varphi}{\partial t}\frac{\partial\varphi}{\partial x}\right) = \frac{\partial^2\varphi}{\partial t^2}\frac{\partial\varphi}{\partial x} + \frac{1}{2}\frac{\partial}{\partial x}\left(\frac{\partial\varphi}{\partial t}\right)^2 \tag{A.19}$$

Upon substitution in (A.18) we obtain

$$\vec{F}_{FS,1-DD} = \frac{\rho}{g}\int_{-\infty}^{\infty} dx \int_{-\infty}^{\infty} dy \frac{\partial^2\varphi}{\partial t^2}\frac{\partial\varphi}{\partial x} - \frac{\rho}{g}\int_{S_W} \frac{\partial^2\varphi}{\partial t^2}\frac{\partial\varphi}{\partial x} ds + \frac{\rho}{2g}\oint_{C_W} dl\ \vec{n}_1 \Big(\frac{\partial\varphi}{\partial t}\Big)^2 \quad \text{(A.20)}$$

In (A.20) Stokes' theorem was invoked over the z=0 plane to reduce the integral of the x-derivative in the last term of (A.19) to an integral over the body waterline. Also the integral of the first term in the right hand side of (A.19) over the body interior waterplane area was added and subtracted. The second and third term to the right of the equal sign in (A.20) are easy to evaluate using the definition (4.2) of the disturbance potential. The evaluation of the infinite integral in (A.20) is discussed next.

Invoking the free surface condition (2.5) satisfied by the total disturbance potential and introducing the velocity potential decomposition into the instantaneous and memory components we obtain

$$\frac{\partial^2\varphi}{\partial t^2}\frac{\partial\varphi}{\partial x} = -g\frac{\partial\varphi}{\partial z}\frac{\partial\varphi}{\partial x} = -g\frac{\partial\varphi^{(M)}}{\partial z}\frac{\partial\varphi^{(M)}}{\partial x} - g\frac{\partial\varphi^{(0)}}{\partial z}\frac{\partial\varphi^{(M)}}{\partial x},\ z=0 \quad \text{(A.21)}$$

The second equality in (A.21) made use of the property that the value and hence the x-derivative of the velocity potential component vanish on the z=0 plane at all times. We therefore are led to the evaluation of the infinite integral

$$\frac{\rho}{g}\int_{-\infty}^{\infty} dx \int_{-\infty}^{\infty} dy \frac{\partial^2\varphi}{\partial t^2}\frac{\partial\varphi}{\partial x} = \frac{\rho}{g}(-g)\int_{-\infty}^{\infty} dx \int_{-\infty}^{\infty} dy \left(\frac{\partial\varphi^{(M)}}{\partial z}\frac{\partial\varphi^{(M)}}{\partial x} + \frac{\partial\varphi^{(0)}}{\partial z}\frac{\partial\varphi^{(M)}}{\partial x}\right) \quad \text{(A.22)}$$

The memory component of the disturbance velocity potential is harmonic in the lower half space for z<0 and it vanishes at infinity. It therefore satisfies the familiar vector identity over a closed surface bounded by the $z = 0$ plane and a semi-spherical surface at infinity over which the integrand vanishes

$$\int_{-\infty}^{\infty} dx \int_{-\infty}^{\infty} dy \Big(\frac{\partial \varphi^{(M)}}{\partial n} \nabla \varphi^{(M)} - \frac{1}{2} \vec{n} \varphi^{(M)} \cdot \varphi^{(M)} \Big) = 0 \tag{A.23}$$

The unit vector $\vec{n}$ points in the vertical direction. The x-component of (A.23) reads

$$\int_{-\infty}^{\infty} dx \int_{-\infty}^{\infty} dy \Big(\frac{\partial \varphi^{(M)}}{\partial n} \frac{\partial \varphi^{(M)}}{\partial x} \Big) = 0 \tag{A.24}$$

Combining (A.22) and (A.24) it follows that

$$\frac{\rho}{g} \int_{-\infty}^{\infty} dx \int_{-\infty}^{\infty} dy \frac{\partial^2 \varphi}{\partial t^2} \frac{\partial \varphi}{\partial x} = -\rho \int_{-\infty}^{\infty} dx \int_{-\infty}^{\infty} dy \frac{\partial \varphi^{(0)}}{\partial z} \frac{\partial \varphi^{(M)}}{\partial x} \tag{A.25}$$

The Rankine source $1/r$ its image $1/r$ and their Z-derivatives admit the following Fourier representations on the $z = 0$ plane

$$\frac{1}{r} = \frac{1}{2\pi} \iint_{-\infty}^{\infty} du_1 dv_1 e^{-(u_1^2+v_1^2)^{1/2}|z-\zeta_1| + iu_1(x-\xi_1) + iv_1(y-\eta_1)}$$

$$\frac{\partial}{\partial z}\Big(\frac{1}{r}\Big)_{r=0} = -\frac{\partial}{\partial z}\Big(\frac{1}{r'}\Big)_{r=0} = -\frac{1}{2\pi} \iint_{-\infty}^{\infty} du_1 dv_1 (u_1^2 + v_1^2)^{1/2} e^{(u_1^2+v_1^2)^{1/2}\zeta_1 + iu_1(x-\xi_1) + iv_1(y-\eta_1)} \tag{A.26}$$

Note that the infinite integrals over u and v are subjected to a summation series for polychromatic waves. Since the final expression for the DD component does not involve the incident wave velocity potential, the effects of irregular waves are implied to be included when computing source strength σ at any time and thus the summation is skipped for simplicity in this derivation.

Combining (A.26) with the definition of the impulsive velocity potential $\varphi^{(0)}$ in (A.5), the z-derivative of the impulsive potential is:

$$\frac{\partial \varphi^{(0)}}{\partial z}(x,y,0,t) = -\frac{1}{4\pi^2}\iint_{-\infty}^{\infty} du_1 dv_1 (u_1^2+v_1^2)^{1/2} \int_{S_B(t)} d\xi_1 \sigma(\vec{\xi_1},t) e^{(u_1^2+v_1^2)^{1/2}\zeta_1 + iu_1(x-\xi_1)+iv_1(y-\eta_1)} \tag{A.27}$$

Following (A.10), the first partial x-derivative of the disturbance potential at $z=0$ is:

$$\frac{\partial \varphi^{(M)}}{\partial x}(x,y,0,t) = -\frac{1}{4\pi^2}\int_0^t d\tau \int_{S_B(\tau)} d\xi_2 \sigma(\vec{\xi_2},\tau) \iint_{-\infty}^{\infty} du_2 dv_2 \; iu_2 e^{k_2\zeta_2}\sqrt{\frac{g}{k_2}}\sin[\sqrt{gk_2}(t-\tau)] e^{iu_2(x-\xi_2)+iv_2(y-\eta_2)} \tag{A.28}$$

Substituting (A.27) and (A.28) into (A.25):

$$\frac{\rho}{g}\int_{-\infty}^{\infty}dx\int_{-\infty}^{\infty}dy\frac{\partial^2\varphi}{\partial t^2}\frac{\partial\varphi}{\partial x}=$$

$$-\rho\iint_{-\infty}^{\infty}dxdy\Bigg\{-\frac{1}{4\pi^2}\iint_{-\infty}^{\infty}du_1dv_1k_1\int_{S_B(t)}d\xi_1\sigma(\vec{\xi_1},t)e^{k_1\zeta_1+iu_1(x-\xi_1)+iv_1(y-\eta_1)}$$

$$\times-\frac{1}{4\pi^2}\int_0^t d\tau\int_{S_B(\tau)}d\xi_2\sigma(\vec{\xi_2},\tau)\iint_{-\infty}^{\infty}du_2dv_2\ iu_2e^{k_2\zeta_2}\sqrt{\frac{g}{k_2}}\sin[\sqrt{gk_2}(t-\tau)]e^{iu_2(x-\xi_2)+iv_2(y-\eta_2)}\Bigg\}$$

$$=-\rho\Big(-\frac{1}{4\pi^2}\Big)^2\Bigg\{\int_{S_B(t)}d\xi_1\sigma(\vec{\xi_1},t)\int_0^t d\tau\int_{S_B(\tau)}d\xi_2\sigma(\vec{\xi_2},\tau)$$

$$\times\iint_{-\infty}^{\infty}du_1dv_1\ k_1e^{k_1\zeta_1-iu_1\xi_1-iv_1\eta_1}$$

$$\times\iint_{-\infty}^{\infty}du_2dv_2\ iu_2\sqrt{\frac{g}{k_2}}\sin[\sqrt{gk_2}(t-\tau)]e^{k_2\zeta_2-iu_2\xi_2-iv_2\eta_2}$$

$$\times\iint_{-\infty}^{\infty}dxdye^{i(u_1+u_2)x+i(v_1+v_2)y}\Bigg\} \tag{A.29}$$

Invoking the identity for delta functions again:

$$\iint_{-\infty}^{\infty}dxdye^{i(u_1+u_2)x+i(v_1+v_2)y}=4\pi^2\delta(u_1+u_2)\delta(v_1+v_2) \tag{A.30}$$

Using also the properties of the delta function:

$$\iint_{-\infty}^{\infty}du_2dv_2F(u_2,v_2)\delta(u_1+u_2)\delta(v_1+v_2)=F(-u_1,-v_1) \tag{A.31}$$

where

$$F(u_2,v_2)=-iu_1\sqrt{\frac{g}{k_1}}\sin[\sqrt{gk_1}(t-\tau)]e^{k_1\zeta_2+iu_1\xi_2+iv_1\eta_2} \tag{A.32}$$

(A.29) becomes:

$$
\begin{aligned}
&= -\rho\frac{1}{4\pi^2}\int_{S_B(t)} d\xi_1\sigma(\vec{\xi_1},t)\int_0^t d\tau\int_{S_B(\tau)} d\xi_2\sigma(\vec{\xi_2},\tau)\\
&\quad\times\iint_{-\infty}^{\infty} du_1dv_1\ (-iu_1)k_1\sqrt{\frac{g}{k_1}}\sin[\sqrt{gk_1}(t-\tau)]e^{k_1(\zeta_1+\zeta_2)-iu_1(\xi_1-\xi_2)-iv_1(\eta_1-\eta_2)}\\
&= -\rho\frac{1}{4\pi^2}\int_{S_B(t)} d\xi_1\sigma(\vec{\xi_1},t)\int_0^t d\tau\int_{S_B(\tau)} d\xi_2\sigma(\vec{\xi_2},\tau)\\
&\quad\times\frac{\partial^2}{\partial\xi_1\partial\zeta_1}\iint_{-\infty}^{\infty} du_1dv_1\ \sqrt{\frac{g}{k_1}}\sin[\sqrt{gk_1}(t-\tau)]e^{k_1(\zeta_1+\zeta_2)-iu_1(\xi_1-\xi_2)-iv_1(\eta_1-\eta_2)}\\
&= \rho\int_{S_B(t)} d\xi_1\sigma(\vec{\xi_1},t)\int_0^t d\tau\int_{S_B(\tau)} d\xi_2\sigma(\vec{\xi_2},\tau)\frac{\partial^2}{\partial\xi_1\partial\zeta_1}H_\tau(\vec{\xi_1},\vec{\xi_2},t-\tau)
\end{aligned}
\tag{A.33}
$$

Therefore the final expression for the DD component of the free-surface impulse force in surge is:

$$
\begin{aligned}
&\vec{F}_{FS,1-DD}(t)\\
&= \rho\int_{S_B(t)} ds_{\xi_1}\sigma(\vec{\xi_1},t)\frac{\partial^2\varphi^{(M)}(\vec{\xi_1},t)}{\partial\xi_1\partial\zeta_1}\\
&\quad-\frac{\rho}{g}\int_{S_W(t)}\frac{\partial^2\varphi^{(M)}}{\partial t^2}\frac{\partial\varphi^{(M)}}{\partial x}ds+\frac{\rho}{2g}\oint_{C_W(t)}\Big(\frac{\partial\varphi^{(M)}}{\partial t}\Big)^2 n_1dl\\
&\text{where}\quad \varphi^{(M)}(\vec{\xi_1},t)=\int_0^t d\tau\int_{S_B(\tau)} ds_{\xi_2}\sigma(\vec{\xi_2},\tau)H_\tau(\vec{\xi_1},\vec{\xi_2},t-\tau)
\end{aligned}
\tag{A.34}
$$

Appendix B

Free-surface impulse force in Heave

Start by using the force expression presented in [30] and (2.42). Taking the free-surface impulse force in the Z-direction up to second order:

$$\begin{aligned}\vec{F}_{FS,3}(t) = &- \rho\frac{d}{dt}\int\limits_{S_I(t)} \varphi(t)\vec{n}_z ds + \rho\vec{k}\int\limits_{S_I(t)} \frac{\partial\varphi(t)}{\partial t} ds \\ &+ \rho\frac{d}{dt}\int\limits_{S_I(t)} \left(\frac{1}{g}\frac{\partial\varphi(t)}{\partial t}\frac{\partial}{\partial z}(\varphi_I(t)+\varphi(t))\right) ds\end{aligned} \tag{B.1}$$

By moving the derivative of the first term of the force expression inside of the integral and keeping terms to the leading order, the first term of the force expression can be shown to cancel with the second term, thus leaving only the last term of the force expression to be computed:

$$\vec{F}_{FS,3}(t) = \frac{\rho}{g}\frac{d}{dt}\int\limits_{S_I(t)} \left(\frac{\partial\varphi(t)}{\partial t}\frac{\partial}{\partial z}(\varphi_I(t)+\varphi(t))\right) ds \tag{B.2}$$

The Z-direction free-surface impulse force can be rewritten into two terms: an ID term which involves cross-products of the incident and disturbance potentials, and a DD term which involves a quadratic product of the disturbance potential:

$$\begin{aligned}
\vec{F}_{FS,3}(t) &= \vec{F}_{FS,3-ID}(t) + \vec{F}_{FS,3-DD}(t) \\
\vec{F}_{FS,3-ID}(t) &= \frac{\rho}{g}\frac{d}{dt}\int\limits_{S_I(t)} \left(\frac{\partial\varphi(t)}{\partial t}\frac{\partial\varphi_I(t)}{\partial z}\right) ds \\
\vec{F}_{FS,3-DD}(t) &= \frac{\rho}{g}\frac{d}{dt}\int\limits_{S_I(t)} \left(\frac{\partial\varphi(t)}{\partial t}\frac{\partial\varphi(t)}{\partial z}\right) ds
\end{aligned} \tag{B.3}$$

Applying the linear free-surface condition for both the incident and the disturbance velocity potential:

$$\frac{\partial\varphi_I(t)}{\partial z} = -\frac{1}{g}\frac{\partial^2\varphi_I(t)}{\partial t^2} \tag{B.4}$$

$\vec{F}_{FS,3-ID}(t)$ becomes:

$$\vec{F}_{FS,3-ID}(t) = -\frac{\rho}{g^2}\frac{d}{dt}\int\limits_{S_I(t)} \left(\frac{\partial\varphi(t)}{\partial t}\frac{\partial^2\varphi_I(t)}{\partial t^2}\right) ds \tag{B.5}$$

The ambient wave free-surface $S_I(t)$ can be rewritten into the difference between the infinte free-surface $S_\infty(t)$ and the ambient wave surface inside of the body $S_W(t)$:

$$\begin{aligned}
\vec{F}_{FS,3-ID}(t) &= -\frac{\rho}{g^2}\frac{d}{dt}\left(\int\limits_{S_\infty(t)} - \int\limits_{S_W(t)}\right)\left(\frac{\partial\varphi(t)}{\partial t}\frac{\partial^2\varphi_I(t)}{\partial t^2}\right) ds \\
&= \frac{d}{dt}\left\{\frac{\rho}{g^2}\int\limits_{S_W(t)} \frac{\partial\varphi(t)}{\partial t}\frac{\partial^2\varphi_I(t)}{\partial t^2} ds - \frac{\rho}{g^2}\int\limits_{S_\infty(t)} \frac{\partial\varphi(t)}{\partial t}\frac{\partial^2\varphi_I(t)}{\partial t^2} ds\right\}
\end{aligned} \tag{B.6}$$

The impulses for this force expression can then be identified to be an integral over $S_W(t)$ and another over $S_\infty(t)$:

$$\begin{aligned}
\vec{F}_{FS,3-ID}(t) &= \frac{d}{dt}\vec{I}_{FS,3-ID}(t) \\
\vec{I}_{FS,3-ID,S_W}(t) &= \frac{\rho}{g^2}\int\limits_{S_W(t)} \frac{\partial\varphi(t)}{\partial t}\frac{\partial^2\varphi_I(t)}{\partial t^2}ds \\
\vec{I}_{FS,3-ID,S_\infty}(t) &= -\frac{\rho}{g^2}\int\limits_{S_\infty(t)} \frac{\partial\varphi(t)}{\partial t}\frac{\partial^2\varphi_I(t)}{\partial t^2}ds
\end{aligned} \tag{B.7}$$

Again, for a polychromatic wave the incident wave velocity potential is:

$$\text{(polychromatic)}\quad \varphi_I(x,y,z,t) = \Re\left\{\sum_j \frac{igA_j}{\omega_j}e^{\nu_j z - i\nu_j x\cos\beta_j - i\nu_j y\sin\beta_j + i\omega_j t + i\chi_j}\right\} \tag{B.8}$$

The first and second partial time derivative of φ_I are:

$$\begin{aligned}
\frac{\partial\varphi_I}{\partial t}(x,y,z,t) &= \Re\left\{\sum_j \frac{igA_j}{\omega_j}(i\omega_j)e^{\nu_j z - i\nu_j x\cos\beta_j - i\nu_j y\sin\beta_j + i\omega_j t + i\chi_j}\right\} \\
\frac{\partial^2\varphi_I}{\partial t^2}(x,y,z,t) &= \Re\left\{\sum_j \frac{igA_j}{\omega_j}(i\omega_j)^2e^{\nu_j z - i\nu_j x\cos\beta_j - i\nu_j y\sin\beta_j + i\omega_j t + i\chi_j}\right\}
\end{aligned} \tag{B.9}$$

And the disturbance velocity potential is:

$$\begin{aligned}
\varphi(x,y,z,t) &= \varphi^{(0)}(x,y,z,t) + \varphi^{(M)}(x,y,z,t) \\
\varphi^{(0)}(x,y,z,t) &= \int_{S_B(\tau)} ds_\xi \sigma(\vec{\xi},t)\left(\frac{1}{r} - \frac{1}{r'}\right) \\
\varphi^{(M)}(x,y,z,t) &= \int_0^t d\tau \int_{S_B(\tau)} d\xi\sigma(\vec{\xi},\tau)H_\tau(\vec{x},\vec{\xi},t-\tau) \\
H_\tau(\vec{x},\vec{\xi},t-\tau) &= -\frac{1}{2\pi}\sum_j \int_0^\infty dk_j\ \sqrt{gk_j}e^{k_j(z+\zeta)}\sin[\sqrt{gk_j}(t-\tau)]J_0(k_jR)
\end{aligned} \tag{B.10}$$

The analysis proceeds by evaluating the free-surface impulse force on $z = 0$; The function H_τ can be rewritten as:

$$\text{let} \quad u_j = k_j \cos\gamma_j; \quad v_j = k_j \sin\gamma_j; \quad \text{thus} \quad du_j dv_j = k_j dk_j d\gamma_j$$

$$H_\tau(\vec{x},\vec{\xi},t-\tau) = -\frac{1}{4\pi^2}\sum_j \int_{-\pi}^{\pi} d\theta_j \int_0^{\infty} dk_j \ \sqrt{gk_j} e^{k_j\zeta} \sin[\sqrt{gk_j}(t-\tau)] e^{ik_j R\cos\theta_j} \tag{B.11}$$

Let $\theta_j = \gamma_j - \psi_j, \quad d\theta_j = d\gamma_j, \quad k_j^2 = u_j^2 + v_j^2$:

$$e^{ik_j R\cos\theta_j} = e^{iu_j(x-\xi)+iv_j(y-\eta)} \tag{B.12}$$

H_τ is then:

$$H_\tau(\vec{x},\vec{\xi},t-\tau) = -\frac{1}{4\pi^2}\sum_j \iint_{-\infty}^{\infty} du_j dv_j \ \sqrt{\frac{g}{k_j}} e^{k_j\zeta} \sin[\sqrt{gk_j}(t-\tau)] e^{iu_j(x-\xi)+iv_j(y-\eta)} \tag{B.13}$$

The first partial time derivative of the disturbance potential at $z = 0$ is then:

$$\frac{\partial\varphi}{\partial t}(x,y,0,t) = \frac{\partial\varphi^{(0)}}{\partial t}(x,y,0,t) + \frac{\partial\varphi^{(M)}}{\partial t}(x,y,0,t) \quad \text{with} \quad \frac{\partial\varphi^{(0)}}{\partial t} = 0.$$

$$\begin{aligned} &\frac{\partial\varphi^{(M)}}{\partial t}(x,y,0,t) = \\ &\quad -\frac{1}{4\pi^2}\int_0^t d\tau \int_{S_B(\tau)} d\xi\sigma(\xi,\tau) \\ &\quad \times \sum_j \iint_{-\infty}^{\infty} du_j dv_j \ e^{k_j\zeta}\sqrt{\frac{g}{k_j}}\sqrt{gk_j}\cos[\sqrt{gk_j}(t-\tau)] e^{iu_j(x-\xi)+iv_j(y-\eta)} \end{aligned} \tag{B.14}$$

Substituting into B.7, the integral over S_∞ becomes:

$$\vec{I}_{FS,3-ID,S_\infty}(t) = -\frac{\rho}{g^2}\iint_{-\infty}^{\infty} dxdy\left(\frac{\partial\varphi(t)}{\partial t}\frac{\partial^2\varphi_I(t)}{\partial t^2}\right)$$

$$= -\frac{\rho}{g^2}\iint_{-\infty}^{\infty} dxdy\Bigg\{\Re\Big\{\sum_j \frac{igA_j}{\omega_j}(i\omega_j)^2 e^{-i\nu_j x\cos\beta_j - i\nu_j y\sin\beta_j + i\omega_j t + i\chi_j}\Big\}$$

$$\times\ -\frac{1}{4\pi^2}\int_0^t d\tau\int_{S_B(\tau)} d\xi\sigma(\xi,\tau)\sum_j\iint_{-\infty}^{\infty} du_j dv_j\ e^{k_j\zeta}\sqrt{\frac{g}{k_j}}\sqrt{gk_j}\cos[\sqrt{gk_j}(t-\tau)]e^{iu_j(x-\xi)+iv_j(y-\eta)}\Bigg\} \tag{B.15}$$

Reorganizing B.15:

$$\vec{I}_{FS,3-ID,S_\infty}(t) = \frac{\rho}{g^2}\frac{1}{4\pi^2}\Re\Bigg\{\int_0^t d\tau\int_{S_B(\tau)} d\xi\sigma(\xi,\tau)$$

$$\times\sum_j\iint_{-\infty}^{\infty} du_j dv_j\Big[e^{\nu_j\zeta}\sqrt{\frac{g}{\nu_j}}\sqrt{g\nu_j}\cos[\sqrt{g\nu_j}(t-\tau)]\frac{igA_j}{\omega_j}(i\omega_j)^2 e^{i\omega_j t+i\chi_j}\Big]$$

$$\times\iint_{-\infty}^{\infty} dxdy\Big[e^{iu_j(x-\xi)-i\nu_j x\cos\beta_j+iv_j(y-\eta)-i\nu_j y\sin\beta_j}\Big]\Bigg\} \tag{B.16}$$

Applying the definitions of the delta dunctions:

$$\begin{aligned}\int_{-\infty}^{\infty} dx e^{ix(u_j-\nu_j\cos\beta_j)} &= 2\pi\delta(u_j-\nu_j\cos\beta_j)\\ \int_{-\infty}^{\infty} dy e^{iy(v_j-\nu_j\sin\beta_j)} &= 2\pi\delta(v_j-\nu_j\sin\beta_j)\end{aligned} \tag{B.17}$$

$$\iint_{-\infty}^{\infty} dxdy e^{iu_j x-i\nu_j x\cos\beta_j+iv_j y-i\nu_j y\sin\beta_j} = 4\pi^2\delta(u_j-\nu_j\cos\beta_j)\delta(v_j-\nu_j\sin\beta_j) \tag{B.18}$$

Substituting into B.16 and performing the infinite integral, the equation becomes:

$$\vec{I}_{FS,3-ID,S_\infty}(t) = \frac{\rho}{g^2}\frac{1}{4\pi^2}\Re\Bigg\{\int_0^t d\tau \int_{S_B(\tau)} d\xi\sigma(\xi,\tau)$$
$$\times\ 4\pi^2\sum_j\left[e^{\nu_j\zeta - i\nu_j\xi\cos\beta_j - i\nu_j\eta\sin\beta_j + i\omega_j t + i\chi_j}\sqrt{\frac{g}{\nu_j}}\sqrt{g\nu_j}\cos[\sqrt{g\nu_j}(t-\tau)]\frac{igA_j}{\omega_j}(i\omega_j)^2\right]\Bigg\} \tag{B.19}$$

Simplifying:

$$\vec{I}_{FS,3-ID,S_\infty}(t)$$
$$= -\rho\Re\Bigg\{\int_0^t d\tau\sum_j\left[iA_j\omega_j e^{i\omega_j t + i\chi_j}\cos[\sqrt{g\nu_j}(t-\tau)]\int_{S_B(\tau)} d\xi\sigma(\xi,\tau)e^{\nu_j\zeta - i\nu_j\xi\cos\beta_j - i\nu_j\eta\sin\beta_j}\right]\Bigg\}$$
$$= -\rho\Re\Bigg\{\int_0^t d\tau\sum_j\left[iA_j\omega_j e^{i\omega_j t + i\chi_j}\cos[\sqrt{g\nu_j}(t-\tau)]K_j(\nu_j,\beta_j,\tau)\right]\Bigg\}$$
$$\text{where}\quad K_j(\nu_j,\beta_j,\tau) = \int_{S_B(\tau)} d\xi\sigma(\xi,\tau)e^{\nu_j\zeta - i\nu_j\xi\cos\beta_j - i\nu_j\eta\sin\beta_j} \tag{B.20}$$

The final expression for $\vec{F}_{FS,3-ID}(t)$ is therefore:s

$$\vec{F}_{FS,3-ID}(t)$$
$$= \frac{\rho}{g^2}\frac{d}{dt}\int_{S_W(t)}\frac{\partial\varphi(t)}{\partial t}\frac{\partial^2\varphi_I(t)}{\partial t^2}ds$$
$$- \rho\frac{d}{dt}\int_0^t d\tau\Re\Bigg\{\sum_j\left[iA_j\omega_j e^{i\omega_j t + i\chi_j}\cos[\sqrt{g\nu_j}(t-\tau)]K_j(\nu_j,\beta_j,\tau)\right]\Bigg\} \tag{B.21}$$

Rewriting the DD integral in (B.3) over the ambient wave free-surface $S_I(t)$ into the difference between the infinte free-surface $S_\infty(t)$ and the ambient wave surface inside of the body $S_W(t)$:

$$\begin{aligned}
\vec{F}_{FS,3-DD}(t) &= \frac{\rho}{g}\frac{d}{dt}\int\limits_{S_I(t)}\left(\frac{\partial\varphi(t)}{\partial t}\frac{\partial\varphi(t)}{\partial z}\right)ds \\
&= \frac{\rho}{g}\frac{d}{dt}\left(\int\limits_{S_\infty(t)} - \int\limits_{S_W(t)}\right)\left(\frac{\partial\varphi(t)}{\partial t}\frac{\partial\varphi(t)}{\partial z}\right)ds \qquad \text{(B.22)} \\
\boxed{\text{linear FSC}} &= \frac{d}{dt}\left\{\frac{\rho}{g^2}\int\limits_{S_W(t)}\frac{\partial\varphi(t)}{\partial t}\frac{\partial^2\varphi(t)}{\partial t^2}ds + \frac{\rho}{g}\int\limits_{S_\infty(t)}\frac{\partial\varphi(t)}{\partial t}\frac{\partial\varphi(t)}{\partial z}ds\right\}
\end{aligned}$$

Seperating the derivative inside the integral over S_∞ into two parts:

$$\frac{\partial\varphi(t)}{\partial t}\frac{\partial\varphi(t)}{\partial z} = \frac{\partial\varphi^{(M)}(t)}{\partial t}\frac{\partial\varphi^{(0)}(t)}{\partial z} + \frac{\partial\varphi^{(M)}(t)}{\partial t}\frac{\partial\varphi^{(M)}(t)}{\partial z} \qquad \text{(B.23)}$$

Assuming small wave steepness, the integral over S_∞ can be evaluated on $z = 0$. Transforming the z derivative of the impulsive potential to a time derivative using the linear FSC:

$$\frac{\partial\varphi^{(M)}(t)}{\partial t}\frac{\partial\varphi^{(0)}(t)}{\partial z} = -\frac{1}{g}\frac{\partial\varphi^{(M)}(t)}{\partial t}\frac{\partial^2\varphi^{(0)}(t)}{\partial t^2} \qquad \text{(B.24)}$$

Recalling:

$$\frac{\partial\varphi^{(0)}(t)}{\partial t} = 0 \qquad \text{(B.25)}$$

Thus the 2nd integral of B.22 is now reduced to:

$$\frac{\rho}{g}\int_{S_\infty}\frac{\partial\varphi^{(M)}(t)}{\partial t}\frac{\partial\varphi^{(M)}(t)}{\partial z}ds \qquad \text{(B.26)}$$

The spatial and temporal derivative of the memory potentials on $z = 0$ are:

$$\text{let} \quad u = k\cos\gamma; \quad v = k\sin\gamma; \quad \text{thus} \quad dudv = kdkd\gamma$$

$$\varphi^{(M)}(x,y,z,t) = \int_0^t d\tau \int_{S_B(\tau)} ds_\xi \sigma(\vec{\xi},\tau) H_\tau(\vec{x},\vec{\xi},t-\tau)$$

$$H_\tau(\vec{x},\vec{\xi},t-\tau) = -\frac{1}{4\pi^2}\iint_{-\infty}^{\infty} dudv\; e^{k\zeta}\sqrt{\frac{g}{k}}\sin[\sqrt{gk}(t-\tau)]e^{iu(x-\xi)+iv(y-\eta)}$$

$$\frac{\partial\varphi^{(M)}(t)}{\partial t} = \int_0^t d\tau_1 \int_{S_B(\tau_1)} ds_{\xi_1}\sigma(\vec{\xi_1},\tau_1)$$
$$\times\Big(-\frac{1}{4\pi^2}\Big)\iint_{-\infty}^{\infty} du_1dv_1\; e^{k_1\zeta_1}\sqrt{\frac{g}{k_1}}\sqrt{gk_1}\cos[\sqrt{gk_1}(t-\tau_1)]e^{iu_1(x-\xi_1)+iv_1(y-\eta_1)}$$

$$\frac{\partial\varphi^{(M)}(t)}{\partial z} = \int_0^t d\tau_2 \int_{S_B(\tau_2)} ds_{\xi_2}\sigma(\vec{\xi_2},\tau_2)$$
$$\times\Big(-\frac{1}{4\pi^2}\Big)\iint_{-\infty}^{\infty} du_2dv_2\; e^{k_2\zeta_2}k_2\sqrt{\frac{g}{k_2}}\sin[\sqrt{gk_2}(t-\tau_2)]e^{iu_2(x-\xi_2)+iv_2(y-\eta_2)} \tag{B.27}$$

Substituting the expressions into impulse B.26

$$
\begin{aligned}
&\frac{\rho}{g}\int_{S_\infty}\frac{\partial\varphi^{(M)}(t)}{\partial t}\frac{\partial\varphi^{(M)}(t)}{\partial z}ds \\
&=\frac{\rho}{g}\iint_{-\infty}^{\infty}dxdy \\
&\quad\times\int_0^t d\tau_1\int_{S_B(\tau_1)}ds_{\xi_1}\sigma(\vec{\xi}_1,\tau_1) \\
&\quad\times\Big(-\frac{1}{4\pi^2}\Big)\iint_{-\infty}^{\infty}du_1dv_1\ e^{k_1\zeta_1}\sqrt{\frac{g}{k_1}}\sqrt{gk_1}\cos[\sqrt{gk_1}(t-\tau_1)]e^{iu_1(x-\xi_1)+iv_1(y-\eta_1)} \\
&\quad\times\int_0^t d\tau_2\int_{S_B(\tau_2)}ds_{\xi_2}\sigma(\vec{\xi}_2,\tau_2) \\
&\quad\times\Big(-\frac{1}{4\pi^2}\Big)\iint_{-\infty}^{\infty}du_2dv_2\ k_2e^{k_2\zeta_2}\sqrt{\frac{g}{k_2}}\sin(\sqrt{gk_2}(t-\tau_2))e^{iu_2(x-\xi_2)+iv_2(y-\eta_2)} \\
&=\rho\Big(-\frac{1}{4\pi^2}\Big)^2\int_0^t d\tau_1\int_{S_B(\tau_1)}ds_{\xi_1}\sigma(\vec{\xi}_1,\tau_1)\int_0^t d\tau_2\int_{S_B(\tau_2)}ds_{\xi_2}\sigma(\vec{\xi}_2,\tau_2) \\
&\quad\times\iint_{-\infty}^{\infty}du_1dv_1\ e^{k_1\zeta_1}\cos[\sqrt{gk_1}(t-\tau_1)]e^{-iu_1\xi_1-iv_1\eta_1} \\
&\quad\times\iint_{-\infty}^{\infty}du_2dv_2\ e^{k_2\zeta_2}\sqrt{gk_2}\sin(\sqrt{gk_2}(t-\tau_2))e^{-iu_2\xi_2-iv_2\eta_2} \\
&\quad\times\iint_{-\infty}^{\infty}dxdy\ e^{i(u_1+u_2)x+i(v_1+v_2)y}
\end{aligned}
\tag{B.28}
$$

Invoking the identity:

$$
\int_{-\infty}^{\infty}dx\int_{-\infty}^{\infty}dye^{i(u_1+u_2)x+i(v_1+v_2)y}=4\pi^2\delta(u_1+u_2)\delta(v_1+v_2) \tag{B.29}
$$

Using also the properties of the delta function:

$$\iint_{-\infty}^{\infty} du_1 dv_1 F(u_1, v_1)\delta(u_1 + u_2)\delta(v_1 + v_2) = F(-u_2, -v_2) \tag{B.30}$$

where

$$F(u_1, v_1) = e^{(u_1^2+v_1^2)^{(1/2)}\zeta_1}\cos[g^{(1/2)}(u_1^2 + v_1^2)^{(1/4)}(t - \tau_1)]e^{-iu_1\xi_1 - iv_1\eta_1} \tag{B.31}$$

Rewriting in B.28 terms of $u_2 = u$ and $v_2 = v$:

$$\begin{aligned}
&\frac{\rho}{g}\int_{S_\infty} \frac{\partial\varphi^{(M)}(t)}{\partial t}\frac{\partial\varphi^{(M)}(t)}{\partial z}ds \\
&= \frac{\rho}{g}\Big(-\frac{1}{4\pi^2}\Big)^2(4\pi^2)\int_0^t d\tau_1 \int_{S_B(\tau_1)} ds_{\xi_1}\sigma(\vec{\xi_1}, \tau_1)\int_0^t d\tau_2 \int_{S_B(\tau_2)} ds_{\xi_2}\sigma(\vec{\xi_2}, \tau_2) \\
&\quad \times \iint_{-\infty}^{\infty} du dv\ g^{(1/2)}(u^2 + v^2)^{(1/4)}e^{(u^2+v^2)^{(1/2)}(\zeta_1+\zeta_2)} \\
&\quad \times \cos[g^{(1/2)}(u^2 + v^2)^{(1/4)}(t - \tau_1)]\sin(g^{(1/2)}(u^2 + v^2)^{(1/4)}(t - \tau_2))e^{iu(\xi_1-\xi_2)+iv(\eta_1-\eta_2)} \\
&= \frac{\rho}{4\pi^2}\int_0^t d\tau_1 \int_{S_B(\tau_1)} ds_{\xi_1}\sigma(\vec{\xi_1}, \tau_1)\int_0^t d\tau_2 \int_{S_B(\tau_2)} ds_{\xi_2}\sigma(\vec{\xi_2}, \tau_2) \\
&\quad \times \iint_{-\infty}^{\infty} du dv\ \sqrt{gk}e^{k(\zeta_1+\zeta_2)}\cos[\sqrt{gk}(t - \tau_1)]\sin(\sqrt{gk}(t - \tau_2))e^{iu(\xi_1-\xi_2)+iv(\eta_1-\eta_2)}
\end{aligned} \tag{B.32}$$

With

$$\begin{aligned}
&\xi_1 - \xi_2 = R\cos\psi; \quad \eta_1 - \eta_2 = R\sin\psi; \\
&u = k\cos\gamma; \quad v = k\sin\gamma; \quad dudv = kdkd\gamma; \quad \theta = \gamma - \psi; \quad d\theta = d\gamma; \\
&\Rightarrow e^{iu(\xi_1-\xi_2)+iv(\eta_1-\eta_2)} = e^{ikR\cos(\gamma-\psi)} = e^{ikR\cos\theta}
\end{aligned} \tag{B.33}$$

The impulse becomes:

$$\begin{aligned}
&\frac{\rho}{g}\int_{S_\infty}\frac{\partial\varphi^{(M)}(t)}{\partial t}\frac{\partial\varphi^{(M)}(t)}{\partial z}ds \\
&=\frac{\rho}{4\pi^2}\int_0^t d\tau_1\int_{S_B(\tau_1)}ds_{\xi_1}\sigma(\vec{\xi}_1,\tau_1)\int_0^t d\tau_2\int_{S_B(\tau_2)}ds_{\xi_2}\sigma(\vec{\xi}_2,\tau_2) \\
&\quad\times\int_{-\pi}^{\pi}d\theta\int_0^\infty kdk\ \sqrt{gk}e^{k(\zeta_1+\zeta_2)}\cos[\sqrt{gk}(t-\tau_1)]\sin(\sqrt{gk}(t-\tau_2))e^{ikR\cos\theta}
\end{aligned} \tag{B.34}$$

Using trigonometric identities:

$$\cos[\sqrt{gk}(t-\tau_1)]\sin(\sqrt{gk}(t-\tau_2))=\frac{1}{2}\Big\{\sin(\sqrt{gk}(\tau_1-\tau_2))+\sin[\sqrt{gk}(2t-(\tau_1+\tau_2))]\Big\} \tag{B.35}$$

Thus:

$$\begin{aligned}
&\frac{\rho}{g}\int_{S_\infty}\frac{\partial\varphi^{(M)}(t)}{\partial t}\frac{\partial\varphi^{(M)}(t)}{\partial z}ds \\
&=-\rho\int_0^t d\tau_1\int_{S_B(\tau_1)}ds_{\xi_1}\sigma(\vec{\xi}_1,\tau_1)\int_0^t d\tau_2\int_{S_B(\tau_2)}ds_{\xi_2}\sigma(\vec{\xi}_2,\tau_2) \\
&\quad\times\frac{1}{2}\Big(-\frac{1}{4\pi^2}\Big)\frac{\partial}{\partial\zeta_1}\Big\{\int_{-\pi}^{\pi}d\theta\int_0^\infty dk\ \sqrt{gk}e^{k(\zeta_1+\zeta_2)}\sin(\sqrt{gk}(\tau_1-\tau_2))e^{ikR\cos\theta} \\
&\quad+\int_{-\pi}^{\pi}d\theta\int_0^\infty dk\ \sqrt{gk}e^{k(\zeta_1+\zeta_2)}\sin[\sqrt{gk}(2t-(\tau_1+\tau_2))]e^{ikR\cos\theta}\Big\}
\end{aligned} \tag{B.36}$$

$$
\begin{aligned}
&\frac{\rho}{g}\int_{S_\infty}\frac{\partial\varphi^{(M)}(t)}{\partial t}\frac{\partial\varphi^{(M)}(t)}{\partial z}ds \\
&= -\frac{\rho}{2}\int_0^t d\tau_1\int_{S_B(\tau_1)} ds_{\xi_1}\sigma(\vec{\xi}_1,\tau_1)\int_0^t d\tau_2\int_{S_B(\tau_2)} ds_{\xi_2}\sigma(\vec{\xi}_2,\tau_2) \\
&\quad\times\frac{\partial}{\partial\zeta_1}\Big[H_\tau(\vec{\xi}_1,\vec{\xi}_2,\tau_1-\tau_2)+H_\tau(\vec{\xi}_1,\vec{\xi}_2,2t-(\tau_1+\tau_2))\Big] \qquad \text{(B.37)}\\
&\quad\text{where}\quad H_\tau(\vec{\xi}_1,\vec{\xi}_2,T) \\
&\qquad = -\frac{1}{4\pi^2}\int_{-\pi}^{\pi}d\theta\int_0^\infty dk\ \sqrt{gk}e^{k(\zeta_1+\zeta_2)}sin[\sqrt{gk}T]e^{ikR\cos\theta}
\end{aligned}
$$

The final expression for $\vec{F}_{FS,3-DD}(t)$ is then:

$$
\begin{aligned}
&\vec{F}_{FS,3-DD}(t) \\
&\quad= \frac{d}{dt}\Bigg\{\frac{\rho}{g^2}\int_{S_W(t)}\frac{\partial\varphi(t)}{\partial t}\frac{\partial^2\varphi(t)}{\partial t^2}ds \\
&\qquad -\frac{\rho}{2}\int_0^t d\tau_1\int_{S_B(\tau_1)} ds_{\xi_1}\sigma(\vec{\xi}_1,\tau_1)\int_0^t d\tau_2\int_{S_B(\tau_2)} ds_{\xi_2}\sigma(\vec{\xi}_2,\tau_2) \qquad \text{(B.38)}\\
&\qquad\quad\times\frac{\partial}{\partial\zeta_1}\Big[H_\tau(\vec{\xi}_1,\vec{\xi}_2,\tau_1-\tau_2)+H_\tau(\vec{\xi}_1,\vec{\xi}_2,2t-(\tau_1+\tau_2))\Big]\Bigg\}
\end{aligned}
$$

Appendix C

Free-surface impulse force in Pitch

Start by using the moment expression presented in [30] and (2.43). Taking the free-surface impulse pitch moment up to second order:

$$\begin{aligned}\vec{M}_{FS,5}(t) = &-\rho\frac{d}{dt}\int\limits_{S_I(t)}\varphi(t)\Big(\vec{X}\times\vec{n}\Big)ds+\rho\int\limits_{S_I(t)}\frac{\partial\varphi(t)}{\partial t}\Big(\vec{X}\times\vec{k}\Big)ds\\&+\rho\frac{d}{dt}\int\limits_{S_I(t)}\left[\frac{1}{g}\frac{\partial\varphi(t)}{\partial t}\Big(\vec{X}\times(\nabla\varphi_I(t)+\nabla\varphi(t))\Big)\right]ds\end{aligned}\tag{C.1}$$

For small wave steepness, the normal vector to the ambient wave free-surface maybe expressed as:

$$\vec{n}=\frac{\nabla(Z-\zeta_I(X,Y,t))}{|\nabla(Z-\zeta_I(X,Y,t))|}=\frac{-\zeta_{I_X}\vec{i}-\zeta_{I_Y}\vec{j}+\vec{k}}{\sqrt{1+\zeta_{I_X}^2+\zeta_{I_Y}^2}}=(-\zeta_{I_X}\vec{i}-\zeta_{I_Y}\vec{j}+\vec{k})[1+O(\delta^2)]\tag{C.2}$$

$\vec{X} \times \vec{n}$, $\vec{X} \times \vec{k}$, $\vec{X} \times \nabla\varphi_I$ and $\vec{X} \times \nabla\varphi$ in the pitch direction are respectively:

$$\begin{aligned}
\Big(\vec{X} \times \vec{n}\Big)_5 &= (z\zeta_{I_X} - x)\vec{j} + O(\delta^2); \\
\Big(\vec{X} \times \vec{k}\Big)_5 &= -x\vec{j}; \\
\Big(\vec{X} \times \nabla\varphi_I\Big)_5 &= \Big(z\frac{\partial\varphi_I}{\partial X} - x\frac{\partial\varphi_I}{\partial Z}\Big)\vec{j}; \\
\Big(\vec{X} \times \nabla\varphi\Big)_5 &= \Big(z\frac{\partial\varphi}{\partial X} - x\frac{\partial\varphi}{\partial Z}\Big)\vec{j};
\end{aligned} \tag{C.3}$$

Substituting C.3 into C.1:

$$\begin{aligned}
\vec{M}_{FS,5}(t) = &-\rho\frac{d}{dt}\int\limits_{S_I(t)} \varphi(t)\Big(z\zeta_{I_X} - x\Big)ds + \rho\int\limits_{S_I(t)} \frac{\partial\varphi(t)}{\partial t}(-x)ds \\
&+ \frac{\rho}{g}\frac{d}{dt}\int\limits_{S_I(t)} \left[\frac{\partial\varphi(t)}{\partial t}\left(\Big(z\frac{\partial\varphi_I}{\partial X} - x\frac{\partial\varphi_I}{\partial Z}\Big) + \Big(z\frac{\partial\varphi}{\partial X} - x\frac{\partial\varphi}{\partial Z}\Big)\right)\right]ds + O(\delta^2)
\end{aligned} \tag{C.4}$$

For small wave steepness, the pitch moment is evaluated on $z = 0$, the remainder of the first and second integral cancels and the moment expression is reduced to:

$$\vec{M}_{FS,5}(t) = -\frac{\rho}{g}\frac{d}{dt}\int\limits_{S_I(t)} x\frac{\partial\varphi(t)}{\partial t}\left(\frac{\partial\varphi_I}{\partial Z} + \frac{\partial\varphi}{\partial Z}\right)ds \tag{C.5}$$

Applying the linear FSC:

$$\frac{\partial\varphi_I}{\partial Z} = -\frac{1}{g}\frac{\partial^2\varphi_I}{\partial t^2}; \quad \frac{\partial\varphi}{\partial Z} = -\frac{1}{g}\frac{\partial^2\varphi}{\partial t^2} \tag{C.6}$$

The pitch moment can be split into:

$$\begin{aligned}
\vec{M}_{FS,5}(t) &= \vec{M}_{FS,5-ID}(t) + \vec{M}_{FS,5-DD}(t) \\
\vec{M}_{FS,5-ID}(t) &= \frac{\rho}{g^2}\frac{d}{dt}\int\limits_{S_I(t)} \left(x\frac{\partial\varphi(t)}{\partial t}\frac{\partial^2\varphi_I(t)}{\partial t^2}\right)ds \\
\vec{M}_{FS,5-DD}(t) &= \frac{\rho}{g^2}\frac{d}{dt}\int\limits_{S_I(t)} \left(x\frac{\partial\varphi(t)}{\partial t}\frac{\partial^2\varphi(t)}{\partial t^2}\right)ds
\end{aligned} \tag{C.7}$$

Rewriting the ID integral as the difference between the impulse over the infinite free-surface and the ambient free-surface inside of the body:

$$\vec{M}_{FS,5-ID}(t) = \frac{\rho}{g^2}\frac{d}{dt}\left(\int\limits_{S_\infty(t)} - \int\limits_{S_W(t)}\right)\left(x\frac{\partial\varphi(t)}{\partial t}\frac{\partial^2\varphi_I(t)}{\partial t^2}\right)ds \tag{C.8}$$

The ID impulse in (C.8) can be split into:

$$\begin{aligned}
\vec{M}_{FS,5-ID}(t) &= \frac{d}{dt}\Big(\vec{I}_{FS,5-ID,S_W}(t) + \vec{I}_{FS,5-ID,S_\infty}(t)\Big);\\
\vec{I}_{FS,5-ID,S_W}(t) &= -\frac{\rho}{g^2}\int\limits_{S_W(t)} x\frac{\partial\varphi(t)}{\partial t}\frac{\partial^2\varphi_I(t)}{\partial t^2}ds\\
\vec{I}_{FS,5-ID,S_\infty}(t) &= \frac{\rho}{g^2}\int\limits_{S_\infty(t)} x\frac{\partial\varphi(t)}{\partial t}\frac{\partial^2\varphi_I(t)}{\partial t^2}ds
\end{aligned} \tag{C.9}$$

Focusing on the second integral over the infinte free-surface:
Substituting into the impulse over S_∞ in C.9:

$$\begin{aligned}
\vec{I}_{FS,5-ID,S_\infty}(t) &= \frac{\rho}{g^2}\iint\limits_{-\infty}^{\infty} dxdy\left(x\frac{\partial\varphi(t)}{\partial t}\frac{\partial^2\varphi_I(t)}{\partial t^2}\right)\\
&= \frac{\rho}{g^2}\iint\limits_{-\infty}^{\infty} dxdy\Bigg\{x\,\Re\Big\{\frac{igA}{\omega}(i\omega)^2 e^{-i\nu x\cos\beta - i\nu y\sin\beta + i\omega t}\Big\}\\
&\times\ -\frac{1}{4\pi^2}\int\limits_0^t d\tau\int_{S_B(\tau)} ds_\xi\sigma(\vec{\xi},\tau)\iint\limits_{-\infty}^{\infty} dudv\ e^{k\zeta}\sqrt{\frac{g}{k}}\sqrt{gk}\cos[\sqrt{gk}(t-\tau)]e^{iu(x-\xi)+iv(y-\eta)}\Bigg\}
\end{aligned} \tag{C.10}$$

Reorganizing (C.10):

$$\vec{I}_{FS,5-ID,S_\infty}(t) = \frac{\rho}{g}\Big(-\frac{1}{4\pi^2}\Big)\Re\Bigg\{\int_0^t d\tau \int_{S_B(\tau)} ds_\xi \sigma(\vec{\xi},\tau)(-igA\omega)e^{i\omega t} \times \iint_{-\infty}^{\infty} dudv\Big[e^{(u^2+v^2)^{(1/2)}\zeta}\cos[g^{(1/2)}(u^2+v^2)^{(1/4)}(t-\tau)]e^{-iu\xi-iv\eta}\Big] \times \iint_{-\infty}^{\infty} dxdy\Big[xe^{ix(u-\nu\cos\beta)+iv(y-\nu\sin\beta)}\Big]\Bigg\} \tag{C.11}$$

Let

$$f(u,v) = e^{(u^2+v^2)^{(1/2)}\zeta}\cos[g^{(1/2)}(u^2+v^2)^{(1/4)}(t-\tau)]e^{-iu\xi-iv\eta} \tag{C.12}$$

Applying the definitions of the delta dunctions:

$$\begin{aligned}\int_{-\infty}^{\infty} dx\ xe^{ix(u-\nu\cos\beta)} &= -2\pi i\delta'(u-\nu\cos\beta)\\ \int_{-\infty}^{\infty} dy\ e^{iy(v-\nu\sin\beta)} &= 2\pi\delta(v-\nu\sin\beta)\end{aligned} \tag{C.13}$$

(C.11) becomes:

$$\vec{I}_{FS,5-ID,S_\infty}(t) = \frac{\rho}{g}\Big(\frac{1}{4\pi^2}\Big)\Re\Bigg\{\int_0^t d\tau \int_{S_B(\tau)} ds_\xi \sigma(\vec{\xi},\tau)(igA\omega)e^{i\omega t} \times (-4\pi^2 i)\iint_{-\infty}^{\infty} dudv f(u,v)\delta'(u-\nu\cos\beta)\delta(v-\nu\sin\beta)\Bigg\} \tag{C.14}$$

Applying again properties of delta functions:

$$\iint_{-\infty}^{\infty} dudv f(u,v)\delta'(u-\nu\cos\beta)\delta(v-\nu\sin\beta) = -f'(\nu\cos\beta,\nu\sin\beta) \tag{C.15}$$

(C.14) becomes:

$$\vec{I}_{FS,5-ID,S_\infty}(t) = \rho A\omega \Re\Big\{ e^{i\omega t} \int_0^t d\tau \int_{S_B(\tau)} ds_\xi \sigma(\vec{\xi},\tau)\Big[- f'(\nu\cos\beta, \nu\sin\beta)\Big]\Big\} \quad \text{(C.16)}$$

$f'(u,v)$ is:

$$\begin{aligned}
&\frac{\partial}{\partial u} f(u,v) = \frac{\partial}{\partial u}\Big\{ e^{(u^2+v^2)^{(1/2)}\zeta} \cos[g^{(1/2)}(u^2+v^2)^{(1/4)}(t-\tau)] e^{-iu\xi - iv\eta}\Big\} \\
&= \Big(\frac{\partial}{\partial u} e^{(u^2+v^2)^{(1/2)}\zeta}\Big) \cos[g^{(1/2)}(u^2+v^2)^{(1/4)}(t-\tau)] e^{-iu\xi - iv\eta} \\
&\quad + \Big(\frac{\partial}{\partial u} \cos[g^{(1/2)}(u^2+v^2)^{(1/4)}(t-\tau)]\Big) e^{(u^2+v^2)^{(1/2)}\zeta} e^{-iu\xi - iv\eta} \\
&\quad + \Big(\frac{\partial}{\partial u} e^{-iu\xi - iv\eta}\Big) e^{(u^2+v^2)^{(1/2)}\zeta} \cos[g^{(1/2)}(u^2+v^2)^{(1/4)}(t-\tau)] \qquad \text{(C.17)} \\
&= \Big(\frac{u\zeta e^{(u^2+v^2)^{(1/2)}\zeta}}{(u^2+v^2)^{(1/2)}}\Big) \cos[g^{(1/2)}(u^2+v^2)^{(1/4)}(t-\tau)] e^{-iu\xi - iv\eta} \\
&\quad + \Big(\frac{-u\sqrt{g}(t-\tau)\sin[g^{(1/2)}(u^2+v^2)^{(1/4)}(t-\tau)]}{2(u^2+v^2)^{(3/4)}}\Big) e^{(u^2+v^2)^{(1/2)}\zeta} e^{-iu\xi - iv\eta} \\
&\quad + \Big(- i\xi e^{-iu\xi - iv\eta}\Big) e^{(u^2+v^2)^{(1/2)}\zeta} \cos[g^{(1/2)}(u^2+v^2)^{(1/4)}(t-\tau)]
\end{aligned}$$

$f'(\nu\cos\beta, \nu\sin\beta)$ is then:

$$\begin{aligned}
&= \Big(\zeta\cos\beta e^{\nu\zeta}\Big) \cos[\sqrt{g\nu}(t-\tau)] e^{-i\nu\xi\cos\beta - i\nu\eta\sin\beta} \\
&\quad + \Big(- \frac{1}{2}\sqrt{\frac{g}{\nu}} \cos\beta (t-\tau)\sin[\sqrt{g\nu}(t-\tau)]\Big) e^{\nu\zeta} e^{-i\nu\xi\cos\beta - i\nu\eta\sin\beta} \qquad \text{(C.18)} \\
&\quad + \Big(- i\xi e^{-i\nu\xi\cos\beta - i\nu\eta\sin\beta}\Big) e^{\nu\zeta} \cos[\sqrt{g\nu}(t-\tau)]
\end{aligned}$$

(C.16) becomes:

$$\begin{aligned}\vec{I}_{FS,5-ID,S_\infty}(t) = \; & \rho A\omega\Re\Bigg\{e^{i\omega t}\int_0^t d\tau\int_{S_B(\tau)} ds_\xi\sigma(\vec{\xi},\tau) \\ & \times\Big[-\zeta\cos\beta\cos[\sqrt{g\nu}(t-\tau)]e^{\nu\zeta-i\nu\xi\cos\beta-i\nu\eta\sin\beta} \\ & +\frac{1}{2}\sqrt{\frac{g}{\nu}}\cos\beta(t-\tau)\sin[\sqrt{g\nu}(t-\tau)]e^{\nu\zeta-i\nu\xi\cos\beta-i\nu\eta\sin\beta} \\ & +i\xi\cos[\sqrt{g\nu}(t-\tau)]e^{\nu\zeta-i\nu\xi\cos\beta-i\nu\eta\sin\beta}\Big]\Bigg\}\end{aligned} \tag{C.19}$$

The free-surface pitch ID moment is then:

$$\begin{aligned}\vec{M}_{FS,5-ID}(t) = & -\frac{\rho}{g^2}\frac{d}{dt}\int_{S_W(t)}\left(x\frac{\partial\varphi(t)}{\partial t}\frac{\partial^2\varphi_I(t)}{\partial t^2}\right)ds \\ & +\rho A\omega\Re\Bigg\{e^{i\omega t}\int_0^t d\tau\int_{S_B(\tau)} ds_\xi\sigma(\vec{\xi},\tau)\Big[Q_1+Q_2+Q_3\Big]e^{\nu\zeta-i\nu\xi\cos\beta-i\nu\eta\sin\beta}\Bigg\}\end{aligned} \tag{C.20}$$

where

$$Q_1 = -\zeta\cos\beta\cos[\sqrt{g\nu}(t-\tau)];$$

$$Q_2 = \frac{1}{2}\sqrt{\frac{g}{\nu}}\cos\beta(t-\tau)\sin[\sqrt{g\nu}(t-\tau)];$$

$$Q_3 = i\xi\cos[\sqrt{g\nu}(t-\tau)].$$

Rewriting the DD integral over the ambient wave free-surface $S_I(t)$ into the difference between the infinte free-surface $S_\infty(t)$ and the ambient wave surface inside of the body $S_W(t)$:

$$\begin{aligned}
\vec{M}_{FS,5-DD}(t) &= -\frac{\rho}{g}\frac{d}{dt}\int\limits_{S_I(t)}\left(x\frac{\partial\varphi(t)}{\partial t}\frac{\partial\varphi(t)}{\partial z}\right)ds \\
&= -\frac{\rho}{g}\frac{d}{dt}\left(\int\limits_{S_\infty(t)} - \int\limits_{S_W(t)}\right)\left(x\frac{\partial\varphi(t)}{\partial t}\frac{\partial\varphi(t)}{\partial z}\right)ds \qquad \text{(C.21)} \\
\boxed{\text{linear FSC}} &= \frac{d}{dt}\left\{-\frac{\rho}{g^2}\int\limits_{S_W(t)} x\frac{\partial\varphi(t)}{\partial t}\frac{\partial^2\varphi(t)}{\partial t^2}ds - \frac{\rho}{g}\int\limits_{S_\infty(t)} x\frac{\partial\varphi(t)}{\partial t}\frac{\partial\varphi(t)}{\partial z}ds\right\}
\end{aligned}$$

Same with the heave free-surface impulse force, as $\partial\varphi^{(0)}/\partial t = 0$, the 2nd integral in (C.21) can be reduced to:

$$-\frac{\rho}{g}\int_{S_\infty} x\frac{\partial\varphi^{(M)}(t)}{\partial t}\frac{\partial\varphi^{(M)}(t)}{\partial z}ds \qquad \text{(C.22)}$$

Substituting the expressions of the derivatives of the memory potentials into (C.22):

$$
\begin{aligned}
&-\frac{\rho}{g}\int_{S_\infty} x\frac{\partial\varphi^{(M)}(t)}{\partial t}\frac{\partial\varphi^{(M)}(t)}{\partial z}ds \\
&= -\rho\Big(-\frac{1}{4\pi^2}\Big)^2\int_0^t d\tau_1\int_{S_B(\tau_1)} ds_{\xi_1}\sigma(\vec{\xi}_1,\tau_1)\int_0^t d\tau_2\int_{S_B(\tau_2)} ds_{\xi_2}\sigma(\vec{\xi}_2,\tau_2) \\
&\quad\times\iint_{-\infty}^{\infty} du_1dv_1\; e^{k_1\zeta_1}\cos[\sqrt{gk_1}(t-\tau_1)]e^{-iu_1\xi_1-iv_1\eta_1} \\
&\quad\times\iint_{-\infty}^{\infty} du_2dv_2\; e^{k_2\zeta_2}\sqrt{gk_2}\sin(\sqrt{gk_2}(t-\tau_2))e^{-iu_2\xi_2-iv_2\eta_2} \\
&\quad\times\iint_{-\infty}^{\infty} dxdy\; xe^{i(u_1+u_2)x+i(v_1+v_2)y} \\
&= -\rho\Big(-\frac{1}{4\pi^2}\Big)^2\int_0^t d\tau_1\int_{S_B(\tau_1)} ds_{\xi_1}\sigma(\vec{\xi}_1,\tau_1)\int_0^t d\tau_2\int_{S_B(\tau_2)} ds_{\xi_2}\sigma(\vec{\xi}_2,\tau_2) \\
&\quad\times\iint_{-\infty}^{\infty} du_1dv_1\; F_1(u_1,v_1)\iint_{-\infty}^{\infty} du_2dv_2\; F_2(u_2,v_2) \\
&\quad\times\iint_{-\infty}^{\infty} dxdy\; xe^{i(u_1+u_2)x+i(v_1+v_2)y}
\end{aligned}
\tag{C.23}
$$

where:

$$
\begin{aligned}
F_1(u_1,v_1) &= e^{(u_1^2+v_1^2)^{(1/2)}\zeta_1}\cos[g^{(1/2)}(u_1^2+v_1^2)^{(1/4)}(t-\tau_1)]e^{-iu_1\xi_1-iv_1\eta_1} \\
F_2(u_2,v_2) &= e^{(u_2^2+v_2^2)^{(1/2)}\zeta_2}g^{(1/2)}(u_2^2+v_2^2)^{(1/4)}\sin[(g^{(1/2)}(u_2^2+v_2^2)^{(1/4)}(t-\tau_2))]e^{-iu_2\xi_2-iv_2\eta_2}
\end{aligned}
\tag{C.24}
$$

Invoking the identity:

$$
\int_{-\infty}^{\infty} dx\int_{-\infty}^{\infty} dy\; xe^{i(u_1+u_2)x+i(v_1+v_2)y} = -4\pi^2 i\delta'(u_1+u_2)\delta(v_1+v_2) \tag{C.25}
$$

Using also the properties of the delta function:

$$\iint_{-\infty}^{\infty} du_1 dv_1 F_1(u_1, v_1)\delta'(u_1 + u_2)\delta(v_1 + v_2) = -F_1'(-u_2, -v_2) \tag{C.26}$$

$F_1'(u_1, v_1)$ is:

$$\begin{aligned}
\frac{\partial}{\partial u_1}F_1'(u_1, v_1) &= \frac{\partial}{\partial u_1}\Big\{e^{(u_1^2+v_1^2)^{(1/2)}\zeta}\cos[g^{(1/2)}(u_1^2 + v_1^2)^{(1/4)}(t - \tau_1)]e^{-iu_1\xi_1 - iv_1\eta_1}\Big\} \\
&= \Big(\frac{u_1\zeta_1 e^{(u_1^2+v_1^2)^{(1/2)}\zeta_1}}{(u_1^2 + v_1^2)^{(1/2)}}\Big)\cos[g^{(1/2)}(u_1^2 + v_1^2)^{(1/4)}(t - \tau_1)]e^{-iu_1\xi_1 - iv_1\eta_1} \\
&\quad + \Big(\frac{-u_1\sqrt{g}(t - \tau_1)\sin[g^{(1/2)}(u_1^2 + v_1^2)^{(1/4)}(t - \tau_1)]}{2(u_1^2 + v_1^2)^{(3/4)}}\Big)e^{(u_1^2+v_1^2)^{(1/2)}\zeta_1}e^{-iu_1\xi_1 - iv_1\eta_1} \\
&\quad + \Big(-i\xi_1 e^{-iu_1\xi_1 - iv_1\eta_1}\Big)e^{(u_1^2+v_1^2)^{(1/2)}\zeta_1}\cos[g^{(1/2)}(u_1^2 + v_1^2)^{(1/4)}(t - \tau_1)]
\end{aligned} \tag{C.27}$$

$F_1'(-u_2, -v_2)$ is then:

$$\begin{aligned}
&= \Big(\frac{-u_2\zeta_1 e^{(u_2^2+v_2^2)^{(1/2)}\zeta_1}}{(u_2^2 + v_2^2)^{(1/2)}}\Big)\cos[g^{(1/2)}(u_2^2 + v_2^2)^{(1/4)}(t - \tau_1)]e^{iu_2\xi_1 + iv_2\eta_1} \\
&\quad + \Big(\frac{u_2\sqrt{g}(t - \tau_1)\sin[g^{(1/2)}(u_2^2 + v_2^2)^{(1/4)}(t - \tau_1)]}{2(u_2^2 + v_2^2)^{(3/4)}}\Big)e^{(u_2^2+v_2^2)^{(1/2)}\zeta_1}e^{iu_2\xi_1 + iv_2\eta_1} \\
&\quad + \Big(-i\xi_1 e^{iu_2\xi_1 + iv_2\eta_1}\Big)e^{(u_2^2+v_2^2)^{(1/2)}\zeta_1}\cos[g^{(1/2)}(u_2^2 + v_2^2)^{(1/4)}(t - \tau_1)]
\end{aligned} \tag{C.28}$$

Revisiting the impulse:

$$\begin{aligned}
&-\frac{\rho}{g}\int_{S_\infty} x\frac{\partial\varphi^{(M)}(t)}{\partial t}\frac{\partial\varphi^{(M)}(t)}{\partial z}ds \\
&= -\rho\Big(\frac{1}{4\pi^2}\Big)^2(-4\pi^2 i)\int_0^t d\tau_1\int_{S_B(\tau_1)} ds_{\xi_1}\sigma(\vec{\xi}_1, \tau_1)\int_0^t d\tau_2\int_{S_B(\tau_2)} ds_{\xi_2}\sigma(\vec{\xi}_2, \tau_2) \\
&\quad \times \iint_{-\infty}^{\infty} du_2 dv_2\ F_2(u_2, v_2)\Big(-F_1'(-u_2, -v_2)\Big)
\end{aligned} \tag{C.29}$$

For $F_2(u_2, v_2)F_1'(-u_2, -v_2)$, simplify it into 3 seperate terms and reduce the expressions with $u = u_2$ and $u^2 + v^2 = k^2$:

$$
\begin{aligned}
&F_2(u,v)F_{1-1}'(-u,-v) \\
&= \Big(\frac{-u\zeta_1 e^{(u^2+v^2)^{(1/2)}\zeta_1}}{(u^2+v^2)^{(1/2)}}\Big)\cos[g^{(1/2)}(u^2+v^2)^{(1/4)}(t-\tau_1)]e^{iu\xi_1+iv\eta_1} \\
&\quad \times e^{(u^2+v^2)^{(1/2)}\zeta_2} g^{(1/2)}(u^2+v^2)^{(1/4)}\sin[(g^{(1/2)}(u^2+v^2)^{(1/4)}(t-\tau_2))]e^{-iu\xi_2-iv\eta_2} \\
&= -u\zeta_1\sqrt{\frac{g}{k}}e^{k(\zeta_1+\zeta_2)}\cos[\sqrt{gk}(t-\tau_1)]\sin[\sqrt{gk}(t-\tau_2)]e^{iu(\xi_1-\xi_2)+iv(\eta_1-\eta_2)} \\
&= -\Big(\frac{1}{iu}\Big)\frac{\partial}{\partial\xi_1}\Big\{u\zeta_1\sqrt{\frac{g}{k}}e^{k(\zeta_1+\zeta_2)}\cos[\sqrt{gk}(t-\tau_1)]\sin[\sqrt{gk}(t-\tau_2)]e^{iu(\xi_1-\xi_2)+iv(\eta_1-\eta_2)}\Big\} \\
&= -\frac{\zeta_1}{i}\frac{\partial}{\partial\xi_1}\Bigg\{\sqrt{\frac{g}{k}}e^{k(\zeta_1+\zeta_2)}e^{iu(\xi_1-\xi_2)+iv(\eta_1-\eta_2)} \\
&\qquad \times\frac{1}{2}\Big\{\sin(\sqrt{gk}(\tau_1-\tau_2))+\sin[\sqrt{gk}(2t-(\tau_1+\tau_2))]\Big\}\Bigg\} \\
&= -\frac{\zeta_1}{2i}\frac{\partial}{\partial\xi_1}\Bigg\{\sqrt{\frac{g}{k}}e^{k(\zeta_1+\zeta_2)}e^{iu(\xi_1-\xi_2)+iv(\eta_1-\eta_2)} \\
&\qquad \times\Big\{\sin(\sqrt{gk}(\tau_1-\tau_2))+\sin[\sqrt{gk}(2t-(\tau_1+\tau_2))]\Big\}\Bigg\}
\end{aligned}
\tag{C.30}
$$

$$
\begin{aligned}
&F_2(u,v)F'_{1-2}(-u,-v) \\
&= \Big(\frac{u\sqrt{g}(t-\tau_1)\sin[g^{(1/2)}(u^2+v^2)^{(1/4)}(t-\tau_1)]}{2(u^2+v^2)^{(3/4)}}\Big)e^{(u^2+v^2)^{(1/2)}\zeta_1}e^{iu\xi_1+iv\eta_1} \\
&\quad \times e^{(u^2+v^2)^{(1/2)}\zeta_2}g^{(1/2)}(u^2+v^2)^{(1/4)}\sin[(g^{(1/2)}(u^2+v^2)^{(1/4)}(t-\tau_2))]e^{-iu\xi_2-iv\eta_2} \\
&= \frac{ug}{2k}(t-\tau_1)e^{k(\zeta_1+\zeta_2)}\sin[\sqrt{gk}(t-\tau_1)]\sin[\sqrt{gk}(t-\tau_2)]e^{iu(\xi_1-\xi_2)+iv(\eta_1-\eta_2)} \\
&= \Big(\frac{1}{iu}\Big)\frac{\partial}{\partial\xi_1}\Bigg\{\frac{u}{2}\frac{g}{k}(t-\tau_1)e^{k(\zeta_1+\zeta_2)}e^{iu(\xi_1-\xi_2)+iv(\eta_1-\eta_2)} \\
&\quad \times \frac{1}{2}\Big\{\cos[\sqrt{gk}(\tau_1-\tau_2)]-\cos[\sqrt{gk}(2t-(\tau_1+\tau_2))]\Big\}\Bigg\} \\
&= \frac{1}{2i}\frac{\partial}{\partial\xi_1}\Bigg\{\frac{g}{k}(t-\tau_1)e^{k(\zeta_1+\zeta_2)}e^{iu(\xi_1-\xi_2)+iv(\eta_1-\eta_2)} \\
&\quad \times \frac{1}{2}\Big\{\Big(\frac{1}{\sqrt{gk}}\Big)\frac{\partial}{\partial\tau_2}\sin[\sqrt{gk}(\tau_1-\tau_2)]-\Big(\frac{-1}{\sqrt{gk}}\Big)\frac{\partial}{\partial\tau_2}\sin[\sqrt{gk}(2t-(\tau_1+\tau_2))]\Big\}\Bigg\} \\
&= \frac{1}{4i}\frac{\partial}{\partial\xi_1}\Bigg\{(t-\tau_1)\frac{1}{k}\sqrt{\frac{g}{k}}e^{k(\zeta_1+\zeta_2)}e^{iu(\xi_1-\xi_2)+iv(\eta_1-\eta_2)} \\
&\quad \times \Big\{\frac{\partial}{\partial\tau_2}\sin[\sqrt{gk}(\tau_1-\tau_2)]+\frac{\partial}{\partial\tau_2}\sin[\sqrt{gk}(2t-(\tau_1+\tau_2))]\Big\}\Bigg\}
\end{aligned}
\tag{C.31}
$$

$$
\begin{aligned}
&F_2(u,v)F'_{1-3}(-u,-v) \\
&= \Big(- i\xi_1 e^{iu\xi_1 + iv\eta_1} \Big) e^{(u^2+v^2)^{(1/2)}\zeta_1} \cos[g^{(1/2)}(u^2+v^2)^{(1/4)}(t-\tau_1)] \\
&\quad \times e^{(u^2+v^2)^{(1/2)}\zeta_2} g^{(1/2)}(u^2+v^2)^{(1/4)} \sin[(g^{(1/2)}(u^2+v^2)^{(1/4)}(t-\tau_2))] e^{-iu\xi_2 - iv\eta_2} \\
&= -i\xi_1 \sqrt{gk} e^{k(\zeta_1+\zeta_2)} \cos[\sqrt{gk}(t-\tau_1)] \sin[\sqrt{gk}(t-\tau_2)] e^{iu(\xi_1-\xi_2)+iv(\eta_1-\eta_2)} \\
&= -i\xi_1 \Big(\frac{1}{k}\Big) \frac{\partial}{\partial \zeta_1} \Bigg\{ \sqrt{gk} e^{k(\zeta_1+\zeta_2)} e^{iu(\xi_1-\xi_2)+iv(\eta_1-\eta_2)} \\
&\qquad \times \frac{1}{2} \Big\{ \sin(\sqrt{gk}(\tau_1-\tau_2)) + \sin[\sqrt{gk}(2t-(\tau_1+\tau_2))] \Big\} \Bigg\} \\
&= -\frac{i\xi_1}{2} \frac{\partial}{\partial \zeta_1} \Bigg\{ \sqrt{\frac{g}{k}} e^{k(\zeta_1+\zeta_2)} e^{iu(\xi_1-\xi_2)+iv(\eta_1-\eta_2)} \\
&\qquad \times \Big\{ \sin(\sqrt{gk}(\tau_1-\tau_2)) + \sin[\sqrt{gk}(2t-(\tau_1+\tau_2))] \Big\} \Bigg\}
\end{aligned}
\tag{C.32}
$$

The impulse now becomes:

$$
\begin{aligned}
&-\frac{\rho}{g}\int_{S_\infty} x\frac{\partial\varphi^{(M)}(t)}{\partial t}\frac{\partial\varphi^{(M)}(t)}{\partial z}ds \\
&=-\rho\Big(\frac{i}{4\pi^2}\Big)\int_0^t d\tau_1\int_{S_B(\tau_1)} ds_{\xi_1}\sigma(\vec{\xi}_1,\tau_1)\int_0^t d\tau_2\int_{S_B(\tau_2)} ds_{\xi_2}\sigma(\vec{\xi}_2,\tau_2) \\
&\quad\times\iint_{-\infty}^{\infty} dudv\left\{\right. \\
&\qquad-\frac{\zeta_1}{2i}\frac{\partial}{\partial\xi_1}\left\{\sqrt{\frac{g}{k}}e^{k(\zeta_1+\zeta_2)}e^{iu(\xi_1-\xi_2)+iv(\eta_1-\eta_2)}\right. \\
&\qquad\quad\left.\times\Big\{\sin(\sqrt{gk}(\tau_1-\tau_2))+\sin[\sqrt{gk}(2t-(\tau_1+\tau_2))]\Big\}\right\} \\
&\qquad+\frac{1}{4i}\frac{\partial}{\partial\xi_1}\left\{(t-\tau_1)\frac{1}{k}\sqrt{\frac{g}{k}}e^{k(\zeta_1+\zeta_2)}e^{iu(\xi_1-\xi_2)+iv(\eta_1-\eta_2)}\right. \\
&\qquad\quad\left.\times\Big\{\frac{\partial}{\partial\tau_2}\sin[\sqrt{gk}(\tau_1-\tau_2)]+\frac{\partial}{\partial\tau_2}\sin[\sqrt{gk}(2t-(\tau_1+\tau_2))]\Big\}\right\} \\
&\qquad-\frac{i\xi_1}{2}\frac{\partial}{\partial\zeta_1}\left\{\sqrt{\frac{g}{k}}e^{k(\zeta_1+\zeta_2)}e^{iu(\xi_1-\xi_2)+iv(\eta_1-\eta_2)}\right. \\
&\qquad\quad\left.\left.\times\Big\{\sin(\sqrt{gk}(\tau_1-\tau_2))+\sin[\sqrt{gk}(2t-(\tau_1+\tau_2))]\Big\}\right\}\right\}
\end{aligned}
\tag{C.33}
$$

$$
\begin{aligned}
&= -\rho\Big(\frac{i}{4\pi^2}\Big)\int_0^t d\tau_1 \int_{S_B(\tau_1)} ds_{\xi_1}\sigma(\vec{\xi}_1,\tau_1)\int_0^t d\tau_2 \int_{S_B(\tau_2)} ds_{\xi_2}\sigma(\vec{\xi}_2,\tau_2)\\
&\quad\times\int_{-\pi}^{\pi} d\theta \int_0^{\infty} k dk \left\{\right.\\
&\qquad -\frac{\zeta_1}{2i}\frac{\partial}{\partial\xi_1}\left\{\sqrt{\frac{g}{k}}e^{k(\zeta_1+\zeta_2)}e^{ikR\cos\theta}\right.\\
&\qquad\quad\left.\times\left\{\sin(\sqrt{gk}(\tau_1-\tau_2))+\sin[\sqrt{gk}(2t-(\tau_1+\tau_2))]\right\}\right\}\\
&\qquad +\frac{1}{4i}\frac{\partial}{\partial\xi_1}\left\{(t-\tau_1)\frac{1}{k}\sqrt{\frac{g}{k}}e^{k(\zeta_1+\zeta_2)}e^{ikR\cos\theta}\right.\\
&\qquad\quad\left.\times\left\{\frac{\partial}{\partial\tau_2}\sin[\sqrt{gk}(\tau_1-\tau_2)]+\frac{\partial}{\partial\tau_2}\sin[\sqrt{gk}(2t-(\tau_1+\tau_2))]\right\}\right\}\\
&\qquad -\frac{i\xi_1}{2}\frac{\partial}{\partial\zeta_1}\left\{\sqrt{\frac{g}{k}}e^{k(\zeta_1+\zeta_2)}e^{ikR\cos\theta}\right.\\
&\qquad\quad\left.\left.\times\left\{\sin(\sqrt{gk}(\tau_1-\tau_2))+\sin[\sqrt{gk}(2t-(\tau_1+\tau_2))]\right\}\right\}\right\}
\end{aligned}
\tag{C.34}
$$

$$
\begin{aligned}
&= \rho \int_0^t d\tau_1 \int_{S_B(\tau_1)} ds_{\xi_1} \sigma(\vec{\xi}_1, \tau_1) \int_0^t d\tau_2 \int_{S_B(\tau_2)} ds_{\xi_2} \sigma(\vec{\xi}_2, \tau_2) \\
&\quad \times \left(\frac{-1}{4\pi^2}\right) \int_{-\pi}^{\pi} d\theta \int_0^{\infty} dk \left\{ \right. \\
&\qquad - \frac{\zeta_1}{2} \frac{\partial}{\partial \xi_1} \left\{ \sqrt{gk} e^{k(\zeta_1+\zeta_2)} e^{ikR\cos\theta} \right. \\
&\qquad\quad \left. \times \left\{ \sin(\sqrt{gk}(\tau_1 - \tau_2)) + \sin[\sqrt{gk}(2t - (\tau_1 + \tau_2))] \right\} \right\} \\
&\qquad + \frac{1}{4} \frac{\partial}{\partial \xi_1} \left\{ (t - \tau_1) \frac{1}{k} \sqrt{gk} e^{k(\zeta_1+\zeta_2)} e^{ikR\cos\theta} \right. \\
&\qquad\quad \left. \times \left\{ \frac{\partial}{\partial \tau_2} \sin[\sqrt{gk}(\tau_1 - \tau_2)] + \frac{\partial}{\partial \tau_2} \sin[\sqrt{gk}(2t - (\tau_1 + \tau_2))] \right\} \right\} \\
&\qquad + \frac{\xi_1}{2} \frac{\partial}{\partial \zeta_1} \left\{ \sqrt{gk} e^{k(\zeta_1+\zeta_2)} e^{ikR\cos\theta} \right. \\
&\qquad\quad \left. \left. \times \left\{ \sin(\sqrt{gk}(\tau_1 - \tau_2)) + \sin[\sqrt{gk}(2t - (\tau_1 + \tau_2))] \right\} \right\} \right\}
\end{aligned}
\tag{C.35}
$$

The impulse is then:

$$
\begin{aligned}
&-\frac{\rho}{g}\int_{S_\infty} x\frac{\partial\varphi^{(M)}(t)}{\partial t}\frac{\partial\varphi^{(M)}(t)}{\partial z}ds \\
&=\rho\int_0^t d\tau_1\int_{S_B(\tau_1)} ds_{\xi_1}\sigma(\vec{\xi}_1,\tau_1)\int_0^t d\tau_2\int_{S_B(\tau_2)} ds_{\xi_2}\sigma(\vec{\xi}_2,\tau_2) \\
&\quad\times\Bigg\{-\frac{\zeta_1}{2}\frac{\partial}{\partial\xi_1}\Big[H_\tau(\vec{\xi}_1,\vec{\xi}_2,\tau_1-\tau_2)+H_\tau(\vec{\xi}_1,\vec{\xi}_2,2t-(\tau_1+\tau_2))\Big] \\
&\qquad+\frac{(t-\tau_1)}{2k}\int d\zeta_1\frac{\partial}{\partial\xi_1}\frac{\partial}{\partial t}\Big[H_\tau(\vec{\xi}_1,\vec{\xi}_2,\tau_1-\tau_2)+H_\tau(\vec{\xi}_1,\vec{\xi}_2,2t-(\tau_1+\tau_2))\Big] \\
&\qquad+\frac{\xi_1}{2}\frac{\partial}{\partial\zeta_1}\Big[H_\tau(\vec{\xi}_1,\vec{\xi}_2,\tau_1-\tau_2)+H_\tau(\vec{\xi}_1,\vec{\xi}_2,2t-(\tau_1+\tau_2))\Big]\Bigg\}
\end{aligned}
\tag{C.36}
$$

where $H_\tau(\vec{\xi}_1,\vec{\xi}_2,T)$

$$
=-\frac{1}{4\pi^2}\int_{-\pi}^{\pi}d\theta\int_0^\infty dk\ \sqrt{gk}e^{k(\zeta_1+\zeta_2)}sin[\sqrt{gk}T]e^{ikR\cos\theta}
$$

The DD free-surface pitch moment is then:

$$
\begin{aligned}
\vec{M}_{FS,5-DD}(t)&=\frac{d}{dt}\Bigg\{-\frac{\rho}{g^2}\int_{S_W(t)} x\frac{\partial\varphi(t)}{\partial t}\frac{\partial^2\varphi(t)}{\partial t^2}ds \\
&\quad+\rho\int_0^t d\tau_1\int_{S_B(\tau_1)} ds_{\xi_1}\sigma(\vec{\xi}_1,\tau_1)\int_0^t d\tau_2\int_{S_B(\tau_2)} ds_{\xi_2}\sigma(\vec{\xi}_2,\tau_2) \\
&\qquad\times\Bigg\{-\frac{\zeta_1}{2}\frac{\partial}{\partial\xi_1}\Big[H_\tau(\vec{\xi}_1,\vec{\xi}_2,\tau_1-\tau_2)+H_\tau(\vec{\xi}_1,\vec{\xi}_2,2t-(\tau_1+\tau_2))\Big] \\
&\qquad\quad+\frac{(t-\tau_1)}{2k}\int d\zeta_1\frac{\partial}{\partial\xi_1}\frac{\partial}{\partial t}\Big[H_\tau(\vec{\xi}_1,\vec{\xi}_2,\tau_1-\tau_2)+H_\tau(\vec{\xi}_1,\vec{\xi}_2,2t-(\tau_1+\tau_2))\Big] \\
&\qquad\quad+\frac{\xi_1}{2}\frac{\partial}{\partial\zeta_1}\Big[H_\tau(\vec{\xi}_1,\vec{\xi}_2,\tau_1-\tau_2)+H_\tau(\vec{\xi}_1,\vec{\xi}_2,2t-(\tau_1+\tau_2))\Big]\Bigg\}\Bigg\}
\end{aligned}
\tag{C.37}
$$

Appendix D

Nonlinear loads on a vertical cylinder in irregular waves of small Ka

This section discuss the method presented by Sclavounos [31] on computing nonlinear surge force acting on a vertical circular cylinder in irregular waves.

For a vertical cylinder fixed in space (a diffraction problem), the Fluid-Impulse Theory can be used to approximate nonlinear loads to leading order by the 2D croos-flow potential.

The ambient waves are assumed to be irregular. The expressions presented in this section are valid for finite values of Ka, where K is a characteristic wavenumber and a is the cylinder radius.

The characteristic wavelegnth in a seastate is often large relative to the cylinder diameters of offshore structures and wind turbines. In such cases Ka is a small parameter and the diffraction potential near the cylinder may be approximated to leading order by the 2D cross-flow potential:

$$\varphi(r,\theta) = -u_1 \frac{a}{r}\cos\theta, \quad u_1 = \frac{\partial \varphi_I}{\partial x}(r=0) \tag{D.1}$$

For a polychromatic wave the incident wave velocity potential is:

$$\text{(polychromatic)} \quad \varphi_I(x,y,z,t) = \Re\left\{ \sum_j \frac{igA_j}{\omega_j} e^{\nu_j z - i\nu_j x\cos\beta_j - i\nu_j y\sin\beta_j + i\omega_j t + i\chi_j} \right\} \tag{D.2}$$

The first x-derivative of φ_I in deep water is:

$$\begin{aligned} \frac{\partial\varphi_I}{\partial x} &= \Re\left\{ \sum_j \frac{igA_j}{\omega_j}(-i\nu_j\cos\beta_j) e^{\nu_j z - i\nu_j x\cos\beta_j - i\nu_j y\sin\beta_j + i\omega_j t + i\chi_j} \right\} \\ &= \Re\left\{ \sum_j A_j\omega_j\cos\beta_j e^{\nu_j z - i\nu_j x\cos\beta_j - i\nu_j y\sin\beta_j + i\omega_j t + i\chi_j} \right\} \end{aligned} \tag{D.3}$$

With uni-directional waves:

$$u_1 = \frac{\partial\varphi_I}{\partial x}(r=0) = \Re\left\{ \sum_j A_j\omega_j e^{\nu_j z + i\omega_j t + i\chi_j} \right\} \tag{D.4}$$

Substituting (D.1) into F-K and disturbance body force, the expressions become equal in the limit of small Ka and their sum is:

$$F_{X,F-K} + F_{X,D} = 2\rho\pi a^2 \int_{-T}^{\zeta_I} dz\dot{u}_1(z)|_{x=0} + 2\rho\pi a^2 \frac{\partial\zeta_I}{\partial t}\Big|_{x=0} u_1|_{x=0,z=\zeta_I} \tag{D.5}$$

The time derivative of u_1 is:

$$\begin{aligned} \frac{\partial}{\partial t}\frac{\partial\varphi_I}{\partial x} &= \Re\left\{ \sum_j \frac{igA_j}{\omega_j}(-i\nu_j\cos\beta_j)(i\omega_j) e^{\nu_j z - i\nu_j x\cos\beta_j - i\nu_j y\sin\beta_j + i\omega_j t + i\chi_j} \right\} \\ &= \Re\left\{ \sum_j iA_j\omega_j^2\cos\beta_j e^{\nu_j z - i\nu_j x\cos\beta_j - i\nu_j y\sin\beta_j + i\omega_j t + i\chi_j} \right\} \end{aligned} \tag{D.6}$$

At $x = 0$ and in unidirectional waves:

$$\dot{u}_1(z)|_{x=0} = \Re\left\{ \sum_j iA_j\omega_j^2 e^{\nu_j z + i\omega_j t + i\chi_j} \right\} \tag{D.7}$$

The wave elevation of irregular waves can be expressed as:

$$\zeta_I = \Re\left\{ \sum_j A_j e^{-i\nu_j x\cos\beta_j - i\nu_j y\sin\beta_j + i\omega_j t + i\chi_j} \right\} \tag{D.8}$$

The time derivative of ζ_I is:

$$\frac{\partial\zeta_I}{\partial t} = \Re\left\{ \sum_j iA_j\omega_j e^{-i\nu_j x\cos\beta_j - i\nu_j y\sin\beta_j + i\omega_j t + i\chi_j} \right\} \tag{D.9}$$

At $x = 0$:

$$\begin{aligned} \zeta_I|_{x=0} &= \Re\left\{ \sum_j A_j e^{i\omega_j t + i\chi_j} \right\} \\ \frac{\partial\zeta_I}{\partial t}|_{x=0} &= \Re\left\{ \sum_j iA_j\omega_j e^{i\omega_j t + i\chi_j} \right\} \end{aligned} \tag{D.10}$$

Numerically:

$$\begin{aligned} \{F_{X,F-K} + F_{X,D}\}_c = 2\rho\pi a^2 \Bigg\{ & \sum_{m=1}^{N_{(T+\zeta_I)}} \triangle z_m \dot{u}_{1_m} \\ & + \Re\Big\{ \sum_{j=1}^{N_\Omega} iA_j\omega_j e^{i\omega_j c + i\chi_j} \Big\} \Re\Big\{ \sum_{j=1}^{N_\Omega} A_j\omega_j e^{i\omega_j t + i\chi_j} \Big\} \Bigg\}_c \end{aligned} \tag{D.11}$$

Introducing (D.1) into (2.58), the DD term vanishs identically.

ID is then the leading order force. It becomes:

$$F_{X,FS} = 2\rho\pi a^2 \int_{-T}^{\zeta_I} dz(u_1 u_{1x} + u_3 u_{1z}) - \rho\pi a^2 u_1 u_3|_{x=0,z=\zeta_I}; \quad u_3 = \frac{\partial\zeta_I}{\partial t} + u_1\frac{\partial\zeta_I}{\partial x}; \tag{D.12}$$

$$
\begin{aligned}
u_{1x} &= \Re\left\{ \sum_j \frac{igA_j}{\omega_j}(-i\nu_j \cos\beta_j)(-i\nu_j \cos\beta_j) e^{\nu_j z - i\nu_j x\cos\beta_j - i\nu_j y \sin\beta_j + i\omega_j t + i\chi_j} \right\} \\
&= \Re\left\{ \sum_j \frac{-iA_j\nu_j^3}{g} \cos^2\beta_j e^{\nu_j z - i\nu_j x\cos\beta_j - i\nu_j y \sin\beta_j + i\omega_j t + i\chi_j} \right\} \\
u_{1z} &= \Re\left\{ \sum_j \frac{igA_j}{\omega_j}(-i\nu_j \cos\beta_j)(\nu_j) e^{\nu_j z - i\nu_j x\cos\beta_j - i\nu_j y \sin\beta_j + i\omega_j t + i\chi_j} \right\} \\
&= \Re\left\{ \sum_j \frac{A_j\nu_j^3}{g} \cos\beta_j e^{\nu_j z - i\nu_j x\cos\beta_j - i\nu_j y \sin\beta_j + i\omega_j t + i\chi_j} \right\}
\end{aligned}
\tag{D.13}
$$

At $x = 0$ and in unidirectional waves:

$$
\begin{aligned}
u_{1x} &= \Re\left\{ \sum_j \frac{-iA_j\nu_j^3}{g} e^{\nu_j z + i\omega_j t + i\chi_j} \right\} \\
u_{1z} &= \Re\left\{ \sum_j \frac{A_j\nu_j^3}{g} e^{\nu_j z + i\omega_j t + i\chi_j} \right\}
\end{aligned}
\tag{D.14}
$$

The x-derivative of ζ_I is:

$$
\frac{\partial \zeta_I}{\partial x} = \Re\left\{ \sum_j -iA_j\nu_j \cos\beta_j e^{-i\nu_j x\cos\beta_j - i\nu_j y \sin\beta_j + i\omega_j t + i\chi_j} \right\} \tag{D.15}
$$

At $x = 0$ and in unidirectional waves:

$$
\begin{aligned}
\frac{\partial \zeta_I}{\partial t} &= \Re\left\{ \sum_j iA_j\omega_j e^{i\omega_j t + i\chi_j} \right\} \\
\frac{\partial \zeta_I}{\partial x} &= \Re\left\{ \sum_j -iA_j\nu_j e^{i\omega_j t + i\chi_j} \right\}
\end{aligned}
\tag{D.16}
$$

Numerically:

$$
F_{X,FS}|_c = \left\{ 2\rho\pi a^2 \Big[\sum_{m=1}^{N_{(T+\zeta_I)}} \triangle z_m (u_1 u_{1x} + u_3 u_{1z})_m \Big] - \rho\pi a^2 \{u_1 u_3\}|_{x=0,z=0} \right\}_c \tag{D.17}
$$

Bibliography

[1] A. Arapogianni, A-B. Genachte, and the members of the European Wind Energy Association's (EWEA) Offshore Wind Industry Group (OWIG) Task Force on deep offshore and new foundation concepts. Deep water - the next step for offshore wind energy. Technical report, European and Energy Association, www.ewea.org/report/deep-water, 2013.

[2] E.E. Bachynski, M. Etemaddar, M. Kvittem, C. Luan, and T. Moan. Dynamic analysis of floating wind turbines during pitch actuator fault, grid loss and shutdown. *Energy Procedia*, 35:210–222, 2013.

[3] S.R. Breit, P.D. Sclavounos, and J.N. Newman. New generation of panel programs for radiation-diffraction problems. Report No.: AD-A-159487/8/XAB, Massachusetts Institute of Technology, Department of Ocean Engineering, Cambridge, MA, 1985.

[4] J.M. Chuang, W. Qiu, and H. Peng. On the evaluation of time-domain green function. *Ocean Engineering*, 34:962–969, 2007.

[5] A. H. Clement. An ordinary differential equation for the green function of time-domain free-surface hydrodynamics. *Journal of Engineering Mathematics*, 33:201–217, 1998.

[6] M. St. Denis and W.J. Pierson. Motions of ships in confused seas. In *Annual Meeting of the Society of Naval Architects and Marine Engineers*, volume 61, pages 280–357, New York, 1953.

[7] O. M. Faltinsen, J.N. Newman, and T. Vinje. Nonlinear wave loads on a slender vertical cylinder. *Journal of Fluid Mechanics*, 289:179–198, 1995.

[8] B. Fox. The offshore grid: The future of america's offshore wind energy potential. *Ecology Law Quaterly*, 42(3):651–698, 2015.

[9] W. Froude. On the rolling of ships. *Transactions of the Institute of Naval Architecture*, 2:180–229, 1861.

[10] A.R. Henderson, R. Leutz, and T. Fujii. Potential for floating offshore wind energy in japanese waters. In *ISOPE Conference*, pages 505–512, Kitakyushu, Japan, 2002.

[11] J.L. Hess and A.M.O. Smith. Calculation of non-lifting potential flow about arbitrary three-dimensional bodies. Report No. E.S. 40622, Douglas Aircraft Company, Inc., Long Beach, CA, 1962.

[12] A. Jami. *Etude Théorique et Numérique de Phénomènes Transitoires en Hydrodynamique Navale. Thèse de Doctorat ès Sciences.* PhD thesis, Paris, ENSTA, 1981.

[13] J. Jonkman and W. Musial. Offshore code comparison collaboration (OC3) for IEA wind task 23 offshore wind technology and deployment. NREL/TP-5000-48191, National Renewable Energy Laboratory, Golden, CO, 2010.

[14] J.M. Jonkman, A.N. Robertson, and G.J. Hayman. *HydroDyn User's Guide and Theory Manual (Draft).* National Renewable Energy Laboratory, Golden, CO, 2014.

[15] J. Katz and A. Plotkin. *Low-Speed Aerodynamics.* McGraw-Hill, 1991.

[16] A. N. Krylov. A new theory of the pitching motion of ships on waves, and the stresses produced by this motion. *Transactions of the Institution of Naval Architectures*, 37:326–359, 1896.

[17] C.-H. Lee and J.N. Newman. *Computation of Wave Effects Using the Panel Method.* Numerical Models in Fluid-Structure Interaction. WIT Press, Southhampton, UK, preprint edition, 2004.

[18] C.H. Lee. *WAMIT theory manual.* Massachusetts Institute of Technology. Department of Ocean Engineering, Cambridge, Mass., 1995.

[19] S. Lee. *A Nonlinear Wave Load Model for Extreme and Fatigue Responses of Offshore Floating Wind Turbines.* PhD thesis, Massachusetts Institute of Technology, 2012.

[20] J. R. Morison, M.P. O'Brien, J. W. Johnson, and S. A. Schaaf. The force exerted by surface waves on piles. *Journal of Petroleum Technology*, 189:149–154, 1950.

[21] W. Musial and S. Butterfield. Future for offshore wind energy in the united states. In *Energy Ocean Proceedings*, Palm Beach, FL, 2004. (NREL/CP-500-36313) Golden, CO. : National Renewable Energy Laboratory.

[22] J.N. Newman. The approximation of free-surface green functions. In F. Ursell, P.A. Martin, and G.R. Wickham, editors, *Wave asymptotics : the proceedings of the meeting to mark the retirement of Professor Fritz Ursell from the Beyer Chair of Applied Mathematics in the University of Manchester*, chapter 7, pages 107–135. Cambridge University Press, New York, 1992.

[23] J.N. Newman and P.D. Sclavounos. The computation of wave loads on large offshore structures,. In *5th International Conference on the behavior of Offshore Structures (BOSS)*, Trondheim, Norway, 1988.

[24] J.N. Newman and E.O. Tuck. Current progress in the slender-body theory of ship motions. In *Proceedings of the 5th symposium naval hydrodynamics*, pages 129–167, 1964.

[25] F.G. Nielsen, T. Hanson, and B. Skaare. Integrated dynamic analysis of floating offshore wind turbines. In *OMAE*, Hamburg, Germany, 2006.

[26] A. Robertson, J. Jonkman, W. Musial, F. Vorpahl, and W. Popko. Offshore code comparison collaboration continued. Phase II results of a floating semi-submersible wind energy system. In *OMAE*, San Francisco, CA, 2014.

[27] A. N. Robertson, F. F. Wendt, J. M. Jonkman, W. Popko, F. Vorpahl, C. T. Stansberg, E. E. Bachynski, I. Bayati, F. Beyer, J. B. de Vaal, R. Harries, A. Yamaguchi, H. Shin, B. Kim, T. van der Zee, P. Bozonnet, B. Aguilo, R. Bergua, J. Qvist, Q. Wang, X. Chen, M. Guerinel, Y. Tu, Y. Huang, R. Li, and L. Bouy. OC5 Project Phase I: validation of hydrodynamic loading on a fixed cylinder. In *ISOPE*, Kona, Hawaii, 2015.

[28] D. Roddier, C. Cermelli, A. Aubault, and A. Weinstein. Windfloat: A floating foundation for offshore wind turbines. *Journal of Renewable and Sustainable Energy*, 2(3):033104, 2010.

[29] P. D. Sclavounos. On the quadratic effect of random gravity waves on a vertical boundary. *Journal of Fluid Mechanics*, 242:475–489, 1992.

[30] P. D. Sclavounos. Nonlinear impulse of ocean waves on floating bodies. *Journal of Fluid Mechanics*, 697:316–335, 2012.

[31] P. D. Sclavounos. Nonlinear loads on a vertical circular in irregular waves. Presented at the 31st International Workshop on Water Waves and Floating Bodies, Plymouth, Michigan, April 2016.

[32] P.D. Sclavounos, S. Lee, J. DiPietro, G. Potenza, P. Caramuscio, and G. De Michele. Floating offshore wind turbines: Tension leg platform and taught leg buoy concepts supporting 3-5 MW wind turbines. In *European Wind Energy Conference (EWEC)*, Warsaw, Poland, 2010.

[33] J. J. Stoker. *Water waves : the mathematical theory with applications*. Wiley-Interscience, New York, 1957.

[34] E.N. Wayman, P.D. Sclavounos, S. Butterfield, J. Jonkman, and W. Musial. Coupled dynamic modeling of floating wind turbine systems. In *Offshore Technology Conference*, Houston, TX, May 2006.

[35] J. V. Wehausen and E. V. Laitone. Surface waves. In *Encyclopaedia of Physics, Vol. IX*, pages 446–778. Springer Verlag, New York, 1960.